The Influence Matrix Approach to Quantum Many-Body Dynamics

Sonner, Michael

UNIVERSITÉ DE GENÈVE
Département de Physique Théorique

FACULTÉ DES SCIENCES
Professeur J. Sonner

The Influence Matrix Approach to Quantum Many-Body Dynamics

présenté à la Faculté des Sciences de l'Université de Genève pour obtenir le grade de docteur ès Sciences, mention Physique

par

Michael Sonner

de

Stuttgart-Bad Canstatt (Allemagne)

Thèse N° 5824

Genève

Archive ouverte

2024

UNIVERSITÉ DE GENÈVE

FACULTÉ DES SCIENCES

DOCTORAT ÈS SCIENCES, MENTION PHYSIQUE

Thèse de Monsieur Michael SONNER

intitulée :

«The Influence Matrix Approach to Quantum Many-Body Dynamics»

La Faculté des sciences, sur le préavis de

Monsieur J. SONNER, professeur ordinaire et directeur de thèse
Département de physique théorique

Monsieur T. GIAMARCHI, professeur ordinaire
Département de physique de la matière quantique

Monsieur D. ABANIN, professeur
Department of physics, Princeton University, Princeton, United States

Monsieur A. LÄUCHLI, professeur
Section de physique, Faculté des sciences de base, École Polytechnique fédérale de Lausanne (EPFL), Lausanne, Suisse - Laboratory for Theoretical and Computational Physics, Center for Scientific Computing, Theory and Data (PSI), Villigen, Suisse

autorise l'impression de la présente thèse, sans exprimer d'opinion sur les propositions qui y sont énoncées.

Genève, le 10 juin 2024

Thèse - 5824 -

Le Décanat

N.B. - La thèse doit porter la déclaration précédente et remplir les conditions énumérées dans les "Informations relatives aux thèses de doctorat à l'Université de Genève".

Summary

Studying the dynamics of complex quantum systems out-of-equilibrium is a central problem in modern physics. This field encompasses fundamental questions, like the nature of thermalization and how it can be avoided by some quantum system as well as practical questions about properties of materials. Recently, experimental techniques like ultracold atom experiments and other platforms for quantum simulation emerged that can access out-of-equilibrium phases such as Floquet time crystals.

However, the theoretical and computational study of out-of-equilibrium phenomena remains challenging. From a computational perspective, the fundamental challenge in quantum many-body physics lies in the exponential number of parameters necessary to describe the wavefunction. If their spatial entanglement is low, wavefunctions can be approximated with relatively few parameters using tensor network techniques. Since equilibrium wavefunctions have low spatial entanglement, this aspect makes computations viable. However, when simulating dynamics, spatial entanglement grows rapidly with the evolution time. In this thesis I present a new approach to many-body dynamics building on Feynman and Vernon's influence functional and combining insights from the field of open quantum systems with matrix product state techniques.

We consider dynamics of a subsystem, and view the rest of the many-body system as a quantum environment. The environment's properties are encoded in the influence matrix on the space of trajectories. Treating the influence matrix as a "wave function" in the temporal domain, we introduce the concept of Temporal Entanglement which can be interpreted as the "quantum memory" of the bath. In several broad and relevant classes of systems, such as some chaotic systems, localized and integral systems, temporal entanglement exhibits favorable scaling. This allows the influence matrix to be efficiently compressed as matrix product state, opening the door to a new family of computational methods based on low temporal rather than spatial entanglement.

Dynamical properties related to many-body localization and chaotic behavior are reflected in the influence matrix, allowing for analytical studies of these phenomena. I further show that this approach can be successfully applied to quantum impurity problems, where an interacting subsystem is coupled to environments consisting of free fermions. These models are of high practical significance as an ingredient in current algorithms used to study the properties of correlated materials

Résumé

Étudier la dynamique des systèmes quantiques complexes hors équilibre est un problème central en physique moderne. Ce domaine englobe des questions fondamentales, telles que la nature de la thermalisation et comment certains systèmes quantiques peuvent l'éviter, ainsi que des questions pratiques concernant les propriétés des matériaux. Récemment, des techniques expérimentales telles que les expériences avec des atomes ultra-froids et d'autres plateformes pour la simulation quantique ont émergé, permettant d'accéder à des phases hors équilibre telles que les cristaux temporels de Floquet.

Cependant, l'étude théorique et numérique des phénomènes hors équilibre reste un défi. D'un point de vue numérique, le défi fondamental dans l'étude des systèmes quantiques à N corps réside dans le nombre exponentiel de paramètres nécessaires pour décrire leur fonction d'onde. Si leur intrication spatiale est faible, les fonctions d'onde peuvent être approximées avec relativement peu de paramètres en utilisant des réseaux de tenseurs. Comme les fonctions d'onde à l'équilibre ont une faible intrication spatiale, cet aspect rend les calculs viables. Cependant, lors de la simulation de dynamiques, l'intrication spatiale augmente rapidement avec le temps d'évolution, compliquant les simulations numériques. Dans cette thèse, je présente une nouvelle approche des dynamiques à N corps en m'appuyant sur la fonctionnelle d'influence de Feynman et Vernon et en combinant des éléments du domaine des systèmes quantiques ouverts avec des techniques d'état de produit tensoriel.

Pour ce faire, nous considérons la dynamique d'un sous-système, et considérons le reste du système à N corps comme un environnement quantique. Les propriétés de l'environnement sont encodées dans la matrice d'influence sur l'espace des trajectoires. En traitant la matrice d'influence comme une « fonction d'onde » dans le domaine temporel, nous introduisons le concept d'Intrication Temporelle qui peut être interprété comme la « mémoire quantique » du bain. Dans plusieurs classes génerales et pertinentes de systèmes, comme certains systèmes chaotiques, localisés et intégrable, l'intrication temporelle présente une mise à l'échelle favorable. Cela permet à la matrice d'influence d'être efficacement compressée comme état de produit tensoriel, ouvrant la porte à une nouvelle famille de méthodes numériques basées sur une faible intrication temporelle plutôt que spatiale.

Les propriétés dynamiques liées à la localisation à N corps et au comportement chaotique se reflètent dans la matrice d'influence, permettant des études analytiques de ces phénomènes. Je montre en outre que cette approche peut être appliquée avec succès aux problèmes d'impureté quantique, où un sous-système avec interaction est couplé à des environnements constitués de fermions libres. Ces modèles sont d'une grande importance pratique comme composants dans les algorithmes actuels utilisés pour étudier les propriétés des matériaux corrélés.

Contents

Publication list

Included as reprints in this thesis

[1] Alessio Lerose, Michael Sonner, and Dmitry A. Abanin. "Influence Matrix Approach to Many-Body Floquet Dynamics". In: *Physical Review X* 11.2 (2021), p. 021040.

[2] Michael Sonner, Alessio Lerose, and Dmitry A. Abanin. "Characterizing Many-Body Localization via Exact Disorder-Averaged Quantum Noise". In: *Physical Review B* 105.2 (2022), p. L020203.

[3] Julian Thoenniss, Michael Sonner, Alessio Lerose, and Dmitry A. Abanin. "Efficient Method for Quantum Impurity Problems out of Equilibrium". In: *Physical Review B* 107.20 (May 2023), p. L201115. DOI: 10.1103/PhysRevB.107.L201115. (Visited on 08/11/2023).

Other works

[4] X. Mi et al. "Noise-Resilient Edge Modes on a Chain of Superconducting Qubits". In: *Science* 378.6621 (Nov. 2022), pp. 785–790. DOI: 10.1126/science.abq5769. (Visited on 08/31/2023).

[5] Alessio Lerose, Michael Sonner, and Dmitry A. Abanin. "Scaling of Temporal Entanglement in Proximity to Integrability". In: *Physical Review B* 104.3 (2021), p. 035137.

[6] Alessio Lerose, Michael Sonner, and Dmitry A. Abanin. "Overcoming the Entanglement Barrier in Quantum Many-Body Dynamics via Space-Time Duality". In: *Physical Review B* 107.6 (Feb. 2023), p. L060305. DOI: 10.1103/PhysRevB.107.L060305. (Visited on 02/01/2024).

[7] Michael Sonner, Maksym Serbyn, Zlatko Papić, and Dmitry A. Abanin. "Thouless Energy across the Many-Body Localization Transition in Floquet Systems". In: *Physical Review B* 104.8 (2021), p. L081112.

[8] Michael Sonner, Alessio Lerose, and Dmitry A. Abanin. "Influence Functional of Many-Body Systems: Temporal Entanglement and Matrix-Product State Representation". In: *Annals of Physics* 435 (2021), p. 168677.

[9] Benedikt Kloss, Julian Thoenniss, Michael Sonner, Alessio Lerose, Matthew T. Fishman, E. M. Stoudenmire, Olivier Parcollet, Antoine Georges, and Dmitry A. Abanin. "Equilibrium Quantum Impurity Problems via Matrix Product State Encoding of the Retarded Action". In: *Physical Review B* 108.20 (Nov. 2023), p. 205110. DOI: 10.1103/PhysRevB.108.205110. (Visited on 04/28/2024).

[10] Giacomo Giudice, Giuliano Giudici, Michael Sonner, Julian Thoenniss, Alessio Lerose, Dmitry A. Abanin, and Lorenzo Piroli. "Temporal Entanglement, Quasiparticles, and the Role of Interactions". In: *Physical Review Letters* 128.22 (2022), p. 220401.

Preface

Structure of thesis

This thesis is structured as follows. In the first chapter, I intoduce the field of out out-of-equilibrium physics and basic concepts which are used throughout the rest of the thesis. The second chapter introduces the influence matrix as well as the notion of temporal entanglement. In the third chapter, I discuss how the influence matrix can be computed in one dimensional systems and explain why temporal entanglement is low for infinite systems which consist of free quasi-particles. The following chapters discuss different application of the influence matrix formalism. They each contain a short introduction along with a reprint of the arXiv version of the corresponding paper. The fourth chapter discusses the exact influence matrices which can be obtained for dual unitary circuits. In the fifth chapter many-body localization is studied using disorder-averaged influence matrices. The sixth chapter employs the IM techniques to numerically compute the real time evolution of impurity models. Finally the seventh chapter summarizes theses developments as well as provide an outlook for future research in this field.

Conventions used in this thesis

In this thesis, I use a version of Einsteins Summation convention to keep the length of equations manageable. Indices which appear exactly twice are understood to be summed over. This only applies to "first-level" indices and not indices of indices. Furthermore, unless specifically mentioned otherwise, Greek indices refer to vectorized density matrix degrees of freedom. Hence density matrices typically have one index per Hilbert space and channels which are operators on the space of density matrices have two.

For example the following matrix product state expansion of a density matrix

$$\rho_{\{\alpha_k\}_{k=1}^4} = v_{\beta_0} \left(\prod_{k=1}^{4} M_{\beta_{k-1},\alpha_k,\beta_k} \right) w_{\beta_4} \tag{0.1}$$

is understood to expand to

$$\rho_{\alpha_1,\alpha_2,\alpha_3,\alpha_4} = v_{\beta_0} M_{\beta_0,\alpha_1,\beta_1} M_{\beta_1,\alpha_2,\beta_2} M_{\beta_2,\alpha_3,\beta_3} M_{\beta_3,\alpha_3,\beta_4} w_{\beta_4} \tag{0.2}$$

and is then be contracted using Einsteins convention as

$$\rho_{\alpha_1,\alpha_2,\alpha_3,\alpha_4} = \sum_{\beta_0=1}^{d^2} \sum_{\beta_1=1}^{d^2} \sum_{\beta_2=1}^{d^2} \sum_{\beta_3=1}^{d^2} \sum_{\beta_4=1}^{d^2} v_{\beta_0} M_{\beta_0,\alpha_1,\beta_1} M_{\beta_1,\alpha_2,\beta_2} M_{\beta_2,\alpha_3,\beta_3} M_{\beta_3,\alpha_3,\beta_4} w_{\beta_4} \tag{0.3}$$

These conventions do not apply to reprints of papers which form part of this thesis.

1 Out of equilibrium dynamics

1.1 Introduction

I begin this thesis by lining out current developments in the study of out-of-equilibrium quantum systems and introduce basic theoretical concepts which will be used throughout the rest of the thesis.

In this thesis, I will discuss quantum systems out-of-equilibrium. Typically and apart from few exceptions such as phosphorescence, quantum systems in highly excited states relax quickly to their equilibrium due to interactions with the environment. This makes it difficult to study out-of-equilibrium physics experimentally. However, the advent of quantum simulation platforms consisting of carefully controlled and isolated quantum systems such as ultra-cold atoms [11, 12], Rydberg atoms[13] and other quantum simulation platforms [14] lead to progress in this field[15]. One typical setup to study out-of-equilibrium dynamics is a *quantum quench*. The quantum system is prepared in the ground state of one Hamiltonian, which is then suddenly changed to a different Hamiltonian. The quantum system finds itself then in a highly excited state and its thermalization or lack thereof can be observed. Thermalization of quantum systems is discussed in more details in Sec. 1.3 below. Out-of-equilibrium physics of a quantum system can also be probed by considering transport. This is most natural in mesoscopic systems [16, 17], but is also possible using other platforms like ultra-cold atoms [18]. Another intriguing possibility are *periodically driven systems*. Periodically changing the Hamiltonian allows for novel exotic phases of matter in out-of-equilibrium systems such as Floquet time-crystals [19–22] or topological phases [23] which are not possible in equilibrium.

Furthermore, out-of-equilibrium behavior can be used to study properties of matter by exciting it using photons and observing its relaxation. One important technique in this class is nuclear magnetic resonance (NMR)[24], where nuclear spins in a strong static magnetic field are excited using pulses of radio waves. The nuclear spins emit a radio echo upon returning to their ground state, which depends on their local environment. This technique is routinely used to identify and determine the structure of chemical compounds.

Quantum circuits used in quantum algorithms can themselves be seen as highly non-equilibrium quantum systems. This enables the use of generic quantum computing platforms such as superconducting qubits[25] which do not directly resemble isolated quantum systems to probe out-of-equilibrium physics[4, 20]. Understanding which classes of quantum circuits can be efficiently simulated on classical computers and which cannot is a promising approach to find problem where quantum computer possess a quantum advantage.

This introduction is structured as follows. First I will discuss the basic formalism of open quantum systems. Then we discuss basic phenomenology of thermalization. Finally, I introduce matrix product states which play an important role throughout this thesis.

1.2 Open quantum systems and Markovian dynamics

This thesis relies extensively on the formalisms used to treat *open quantum systems*. In this section, I introduce the most important concepts and definitions, which are used throughout the rest of this thesis. One excellent review, which uses similar conventions is Ref. [26]

The major challenge in building quantum computers and other controllable quantum systems are its interactions with their environment. Quantum environments, which can encompass everything from the measurement devices to the scientist performing the experiment are themselves very large and complicated quantum systems. Interactions with the large environment quantum system result in entanglement between these two quantum systems, which in turn manifests as dissipation on the small quantum system. To avoid describing large quantum environments system exactly, we derive an effective description of a subsystem embedded in a large quantum system.

Consider a quantum system defined on a Hilbert space $\mathcal{H}$ which factorizes into a large *environment* Hilbert space $\mathcal{H}^{env}$ and a *subsystem* Hilbert space $\mathcal{H}^{sub}$,

$$\mathcal{H} = \mathcal{H}^{\text{sub}} \otimes \mathcal{H}^{\text{env}}. \tag{1.1}$$

By definition we can write any wavefunction $|\psi\rangle$ on the full Hilbert space as linear combination of tensor products:

$$|\psi\rangle = \sum_{k}^{d} \lambda_k |\psi_k^{\text{sub}}\rangle |\psi_k^{\text{env}}\rangle. \tag{1.2}$$

This decomposition is not unique, but it is always possible to choose the vectors in each part of the Hilbert space to be orthonormal [26, 27]. This is called the *Schmidt-decomposition* and the non-negative, real values λ_k, conventionally sorted in descending order are the *Schmidt-values*. We hence use

$$\langle \psi_k^{\text{sub}} | \psi_l^{\text{sub}} \rangle = \langle \psi_k^{\text{env}} | \psi_l^{\text{env}} \rangle = \delta_{kl}. \tag{1.3}$$

The number of Schmidt-values d is called the *Schmidt-rank* and is bounded by

$$d \leq \min\left(\dim(\mathcal{H}^{\text{sub}}), \dim(\mathcal{H}^{\text{env}})\right). \tag{1.4}$$

Suppose one wants to measure an observable which is only supported on the subsystem Hilbert space $\mathcal{H}^{\text{sub}}$. Its expectation value can be expressed as

$$\langle \psi | O | \psi \rangle = \sum_{k,l}^{d} \lambda_k \lambda_l \langle \psi_k^{\text{env}} | \langle \psi_k^{\text{sub}} | O | \psi_k^{\text{sub}} \rangle | \psi_k^{\text{env}} \rangle, \tag{1.5}$$

using the orthogonality of the Schmidt-vectors in the environment space and we can rewrite this expression as:

$$\langle\psi|O|\psi\rangle = \mathrm{Tr}(O\rho^{\mathrm{sub}}) \tag{1.6}$$

where ρ^{sub} is the *reduced density matrix* (RDM) and can be written as

$$\rho^{\mathrm{sub}} = \sum_k^d \lambda_k^2 |\psi_k^{\mathrm{sub}}\rangle\langle\psi_k^{\mathrm{sub}}| = \mathrm{Tr}_{\mathrm{env}}(|\psi\rangle\langle\psi|). \tag{1.7}$$

where $\mathrm{Tr}_{\mathrm{env}}$ corresponds to the trace over the environment Hilbert space. Remarkably the RDM is the only object necessary to compute any observable. In particular the exact structure of the wavefunction within the environment Hilbert space is no longer necessary! The full wavefunction corresponding to a given RDM ρ is not unique, a wavefunction $|\psi\rangle$ that satisfies Eq. (1.7) is called *purification* of ρ. The number of parameters of the RDM is given by $\dim(\mathcal{H}^{\mathrm{sub}})^2 = \dim(\mathcal{H}^{\mathrm{sub}}) \times \dim(\mathcal{H}^{\mathrm{sub}})$ and does not depend on the Hilbert space dimension of the environment. The expression in Eq. (1.7) can be viewed as a diagonalization of ρ, where the eigenvalues are given by λ_k^2. Hence, a RDM is a positive semidefinite, hermitian matrix. Normalization of the full wavefunction $|\psi\rangle$ yields the additional constraint that the trace is one

$$\mathrm{Tr}(\rho) = \sum_k \lambda_k^2 = 1. \tag{1.8}$$

Any positive definite, hermitian matrix with trace one can be purified using an environment Hilbert space equivalent to the subsystem Hilbert space. This is called the purification theorem[28–30].

The notion of density matrix can also be understood without reference to any purification. Consider a quantum system which is with probability p_k in a state with wavefunction $|\Phi_k\rangle$. These wavefunctions do not necessarily need to be orthogonal. We can compute any observables of this mixed state by computing

$$\langle O\rangle = \sum_k p_k \langle\Phi_k|O|\Phi_k\rangle = \mathrm{Tr}(O\sum p_k|\Phi_k\rangle\langle\Phi_k|) = \mathrm{Tr}(O\rho) \tag{1.9}$$

with the density matrix ρ defined as:

$$\rho = \sum_k p_k |\Phi_k\rangle\langle\Phi_k| \tag{1.10}$$

A subsystem of a large quantum system thus behaves with respect to measurements like a *classical mixture* of pure states. Conversely and classical mixture can be understood as a subsystem of a large quantum system. This allows us to represent various classical ensembles using density matrices: Thermal states with an inverse temperature β in a system with a local Hamiltonian H can be expressed as density matrix

$$\rho = \frac{e^{\beta H}}{\mathrm{Tr}(e^{\beta H})} \tag{1.11}$$

In the limit of infinite temperature $\beta \to 0$ we obtain the *infinite temperature* or *maximally mixed* state

$$\rho = \frac{1}{\dim(\mathcal{H}^{\text{sub}})} \mathbb{1}^{\text{sub}}. \tag{1.12}$$

The density matrix corresponding to a quantum state described by a single local wavefunction $|\psi\rangle$, a *pure state*, is given by the projector onto the wavefunction:

$$\rho = |\psi\rangle\langle\psi|. \tag{1.13}$$

Interpreting the eigenvalues of the density matrix as probabilities suggests using the notion of *entropy* from the field of information theory[31] to quantify the "mixedness" of a density matrix. We can write the von-Neumann entropy of a density matrix[32]

$$S = \sum_{n=1}^{d} p_n \log(p_n) = \text{Tr}(\rho \log(\rho)). \tag{1.14}$$

For thermal states as in Eq. (1.11), this coincides with the thermodynamic entropy[33][1].

If quantum system is in a pure state, we call the entropy of the RDM of a subsystem its *entanglement entropy*. The scaling of the entanglement entropy with the size of the subsystem is widely used ad a witness to diagnose physical phases[34]. If the entanglement entropy scales linearly with the volume, that is the number of degrees of freedom, in a subsystem it is said to scale as a *volume law*. This is for example the case for random quantum states[34]. Scaling with the surface of the subsystem is called *area-law* scaling. Ground states of gapped local Hamiltonians scale are an example of area law states. In one dimension, the surface of any interval is a point, which means that entanglement entropy of area law state does not scale with system size in one dimension. The ground states of critical states in one dimension scales logarithmically in system size[35]. Despite its usefulness as a computable quantity, it is difficult to measure entanglement entropy in experiments, since it is non-linear in the density matrix and hence not an observable in the normal sense. However, experimental protocols to measure entanglement entropies by using multiple copies of the same state have been devised[36–38].

To derive the time evolution of mixed states, we return to the idea that potentially mixed quantum systems can be understood as small subsystem embedded in a large quantum system in a pure state. Any physical time evolution of the entire quantum system composed of subsystem and environment can be expressed by applying a time evolution operator U to the wavefunction $|\psi\rangle$ of the large quantum system:

$$|\psi'\rangle = U|\psi\rangle. \tag{1.15}$$

where $|\psi'\rangle$ is the time evolved wavefunction. Unitarity of U guarantees that orthogonal states remain orthogonal and that norm is preserved. The action of U on mixed states of the subsystem is fully defined by specifying its action on pure states. We can hence

[1] The historical development was opposite: thermodynamic entropy was introduced first[33] then von Neumann entropy[32], and finally the information theory notion[31].

choose the initial wavefunction as a product state between a pure subsystem state $|\psi^{\text{env}}$ with an arbitrary pure environment state $|0\rangle$, that is $|\psi\rangle = |\psi^{\text{sub}}\rangle \otimes |0\rangle$. We can compute the time evolved reduced density matrix by performing the trace over the environment Hilbert space

$$\rho' = \text{Tr}_{\text{env}}(|\psi'\rangle\langle\psi'|) = \text{Tr}_{\text{env}}(U|\psi\rangle\langle\psi|U^\dagger) = \text{Tr}_{\text{env}}(U|0\rangle|\psi^{\text{sub}}\rangle\langle\psi^{\text{sub}}\langle 0|U^\dagger) \tag{1.16}$$

By defining the *Krauss operators*

$$M_a =_{\text{env}} \langle 0|U|a\rangle_{\text{env}} \tag{1.17}$$

we can write the density matrix time evolution as

$$\rho' = \sum_{a=1}^{\mathscr{H}^{\text{env}}} M_a^\dagger \rho M_a. \tag{1.18}$$

The Krauss operators fulfill the condition

$$\mathbb{1} = \sum_{a=1}^{\mathscr{H}^{\text{env}}} M_a^\dagger M_a, \tag{1.19}$$

which follows from unitarity of U. It turns out that with at most $\dim(\mathscr{H}^{\text{sub}})^2$ Krauss-operators, *any* linear map which is completely positive and trace preserving (CPTP), i.a. maps valid density matrices to valid density matrices can be represented using the *operator sum* representation in Eq. (1.18) with condition Eq. (1.19)[26]. Such maps are called, depending on context *quantum channels*[26], *superoperators*[39] or *CPTP-maps*[40, 41]. The limit of $\dim(\mathscr{H}^{\text{sub}})^2$ Krauss-operators also define the maximal additional Hilbert space size the environment needs to have in order to be able to represent all channels using a unitarity time evolution. The representation of channels using a unitary time evolution is called the *Stine-spring dilation*[42]. Successive application of quantum channels correspond to Markovian time evolution, since the time evolved density matrix only depends on the previous density matrix and not on any internal state of the environment. Extensions to non-Markovian time evolutions have been proposed[43–45] and in fact lead to a very similar construction to what the one described in this thesis in Chap. 2. Furthermore it is common in the literature to consider the continuous time of Markovian system using Lindbladian master equations[46]. However, for the purposes of this thesis discrete time evolution is sufficient.

Physically a set of operators in the form of Eq. (1.19) can be understood as a generalized measurement of the subsystem by the environment in form of a *postive operator valued measurement* (POVM). Each Krauss operator corresponds to a measurement outcome, with the associated probability given by

$$p_a = \text{Tr}(\rho M_a^\dagger M_a). \tag{1.20}$$

This allows us to identify and interpret some important channels: If there is only one Krauss operator, it has to be unitary and it corresponds to the absence of a measurement.

Instead the subsystem evolves unitarily without interacting with the environment. We can write such a unitary channel as:

$$C_U[\rho] = (U \otimes U^\dagger)[\rho] = U\rho U^\dagger. \tag{1.21}$$

Consider now a single spin as subsystem. If the environment measures the spin in the z basis, we can write the corresponding channel as

$$C_{\text{dephasing}}[\rho; \gamma = 1] = |\uparrow\rangle\langle\uparrow|\rho|\uparrow\rangle\langle\uparrow| + |\downarrow\rangle\langle\downarrow|\rho|\downarrow\rangle\langle\downarrow| = \frac{1}{2}\mathbb{1}\rho\mathbb{1} + \frac{1}{2}\sigma^z\rho\sigma^z. \tag{1.22}$$

This is called a (perfectly) *dephasing* or *phase-damping* channel [26]. On the density matrix it acts by completely suppressing the off-diagonal elements, thereby projecting the density matrix onto the z axis. Instead of performing a strong measurement, the environment can also only measure with a given probability p. In this case, we obtain the more generic dephasing channel:

$$C_{\text{dephasing}}[\rho] = (1 - \frac{p}{2})\mathbb{1}\rho\mathbb{1} + \frac{p}{2}\sigma^z\rho\sigma^z \tag{1.23}$$

If we understand each application of the channel as a discrete timestep, this means that the off-diagonal element are exponentially dampened in time.

We can also consider an environment that perform what is called an *information complete* measurement which transfers all information from the subsystem into the environment, leaving the subsystem in a maximally mixed state. We can write this measurement by using all Pauli matrices as Krauss operators, resulting in a channel that always yields the maximally mixed state:

$$C_{\text{depolarizing}}[\rho] = \frac{1}{4}\mathbb{1}\rho\mathbb{1} + \frac{1}{4}\sigma^x\rho\sigma^x + \frac{1}{4}\sigma^y\rho\sigma^y + \frac{1}{4}\sigma^z\rho\sigma^z = \frac{\mathbb{1}}{2}\text{Tr}(\rho) \tag{1.24}$$

This channel is called a (perfectly) *depolarizing* channel. Note that we need the maximal number of $d^2 = 4$ Krauss operators to represent it in operator-sum form.

In this thesis, I generally use *vectorized* indexing for density matrices, operators and channels in order to make expressions more concise. This means that a density matrix or operator is indexed by a single (Greek) index running through the dimension of the doubled Hilbert space. Correspondingly, channels possess two indices. This convention does not apply to reprints which form part of the thesis.

1.3 Thermalization and MBL

In this section, I briefly discuss the presence and absence of thermalization in quantum systems, characterizing their long time behaviors. For comprehensive reviews, I refer to Refs. [47, 48].

If we pour ourselves a hot cup of coffee and let it sit on the desk for too long, it gets colder until it reaches room temperature. From daily experience we know that most physical systems have a tendency to return to a thermal equilibrium. This means that

macroscopic observables, such as particle or energy density, evolve towards a state only defined by the conservation laws in a system, irrespective of their initial conditions. This *thermalization* process hence defines a direction of time. The fact that there seems to be a preferred direction of time evolution is surprising, since the laws of motions governing the microscopic constituents of physical systems are generally [2] invariant under time reversal. In classical physics, this apparent paradox can be resolved by considering the number of individual microscopic configurations corresponding to each macroscopic state. We find that there are vastly more microscopic states corresponding to the thermal equilibrium, then to out-of-equilibrium states. This is quantified by the *thermodynamic entropy* of a given macroscopic state, which roughly corresponds to the logarithm of the number of microscopic configurations. Chaotic systems, which are defined by the property that trajectories corresponding to slightly different initial state diverge exponentially, are expected to be *ergodic*. This means that after a long time the system is equally likely to be found in any microscopic state conforming to the same conserved quantities as the initial state. Since most microscopic states correspond to macroscopic states close to thermal equilibrium, the system will move towards thermal equilibrium. This explains how the thermodynamic arrow of time can arise from time-reversal symmetric microscopic laws of nature. Ergodicity has been proven for some special cases like hard spheres[50] on a torus, or some billards[51, 52]. However, even in classical systems, determining whether a system is ergodic or not is, in general a difficult proposition[53].

For quantum systems the situation is a bit different. Since quantum systems are governed by the linear Schroedinger equation, they cannot behave chaotically in the classical sense. Unitarity further implies that states that are completely distinguishable, i.e. orthogonal at the initial time, remain orthogonal throughout their time evolution. Overlaps with the eigenstates of the Hamiltonian are constant in time, yielding an extensive set of integrals of motions. Despite this, the physical intuition that most systems thermalize still holds. Instead of considering the entire wavefunction, we can consider the expectation value local or few site operators. A system thermalizes, if the long term average of local operators O returns to its thermal values. In systems without any additional conservation laws, this is given by the Gibbs ensemble:

$$\overline{O} = \frac{\mathrm{Tr}(Oe^{-\beta H})}{\mathrm{Tr}(e^{-\beta H})} \tag{1.25}$$

where the inverse temperature β is determined by the energy of the initial state. Physically this thermalization can be understood as the system acts as a thermal bath on its subsystems. Information about the initial state is still present in the full wavefunction of the quantum system. However, it is spread over the entire system and thus essentially unrecoverable.

To understand how thermalization can arise from quantum mechanics, we consider a microcanonical ensemble description. Provided the entropy is a fast rising function of the energy, as in typical physical systems, we can write the thermalization condition in

[2] Apart from some tiny deviations related to the weak force [49]

Eq. (1.25) equivalently as[54]

$$\overline{O} = \sum_n \Delta(E,n)\langle n|O|n\rangle, \tag{1.26}$$

where $\Delta(E,n)$ is normalized in n and peaked around $E = E_n$ and the energy E is given by the initial state $E = \langle\psi|H|\psi\rangle$. We can write down the time evolution of operator O by expanding the wavefunction in terms of energy eigenstates

$$|\psi(t)\rangle = \sum_n c_n|n\rangle, \tag{1.27}$$

and obtain

$$\langle\psi(t)|O|\psi(t)\rangle = \sum_n |c_n|^2\langle n|O|n\rangle + \sum_{n,m} e^{i(E_n-E_m)t}c_n^* c_m\langle m|O|n\rangle. \tag{1.28}$$

In the long time average, the terms proportional to the off-diagonal matrix elements do not contribute, as the phases average to zero. Hence, for thermalizing systems, energy eigenstates themselves act locally as thermal states. This implies for example volume law entanglement entropy for energy eigenstates of thermalizing Hamiltonians. The analysis can be be extended to off-diagonal elements, by assuming that local observables behave like random matrices in the basis of energy eigenstates which are close in energy[55]. The off-diagonal elements are then given by overlaps of random vectors with similar energy and hence suppressed by the thermodynamic entropy $e^{-\frac{1}{2}S(E)}$. We hence write the Eigenstate thermalization hypothesis (ETH)[54, 56] ansatz for matrix elements of operators O:

$$\langle n|O|m\rangle \approx \delta_{mn}\overline{O}(E) + e^{-\frac{1}{2}S(E)}f_O(E,\omega)R_{mn}. \tag{1.29}$$

where $\overline{O}(E)$ and $f_O(E,\omega)$ are smooth function of the energy $E = \frac{E_n+E_m}{2}$ and $\omega = E_n - E_m$. R_{mn} denotes a random variable with zero average and variance one. The connection to random matrices has implications for the spectrum of thermalizing Hamiltonians. For example, the level spacing between neighbouring levels exhibit a level repulsion and are distributed by the Wigner-Dyson distribution

$$P(\Delta) \propto \Delta^2 e^{-c\Delta} \tag{1.30}$$

instead of being Poisson distributed

$$P(\Delta) \propto e^{-c\Delta} \tag{1.31}$$

which would correspond to independently chosen levels and is common in non-thermalizing systems. These probes are commonly used to identify thermalizing quantum systems [7, 57]

However, not all quantum systems exhibit thermalization. Similar to classical systems, it is possible to fine-tune Hamiltonians such that they commute with an extensive number

of integrals of motions that can be expressed in terms of local operators. Such so-called *integrable* systems include non-interacting fermions and bosons as well as Bethe-integrable models like the XXZ chain[58]. In this case typical eigenstates still observe ETH[48, 59, 60], but there is a small number of eigenstates which does violate ETH. This is called *weak* ETH.

Surprisingly it was found that even generic quantum systems can escape thermalization by being strongly disordered[61–63]. These *Many-body localized* (MBL) systems can be thought of interacting extension of *Anderson localization*[64]. Localized systems are characterized by the suppression of transport and retention of information of the initial state in local observables. This can be understood by the emergence of local integrals of motions [65–67]. In MBL systems, entanglement entropy grows logarithmically in time[68], in contrast to the typical linear growth observed in thermalizing and integrable systems [69–71]. For comprehensive reviews about MBL see Refs. [72–75]

1.4 Matrix Product States

In this section I will briefly review basic Matrix Product State (MPS) techniques which are used throughout this thesis. For a more comprehensive introduction I refer to the reviews [76–79].

The Hilbert space dimension of a quantum many-body system is exponential in the system size. This puts severe limits on computational methods which rely on manipulating the entire state in vector form. Finding an efficient parametrization of relevant states using fewer parameters allows for larger system size at the cost of making an approximation. The quality of the approximation generally depends on the number of parameters used, as well as the state which is being represented.

For one dimensional systems, the *Matrix product state* (MPS)[80–82] representation, which is also called *Tensor Train decomposition*[83] can be such an efficient representation. A MPS representation of a wavefunction ψ of a quantum system with L sites which are indexed by the *physical indices* i_n is given by:

$$\psi_{\{i_n\}_{n=1}^L} = \prod_{n=1}^{L} M^{(\psi,n)}_{k_n,i_n,k_{n+1}}|_{k_1=k_{L+1}=1} \tag{1.32}$$

where the tensors M are called the *MPS kernels*, and the indices k_n are the *virtual indices*. The dimensionality of this virtual space indexed by the virtual indexes is called the *bond dimension* χ_n. To simplify notation, one usually uses the maximal bond dimension $\chi = \max(\chi_n)$ as the parameter which controls the expressiveness of the MPS representation. The MPS parametrization uses $O(Ld\chi^2)$ complex parameters. Arbitrary states can be represented as MPS, one way to do this is for example by using identities for all MPS kernels except from the first:

$$\psi_{\{i_n\}_{n=1}^L} = \psi_{i_1,\{i_k\}_{k=2}^L} \prod_{n=2}^{L} \mathbb{1}_{\{i_k\}_{k=n}^L,i_n,\{i_k\}_{k=n+1}^L}|_{k_{L+1}=1} \tag{1.33}$$

Of course the bond dimension χ of the exact representation of an arbitrary state scales exponentially in the system size L. An important building block of many MPS algorithm are hence algorithms to *compress* an MPS, i.e. finding an MPS with lower bond dimension which approximates the same vector.

To approach the problem of compression, it is useful to focus on a single bond. By writing the summation over this bond k explicitly, this defines effectively a linear decomposition of the wavefunction in terms of product states. We can find the Schmidt decomposition corresponding to Eq. (1.34) [27]:

$$\psi_{\{i_n\}_{n=1}^L} = \sum_{m=1}^{\chi_k} \lambda_k \psi^{(L,k,m)}_{\{i_n\}_{n=1}^k} \psi^{(R,k,m)}_{\{i_n\}_{n=k+1}^L}, \tag{1.34}$$

where the left and right factors are orthonormal:

$$\psi^{(L,k,l)}_{\{i_n\}_{n=1}^k} \psi^{(L,k,m)*}_{\{i_n\}_{n=1}^k} = \delta_{lm}. \tag{1.35}$$

We can now describe a local truncation to bond dimension χ_k by only performing this sum over the χ_k' largest Schmidt values. While each of these local truncation step is *globally optimal*, this does not apply if multiple bonds are truncated.

For an efficient algorithm, the Schmidt decomposition needs to be computed by only using local degrees of freedom. We start by noting that the MPS representation defined in Eq. (1.32) is not unique. On each bond between two kernels, one can introduce a resolution of identity in form of an invertible matrix $\mathbb{1} = X^{-1}X$. This *gauge freedom* allows us to find a *canonical* forms of MPS. The *left-canonical* form is defined by

$$\psi_{\{i_n\}_{n=1}^L} = \left(\prod_{n=1}^{L-1} A^{(\psi,n)}_{j_n,i_n,j_{n+1}} \right) M^{(\psi,L)}_{j_L,i_L,j_{L+1}}|_{j_1=j_{L+1}=1} \tag{1.36}$$

where the tensors A fulfill a similar isometry condition

$$\delta_{k_{n+1},k'_{n+1}} = \delta_{k_n,k'_n} A^{(\psi,n)}_{k_n,i_n,k_{n+1}} A^{*(\psi,n)}_{k'_n,i_n,k'_{n+1}} \tag{1.37}$$

It is possible to bring any MPS to left-canonical form, by using successive QR-decomposition, which decomposes a matrix $M = QR$ in a product of a orthogonal matrix Q with $Q^\dagger = Q^{-1}$ and a upper triangular matrix R. Assuming that all matrices to the left of bond $k-1$ fulfill the isometry condition Eq. (1.37), we can obtain a MPS where all matrices to the left of bond k are isometric by decomposing the first non-isometric matrix.

$$M^{(\psi,k)}_{j_k,i_k,j_{k+1}} = Q_{j_k,i_k,m} R_{m,j_{k+1}} \tag{1.38}$$

and absorb R into the next non-isometric matrix $M^{(\psi,k+1)}$. Repeating this step until $k = L$ results in an MPS in left-canonical form.

Analogous, we define a *right-canonical* form

$$\psi_{\{i_n\}_{n=1}^L} = M^{(\psi,1)}_{k_1,i_1,k_2} \prod_{n=2}^{L} B^{(\psi,n)}_{k_n,i_n,k_{n+1}}|_{k_1=k_{L+1}=1} \tag{1.39}$$

Where the tensors B fulfill the isometry condition:

$$\delta_{k_n,k'_n} = B^{(\psi,n)}_{k_n,i_n,k_{n+1}} B^{*(\psi,n)}_{k'_n,i_n,k'_{n+1}} \delta_{k_{n+1},k'_{n+1}} \tag{1.40}$$

Combining those definitions allow us to define the *mixed-canonical* form:

$$\psi_{\{i_n\}_{n=1}^L} = \left(\prod_{n=1}^{m-1} A^{(\psi,n)}_{k_n,i_n,k_{n+1}} \right) M^{(\psi,m)}_{k_L,i_L,k_{L+1}} \left(\prod_{n=m+1}^{L} B^{(\psi,n)}_{k_n,i_n,k_{n+1}} \right) |_{k_1=k_{L+1}=1}. \tag{1.41}$$

The non-isometric tensor M at position m is called the *orthogonality center*. The orthogonality center can be moved to the left using QR-decomposition using Eq. (1.38). Analogous, we can use the RQ decomposition to move the orthogonality center one kernel to the left. For both movements the only requirement of the decomposition is the property of the orthogonal matrix. In particular, we can also move the orthogonality using the singular value decomposition (SVD) $M = U\Sigma V^\dagger$, where U and $V^\dagger$ are left (right) isometries and Σ is diagonal. By setting $Q = U$ and $R = \Sigma V^\dagger$, we can use this decomposition in place of the QR-decomposition. However, this only makes sense if SVD needs to be computed for a different reason, since SVD algorithms are generally more expensive and not parallelizable then QR algorithms.

Bringing MPS into a canonical form is helpful, since it allows expressing the Schmidt decomposition only in terms of the orthogonality center without referencing other MPS kernels. Decomposing the orthogonality center using the singular value decomposition (SVD) yields

$$M_{j_k,i_k,j_{k+1}} = \sum_{m=1}^{\chi_k} \Sigma_m U_{j_k,i_k,m} V^\dagger_{m,j_{k+1}} \tag{1.42}$$

where U fulfills the left-isometry condition in Eq. (1.37) and $V^\dagger$ fulfills the right isometry condition. By inserting this decomposition into the formula for the mixed canonical form Eq. (1.41), we can see that the sum over the bond k actually corresponds to computing the Schmidt decomposition! This means, we can truncate the lowest Schmidt values by only performing local SVD.

The formulation of the full truncation procedure is the following: Start by bringing the MPS in left canonical form using repeated QR decomposition as described above. Perform a singular value decomposition on the orthogonality center and truncated to the desired bond dimension. Use the SVD result to shift the orthogonality center by one site and repeat until reaching the end of the MPS. Typically truncation is relatively weak; in this case the different local truncation steps approximately commute and the entire procedure becomes close to globally optimal. However, it requires L expensive SVD operations. For this reason, alternative compression schemes based on the variational method[76] or QR decomposition[84] are used.

Not all states in the Hilbert space can be efficiently represented as MPS. To have a representation with few parameters it is required that the Schmidt values of each bipartition decay fast. The entanglement entropy between bipartition can be used to estimate how fast the Schmidt values decay. If entanglement entropy is low, Schmidt

values decay fast, which in turn means that such states can be closely approximated by MPS of low bond dimension. Since ground states of gapped Hamiltonian have area law entanglement entropy[34], this means that MPS are in one dimension an effective tool to study equilibrium physics. However, in chaotic and integrable quantum systems, entanglement entropy scales linear with evolution time after quantum quenches[69–71]. This makes treating out-of-equilibrium problems challenging.

Even though time evolved states generically have entanglement entropy linear in evolution time, we can formulate algorithms to compute their MPS representation. High entanglement entropy will eventually limit the reachable time scales. One straight forward way is to utilize a trotter decomposition of the time evolution operator. This allows us to approximate the time evolution operator as matrix product operator with low bond dimension. Repeatedly applying this operator and compressing the result yields a time evolution algorithm which is called *Time evolving block decimation* (TEBD) [85, 86]. For continuous time evolution, it is also possible to pose the time evolution problem as a local optimization problem, which is called *Time evolving variational principle* (TDVP) [87]. These algorithms are reviewed in detail in Refs. [88–90].

In recent years a number of ideas have been introduced to mitigate the high temporal entanglement for time evolved states. The recurring idea is to remove correlations which contribute to high entanglement entropy, but are not necessary to compute the time evolution of operators. This can be done by truncation while preserving symmetries[91], which also works for the time evolution of mixed states, called *Density matrix truncation* (DMT) [92, 93]. An alternative approach is to convert entangled degrees of freedom into classical mixture[94] or to manually add dissipation operators which reduce long range entanglement, as in *dissipation assisted operator evolution* (DAOE) [95, 96]

Another approach to the problem of entanglement growth are *transversal* contraction schemes [6, 97–100], which are closely related to the IM approach laid out in this thesis. More details on these approaches can be found in Chap. 3.

2 Influence matrix

2.1 Introduction

Simulating the dynamics of observables in quantum-many body systems is a central challenge in the field of computational quantum physics. For generic quantum system, the conventional approach to this problem is to find an efficient approximation of the wavefunction. While ground states of local Hamiltonians in low dimensions can be parametrized efficiently as matrix product states [34, 78], the complexity of time evolved states increases exponentially with evolution time in thermalizing systems [69–71]. This limits the simulation time of algorithms like time evolving block decimation (TEBD) [85, 86, 101] or the time dependent variational principle (TDVP)[87].

This complexity largely encodes for quantum correlations between distant parts of thermalizing systems. For the computation of local observables, many of these long range correlations are not relevant. Approaches like dissipation assisted operator evolution [95, 96], density matrix truncation [92, 93] or local purification [102, 103], take advantage of this fact by truncating some of those irrelevant correlations and are hence able to improve the simulation times. However, these approaches require insight of the physics in a given quantum system to determine which correlations can safely be discarded.

Here I introduce a generic approach to the problem of local dynamics based on Feynman and Vernon's influence functional [104] and inspired by the theory of open quantum systems as well as transversal folding algorithms [97, 99]. We consider the discrete time evolution of a quantum many-body system and express it as a tensor network. Now, we focus on a subsystem and view the rest of the many-body system as its quantum environment. By contracting all legs associated with bath degrees of freedom of the tensor network we obtain the *Influence Matrix* (IM) of the bath. All of the environment's properties are now encoded in the IM. Analogous to how the knowledge of the density matrix of a quantum state is sufficient to predict the probability distribution of results of all possible quantum measurements, the knowledge of the IM of an environment is sufficient to predict dynamics for arbitrary quantum systems coupled to this environment.

Treating the influence matrix as a "wave function" in the temporal domain we introduce a *Matrix Product State* (MPS) representation of the IM. This step corresponds to replacing a large complicated quantum environment by a smaller environment where the size is given by the MPS bond dimension, effectively truncating degrees of freedom irrelevant for local time evolution. The compression of the environment can be performed automatically and independently of further analytical insight, using conventional singular value decomposition. To quantify for which quantum environments such an efficient IM representation exists, the concept of *Temporal Entanglement* (TE) is introduced. Physically, TE can be interpreted as the amount of "quantum memory" of the bath has.

Low TE indicates the existence of an efficient MPS representation of the IM. In later chapters of this thesis, several classes of quantum systems where TE is low are explored, such as near dual-unitary circuits in Chap. 4, many-body localized systems in Chap. 5, or free fermion systems in Chap.6. Besides being an effective numerical tool, the IM approach can also serve as a starting point for analytical studies. Treating parts of a homogeneous quantum system as environment for the remaining subsystem connects dynamical properties of the quantum system to properties of the IM.

This chapter is structured as follows. First we define the IM in terms of the discrete time evolution of a quantum system coupled to an environment. In the next section, we discuss how the IM can be represented as MPS and introduce the TE, which determines whether this representation is efficient. We then discuss how we can compute the time evolution of observables as well as the time evolution of the local density matrix using the MPS representation. Finally we connect this discussion to the Keldysh path integral and the influence functional introduced by Feynman and Vernon.

2.2 Influence matrix

In this section, I derive the IM as a representation of a quantum environment by considering the time evolution of a quantum system coupled to it.

For the purposes of this thesis, a *quantum environment* can be any part of a larger quantum system. The targeted local observables can not have support within the environment. While this discussion can be extended to more general initial states, here we will focus on quenches from a decoupled environment. Beyond these points, there are no restriction on the dynamics or structure of a quantum environment. This is in contrast to the typical treatment of environments in the field of open quantum system, where the Markovianity approximation usually implies that the environment degrees of freedom are faster then the ones of the subsystem coupled to it[105].

We consider the time evolution of a quantum system consisting of the *environment* coupled to a *subsystem*. The Hilbert space of the subsystem is further factorized into the Hilbert space of the *interface* which couples to the environment and the *rest*, which does not. Hence our total Hilbert space $\mathcal{H}$ can be expressed as

$$\mathcal{H} = \mathcal{H}^{\text{env}} \otimes \mathcal{H}^{\text{if}} \otimes \mathcal{H}^{\text{rest}}. \tag{2.1}$$

In the following, the state of the entire quantum system can be mixed and is hence described by a density matrix. The time evolution can be dissipative and is described by quantum channels. For a brief review of the theory of open quantum systems refer to Sec. 1.2.

The state of the quantum system at each point in time will be described by a density matrix $\rho_{\boldsymbol{\alpha}\mu\boldsymbol{\lambda}}(\tau)$ where the vectorized indices correspond to the environment, interface and rest Hilbert space respectively. We consider a quantum quench where the coupling of the subsystem to the environment at time is switched on at $\tau = 0$. The initial state of the environment is chosen to be a product state between environment and subsystem:

$$\rho(0)_{\boldsymbol{\alpha}\mu\boldsymbol{\lambda}} = \rho^E_{\boldsymbol{\alpha}} \rho^S_{\mu\boldsymbol{\lambda}}. \tag{2.2}$$

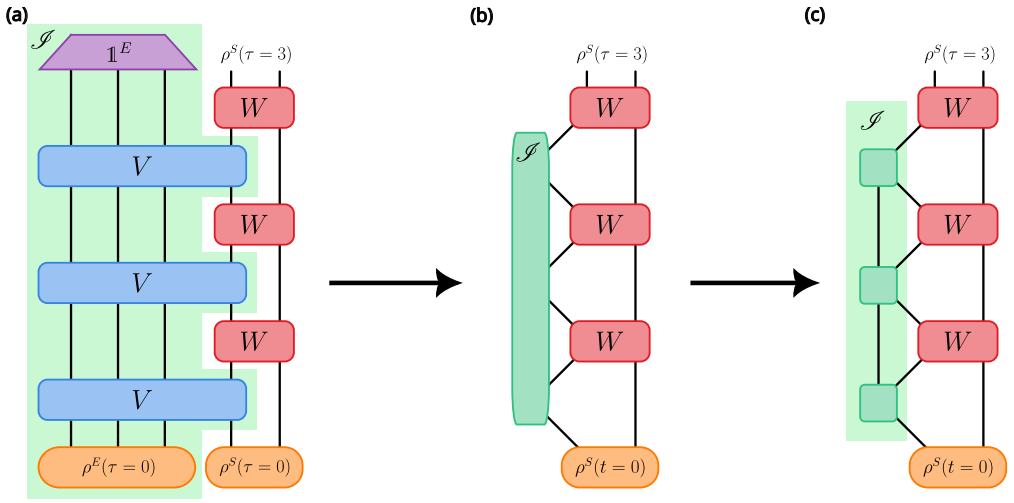

Figure 2.1: The effect of the environment on local time evolution can be captured by the IM. *(a)* Tensor network representing the time evolved reduced density matrix $\rho^S(t=3)$ of a subsystem coupled to a quantum environment. The initial state is a product state between the environment and the subsystem (orange ovals). The time evolution alternates between the channel V acting on the environment and part of the subsystem (blue rounded boxes) and a channel W acting only on the subsystem (red rounded boxes). After the last step, the environment is traced out (purple trapezoid). *(b)* The quantum environment can replaced by the IM tensor (green rounded box) without any regards to its internal structure (green shaded region of (a)). *(c)* This tensor can in turn be parametrized by a MPS.

We consider a discrete time evolution which is split between the time evolution of the environment including the coupling to the subsystem and the time evolution of the subsystem. This is realized by applying a channel $V_{\boldsymbol{\beta}\nu,\boldsymbol{\alpha}\mu}$ acting on the vectorized environment and interface density matrix space on integer time steps and a channel $W_{\nu\boldsymbol{\lambda},\mu\boldsymbol{\kappa}}$ acting on the vectorized subsystem density matrix space on half-integer time steps. The discrete time evolution of the density matrix is given by

$$\begin{aligned}\rho(\tau+\frac{1}{2})_{\boldsymbol{\beta}\nu\boldsymbol{\kappa}} &= V_{\boldsymbol{\beta}\nu,\boldsymbol{\alpha}\mu}\rho(\tau)_{\boldsymbol{\alpha}\mu\boldsymbol{\kappa}}\\ \rho(\tau+1)_{\boldsymbol{\alpha}\nu\boldsymbol{\lambda}} &= W_{\nu\boldsymbol{\lambda},\mu\boldsymbol{\kappa}}\rho(\tau+\frac{1}{2})_{\boldsymbol{\alpha}\mu\boldsymbol{\kappa}}.\end{aligned} \tag{2.3}$$

This structure of time evolution is generic in the sense that any stroboscopic time evolution represented by channels on the entire quantum system can be approximated using such decomposition given sufficient additional time steps. For a concrete example of how such a time discretization can be obtained for a continuous time, Hamiltonian model, refer to chapter 3.

At any time step, the density matrix of the subsystem can be obtained by tracing over the environment:

$$\rho^S_{\mu^T\boldsymbol{\kappa}^T}(\tau) = \mathbb{1}^E_{\boldsymbol{\alpha}^T}\rho_{\boldsymbol{\alpha}^T\mu^T\boldsymbol{\kappa}^T}(\tau). \tag{2.4}$$

To compute the density matrix of the subsystem at time T, we iterate the time evolution Eq. (2.3) and trace out the environment as in Eq. (2.4).

$$\rho^S_{\nu^T\boldsymbol{\lambda}^T}(T) = \mathbb{1}^E_{\boldsymbol{\beta}^T}\left(\prod_{\tau=1}^{T-1} W_{\mu^{\tau+1}\boldsymbol{\kappa}^{\tau+1},\nu^\tau\boldsymbol{\kappa}^\tau}V_{\boldsymbol{\alpha}^{\tau+1}\nu^\tau;\boldsymbol{\alpha}^\tau\mu^\tau}\right)\rho^E_{\boldsymbol{\alpha}^1}\rho^S_{\mu^1\boldsymbol{\kappa}^1} \tag{2.5}$$

This contraction is depicted as a tensor network diagram in Fig. 2.1. We now want to encapsulate the effect of the environment by collecting terms which depend on the environment's internal state, i.e. all terms which possess environment indices $\boldsymbol{\alpha}, \boldsymbol{\beta}$. This leaves us with the following tensor which we call the *Influence Matrix* (IM):

$$\mathscr{I}_{\{\mu^\tau,\nu^\tau\}_{\tau=1}^{T-1}} = \mathbb{1}^E_{\boldsymbol{\alpha}^T}\left(\prod_{\tau=1}^{T} V_{\boldsymbol{\alpha}^{\tau+1}\nu^\tau;\boldsymbol{\alpha}^\tau\mu^\tau}\right)\rho^E_{\boldsymbol{\alpha}^1}. \tag{2.6}$$

The time-evolved density matrix of the subsystem can be expressed in terms of this new tensor (see Fig. 2.1):

$$\rho(T)_{\nu^T\boldsymbol{\lambda}^T} = \mathscr{I}_{\{\mu^\tau,\nu^\tau\}_{\tau=1}^{T}}\left(\prod_{\tau=1}^{T-1} W_{\mu^{\tau+1}\boldsymbol{\kappa}^{\tau+1},\nu^\tau\boldsymbol{\kappa}^\tau}\right)\rho^S_{\mu^1\boldsymbol{\kappa}^1}. \tag{2.7}$$

Note that the time evolution of the subsystem can now entirely be expressed in terms of the subsystem time evolution represented by the channel W and the IM of the environment. The internal structure of the environment given by the environment time evolution channel V and the initial state ρ^E is no longer referenced when computing the

local time evolution of the subsystem. While this implies that it is no longer possible to compute any observable with support inside of the environment Hilbert space, it also means that we can switch out a complicated, large environment with a simpler, smaller environment as long as their IM are the same.

The IM represent the minimal amount of information necessary to fully characterize a quantum environment. It can be seen as a kind of density matrix for quantum environments: A density matrix is sufficient to predict the distribution of measurement outcomes for arbitrary measurements, regardless of how the state is prepared or what its purification is (see 1.2). The IM is sufficient to predict the time evolution of arbitrary subsystems coupled to a quantum environment, regardless of how the environment is internally realized. We can hence view the IM as a tool to classify generic, non-Markovian quantum environments. Indeed, a similar object to the IM called *Process tensor* has been introduced in the field of open quantum systems to generalize channels beyond Markovian environments [43–45].

The legs of the IM can be understood as pairs of *input* and *output* legs where at each time step the state of the interface is acted upon by the environment. The IM has therefore $2T$ legs where each leg corresponds to the vectorized Hilbert space of the interface. The dimensionality of the IM is hence given by

$$\dim[\mathscr{I}] = (\dim(\mathcal{H}^{\mathrm{if}}))^{4T}. \tag{2.8}$$

If we take only a single time step, the space of IM reduces to the space of channels on the interface Hilbert space. Longer IM can be interpreted as a channel between all input legs and all output legs. However, causality implies further constraints on the IM tensor. The channel structure of the IM implies that the IM when viewed as a state on a virtual vectorized Hilbert space formed by the input and output legs is proportional to a density matrix, called the Choi matrix[41, 43, 106] (see Sec. 1.2).

The distinction between environment and subsystem is an arbitrary choice. The only restriction is that the time evolution of the entire quantum system can be efficiently cast in the form of Eq. (2.3). In particular, we can use the IM approach to analyze homogeneous systems by studying how parts of the system acts on other parts. Thermalization in ergodic system can be understood as the quantum system acting as an efficient thermal bath on its subsystem. In localized systems, local environment are not thermal bath. This dynamical property of quantum systems is therefore encoded in the IM of its subsystems. We explore how the IM can be used as an analytical starting point to study thermalization in large quantum systems in Chapters 4 and 5.

It is possible to apply this procedure of splitting of the environment and encapsulating its effect in an IM recursively. For example the bulk of an infinite chain can be seen as a subsystem coupled to two environments, one representing the left semi-infinite chain and one representing the right semi-infinite chain. For details of how observables can be computed in such a setup, see Sec. 2.4 below. It is also possible to consider more complex geometries, where each IM can be used as a building block, representing an entire, potentially infinite, environment. This was explored in the context of a related approach called Time evolving matrix product operator (TEMPO)[107–110].

For specific environment exact expressions for the IM have been found. One such example is dual unitary circuits [111, 112] with infinite temperature initial conditions which is discussed in [1] as well as in Chap. 4 of this Thesis. Furthermore exact solutions have been found for Rule 54 quantum cellular automata [113], and more general initial conditions for certain dual unitary circuits [10, 114].

2.3 Temporal entanglement and MPS representation

In this section, it is explored how the IM tensor defined in Eq. (2.6) can be efficiently parametrized as matrix product state (MPS).

When viewed as a tensor, the dimensionality of the IM given by Eq. (2.8) scales exponentially in the number of time steps T. For numerical methods based on the IM, this puts strong limits on the number of time steps one can reach if the IM is implemented as a full vector. In order to perform numerical computations, it is thus necessary to find an efficient parametrization of this object with fewer parameters. The IM has a temporal structure, where different legs are associated with different times. For thermalizing systems where information is quickly dissipated, we expect little correlation between early and late times. This suggests representing the IM as MPS.

In trotterized Hamiltonian models, the bath changes the subsystem only slightly at each time step, resulting in maximal entanglement between the input and output legs. It is thus efficient to group the corresponding input and output legs on the same MPS kernel. This means that the physical dimension is given by d^4 where $d = \dim(\mathcal{H}^{\mathrm{if}})$ is the interface Hilbert space dimension. Using the definition and conventions in Eq. (1.32) the MPS representation of the IM is given by:

$$\mathscr{I}_{\{\mu^\tau,\nu^\tau\}_{\tau=1}^{T}} = \prod_{\tau=1}^{T} M^{\tau}_{i^\tau,\mu^\tau,\nu^\tau,i^{\tau+1}}\big|_{i^1=i^{T+1}=1}. \tag{2.9}$$

where M^τ are the MPS kernels associated with each time step and i, j correspond to the virtual indices.

Let us compare the MPS representation in Eq. (2.9) with the definition of the IM in Eq. (2.6). We can interpret the MPS kernels as defining the time evolution of a virtual environment with the same IM as the original environment. This interpretation will be used extensively in Sec. 2.4 to efficiently compute observables for quantum systems where environments are described by IM in MPS form. However, the MPS kernels M^τ are in general not channels; their properties depend on the *gauge* of the MPS. However, we can still understand the square root of the bond dimension as an estimate of the size of the Hilbert space such an effective environment would have.

The number of parameters for the MPS parametrization and hence the memory complexity is given by $O(T\chi^2 d^4)$ which scales quadratically with the bond dimension. For this reason it is important to find an approximate MPS representation with a low bond dimension. This can be achieved by truncating the lowest singular value, which is a well-known algorithm for MPS and described in Sec. 1.4. This procedure ensures that for each truncation steps the overlap according to the square norm of the compressed

MPS with the original MPS is maximized while constraining the bond dimension of the compressed MPS. It should be noted that the square norm as measure for distance between IM is not perfect, as it does not represent the difficulty of distinguishing different IMs. However, even the easier problem of finding a good measure of distances between channels is a problem under active research[115, 116].

To compress a MPS efficiently it is important that legs are ordered in a way where strongly entangled legs are close to each other. The ordering implied by Eq. (2.9) is efficient, in particular it turns out to be crucial to use the vectorized Hilbert space for each leg. While this order is intuitive in the derivation laid out in this work, it is not obvious if the IM is derived from Keldysh tensor networks for unitary baths. On the Keldysh contour the vectorized legs is split between the forward and backward contour, see Sec. 2.5 below. However, it was found by works using this approach [97–99] that "folding" the Keldysh contour and effectively using vectorized legs is required for obtaining low bond dimensions. The difference between "folded" and "unfolded" IM entanglement entropy is briefly discussed in Chapter 5. Physically, correlations between equal times on the forward and backward contour that is, within the vectorized space, correspond to dissipation. The compression of unitary baths can therefore be understood as trading a large unitary bath for a small dissipative bath.

The IM-MPS bond dimension χ necessary for a given accuracy is an intrinsic property of the quantum environment. It does not depend on the concrete realization and can be understood as the quantum memory of the environment. This bond dimension also corresponds to the computational complexity of simulating such an environment. Since it is difficult to estimate the minimum bond dimension corresponding to a given accuracy, we introduce the quantity *temporal entanglement* (TE) to measure the complexity of the IM. TE is defined as the maximal bipartite von-Neumann entanglement entropy of the IM as defined in Eq. (2.6) when square normalized like a wavefunction. Formally this means that the TE for a bipartition at timestep τ' can be defined in terms of a temporal reduced density matrix $\mathscr{P}$ as [117]

$$\mathscr{P}^{(\tau)}_{\{\mu^\tau,\nu^\tau\}_{\tau=1}^{\tau'},\{\eta^\tau,\xi^\tau\}_{\tau=1}^{\tau'}} = \frac{1}{\|\mathscr{I}\|^2}\mathscr{I}_{\{\mu^\tau,\nu^\tau\}_{\tau=1}^{T}}\mathscr{I}^*_{\{\eta^\tau,\xi^\tau\}_{\tau=1}^{T}}\prod_{\tau=\tau'}^{T}\delta_{\mu_\tau,\eta_\tau}\delta_{\nu_\tau,\xi_\tau} \tag{2.10}$$

$$S(\tau) = -\mathrm{Tr}(\mathscr{P}^{(\tau)}\log\mathscr{P}^{(\tau)}) \tag{2.11}$$

with the square norm of the influence matrix $\|\mathscr{I}\|^2 = \mathscr{I}_{\{\mu^\tau,\nu^\tau\}_{\tau=1}^{T}}\mathscr{I}^*_{\{\mu^\tau,\nu^\tau\}_{\tau=1}^{T}}$. For product states which correspond to Markovian baths, TE is zero. If TE is high, the expectation is that a high bond dimension χ is necessary to approximate the IM well. Since the IM is proportional to a density matrix, TE can be seen as an *operator space entanglement entropy* [118]. While such entropies are widely used to estimate the complexity of density matrices, they do not correspond to bounds on the bond dimension like the conventional entanglement entropy of wave function. For TE, in particular the Trotter limit of Hamiltonian dynamics can be dangerous, as TE often vanishes in this limit, even for models which can not be approximated as product states [8]. However, even with this caveat TE remains a useful measure to estimate IM complexity.

In recent years, TE has been extensively studied for different systems. In integrable

systems with [10] and without [5, 6, 119] interaction was shown to scale sublinearly in time. An intuitive argument for the case of free quasi-particles is presented in Chapter 3 and Ref. [6]: The key point is that quasi-particles travelling away from the subsystem can never return and hence can be truncated for the purposes of time evolution, analogous to some dissipation assisted operator evolution schemes[95, 96], except that this is done implicitely and automatically by singular value truncation. Low TE for environments consisiting of free fermions enables the use of the IM approach for quantum impurity problems, which is described in Chapter 6 and Refs. [3, 119]. Another intuitive case where TE is low is if the environment is intrinsically dissipative [8]. Here the dissipation time sets the memory time scale limiting TE. This was utilized to simulate an experiment on a real quantum computer in Ref. [4]. Many-Body localized systems where strong disorder prevents thermalization are another cathegory of environments with low TE. While in this case memory time is long, the bath is effectively a shallow bath of only a few qubits which limits the TE. This is further discussed in Chapter 5 and Ref. [2]. Analytically it was found that TE in generic, chaotic systems scales as a volume law with evolution time [114, 117]. A priori this is surprising since thermalizing systems act dissipatively on local subsystems. For now it is an open question what the multi-time correlation, which contribute to high TE encode. However, in the proximity to dual unitary points[111, 112] for infinite temperature initial states, TE is parametrically low as shown in Chapter 4 as well as Ref. [1]. This allows for relatively long evolution times.

For environments with small Hilbert space dimension $\dim(\mathcal{H}^{env})$, an efficient MPS representations can be obtained via compression from the definition in Eq. (2.6). For large or even infinite environments this is infeasible. Hence algorithms which can compute the MPS form of the IM of such environments are required. In Chapters 3 and 6 two such approaches for one dimensional respectively free fermionic systems are described.

2.4 Compute observables

In this section we discuss how one can compute the full time evolution of the density matrix including for intermediate steps of a subsystem coupled to one or multiple environments described by IMs.

While we can use Eq. (2.7) to compute the reduced density matrix of the subsystem for the final time, we usually also want to compute the reduced density matrix for all intermediate times in order to fully understand the trajectory of the system. Instead we view the MPS kernels of the IM as a kind of time evolution operators on the environment and interface. We have that in typical models, the environment is composed of multiple independent environments. For example if one wants to compute the dynamics of a subsystem in the bulk of a infinite chain, the environment is formed by two effectively independent semi-infinite chains which are only coupled via the subsystem. We can take advantage of this structure by encoding independent environments in separate IMs. Formally this can be done by using the definition Eq. (2.6) recursively.

For concreteness, I formulate here the algorithm for a subsystem coupled to two environments, which I will call left and right environments. Those environments will be

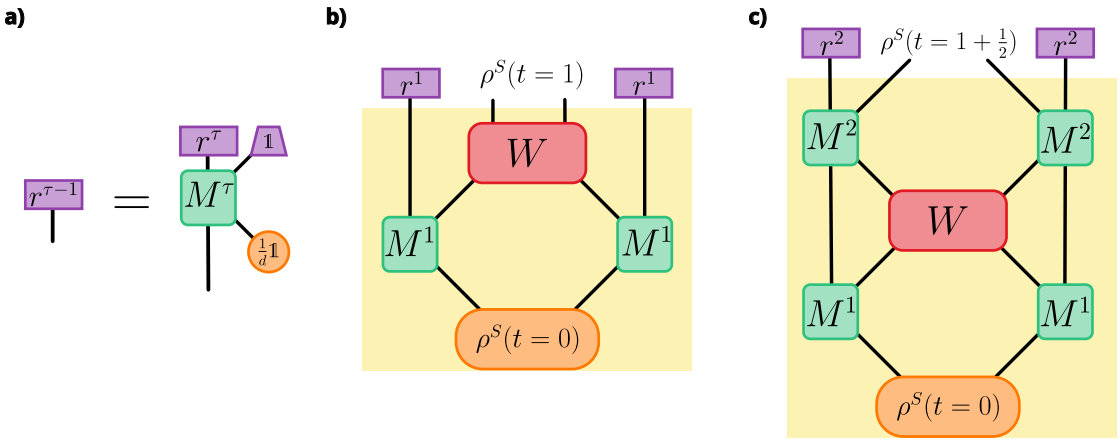

Figure 2.2: Computing the time evolved density matrix $\rho^S(t)$ of a subsystem coupled to two environments described by IMs in MPS form $\{M^\tau\}_{\tau=1}^T$. *(a)* Recursion for the vectors r^τ in virtual MPS space representing the trace over the environment. *(b)* Computation of an integer time step subsystem density matrix $\rho^S(t=1)$ *(c)* Contraction corresponding to the computation of the subsystem density matrix at a half-integer time step $\rho^S(t=1+\frac{1}{2})$

represented by the IM-MPS $\{M^{\tau,(L)}\}_{\tau=1}^T$ and $\{M^{\tau,(R)}\}_{\tau=1}^T$ respectively. We define the *augmented density matrix* (ADM) $\tilde{\rho}_{i,\alpha\boldsymbol{\lambda}\beta,j}$ as a tensor with 5 indices, one index i corresponding to the virtual space of the left IM-MPS, two indices α,β corresponding to the vectorized Hilbert space $\mathcal{H}^{if,(L/R)}$ of the interface between the subsystem and the left/right environment, one index $\boldsymbol{\lambda}$ for the vectorized Hilbert space of the remaining Hilbert space $\mathcal{H}^{rest}$ of the subsystem and one index j corresponding to the virtual space of the right IM-MPS. This tensor will represent the internal state during our algorithm. We compute the time evolution of the ADM as in Fig. 2.2, where the ADM is depicted by the yellow shaded region:

$$\tilde{\rho}_{i,\alpha\boldsymbol{\lambda}\beta,j}(\tau) = W_{\alpha\boldsymbol{\lambda}\beta,\alpha'\boldsymbol{\lambda}'\beta'}\tilde{\rho}_{j,\alpha'\boldsymbol{\lambda}'\beta',k}(\tau-\frac{1}{2}) \tag{2.12}$$

$$\tilde{\rho}_{i,\alpha\boldsymbol{\lambda}\beta,j}(\tau+\frac{1}{2}) = M^{\tau,(L)}_{i',\alpha\alpha',i}\tilde{\rho}_{i',\alpha'\boldsymbol{\lambda}\beta',j'}M^{\tau,(R)}_{j',\beta\beta',j}. \tag{2.13}$$

To compute the reduced density matrix of the subsystem from the ADM, we need to understand what "tracing out the environment" means for the virtual space. At the last step this is not necessary, since the trace over the environment is already included in the definition of the IM (c.f. Eq. (2.6)). For all other time steps τ we can find a vector $r^{L/R,\tau}$ in virtual space which corresponds to computing the trace over the environment.

We can recursively compute the trace vectors $r^{L/R,\tau}$ by contracting the IM-MPS kernels with a possible time evolution, according to Fig. 2.2

$$r^{T,(L/R)} = 1 \tag{2.14}$$

$$r_i^{\tau,(L/R)} = \frac{1}{d^{(L/R)}}r_j^{\tau+1,(L/R)}M^{\tau,(L/R)}_{i,\alpha\beta,j}\mathbb{1}_\alpha\mathbb{1}_\beta. \tag{2.15}$$

where $d^{(L/R)} = \dim(\mathcal{H}_{\text{if}}^{(L/R)}$ is the (unvectorized) Hilbert space dimension of the interface corresponding to the left and right environment respectively. The reduced density matrix of the subsystem can now be computed by contracting the internal ADM with the trace vectors as shown in Fig. 2.2:

$$\rho^S_{\alpha\boldsymbol{\lambda}\beta}(\tau) = r_i^{\tau,L}\tilde{\rho}_{i,\alpha\boldsymbol{\lambda}\beta,j}(\tau)r_j^{\tau,L}, \tag{2.16}$$

$$\rho^S_{\alpha\boldsymbol{\lambda}\beta}(\tau+\frac{1}{2}) = r_i^{\tau+1,L}\tilde{\rho}_{i,\alpha\boldsymbol{\lambda}\beta,j}(\tau)r_j^{\tau+1,L}. \tag{2.17}$$

Let us briefly analyze the time and memory complexity of this algorithm. For computing the time evolution of a subsystem with Hilbert space dimension D coupled to n environments represented by IM-MPS with bond dimension χ, this the ADM requires $\mathcal{O}(\chi^n D^2)$ memory. The IM itself requires $\mathcal{O}(T\chi^2 d^4)$ memory, where d is the dimension of the interface Hilbert space. The time complexity of the contraction algorithm is given by $O(n\chi^\omega d^{2\omega} + D^{2\omega})$ where ω depends on the matrix multiplication algorithm used and is $\omega = 3$ for the "OpenBLAS" implementation [120, 121] used for the numerics in this thesis. However, the time complexity is less useful then it appears, since matrix multiplication can be parallelized efficiently and accelerated by using GPUs or TPUs. Hence the question of whether the ADM fits into the memory of those devices is often the relevant question when assessing the computational limits.

2.5 Keldysh path integral

We discuss how to connect the IM to Feynman and Vernon's Influence functional [104] which arises from the Keldysh path integral.

Before introducing the path integral formalism, it is necessary to specify the structure of the Hilbert spaces $\mathcal{H}^{\text{env}}, \mathcal{H}^{\text{if}}$ and $\mathcal{H}^{\text{rest}}$. For the purposes of this section, we will assume that these Hilbert spaces are bosonic or fermionic Fock spaces generated by the vectors of raising operators denoted by $\mathbf{a}^\dagger, b^\dagger$ and $\mathbf{c}^\dagger$ respectively. We introduce the coherent states on these Fock spaces as

$$\begin{aligned}
|\boldsymbol{\psi}\rangle &= \int e^{i\boldsymbol{\psi}\mathbf{a}^\dagger}\mathrm{d}\boldsymbol{\psi}|0\rangle_{\text{env}}, \\
|\eta\rangle &= \int e^{i\eta b^\dagger}\mathrm{d}\eta|0\rangle_{\text{if}}, \\
|\boldsymbol{\varphi}\rangle &= \int e^{i\boldsymbol{\varphi}c^\dagger}\mathrm{d}\boldsymbol{\varphi}|0\rangle_{\text{rest}}.
\end{aligned} \tag{2.18}$$

where $|0\rangle$ are the vacuum states and $\boldsymbol{\psi}, \eta, \boldsymbol{\varphi}$ are vectors of normal or Grassmann variables, depending on whether the respective Hilbert spaces are bosonic or fermionic. We find the *resolutions of identity* on the environment Hilbert space in terms of coherent states:

$$\mathbb{1}_{\text{env}} = \int \mathrm{d}\boldsymbol{\psi}\mathrm{d}\overline{\boldsymbol{\psi}}e^{-\boldsymbol{\psi}\overline{\boldsymbol{\psi}}}|\boldsymbol{\psi}\rangle\langle\boldsymbol{\psi}|, \tag{2.19}$$

and analogous for the other two Hilbert spaces.

With these tools, we can now define the Keldysh path integral based on the time evolution of the density matrix in Eq. (2.3). Let us consider a system where the underlying dynamics is *Hamiltonian*. The time evolution of the form in Eq. (2.3) can then be defined by the operators

$$V \approx (\mathbb{1} + i\delta t H^{\mathrm{ec}}) \otimes (\mathbb{1} - i\delta t H^{\mathrm{ec}}) \tag{2.20}$$
$$W \approx (\mathbb{1} + i\delta t H^{\mathrm{sub}}) \otimes (\mathbb{1} - i\delta t H^{\mathrm{sub}}). \tag{2.21}$$

where $\delta t \to 0$ is a small time step, $H^{\mathrm{ec}} = H^{\mathrm{env}} + H^{\mathrm{coup}}$ the sum of the environment and coupling Hamiltonian and H^{sub} the Hamiltonian for the subsystem. We can express the Keldysh partition function, which is really just the trace over the final density matrix as:

$$\begin{aligned} Z[0] &= \mathrm{Tr}\left[\rho(T)\right] = 1 \\ Z[0] &= \mathrm{Tr}\left[((\mathbb{1} + i\delta t H^{\mathrm{ec}})(\mathbb{1} + i\delta t H^{\mathrm{sub}}))^T \rho(0) ((\mathbb{1} - i\delta t H^{\mathrm{ec}})(\mathbb{1} - i\delta t H^{\mathrm{sub}}))^T\right] \end{aligned} \tag{2.22}$$

Using the cyclicity of the trace, this can be seen as a time evolution along a closed loop in time. Up to time t_{max} we evolve *forward* in time, afterwards the direction of time is changed and we evolve *backwards* in time. This defines the *Keldysh contour*.

We now write this expression as a *Keldysh path integral* by inserting the resolutions of identity Eq.(2.19) between each time steps and taking the continuoum limit $\delta t \to 0$. We obtain:

$$\begin{aligned} Z[0] &= \int \mathcal{D}\boldsymbol{\psi}\mathcal{D}\overline{\boldsymbol{\psi}}\mathcal{D}\eta\mathcal{D}\overline{\eta}\mathcal{D}\boldsymbol{\varphi}\mathcal{D}\overline{\boldsymbol{\varphi}} e^{-S[\boldsymbol{\psi},\overline{\boldsymbol{\psi}},\eta,\overline{\eta},\boldsymbol{\varphi},\overline{\boldsymbol{\varphi}}]} \\ S[\boldsymbol{\psi},\overline{\boldsymbol{\psi}},\eta,\overline{\eta},\boldsymbol{\varphi},\overline{\boldsymbol{\varphi}}] &= \int_C \mathrm{d}t \overline{\boldsymbol{\psi}}\partial_t\boldsymbol{\psi} + \overline{\eta}\partial_t\eta + \overline{\boldsymbol{\varphi}}\partial_t\boldsymbol{\varphi} + i\sigma(t)H^{\mathrm{ec}}(\boldsymbol{\psi},\overline{\boldsymbol{\psi}},\eta,\overline{\eta}) + i\sigma(t)H^{\mathrm{sub}}(\boldsymbol{\varphi},\overline{\boldsymbol{\varphi}},\eta,\overline{\eta}) \end{aligned} \tag{2.23}$$

where $H^{\mathrm{ec}}(\boldsymbol{\psi},\overline{\boldsymbol{\psi}},\eta,\overline{\eta})$ and $H^{\mathrm{sub}}(\boldsymbol{\varphi},\overline{\boldsymbol{\varphi}},\eta,\overline{\eta})$ are the coherent state Hamiltonian matrix elements corresponding the environment with coupling and the subsystem respectively. They are defined as:

$$\begin{aligned} H^{\mathrm{ec}}(\boldsymbol{\psi},\overline{\boldsymbol{\psi}},\eta,\overline{\eta}) &= \langle\boldsymbol{\psi}|\langle\eta|H^{\mathrm{ec}}|\eta\rangle|\boldsymbol{\psi}\rangle \\ H^{\mathrm{sub}}(\boldsymbol{\varphi},\overline{\boldsymbol{\varphi}},\eta,\overline{\eta}) &= \langle\boldsymbol{\varphi}|\langle\eta|H^{\mathrm{sub}}|\eta\rangle|\boldsymbol{\varphi}\rangle \end{aligned} \tag{2.24}$$

The integrals $\int_C$ run along the Keldysh contour, which corresponds to the forward integral from 0 to t_{max} and the backward integral from t_{max} to 0. To distinguish these Keldysh branches we use $\sigma(t) = +1$ on the forward contour and $\sigma(t) = -1$ for the backward contour.

Separating the environment terms from the terms corresponding to the subsystem in Eq. (2.23) and we obtain a version of Feynman and Vernon's celebrated influence functional[104, 122]:

$$I[\eta,\overline{\eta}] = \int \mathcal{D}\boldsymbol{\psi}\mathcal{D}\overline{\boldsymbol{\psi}} e^{-\int_C \mathrm{d}t \overline{\boldsymbol{\psi}}\partial_t\boldsymbol{\psi} + i\sigma(t)H^{\mathrm{ec}}(\boldsymbol{\psi},\overline{\boldsymbol{\psi}},\eta,\overline{\eta})} \tag{2.25}$$

The Keldysh path-integral can be recovered analagous to Eq. (2.7)

$$Z[0] = \int \mathcal{D}\boldsymbol{\varphi}\mathcal{D}\overline{\boldsymbol{\varphi}}\mathcal{D}\eta\mathcal{D}\overline{\eta} I[\eta,\overline{\eta}] e^{-\int_C \mathrm{d}t \boldsymbol{\psi}\partial_t\boldsymbol{\psi} + i\sigma(t)H^{\mathrm{sub}}(\boldsymbol{\varphi},\overline{\boldsymbol{\varphi}},\eta,\overline{\eta})} \tag{2.26}$$

Note that the effective action of the subsystem does not contain any environment terms anymore. The Influence functional formalism was used to study harmonic oscillators[122] or particle reservoirs [123, 124].

Using the definition Eq. (2.18) we can explicitely write the influence matrix in terms of coherent states.

$$\mathscr{I} = \int \mathcal{D}\eta\mathcal{D}\overline{\eta} I[\eta,\overline{\eta}] |\eta\rangle\langle\eta| \tag{2.27}$$

where the bra corresponds to the "input" legs and the ket correspond to the output leg. The IM can hence be understood as a discrete version of the Feynman vernon infuence functional[3, 107, 109, 119] . For more details and concrete examples on how path-integral expressions can be used in the context of the IM formalism, refer to Chapters 4 and 6.

2.6 Acknowledgements

This chapter is based in parts on the articles [1] and [8] which were written in collaboration with Alessio Lerose and Dmitry Abanin.

3 Influence Matrix in 1+1 dimensions

3.1 Computing the Influence Matrix

In the previous chapter, I established how the effect of a quantum environment on the dynamics of any quantum system coupled to it can be parametrized in the form of an *influence matrix* (IM). For certain quantum environments, specifically those with low *temporal entanglement* (TE), the influence matrix can be closely approximated by a *matrix product state* (MPS) with low bond dimension. However, Finding such a low bond dimension MPS representation of the IM for large quantum environments, is a separate challenge.

In this chapter, I consider one-dimensional environments in the form of chains. Each component of these environments is a quantum system with a small local Hilbert space; for example a quantum spin or a qubit, which can only interact with its two nearest neighbours. Due to the light-cone effect [125, 126] in quantum chains, the limit of an IM corresponding to a semi-infinite chain with a fixed maximal evolution time is well defined. The focus of this chapter will be on computing this *thermodynamic* IM. The key idea is that the last component of a chain is itself a quantum system which is coupled to the environment with the last component removed. Formalizing this idea leads to a recursion relation which relates the IM of the environment with n components, to the IM of the environment with $n-1$ components. In the case of a spatially homogeneous environment, this recursion relation is also a self-consistency equation for the thermodynamic IM.

Contracting the tensor network corresponding to the time evolution of a quantum chain in the transversal direction [97–99] can be understood as recursively computing the thermodynamic IM. We observe that during this *transverse contraction algorithm* (TCA), intermediate IMs, which correspond to finite chains, generically have volume law TE. This holds even if the final, thermodynamic IM has low TE. We call this phenomenon, which limits the efficiency of the TCA, the *temporal entanglement barrier* (TEB). Utilizing the entanglement entropy formula by Calabrese and Cardy [69] the origin of the TEB in integrable models can be traced back to the reflection of quasi-particles. Those quasi-particles are reflected at the spatial boundary of finite chains. This explains the dependence of the TEB on the spatial boundary conditions, as well as the volume law nature and shape of the TEB. Numerical computation support the assumption that this idea generalizes beyond integrable models Armed with this insight, we formulate the Light-cone growth algorithm (LCGA) [6, 100], where the maximal evolution time is increased with the environment size along the light-cone. This ensures that the intermediate IMs in this algorithm are also thermodynamic IMs, only with a shorter maximal evolution time then the final IM. In the translation invariant case, TE is monotonously increasing with maximal evolution time for thermodynamic IMs. Hence

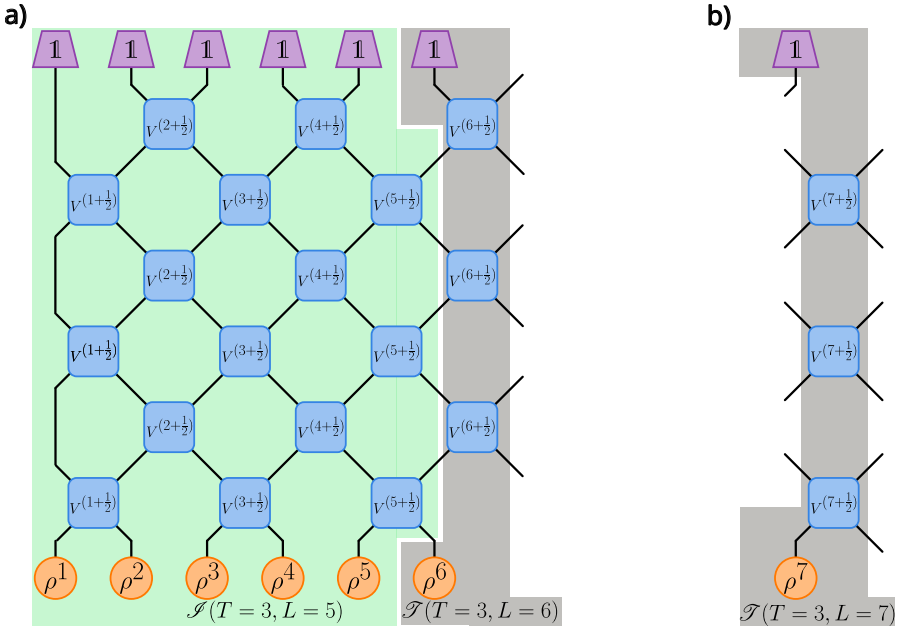

Figure 3.1: *(a)* Tensor network diagram of the IM $\mathscr{I}(T=3,L=6)$ corresponding to a one dimensional brickwork circuit as defined in Eq. (3.9). The two component channels V are depicted by blue rounded rectangles, the initial density matrices by orange circles and the final trace operation by purple trapezoids. The IM $\mathscr{I}(T=3,L=6)$ can be obtained recursively using Eq. (3.12) by applying the (even layer) dual transfer matrix $\mathscr{T}(T=3,L=6)$, which is defined in Eq. (3.10) and is shaded in grey, to the IM of the shorter chain $\mathscr{I}(T=3,L=5)$ which is shaded in green. *(b)* Depiction of an odd layer transfer matrix $\mathscr{T}(T=3,L=7)$ corresponding to Eq. (3.11).

for translationally invariant one dimensional environments with low TE, LCGA is an efficient algorithm to compute local dynamics.

This chapter is structured as follows: In the first section we introduce brickwork circuits and the TCA. In the next section we establish the TEB in this algorithm and discuss its origin using the quasi-particle picture. Then we formulate the LCGA and show that it avoids the TEB. Finally, we demonstrate that the LCGA approach is competitive with other state of the art methods.

3.2 Transversal contraction of semi-infinite chains

In this section, we introduce the transverse contraction algorithm (TCA) which computes the IM of a semi-infinite chain by iteratively computing the IM with fixed maximal evolution time of chains with increasing length.

One dimensional systems with local interaction have a finite speed of information propagation v_g which is called the Lieb-Robinson velocity[125, 126]. Correlations outside

of the light-cone are exponentially suppressed, i.e.

$$|\langle O(t=0,x=x')O(x=0,t=t')\rangle| < c_2 e^{-c_1(x'-v_g t')}, \tag{3.1}$$

where c_1, c_2 are some numerical constants. In particular this also means that the effects of initial conditions and dynamics on the local evolution outside of the light-cone are exponentially suppressed. Since IM have a finite maximal evolution time $t_{\max}$, up to which it can be used to compute local observables, IMs $\mathscr{I}(t_{\max}, L)$ of a large finite environment of length $L \gg v_g t_{\max}$ converge exponentially to the thermodynamic IM $\mathscr{I}(t_{\max}, \infty)$,

$$\mathscr{I}(t_{\max}, L \gg v_g t_{\max}) = \mathscr{I}(t_{\max}, \infty) + O(e^{-c_1 L)}). \tag{3.2}$$

This allows us to obtain the thermodynamic IM by considering the limit of a sequence of IM corresponding to chains of increasing length L and constant maximal evolution time $t_{\max}$.

We consider a chain of $L+1$ components with nearest neighbour interactions, where the first L components form the environment acting on the subsystem consisting only of the last component. To compute the IM corresponding to the environment of the first L components, we start with a Hamiltonian for the entire chain with $L+1$ components. This Hamiltonian can be expressed as sum of nearest neighbour terms $H(n+\frac{1}{2})$ which are only supported on the n-th and $n+1$-th component,

$$H = \sum_{n=1}^{L} H\left(n+\frac{1}{2}\right). \tag{3.3}$$

Next, we discretize time into equal steps of length δt and find the time evolution operator U as well as the time evolution channel V over one time interval as

$$U = e^{iH\delta t} \quad V = U \otimes U^\dagger. \tag{3.4}$$

To make the following expressions more transparent, we assign vectorized indices α_n to the vectorized degree of freedom of component n. The channel V will hence be defined by its components $V_{\{\beta_n\}_{n=1}^{L+1};\{\alpha_n\}_{n=1}^{L+1}}$. With this time evolution channel, the initial density matrix of the environment $\rho^E_{\{\alpha_n^1\}_{n=1}^L}$ and the trace operation at the final time step T on the environment $\mathbb{1}^E_{\{\beta_n^T\}_{n=1}^L}$, we can now find formally the IM by employing Eq. (2.6) and relabelling the index of the last component as it forms the subsystem $\alpha_{L+1}^\tau = \mu^\tau; \beta_{L+1}^\tau = \nu^\tau$:

$$\mathscr{I}_{\{\mu^\tau,\nu^\tau\}_{\tau=1}^T}(T,L) = \mathbb{1}^E_{\{\beta_n^T\}_{n=1}^L}\left(\prod_{\tau=1}^{T-1} V_{\{b_n^\tau\}_{n=1}^L \mu^\tau;\{\alpha_n^{\tau+1}\}_{n=1}^L \nu^{\tau+1}}\right)\rho^E_{\{\alpha_n^1\}_{n=1}^L} \tag{3.5}$$

In practice it is infeasible to evaluate this expression directly since the Hilbert space dimension of the environment grows exponentially in L. This is especially problematic since we are interested in the large $L \to \infty$ limit. Instead we will compute the IM corresponding to length L recursively from the IM corresponding to length $L-1$.

To set up such a recursion relation, we separate the interaction term of the last component of the environment with the subsystem, i.e. the L-th component with the $L+1$-th component of the chain. We can achieve this by approximating the time evolution channel V using the first order Suzuki-Trotter decomposition:

$$V_{\{\beta_n\}_{n=1}^{L+1};\{\alpha_n\}_{n=1}^{L+1}} = \left(\prod_{n=1}^{L/2} V^{(2n+\frac{1}{2})}_{\beta_{2n}\beta_{2n+1};\alpha_{2n}\alpha_{2n+1}}\right)\left(\prod_{n=1}^{L/2-1} V^{(2n+\frac{3}{2})}_{\beta_{2n+1}\beta_{2n+2};\alpha_{2n+1}\alpha_{2n+2}}\right) + O(\delta t^2) \tag{3.6}$$

$$V^{(n+\frac{1}{2})} = e^{i\delta t H(n+\frac{1}{2})} \otimes e^{-i\delta t H(n+\frac{1}{2})}. \tag{3.7}$$

This gives us a quantum circuit representation consisting of two component gates of the many-body channel V. We call a circuit with this structure a *brickwork* circuit. It is important to note that we could also start from a circuit with this structure, i.e. a environment where the time evolution is given by channels of the structure described in Eq. (3.6). In the following we will not require that the channels are unitary, close to identity or that they are constant in time. This allows us for example to treat Floquet systems within the same framework, use a second order Suzuki-Trotter decomposition or describe intrinsically dissipative systems. To reflect this, we will refer from now on primarily to the number of timesteps denoted by the Greek letter τ instead of the physical time $t = \tau\delta t$ of the underlying Hamiltonian. Capital T refers to the total number of time steps corresponding to the maximal evolution time $t_{\max} = T\delta t$.

We assume that the initial density matrix of the environment, ρ^E is a product state, i.e.:

$$\rho^E_{\{\alpha_n\}_{n=1}^{L}} = \prod_{n=1}^{L} \rho^n_{\alpha_n}. \tag{3.8}$$

While this derivation can be generalized to entangled initial state, the details of how to achieve this are out of the scope of this chapter. One possibility is adding additional brickwork time evolution steps which evolve the entangled initial state from a product initial state. Another possibility is, to take the density matrix of the entangled initial state in MPO form and add an extra leg to the IM corresponding to the virtual bond of this MPO.

Even if the underlying Hamiltonian was translationally invariant, the brickwork circuit in Eq. (3.6) breaks the translational symmetry by distinguishing even and odd sites. Of course, in the Suzuki-Trotter limit $\delta t \to 0$, any translational symmetry of the Hamiltonian model is restored. For concreteness, we will assume in the following two equations that L is even, the formulas for odd values of L are analogous.

We now substitute the brickwork representation of V, as well as the factorized initial state ρ^E into the expression for the IM Eq. (3.5).

$$\mathscr{I}_{\{\mu^\tau,\nu^\tau\}_{\tau=1}^{T}}(T,2N) = \prod_{n=1}^{N} \mathbb{1}_{\beta^T_{2n-1}} \mathbb{1}_{\beta^T_{2n}} \left(\prod_{\tau=1}^{T-1} (V^{(2n-\frac{1}{2})}_{\beta_{2n-1}\beta_{2n};\alpha_{2n-1}\alpha_{2n}} V^{(2n+\frac{1}{2})}_{\beta_{2n}\beta_{2n+1};\alpha_{2n}\alpha_{2n+1}}\right) \rho^{2n-1}_{\alpha^1_{2n-1}} \rho^{2n}_{\alpha^1_{2n}} \tag{3.9}$$

This equation represents the IM as a tensor network contraction, which is graphically depicted in Fig. 3.1. We find that a subset of this tensor network contracts to the IM $\mathscr{I}(T, L-1)$ of the environment consisting of the first $L-1$ components acting on the L-th component (green shaded region in Fig. 3.1). The rest of the tensor network (grey shaded area in Fig. 3.1) can be understood as a *dual transfer matrix* $\mathscr{T}(T, L)$ acting on the space of IMs, which maps the IM $\mathscr{I}(T, L-1)$ to the IM $\mathscr{I}(T, L)$. This defines an "evolution" in the space dimension instead of the conventional time evolution. Its component are defined by

$$\mathscr{T}_{\{\mu^\tau,\nu^\tau\}_{\tau=1}^T,\{\kappa^\tau,\lambda^\tau\}_{\tau=1}^T}(T, 2N) = \mathbb{1}_{\kappa^{T+1}} \left(\prod_{\tau=1}^{T} V_{\kappa^{\tau+1}\nu^\tau;\lambda^\tau\mu^\tau} \right) \rho^L_{\kappa^1} \tag{3.10}$$

for even L (grey shaded region in Fig. 3.1(a)) and

$$\mathscr{T}_{\{\mu^\tau,\nu^\tau\}_{\tau=1}^T,\{\kappa^\tau,\lambda^\tau\}_{\tau=1}^T}(T, 2N+1) = \mathbb{1}_{\lambda^T} \left(\prod_{\tau=1}^{T} V_{\kappa^\tau\nu^\tau;\lambda^{\tau-1}\mu^\tau} \right) \rho^L_{\lambda^0} \tag{3.11}$$

for L odd (depicted in Fig. 3.1(b)). This leads us to a recursion relation for the IM

$$\mathscr{I}_{\{\mu^\tau,\nu^\tau\}_{\tau=1}^T}(T, L) = \mathscr{T}_{\{\mu^\tau,\nu^\tau\}_{\tau=1}^T,\{\kappa^\tau,\lambda^\tau\}_{\tau=1}^T}(T, L)\mathscr{I}_{\{\kappa^\tau,\lambda^\tau\}_{\tau=1}^T}(T, L-1). \tag{3.12}$$

using the boundary IM as initial condition. For example, open boundary conditions are encoded by the IM

$$\mathscr{I}^{OBC}_{\{\mu^\tau,\nu^\tau\}_{\tau=1}^T}(T, 0) = \prod_{\tau=1}^{T} \delta_{\mu^\tau,\nu^\tau} \tag{3.13}$$

whereas perfect dephaser boundary conditions which correspond to boundary conditions where a perfectly dephasing channel (see Sec. 1.2) is applied to the boundary at each step, are encoded by the IM

$$\mathscr{I}^{PD}_{\{\mu^\tau,\nu^\tau\}_{\tau=1}^T}(T, 0) = \prod_{\tau=1}^{T} \delta_{\mu^\tau,\nu^\tau}\mathbb{1}_{\mu^\tau}. \tag{3.14}$$

Based on this recursion relation the *transverse contraction algorithm* (TCA) [1, 8, 108] to compute the MPS representation of the IM for one dimensional systems can be formulated similar to conventional TEBD (see Sec.1.4): Start with expressing the boundary IM defined by Eq. (3.13) as a product state. Use Eq. (3.12) by applying the transfer matrix $\mathscr{T}$ is given by Eqs. (3.10),(3.11) as matrix product operator to the MPS representation of the IM. Since this step will increase the bond dimension of the MPS representation of the IM by a factor of 4, this MPS is truncated using singular value decomposition. After repeating these steps L times increasing the length of the environment each time, a MPS representation of $\mathscr{I}(T, L)$ is obtained. Computing the IM using this algorithm is closely related to the approach described in Refs. [97–99].

Circuits with brickwork structure Eq. (3.9) have a strict light-cone with a speed of information given by $v_L = 2$ in units of time steps. All correlations outside of the light-cone vanish exactly:

$$|\langle O(T=0, x=x')O(x=0, T=T')\rangle| = 0 \text{ for } \frac{x'}{T'} > v_L = 2. \tag{3.15}$$

This means that for exact contraction of Eq (3.12) for IM $L > 2t$ the choice of boundary condition does not matter. However, in practice the intermediate IMs have to be truncated which makes this statement no longer true. This will be discussed in more detail below. The strict light-cone property is additional to the Lieb-Robinson light-cone for Hamiltonian systems. In the Trotter limit $\delta t \to 0$, the brickwork light speed in physical time units goes to infinity, making it consistent with the exponential Lieb-Robinson light-cone.

Let us now focus on translational invariant systems,

$$\mathscr{T}(T, 2N) = \mathscr{T}(T, \text{even}) \qquad \mathscr{T}(T, 2N+1) = \mathscr{T}(T, \text{odd}). \tag{3.16}$$

where we can now define the even and odd thermodynamic IM for the semi-infinite chain

$$\mathscr{I}(T, L = 2N > 2T) = \mathscr{I}(T, \infty, \text{even}) \text{and} \mathscr{I}(T, L = 2N+1 > 2T) = \mathscr{I}(T, \infty, \text{odd}). \tag{3.17}$$

These thermodynamic IM can be obtained by using the algorithm above and stopping after $L > 2T$. By applying the recursion relation Eq. (3.12) twice, the thermodynamic IM can be found as the unique solution to a self-consistency equation,

$$\mathscr{I}(T, \infty, \text{even}) = \mathscr{T}(T, \text{even})\mathscr{T}(T, \text{odd})\mathscr{I}(T, \infty, \text{even}). \tag{3.18}$$

This can be seen as the eigenvalue equation for the doubled transfer matrix

$$\mathscr{T}^2(T) = \mathscr{T}(T, \text{even})\mathscr{T}(T, \text{odd}). \tag{3.19}$$

The light-cone property implies that this matrix has a pseudo projection property with a unique eigenvector to eigenvalue one. Finite size IM are encoded in the nil-potent part. In principle one could directly find the IM by solving Eq. (3.18) directly, for example by using the DMRG algorithm [2]. However, the non-Hermitian nature of this eigenvalue problem makes this approach often more difficult in practice. The TCA can be understood as a power method approach of computing this eigenvector.

3.3 Temporal Entanglement Barrier

In this section we study the TE of intermediate IM of the transversal contraction algorithm and find that it can be volume-law even if the thermodynamic IM has area law TE. Using a semi-classical quasi-particle picture, we elucidate the physical origin of this temporal entanglement barrier.

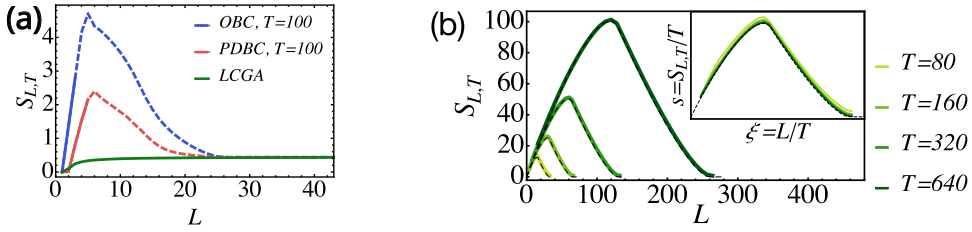

Figure 3.2: *(a)* TE of finite chains computed with TCA vs length for the non-integrable KIC defined by Eq. (3.20) with parameters $J = 0.31, g = 0.638, h = 0.2$ and Open Boundary conditions (OBC, Eq. (3.13)) as well as Perfect dephaser boundary conditions (PDBC, Eq. (3.14)). For comparison the thermodynamic IM of different maximal evolution time T which form the intermediate states of the LCGA. *(b)* TE of finite chains for the integrable KIC with parameters $J = 0.6\pi/4, g = \pi/4, h = 0$ computed as described in Ref. [5]. The TEB scales according to a volume law with evolution time and its maximum is at $L/T = v_L/4$. Inset: The rescaled entanglement entropy computed directly (green) matches the results from the semi-classical formula (dashed) in Eq. (3.21) using the empirically found $\omega = 0.93\log(2) = \text{const.}$. Figure adapted from Ref. [6].

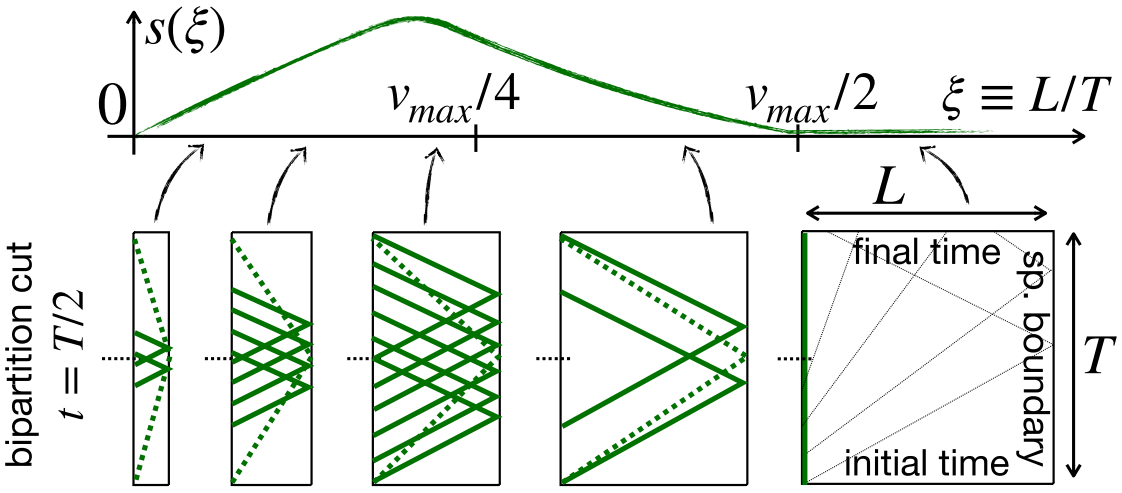

Figure 3.3: The TEB can be explained by quasi particle reflection at the spatial boundary. The bottom panels show possible trajectories of the slowest (dashed) and fastest (solid) quasi-particles for environments of different lengths which contribute to TE. Figure adapted from Ref. [6].

By combining the TCA described above with the computation of observables described in Section 2.4, we have a complete algorithm to compute local observables of quantum systems coupled to one-dimensional chains. The accuracy of this approach is controlled by the *maximal bond dimension* we can use during the iteration and for the final IM. For fixed accuracy, the bond dimension for the final IM depends only on the physics of the environment and can be estimated using the scaling of TE. In particular, it does not depend on the algorithm used to compute the final IM. However, the intermediate IMs encountered during the TCA iterations are truncated as well. Hence the performance of the TCA also depends on the TE of those intermediate IMs.

To understand the TE of intermediate IMs, we consider the kicked Ising chain (KIC) defined by the discrete unitary time evolution operator U acting on a chain of qubits

$$U = e^{iJ\sum_{j=1}^{\infty} Z_j Z_{j+1} + ih\sum_{j=1} Z_j} e^{ig\sum_{j=1}^{\infty} X_j} \tag{3.20}$$

where Z_j, X_j are Pauli operators acting on the j-th qubit. This is non-integrable for generic J, g, h, but can be solved in terms of non-interacting Majorana quasi particles for $h = 0$. For the non-integrable parameters $J = 0.31, g = 0.638, h = 0.2$, the TE of the thermodynamic IM is observed to be low [5]. The TE of finite chains, which correspond to the intermediate states of the TCA, is plotted vs the length of the chain L for this model and different spatial boundary conditions in Fig. 3.2(a). We observe that for both open boundary conditions defined by Eq. (3.13) (blue line) and perfect dephaser boundary conditions defined by Eq. (3.14) (red line), TE increases rapidly with environment size until it cannot be captured anymore due to the finite bond dimension $\chi = 128$. On the other hand, the thermodynamic TE is area law, as depicted by the green line. This phenomenon of highly entangled intermediate IMs, which we call the *temporal entanglement barrier* (TEB), was also observed in Refs. [8, 108]. The TEB can be lowered, by choosing a different boundary condition such as the perfect dephaser boundary condition[8].

Curiously we observe in Fig. 3.2(a) that by continuing iterating despite the drastic truncation, we recover the TE of the thermodynamic IM. This can be explained by the pseudo-projection property of the dual transfer matrix. At every iteration step, the truncation error gets partially projected out, until the full iteration step composed of dual transfer matrix application and truncation is self consistent. However relying on this effect potentially requires a large number of iterations and is hard to control. This makes the TCA a viable option in situations where the light cone growth algorithm discussed below is not applicable such as imaginary times variants of the MPS [9] or tilted versions of the IM[117].

To study the exact shape of the TEB without truncation effects inherent in MPS computations, we defer to the integrable case $h = 0$. For this model it is possible to exactly compute the TE even for highly entangled IM and long times using Grassmann path integral techniques [5]. From the TE for different times in the integrable case in Fig. 3.2 b), we find that the maximum of the TEB at around $L/T = \frac{v_L}{4}$ scales linearly in time, as a *volume-law*. For short times T, the slope is linear in L, and for long times the TE saturates to a constant value independent of evolution time T and environment size L.

To understand the behavior of the temporal entanglement with respect to system size and evolution time, we employ a variation of the picture employed by Calabrese and Cardy in Ref. [69]: Consider the spatial entanglement of a time evolved excited product state in a unitary model with stable quasi-particles. Each site emits highly entangled pairs of quasi-particles which move ballistically. Quasi-particles emitted from different sites are not entangled. We can compute the entanglement across a bipartition in the time evolved state by counting the number of quasi-particle pairs where one partner arrives in one partition and the other partner arrives in the other partition. This idea can be applied directly if the model is *dual-unitary*[111, 112], which means that the spatial "evolution" employed in the TCA is also a unitary evolution. In the dual-unitary case, all quasi-particles move with the light-cone speed $v_L = 2$. We can view the IM $\mathscr{I}(L,T)$ vector as the boundary conditions vector $\mathscr{I}(0,T)$ time evolved under the dual unitary evolution. The open boundary conditions corresponds to maximally entangled pairs of quasi-particles travelling along the light-cone in opposite directions. The temporal boundary corresponding to the trace operation at $\tau = T$ absorbs quasi-particles. In case of infinite temperature initial conditions, this is also true for the temporal boundary at $\tau = 0$. This model is sufficient to qualitatively explain the TEB: For short times, only few quasi-particles are able to cross the bipartition cut, leading to an increase in TE. Eventually all quasi-particles reach a boundary and get absorbed leaving us with zero TE and a product state for the thermodynamic IM. This is indeed the correct result for the thermodynamic IM of a dual-unitary model, as will be discussed in more detail in Chap. 4.

To generalize this idea beyond dual-unitarity and make it more physically transparent, we return to the usual direction of time evolution. The production of quasi particle pairs at the spatial boundary can be understood as *reflection*. The production cross-section in the Calabrese Cardy picture[69] relates to the reflection coefficient. We can estimate the TE over a cut at time step τ_c by computing the density of quasi-particles which can be injected into the environment from the subsystem before time step τ_c, get reflected at the spatial boundary and returns to the subsystem before the final time step T. This idea is visualized in Fig. 3.3 for $\tau_c = T/2$. For very short environments, only few quasi-particles can be reflected in a way that they cross τ_c and contribute to entanglement. The fraction of such quasi-particles increases with the size of the environment, until for environments around $v/4$ the fastest quasi-particles from any point before $T/2$ will return to the subsystem, leading to a maximum in the TE. For longer environments, fewer and fewer particles reach the spatial boundaries and return before the final time $t_{\max}$, until the only remaining contribution to TE stems from edge modes and short time effects leading to area law TE.

We can formalize this variant of the Calabrese Cardy picture into a semi-classical formula for the leading contribution for long maximal evolution time $t_{\max}$ to the TE across a bipartition t_c in continuous time:

$$S(t_{\max}, L, t_c) = \int_0^t \mathrm{d}t_i \int_t^{t_{\max}} \mathrm{d}t_f \int_{\omega_{\min}}^{\omega_{\max}} \frac{\mathrm{d}\omega}{2\pi} w(\omega) \delta\left(t_i - t_f - \frac{2L}{v(\omega)}\right) \tag{3.21}$$

where $v(\omega) = \frac{\mathrm{d}\omega}{\mathrm{d}k}$ is the group velocity bonded by the Lieb-Robinson velocity $v(\omega) \leq v_{LC}$, t_i is the point in time before t_c when the quasi-particle enters the environment, t_f the point in time after t_c when the quasi-particle returns to the subsystem. The quasi-particle weight $w(\omega)$ corresponds to the entanglement contribution per quasi-particle which can bounded by $w(\omega) \leq 2\log(2)$ by considering the dimension of the vectorized Hilbert space. At dual unitarity the quasi-particle weight is given by $w = \log(2)$ exactly. We will focus on the case $t_c = t_{\max}/2$, since this cut will have maximal entanglement and hence determines the complexity of the finite size IM.

We first consider the limit of long times and short environment sizes. In this case we get from Eq. (3.21) that TE increases linearly with environment size L:

$$S(t_{\max} >> L, L, t_{\max}/2) = v_{\mathrm{TE}} L, \tag{3.22}$$

$$v_{\mathrm{TE}} = 2\int_{\omega_{\min}}^{\omega_{\max}} \frac{\mathrm{d}\omega}{2\pi} \frac{w(\omega)}{v(\omega)}. \tag{3.23}$$

The speed of TE v_{TE} is bounded by $v_{\mathrm{TE}} \leq 2\log(2)$ due to the bond dimension $\chi = 4^L$ of the exact IM of finite environments of length L. For finite times $t_{\max}$ and environment lengths L, the semi-classical formula Eq. (3.21) predicts that the TE at the central cut $t_c = t_{\max}$ can be parametrized by $\xi = \frac{L}{T}$ by

$$s(\xi) = \frac{S(t_{\max}, L, t_{\max}/2)}{t_{\max}}. \tag{3.24}$$

For finite ξ some of the slower quasi-particles with velocity $v(\omega) < 4\xi$ get traced out at the final time $t_{\max}$ inside of the environment. We hence have the small ξ behavior of $s(\xi)$ given by:

$$\frac{\mathrm{d}s}{\mathrm{d}\xi}|_{\xi=0} = v_{TE}, \qquad\qquad s(\xi) < v_{TE}\xi. \tag{3.25}$$

At $\xi > v_{LC}/4$, even some of the fastest quasi-particles get traced out, leading to a maximum in $s(\xi)$. For $\xi > v_{LC}/2$, no quasi-particle can return to the system, and the extensive part of the TE vanishes $s(\xi > v_{LC}/2) = 0$. This means that the TE has a volume-law barrier. For the dual unitary case all quasi-particles move with the brickwork light-speed $v_{LC} = 2$ and the formula becomes exact:

$$s_{\mathrm{d}}(\xi) = \log(2)\min(\xi, \frac{1}{2}\xi). \tag{3.26}$$

In Fig. 3.2 b), we can see that the shape of the TEB obtained using the semi-classical formula Eq. (3.21) with constant quasi-particle weight $w = 0.93\log(2)$ (black dashed line) is close to the exact TEB (green line) in the integrable model even away from dual-unitarity at parameters $J = 0.6\pi/4, g = \pi/4$.

This image qualitatively explains the low TE of thermodynamic IM in integrable systems. In the thermodynamic TE no quasi-particle with finite velocity can reach the spatial boundary to be reflected, which is indicated by a vanishing of the extensive part

of the TE quantified by $s(\xi > v_{LC}/2) = 0$. The only remaining contributions to TE are non-extensive in $t_{\max}$ and are hence not captured by Eq. (3.21). They stems from localized edge modes as well as short-time effects relating to the overlap of departing quasi-particles with the subsystem site. For a more general and rigorous analysis on the thermodynamic limit of the TE in integrable systems including different initial states, I refer to Refs. [5, 10, 119]. The low TE in integrable systems opens the door for the IM approach to be used in quantum impurity problems as demonstrated in [3, 119, 127, 128] as well as in Chapter 6.

The TEB in the non-integrable model shown in Fig. 3.2(a) as well as previous observations of the TEB in generic systems [8, 108] are empirical evidence that the phenomenon of the TEB generalizes beyond systems consisting of quasi-particles. Instead the back flow of information from the environment to the subsystem, which is enhanced for finite environments is the fundamental reason for the increase in TE. We also observe in Fig. 3.2 a) that the choice of boundary condition changes the maximum TE of the TEB. In the quasi-particle picture the spatial boundary condition represent a reflection coefficient and is encoded in $w(\omega)$.

Superficially, the TEB is reminiscent of the real space entanglement barrier[129–131]. Starting from a low entangled state, reduced density matrices of a fixed interval of a generic 1+1 dimensional quantum system become complex, before reaching a thermal state with low entanglement. So far it is unclear how those two phenomena are related. The non-monotonicity of entanglement during such contraction was also observed during the contraction of random 2D tensor networks[132]

3.4 Light cone growth algorithm

We now formulate an algorithm, which can avoid the TEB discussed in the previous section. Its accuracy is thus only bounded by the bond dimension and TE of the thermodynamic IM.

The fundamental reason for the intermediate states with high TE in the TCA are that those IM correspond to finite environments. Hence, one solution to the TEB problem is to formulate a recursive scheme where all intermediate states are thermodynamic IM. This means, that instead of keeping the number of timesteps T fixed and increasing the environment size L as was done in TCA, we stay in the thermodynamic limit $L > 2T$ and increase the number of time steps.

To find such a recursion relation, we consider the brickwork tensor network for the IM (Fig. 3.4(a)). By applying the trace preservation property (Fig. 3.4(b)) and repeatedly removing channels which are traced out on both outgoing legs from the full tensor network, we obtain a reduced, light-cone tensor network (Fig. 3.4(c)). Physically this corresponds to removing all channels which can not causally affect the local dynamics of the subsystem. Upon exact contraction, the light-cone tensor network is equivalent to the full tensor network. If we consider transverse contraction of this tensor network, we find that the number of timesteps of the intermediate IMs grows. At each odd step, the number of timesteps of the IM increases by one and on each even step the number

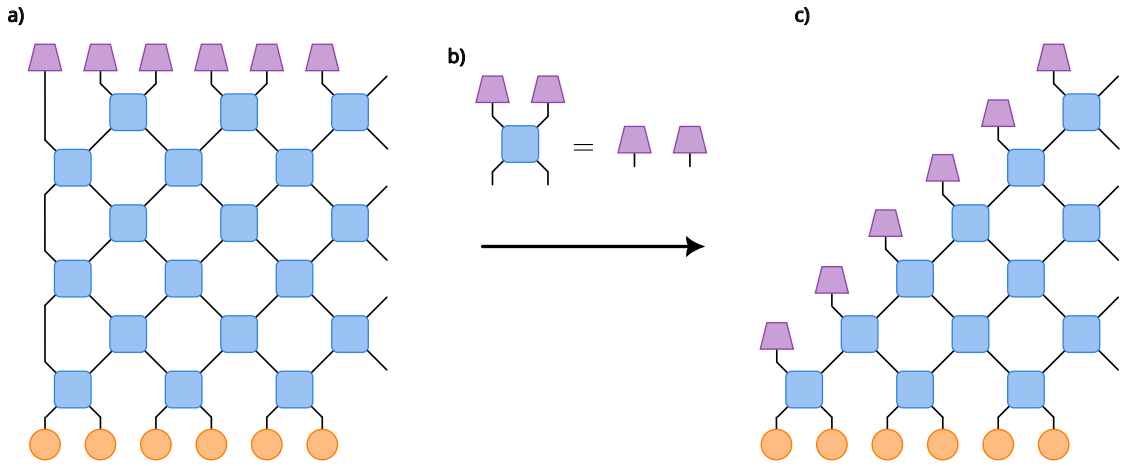

Figure 3.4: Depiction of the light-cone growth algorithm (LCGA). *(a)* shows the full tensor network corresponding to the IM (compare Fig. 3.1. The trace preserving property of channels depicted in *(b)* allows erasure of channels outside of the light-cone. This leaves us with the light cone tensor network in *(c)*. Contracting this tensor network in the transversal direction corresponds to the LCGA defined by Eqs. (3.27),(3.28).

of timesteps stays the same. Since the strict light-cone velocity of a brickwork circuit is given by $v_{LC} = 2$ this means that all the intermediate IMs are thermodynamic IMs corresponding to infinite environment size. This immediately implies the absence of a TEB, since the thermodynamic IMs for any shorter time can be recovered from the IM for a longer time by simply attaching traces $\mathbb{1}$ to the last legs, c.f. Sec. 2.4. Since this procedure does not increase bond dimension, we have that if the longer IM can be represented efficiently with a given bond dimension, so can all IMs of shorter time which form the intermediate states in the LCGA.

Now we can formulate the recursion relation as transverse contraction of the light cone tensor network for even and odd values of L:

$$\mathscr{I}(T+1,\infty,\mathrm{odd})_{\{\mu^\tau,\nu^\tau\}_{\tau=1}^T} = \mathscr{T}(T+1)_{\{\mu^\tau,\nu^\tau\}_{\tau=1}^T,\{\kappa^\tau,\lambda^\tau\}_{\tau=1}^T} \mathscr{I}(T,\infty,\mathrm{even})_{\{\kappa^\tau,\lambda^\tau\}_{\tau=1}^T} \delta_{\kappa^{T+1},\lambda^{T+1}}, \tag{3.27}$$

$$\mathscr{I}(T,\infty,\mathrm{even})_{\{\mu^\tau,\nu^\tau\}_{\tau=1}^T} = \mathscr{T}(T)_{\{\mu^\tau,\nu^\tau\}_{\tau=1}^T,\{\kappa^\tau,\lambda^\tau\}_{\tau=1}^T} \mathscr{I}(T,\infty,\mathrm{odd})_{\{\kappa^\tau,\lambda^\tau\}_{\tau=1}^T}, \tag{3.28}$$

where $\mathscr{T}$ are the dual transfer matrices defined in Eqs.(3.10) and (3.11). Analogous to the TCA, we can formulate the *Light-cone growth algorithm* (LCGA): Starting from $\mathscr{I}(0,\infty,\mathrm{even}) = 1$, we employ the recursion relations Eqs.(3.27) and (3.28) and compress the result. The last two steps are repeated until we reach the desired number of timesteps.

For the LCGA we used the strict brickwork light cone. It is possible to improve the performance further for Hamiltonian systems by increasing T along the slower Lieb-Robinson light-cone. This was pointed out in Ref. [100].

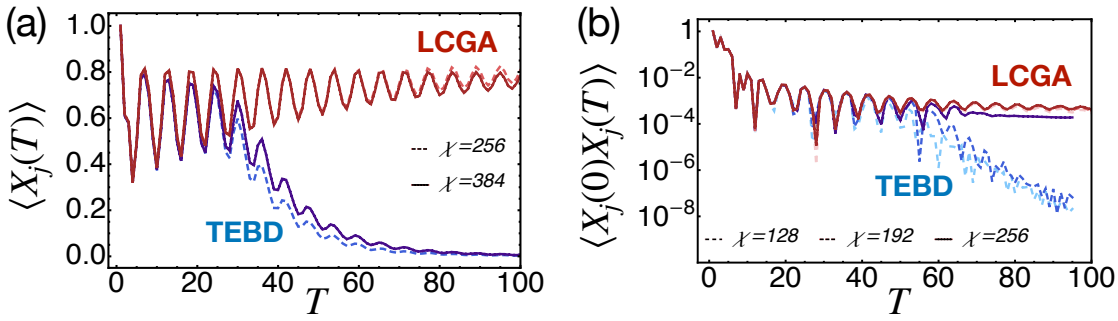

Figure 3.5: Comparison between time evolution of observables computed with TEBD (blue lines) and LCGA (red lines) for the kicked Ising chain defined in Eq. (3.20) with the parameters $J = 0.31, g = 0.638, h = 0.2$. For both algorithms, different lines correspond to different maximal bond dimension. *(a)* Evolution of local polarization $\langle X_j \rangle$ starting from a fully polarized initial state. *(b)* Autocorrelator $\langle X(0)X(T)\rangle$ for the infinite temperature state. Figure adapted from Ref. [6]

Using the LCGA together with the algorithm for the observables described in Sec. 2.4, we can compute dynamics of local observables. We compute the autocorrelator of the x operator at infinite temperature (Fig. 3.5(a)) as well as the time evolution of the expectation value for a state polarized in the x-direction (Fig. 3.5(b)) with LCGA and conventional time-evolving block decimation (TEBD) in the Heisenberg-picture for the KIC at the same parameters $J = 0.31, g = 0.638, h = 0.2$, fixing the same maximum bond dimension. We find that the data computed with TEBD is only converged for short times, whereas LCGA gives access to the long time dynamics at least in this particular model. For very long times, the chosen bond dimension is no longer sufficient to capture the IM accurately, which ultimately also limits LCGA.

3.5 Acknowledgements

This chapter is based on and extends the paper [6], which was written in collaboration with Alessio Lerose and Dmitry A. Abanin. The computations were performed at University of Geneva using Baobab HPC service.

4 Dual unitary circuits and Perfect Dephasers

4.1 Introduction

Generically the "evolution" in the transverse direction as utilized for example in the transverse contraction algorithm (TCA) described in Chapter 3 does not correspond to any physical time evolution. *Dual unitary* circuits[111, 133] are quantum circuits where the transverse evolution corresponds to a unitary time evolution. Despite being generically non-integrable and belonging, depending on the parameters, to the ergodic phase, the dual unitary property allows for analytical approaches. In particular, temporal correlations of local operators[112, 114, 134] and the spectral form factor[133] have been computed for these models. In this chapter we study the influence matrix (IM) at and near dual unitary points to gain insight into the structure of IMs corresponding to thermalizing environments.

For concreteness we study the kicked Ising chain, defined by the Floquet operator

$$U = e^{iJ\sum_{k=1}^{L-1} S_k^z S_{k+1}^z + ih\sum_{k=1}^{L} S^z} e^{ig\sum_{k=1}^{L} S^x} \tag{4.1}$$

where S_k^z, S_k^x are the Pauli operators acting on site k. This model is dual unitary at $J = g = \pi/4$ for any value of the longitudinal field h[111] and non-integrable if all parameters are non-zero. We write the self-consistency equation for the IM corresponding to a semi-infinite chain coupled to the remaining chain via a single interface spin as in Chap. 3. For the dual unitary case, this equation can be solved exactly, yielding a product state IM consisting of perfect dephasing channels[26], which we call *Perfect Dephaser*. This means that the environment is a Markovian bath which measures the interface spin at each period of time evolution, cancelling the off-diagonal elements of its density matrix. This is surprising, since Markovianity is commonly an approximation arising from an environment with faster dynamics then the system coupled to it. Here the environment and the subsystem are homogeneous and there is no separation of time scales.

By solving the self-consistency equation, we further show that dual-unitary models with diagonal, "Ising" coupling and higher spins also yield Perfect Dephaser IMs. In fact, by considering the tensor network representation, we show that for Ising chains, dual-unitarity together with infinite-temperature initial conditions directly implies that the IM is a perfect dephaser: Using the dual-unitary property on each gate, we can successively erase every gate in the tensor network, leaving only a product state where each leg is a trace operator. In the case of a diagonal coupling between the environment and the subsystem, this corresponds to a perfect dephaser IM. Furthermore we show

that *Haar random circuits*, averaged over spatio-temporal noise, also correspond to a perfect dephaser IM.

To go beyond the fine-tuned dual-unitary points, we start by employing MPS representation of the IM obtained using the transversal contraction algorithm described in Chap. 3. Since Perfect Dephasers are product states in the MPS sense, TE is exactly zero at the dual unitary point. When detuning from the dual unitary points, TE remains parametrically low, making an MPS approach viable. This allows us to compute the decay of local correlation functions. We find that in the vicinity of the dual unitary point, TE scales as a volume law in time although with a small prefactor which increases with the detuning from dual unitarity.

In Ising models, the argument of the Influence functional discussed in Sec. 2.5 corresponds to the S^z projection of the interface spin. Matrix elements of the IM can be interpreted as complex weights of interface spin trajectories on the Keldysh contour. The interface spin effectively acts as a magnetic field on the last environment spin. This allows us to interpret the IM matrix elements as overlap between the time evolved environment states subject to the magnetic fields defined by the forward and backward contour. This view immediately gives us that all entries are bounded by one. Classical trajectories, where forward and backward are the same are unity. Quantum trajectories where forward and backward parts are different, correspond to the Lohschmidt echo[135, 136] and vanish at the dual unitary points. For thermalizing systems away from the dual unitary points, the Loschmidt echo decay on average exponentially; this is verified numerically for our model. We can study the IM structure using the tools laid out by Legget et. al. in Ref. [122]: Classical time intervals of the trajectory where the forward and backward spin are the same are called *sojourn* and quantum time intervals where they are different are called *blips*. The influence matrix can be described in terms of an *influence action* which encode the complex statistical weight for configurations of blip and sojourn sequences. In this statistical mechanics theory, blips correspond to massive quasi-particles. Without interactions, the influence action would be the product of the single-blip influence actions. We define the interaction between neighbouring blips separated by a sojourn as difference of the influence action from the non-interacting influence action. Numerically it is shown that these interactions decay with distance, which can be related to the decay of temporal correlations.

This statistical mechanics picture is applied to the problem of a slow impurity coupled to a chain detuned from dual unitarity. The slow impurity introduces weights suppressing blips, and effectively imposes a low density of blips. Together with the fast decay of interactions, this justifies the Non-interacting blip approximation (NIBA). We show that the decay rates predicted by the NIBA match the MPS computations closely to dual-unitarity. In principle this theory can be extended to higher order by considering clusters of blips and sojourns as quasi-particles.

Influence matrix approach to many-body Floquet dynamics

Alessio Lerose,[1,*] Michael Sonner,[1,*] and Dmitry A. Abanin[1]

[1] *Department of Theoretical Physics, University of Geneva, Quai Ernest-Ansermet 30, 1205 Geneva, Switzerland*

(Dated: February 19, 2021)

Recent experimental and theoretical works made much progress towards understanding non-equilibrium phenomena in thermalizing systems, which act as thermal baths for their small subsystems, and many-body localized ones, which fail to do so. The description of time evolution in many-body systems is generally challenging due to the dynamical generation of quantum entanglement. In this work, we introduce an approach to study quantum many-body dynamics, inspired by the Feynman-Vernon influence functional. Focusing on a family of interacting, Floquet spin chains, we consider a Keldysh path-integral description of the dynamics. The central object in our approach is the *influence matrix* (IM), which describes the effect of the system on the dynamics of a local subsystem. For translationally invariant models, we formulate a self-consistency equation for the influence matrix. For certain special values of the model parameters, we obtain an exact solution which represents a *perfect dephaser* (PD). Physically, a PD corresponds to a many-body system that acts as a perfectly Markovian bath on itself: at each period, it measures every spin. For the models considered here, we establish that PD points include dual-unitary circuits investigated in recent works. In the vicinity of PD points, the system is not perfectly Markovian, but rather acts as a bath with a short memory time. In this case, we demonstrate that the self-consistency equation can be solved using matrix-product states (MPS) methods, as the IM *temporal entanglement* is low. A combination of analytical insights and MPS computations allows us to characterize the structure of the influence matrix in terms of an effective "statistical-mechanics" description. We finally illustrate the predictive power of this description by analytically computing how quickly an embedded impurity spin thermalizes. The influence matrix approach formulated here provides an intuitive view of the quantum many-body dynamics problem, opening a path to constructing models of thermalizing dynamics that are solvable or can be efficiently treated by MPS-based methods, and to further characterizing quantum ergodicity or lack thereof.

I. INTRODUCTION

Describing non-equilibrium quantum matter and harnessing it for quantum technology is one of the central challenges in modern physics. The problem of highly non-equilibrium dynamics of many-body systems, both isolated and open, has been attracting intense experimental and theoretical interest over the past years [1–3]. Ergodic isolated systems are believed to thermalize as a result of their quantum evolution; qualitatively, such a system can act as an efficient thermal bath for its sufficiently small subsystems. Recent breakthroughs identified classes of systems that do not reach thermal equilibrium [4–7] and therefore may exhibit new phenomena not envisioned within the framework of statistical mechanics.

Floquet systems, where the Hamiltonian is periodically varied in time, play a special role in the family of non-equilibrium systems, thanks to their natural experimental realizations. Although periodic driving sequences have been utilized in nuclear magnetic resonance for decades [8], recent works revealed a range of new surprising phenomena in Floquet systems. In particular, it was shown that many-body Floquet systems may exhibit new topological properties [9]. Many-body localization in Floquet systems can protect them from heating [10–12], enabling new non-equilibrium states of matter with remarkable properties not attainable in thermal equilibrium [13–17].

The central difficulty in describing dynamics of many-body systems that do thermalize stems from the rapid generation of quantum entanglement. Initially simple, non-entangled states, quickly develop non-local correlations; faithfully describing a time-evolved state requires, in general, a number of parameters which grows exponentially with the evolution time. Various efficient numerical methods based on tensor networks have been introduced [18–21]. Examples of tractable interacting Floquet models, both integrable and thermalizing, have been found and are being actively investigated [22–26].

The goal of this paper is to formulate what we call the *influence matrix* approach to quantum many-body Floquet dynamics. This approach can be viewed as an extension of the celebrated Feynman-Vernon influence functional approach [27] to interacting Floquet systems. In the original formulation, Feynman and Vernon developed a path-integral description of a quantum-mechanical system coupled to a bath. Typically, the bath consists of physical degrees of freedom that are of different nature than those composing the system itself, such as in the case of two-level systems coupled to a bath of harmonic oscillators [28, 29] or particle reservoirs [30]. In our case, in contrast, the bath and the system will be composed of the same physical constituents.

We will consider quantum systems on a lattice, and

* These two authors contributed equally to this work

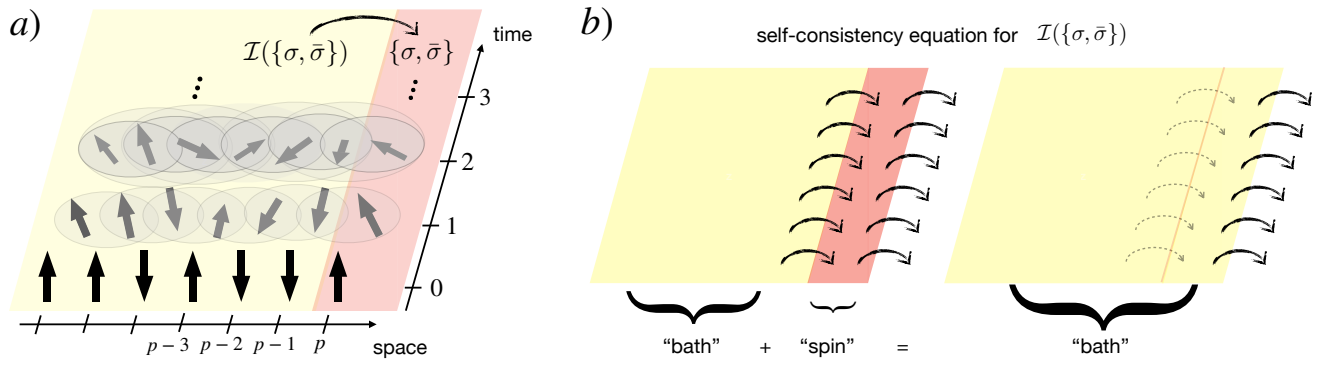

Figure 1. a) Cartoon illustration of the influence matrix approach to many-body Floquet dynamics. The many-body quantum state of a spin system becomes increasingly entangled due to periodic local interactions and kicks. The influence matrix $\mathcal{I}$, defined in Eq. (15) below, describes the dynamical effects of all spins $k < p$ on a spin p, in terms of a path integral weight affecting the trajectories $\{\sigma, \bar\sigma\}$ of spin p forward and backward in time. b) In translationally-invariant one-dimensional systems, the influence matrix is the same for all p, which, as illustrated, leads to a self-consistency equation for it.

will be interested in the dynamics of a finite subsystem, treating its complement as a bath. The effect of this bath on the subsystem can be described by the influence functional. Although here we focus on Floquet systems, generalizations to Hamiltonian systems appear possible. More specifically, we will study a class of kicked Floquet systems, which can be viewed as many-body extensions of the celebrated quantum rotor model [31]. In this case, the influence functional becomes discrete and we will therefore refer to it as the influence matrix (IM).

The setup and the key idea of the approach are summarized in Fig. 1. We consider a one-dimensional system of quantum spins, or qudits, σ_k (with local Hilbert space dimension q). We choose spin p, and treat all degrees of freedom to the left as a bath, as illustrated in Fig. 1a. The starting point of our analysis is the Keldysh path-integral formulation of time evolution. In this formalism, forward and backward trajectories of spins arise; for spin k they are denoted by $\sigma_k^\tau, \bar\sigma_k^\tau$, $\tau = 0, 1, 2, \ldots$. To capture the effect of the bath on spin p, we trace out the bath degrees of freedom, which gives rise to the influence matrix $\mathcal{I}(\{\sigma_p^\tau, \bar\sigma_p^\tau\})$. It enters as an additional weight into the path integral describing the evolution of the reduced density matrix of spin p. In general, this influence matrix is non-local in time.

For translationally invariant systems, spin p, subject to the IM $\mathcal{I}(\{\sigma_p^\tau, \bar\sigma_p^\tau\})$, should produce exactly the same IM for its right neighbor. Using this observation, we will formulate a self-consistency equation for the IM, pictorially illustrated in Fig. 1b. This equation is a key ingredient of our approach.

The knowledge of the IM allows to determine the local dynamical properties of the system, including all temporal correlation functions. The IM naturally incorporates the initial state, and allows averaging over ensembles of initial states. The self-consistent IM describes how a system acts as a bath on itself. This approach thus gives access to detailed information regarding thermalization time scales and memory time of the bath. As discussed below, it also allows one to analyze the effect of the bath on an impurity spin. In this sense, the self-consistent IM provides a more complete characterization of a many-body system as a bath, compared to spectral properties (such as presence or absence of level repulsion [7]), and the statistics of matrix elements studied both in the context of the eigenstate thermalization [3] and many-body localization [32].

While in general the self-consistency equation for the IM is complicated, it admits exact solutions in special cases. For kicked Ising models (see, e.g., Ref. [24] and references therein) with certain parameter values, we find that the infinite-temperature IM can be obtained exactly. This solution describes a bath that is a *perfect dephaser* (PD), that is, its effect on a spin at each step of the Floquet evolution is to exactly cancel off-diagonal matrix elements of its reduced density matrix. Phrased differently, the bath measures every spin of the system at each time step. Interestingly, for the case of kicked Ising models, the perfect dephaser class coincides with models that can be recast as dual-unitary circuits introduced recently [24, 25]. In addition, as discussed below, the PD form of the IM arises upon ensemble-averaging over random realizations of the model.

Perfect dephaser systems serve as remarkably simple quantum baths: when coupled to an impurity spin, the system would act on it as an exactly Markovian bath, with a relaxation rate that depends on the coupling strength. This is remarkable, as Markovianity is usually an approximation which requires the internal dynamics of the bath to be much faster than the quantum system that it measures. Thus, the IM approach allows one to identify quantum systems which act as Markovian baths.

At the mathematical level, the IM approach bears a similarity to a tensor-network numerical method introduced by Bañuls *et al.* [19] for modelling dynamics of Hamiltonian systems. Building on the previous insights [19], we apply a matrix-product state (MPS) ansatz to construct the IM away from the PD points.

This tool allows us to shed light on the more general structure of the IM in ergodic Floquet systems.

At the PD points, the IM, viewed as a "wave function" in the space of single-spin trajectories, is effectively non-entangled. We further find that away from PD points, the IM "wave function" exhibits slow growth of temporal entanglement, which allows us to analyze the system's dynamics at longer times than those accessible via exact diagonalization. This observation provides a tool for identifying regimes of thermalizing Floquet dynamics that are amenable to efficient MPS-based methods.

To characterize the structure of IMs in ergodic systems detuned away from PD points, we adopt a statistical-mechanics-like description, viewing "quantum" intervals of a spin trajectory (i.e., the intervals where the forward and the backward path differ, $\sigma \neq \bar{\sigma}$) as "particles". We study the weights of these particles and their interactions, demonstrating that in thermalizing systems they decay with their temporal distance. We further use this insight to predict how the system thermalizes a slower impurity spin, finding a good agreement with numerical simulations.

The influence matrix approach has several additional attractive features. Perhaps most importantly, it provides a direct, physically intuitive way to describe a many-body system as a quantum bath for its constituent parts, giving access to relevant time scales and various correlation functions, including the Loschmidt echo (see below). Furthermore, it allows one to describe dynamics for different ensembles of initial states and in the thermodynamic limit. As mentioned above, the IM approach admits certain exact solutions that are likely not limited to PDs which will be our focus here.

The rest of the paper is organized as follows. In Section II we introduce the IM approach, and formulate the self-consistency equation for the IM. In Section III we will discuss the cases where the IM can be found exactly, and has a perfect dephaser form. Further, Section IV is dedicated to dynamics away from PD points; we introduce and justify the use of MPS-based methods, develop an analytical characterization of the IM structure, and discuss implications for dynamics. Finally, in Section V we will summarize our results, and provide an outlook.

II. INFLUENCE MATRIX FORMULATION

We will start by introducing the models to be considered. We then describe a path integral representation of the dynamics. The correlation functions are expressed in terms of a transfer matrix which acts on the space of single-spin trajectories. We discuss general properties of such transfer matrices, arguing in particular that they have a *pseudoprojection* property. The eigenvector of the transfer matrix encodes the dynamical properties in the thermodynamic limit, and allows one to find all temporal correlation functions. We interpret the eigenvector as an influence matrix, and formulate a self-consistency equation for it.

A. Model

We consider a class of kicked one-dimensional Floquet systems. At each site of a periodic chain of length L, we place a spin, or qudit, with q basis states, denoted by $|\sigma\rangle$. During each driving period, a two-spin operator $\hat{P}_{j+1/2}$ acts on all neighboring pairs $j,\ j+1$. This operator represents an Ising-type coupling: it is diagonal in the $|\sigma_j, \sigma_{j+1}\rangle = |\sigma_j\rangle \otimes |\sigma_{j+1}\rangle$ basis, and symmetric under exchange $j \leftrightarrow j+1$:

$$\hat{P}_{j+1/2}|\sigma_j, \sigma_{j+1}\rangle = e^{i\phi_{j+1/2}(\sigma_j,\sigma_{j+1})}|\sigma_j, \sigma_{j+1}\rangle \qquad (1)$$

with $\phi(\sigma, \sigma') = \phi(\sigma', \sigma)$. This is followed by unitary single-spin operators $\hat{W}_j$ ("kicks"). The combination of the two steps gives the following Floquet operator (evolution operator over one driving period):

$$\hat{F} = \hat{W}\hat{P} = \prod_j \hat{W}_j \prod_j \hat{P}_{j+1/2}\,. \qquad (2)$$

A graphical representation of the corresponding Floquet evolution is provided in Fig. 2. Here we choose to focus on this class of models for clarity of presentation. The following discussion, however, can be extended to more general Floquet systems, where a shallow quantum circuit is applied periodically in time. For $q = 2$, this model reduces to the kicked Ising model (KIM), which we will frequently use for illustration purposes.

B. Dual transfer matrix

Next, we use a discrete path-integral representation of the dynamics of the system. An amplitude for the evolution over t periods, from an initial product state $|\{\sigma_j^0\}\rangle = \otimes_j |\sigma_j^0\rangle$ at $\tau = 0$ to a state $|\{\sigma_j^t\}\rangle$ at time $\tau = t$, is given by

$$A_{\{\sigma_j^0\}\to\{\sigma_j^t\}} = \langle\{\sigma_j^t\}|\hat{F}^t|\{\sigma_j^0\}\rangle.$$

This amplitude can be expressed by a path integral:

$$A_{\{\sigma_j^0\}\to\{\sigma_j^t\}} = \sum_{\{\sigma_j^\tau\}} \prod_{\tau=0}^{t-1} \prod_j e^{i\phi_{j+1/2}(\sigma_j^\tau,\sigma_{j+1}^\tau)} [W_j]_{\sigma_j^{\tau+1}\sigma_j^\tau} \qquad (3)$$

where we have defined $[W_j]_{\sigma_j^{\tau+1}\sigma_j^\tau} = \langle\sigma_j^{\tau+1}|\hat{W}_j|\sigma_j^\tau\rangle$. The sum runs over all possible trajectories of L spins, with fixed initial and final configurations.

To describe the evolution of the density matrix, we will employ a Keldysh-type formalism. To that end, let us introduce a superoperator R which describes the evolution of the system's density matrix (DM). It is the tensor

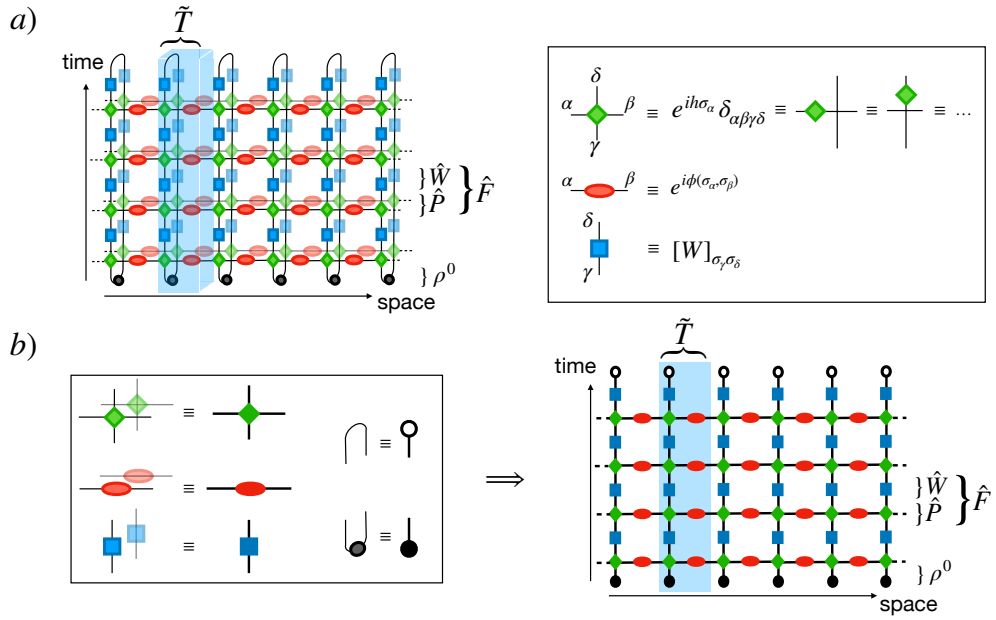

Figure 2. a) Graphical circuit representation of the Floquet dynamics of the model in Eq. (2). The periodic unitary time evolution of the initial unentangled density matrix ρ^0 is pictured by a Keldysh closed-time contour made up of a forward and a backward branch. The red-ellipse and blue-square tensors represent $\hat{P}$ and $\hat{W}$ unitary operators, respectively. The black tensors denote the initial density matrices of individual spins. For later convenience, we have separated possible phases due to on-site magnetic fields, $e^{ih\sigma}$, denoted by green-diamond tensors; the four-index Kroenecker delta tensor $\delta_{\alpha\beta\gamma\delta}$, denoted by a cross, allows to "slide" a green diamond leftward/rightward or upward/downward, indicating that the field h can be thought of as being part of either $\hat{W}$ or $\hat{P}$. The dual transfer matrix $\tilde{T}$ defined in Eq. (8) is highlighted by a blue shaded region. b) In the spirit of the Keldysh formalism, the folded picture is obtained by constructing the composite, q^2-dimensional Hilbert spaces of the forward and backward spins at equal times, spanned by the states $\{|\sigma_j^\tau, \bar{\sigma}_j^\tau\rangle\}$. The local operators acting on this folded space are given by the tensor product of each forward-branch operator $\hat{O} = \hat{W}_j, \hat{P}_{j+1/2}$ and its conjugate $\hat{O}^*$ acting on the backward branch, as illustrated in the left panel. Accordingly, the initial density matrices $[\rho_j^0]_{\sigma_j^0,\bar{\sigma}_j^0}$ are reshaped into vectors $[\rho_j^0]_{(\sigma_j^0,\bar{\sigma}_j^0)}$, and the final-time contractions (traces) $\delta_{\sigma_j^t,\bar{\sigma}_j^t}$ are reshaped into vectors $\delta_{(\sigma_j^t,\bar{\sigma}_j^t)}$, denoted by black and white single-leg tensors, respectively; in either case, summation over $\sigma_j^0, \bar{\sigma}_j^0$ or $\sigma_j^t, \bar{\sigma}_j^t$ is implied by tensor contraction.

product of A and its conjugate A^*, so that its matrix elements are given by

$$R^{\sigma_1^t\bar{\sigma}_1^t\ldots\sigma_L^t\bar{\sigma}_L^t}_{\sigma_1^0\bar{\sigma}_1^0\ldots\sigma_L^0\bar{\sigma}_L^0} = A_{\{\sigma_j^0\}\to\{\sigma_j^t\}} A^*_{\{\bar{\sigma}_j^0\}\to\{\bar{\sigma}_j^t\}}. \tag{4}$$

Note that $\{\sigma\}$ and $\{\bar{\sigma}\}$ denote two independent "paths" or "trajectories", which are conventionally referred to as forward and backward in time. For a given initial DM of the system $\left[\rho^0\right]_{\sigma_1^0\bar{\sigma}_1^0\ldots\sigma_L^0\bar{\sigma}_L^0}$, the DM at time t is obtained by contracting R with ρ^0. In particular, R gives the probability of the system's transition from an initial classical state to a final classical state, if we put $\sigma_j^0 = \bar{\sigma}_j^0$ and $\sigma_j^t = \bar{\sigma}_j^t$ for all j.

Further, following Ref. [19], we introduce a *dual transfer matrix* T_j, which will provide a convenient alternative representation of the reduced density matrix evolution, with time and space interchanged (see Fig. 2). Its matrix elements are given by

$$\langle\sigma_{j+1}^1\,\bar{\sigma}_{j+1}^1\,\ldots\,\bar{\sigma}_{j+1}^{t-1}|\,[T_j]^{\sigma_j^t\bar{\sigma}_j^t}_{\sigma_j^0\bar{\sigma}_j^0}\,|\sigma_j^1\,\bar{\sigma}_j^1\,\ldots\,\bar{\sigma}_j^{t-1}\rangle = \prod_{\tau=0}^{t-1} e^{i\phi_{j+1/2}(\sigma_j^{\tau+1},\sigma_{j+1}^{\tau+1})-i\phi_{j+1/2}(\bar{\sigma}_j^{\tau+1},\bar{\sigma}_{j+1}^{\tau+1})}\,[W_j]_{\sigma_j^{\tau+1}\sigma_j^\tau}[W_j^*]_{\bar{\sigma}_j^{\tau+1}\bar{\sigma}_j^\tau}\,. \tag{5}$$

We treat initial and final spin configurations as parameters. The matrix acts on the $q^{2(t-1)}$-dimensional space of single-spin forward and backward trajectories at times $1 \le \tau \le t-1$.

Then, for a periodic system, Eq. (4) can be expressed via the dual transfer matrices at different sites as follows [33]:

$$R^{\sigma_1^t\bar{\sigma}_1^t\ldots\sigma_L^t\bar{\sigma}_L^t}_{\sigma_1^0\bar{\sigma}_1^0\ldots\sigma_L^0\bar{\sigma}_L^0} = \mathrm{Tr}\left([T_1]^{\sigma_1^t\bar{\sigma}_1^t}_{\sigma_1^0\bar{\sigma}_1^0}\ldots[T_L]^{\sigma_L^t\bar{\sigma}_L^t}_{\sigma_L^0\bar{\sigma}_L^0}\right). \tag{6}$$

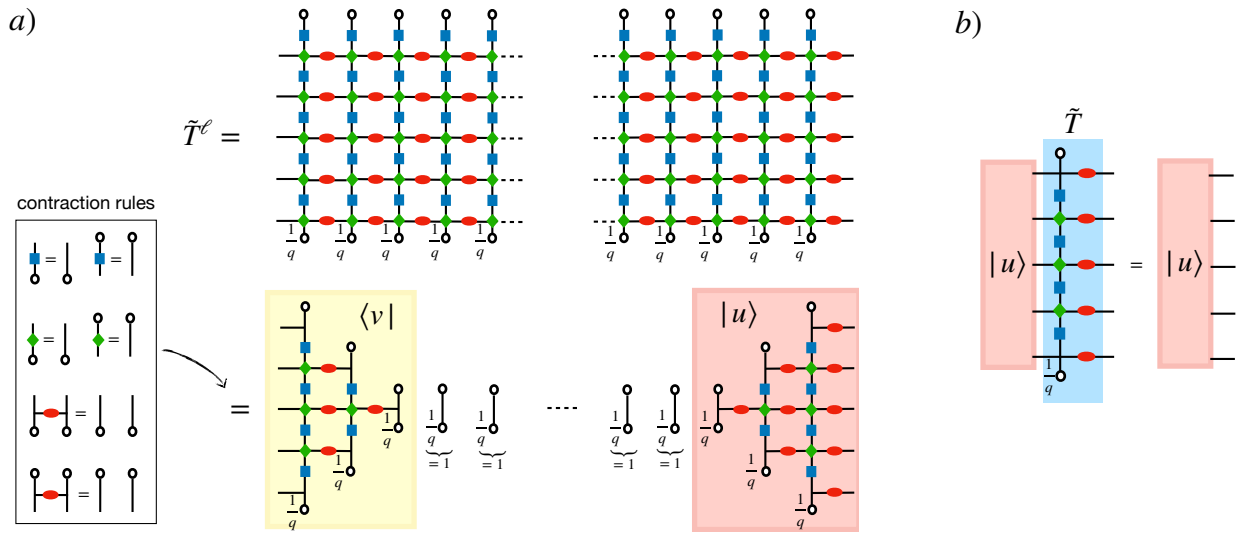

Figure 3. a) Graphical illustration of the pseudoprojection property in Eq. (10). The Keldysh path integral can be represented by a folded circuit and hence evaluated sequentially in the space direction, yielding the iteration $\tilde{T}^\ell$ of the dual transfer matrix (blue shaded tensor) as in Eq. (9) (cf. Fig. 2). Unitarity of time-evolution allows the contraction of the network using the rules in the framed box on the left. Performing all possible contractions, one finds that for $\ell > t$ the input (left) and output (right) legs belong to disconnected networks, bounded by the upper and lower light cones. These two networks define vectors $\langle v|$ and $|u\rangle$, respectively. Hence, the result can be interpreted as the decomposition in Eq. (10). b) Graphical illustration of the eigenvector equation of the dual transfer matrix, which gives the self-consistency equation for the influence matrix of the system (see below).

In the tensor-network language, this representation corresponds to contracting the network in the space direction, as discussed in Ref. [19] which introduced a new numerical method for Hamiltonian systems based on this idea.

As we will see below, this representation has several advantages. It is particularly suited for describing ensembles of initial product states (or, more generally, weakly entangled states). For product states, the initial DM is a tensor product of individual spins DMs $\left[\rho_j^0\right]_{\sigma_j^0\bar{\sigma}_j^0}$:

$$\left[\rho^0\right]_{\sigma_1^0\bar{\sigma}_1^0\ldots\sigma_L^0\bar{\sigma}_L^0} = \prod_j \left[\rho_j^0\right]_{\sigma_j^0\bar{\sigma}_j^0} . \tag{7}$$

In this case, to obtain ρ^t we can conveniently contract T_j with the corresponding initial DM of spin j. Moreover, if we are interested in the evolution of a given spin p, we should contract the final indices for all other spins, by putting $\sigma_j^t = \bar{\sigma}_j^t$, and summing over them. This new dual transfer matrix, illustrated graphically in Fig. 2, can be expressed using Einstein notation for tensor contraction as

$$\tilde{T}_j = \left[\rho_j^0\right]_{\sigma_j^0\bar{\sigma}_j^0} \left[T_j\right]^{\sigma_j^t\sigma_j^t}_{\sigma_j^0\bar{\sigma}_j^0} . \tag{8}$$

Then, the evolution of spin p's DM is generated by the superoperator

$$R^{\sigma_p^T\bar{\sigma}_p^T}_{\sigma_p^0\bar{\sigma}_p^0} = \mathrm{Tr}\left(\tilde{T}_1\ldots\tilde{T}_{p-1}\left[T_p\right]^{\sigma_p^T\bar{\sigma}_p^T}_{\sigma_p^0\bar{\sigma}_p^0}\tilde{T}_{p+1}\ldots\tilde{T}_L\right). \tag{9}$$

It is straightforward to adapt this formalism to different boundary conditions.

Furthermore, for *translationally invariant* systems and initial states, all dual transfer matrices are the same, $\tilde{T}_j = \tilde{T}$. To further simplify Eq. (9), we first discuss properties of $\tilde{T}$.

Dual transfer matrices constructed as above share the following *pseudoprojection* property. Unitarity of time evolution implies that $\mathrm{Tr}(\tilde{T}^L) = 1$ for all integer powers L. Thus, $\tilde{T}$ has a single non-vanishing eigenvalue $\lambda = 1$. We denote by $|u\rangle$ the corresponding right eigenvector, with components $u_{\{\sigma,\bar{\sigma}\}}$. All other eigenvalues are zero. As a result, iterations of $\tilde{T}$ eventually produce a projection onto $|u\rangle$. The system size dependence is encoded in the Jordan blocks of $\tilde{T}$. Indeed, the strictly linear light-cone effect in such Floquet models graphically illustrated in Fig. 3, implies that

the dimensions of Jordan blocks are upper bounded by $\ell^* = 2t$ in general (and $\ell^* = t$ for infinite-temperature initial ensembles, as in the Figure). In fact, points located at distance $r > t$ from the considered site p cannot affect the dynamics of spin p before time t, which thus becomes size-independent for sufficiently long chains. Hence, for $\ell > \ell^*$, we have

$$\tilde{T}^\ell = |u\rangle\langle v|, \tag{10}$$

where the normalization is such that $\langle v|u\rangle = 1$. From Fig. 3a, it is apparent that the left eigenvector $\langle v|$ differs from the right eigenvector by a multiplication by one vertical layer of the circuit, precisely the kick part of the dual transfer matrix in Eq. (5):

$$v_{\{\sigma,\bar\sigma\}} = u_{\{\sigma,\bar\sigma\}} \left[\rho^0\right]_{\sigma^0\bar\sigma^0} \delta_{\sigma^t,\bar\sigma^t} \prod_{\tau=0}^{t-1} [W]_{\sigma^{\tau+1}\sigma^\tau} [W^*]_{\bar\sigma^{\tau+1}\bar\sigma^\tau} \ . \tag{11}$$

The evolution superoperator R of the density matrix of spin p in an infinite homogeneous system [34], Eq. (9), can be conveniently expressed via the eigenvector $|u\rangle$ as

$$R^{\sigma_p^t\bar\sigma_p^t}_{\sigma_p^0\bar\sigma_p^0} = \langle v| \left[T_p\right]^{\sigma_p^t\bar\sigma_p^t}_{\sigma_p^0\bar\sigma_p^0} |u\rangle \quad = \sum_{\{\sigma_p,\bar\sigma_p\}} u^2_{\{\sigma_p,\bar\sigma_p\}} \prod_{\tau=0}^{t-1} [W_p]_{\sigma_p^{\tau+1}\sigma_p^\tau} [W_p^*]_{\bar\sigma_p^{\tau+1}\bar\sigma_p^\tau} \, . \tag{12}$$

Knowledge of R allows us to compute all temporal correlation functions of a single spin. Thus, the problem of describing the dynamics of subsystems reduces to characterizing the properties of the eigenvector of the transfer matrix $\tilde{T}$. We remind the readers that this transfer matrix depends on the ensemble of initial states, see Eq. (8).

C. Self-consistency equation for the influence matrix

Let us take a closer look at the eigenvalue equation for $\tilde{T}$, and give it a transparent physical interpretation. We will assume translational invariance. We now denote the components of the eigenvector $|u\rangle$ (in the space of trajectories of a spin on the Keldysh contour) via

$$|u\rangle = \sum_{\{\sigma,\bar\sigma\}} \mathcal{I}(\{\sigma,\bar\sigma\}) |\sigma^0\bar\sigma^0 \ldots \sigma^{t-1}\bar\sigma^{t-1}\rangle, \tag{13}$$

where $\{\sigma,\bar\sigma\}$ denotes a trajectory of a spin, i.e., $\sigma^0, \bar\sigma^0, \ldots, \sigma^{t-1}, \bar\sigma^{t-1}$. Then, using Eq. (5), we can rewrite the eigenvalue equation as

$$\mathcal{I}(\{\sigma,\bar\sigma\}) = \sum_{\{s,\bar s\}} \mathcal{I}(\{s,\bar s\})\, \delta_{s^t,\bar s^t} \left(\prod_{\tau=0}^{t-1} e^{i\phi(s^\tau,\sigma^\tau) - i\phi(\bar s^\tau,\bar\sigma^\tau)} \, [\mathcal{W}]^{s^{\tau+1}\bar s^{\tau+1}}_{s^\tau \bar s^\tau} \right) \left[\rho^0\right]_{s^0\bar s^0} , \tag{14}$$

where $\mathcal{W}$ is the "folded" kick operator, which is the tensor product of $\hat{W}$ acting along the forward path $\{s\}$, and $\hat{W}^*$ acting along the backward path $\{\bar s\}$.

Next, note that Eq. (14) has a simple physical origin. We can think of the r.-h.s. as describing the propagation in time of a spin $\{s,\bar s\}$, which experiences on-site kicks $\mathcal{W}$, and which is coupled to a neighboring spin $\{\sigma,\bar\sigma\}$. Finally, the term $\mathcal{I}(\{s,\bar s\})$ describes the effect of all the degrees of freedom to the left of our spin on its evolution. Viewing it now as a functional of the trajectory, rather than a vector, we can interpret it as the Feynman-Vernon influence functional (see Ref. [27] and Appendix A), or, rather, *influence matrix*, given the discreteness of time. In fact, the influence functional is obtained by tracing out the degrees of freedom to the left of a given spin p (see Fig. 3):

$$\mathcal{I}(\{\sigma_p,\bar\sigma_p\}) = \sum_{\substack{\{\sigma_k^\tau,\bar\sigma_k^\tau\} \\ k<p,\, 0\le\tau\le t}} \prod_{k<p} \left[\rho_k^0\right]_{\sigma_k^0\bar\sigma_k^0} \delta_{\sigma_k^t,\bar\sigma_k^t} \prod_{\tau=0}^{t-1} e^{i\phi_{k+1/2}(\sigma_k^\tau,\sigma_{k+1}^\tau) - i\phi_{k+1/2}(\bar\sigma_k^\tau,\bar\sigma_{k+1}^\tau)} \, [\mathcal{W}_k]^{\sigma_k^{\tau+1}\bar\sigma_k^{\tau+1}}_{\sigma_k^\tau\bar\sigma_k^\tau} \, . \tag{15}$$

This expression describes the effect of the environment, composed of all spins $k < p$, on the time evolution of

spin p. Thus, Eq. (14) states that a spin, subject to an influence matrix $\mathcal{I}$ created by a bath to its left, creates an equal influence matrix for its neighboring spin to its right. This self-consistency equation for $\mathcal{I}$ is pictorially illustrated in Fig. 1b.

In more abstract terms, the influence matrix $\mathcal{I}(\{\sigma_p, \bar{\sigma}_p\})$ can be regarded as the overlap between the forward and the backward propagations of the environment formed by the spins $k < p$, subject to the trajectories $\{\sigma_p\}$, $\{\bar{\sigma}_p\}$ of the spin p, respectively:

$$\mathcal{I}(\{\sigma_p, \bar{\sigma}_p\}) = \mathrm{Tr}\Big(U_{k<p}[\{\sigma_p^\tau\}]\, \rho^0_{k<p}\, U^\dagger_{k<p}[\{\bar{\sigma}_p^\tau\}]\Big). \quad (16)$$

By unitarity of quantum evolution, one has $|\mathcal{I}(\{\sigma, \bar{\sigma}\})| \leq 1$. We will call trajectories where the forward and backward paths are identical $\bar{\sigma}_p^\tau = \sigma_p^\tau$ *classical trajectories* since they are the equivalent of classical field configurations in the Keldysh formalism. For classical trajectories, one has $\mathcal{I}(\{\sigma, \sigma\}) = 1$. Other general properties of the influence matrix can be obtained by extending the analysis of Ref. [27] to a discrete-time evolution, and are reported in Appendix A.

Although the self-consistency equation (14) encodes much of the complexity of a many-body system's dynamics, we will show below that there are cases when it can be solved analytically. Furthermore, we will show that the local relaxation dynamics can be naturally linked to a statistical-mechanics interpretation of the influence matrix elements $\mathcal{I}(\{\sigma, \bar{\sigma}\})$.

Below we will be interested in averaging over the infinite-temperature ensemble. Thus we put $\left[\rho_j^0\right]_{\sigma_j^0 \bar{\sigma}_j^0} = \delta_{\sigma_j^0 \bar{\sigma}_j^0}/q$. Other initial product states will lead to different transfer matrices. It is also possible to consider entangled initial states, at the expense of increasing the dimensionality of the transfer matrix.

III. PERFECT DEPHASERS

The process of thermalization starting from an initial product state is accompanied by the growth of entanglement between a spin and the rest of the system. In the language of the influence matrix, this corresponds to the suppression of non-classical paths, $|\mathcal{I}(\{\sigma \neq \bar{\sigma}\})| < 1$. The exact form of this suppression encodes the dynamics of thermalization and the decay of correlation functions in a many-body system. In general, we may expect the IM to be a complicated functional that depends on the precise nature of the path $\{\sigma, \bar{\sigma}\}$; parametrizing such a functional requires a number of parameters which is exponential in evolution time.

Surprisingly, there is a class of models for which the exact form of the IM is extremely simple: it vanishes exactly for all non-classical trajectories. This solution of the self-consistency equation (14) has a direct physical interpretation: The environment cancels out all the interference terms. Phrased differently, the environment completely dephases a spin at each evolution step, erasing the off-diagonal elements of its density matrix. Thus, we call such models *perfect dephasers* (PD).

Below we discuss examples of such solvable points for $q = 2$ (kicked Ising model of spins 1/2), and generalizations of KIMs to higher spins, $q > 2$. We find that for this family of models, the perfect dephaser points coincide with the self-dual points introduced by Akila *et al.* [24], and subsequently studied in Refs. [25, 35, 36]. Indeed, it is possible to show that dual-unitarity implies PD property, see Refs. [25, 37] and Subsection C below. There, we further show how this property is reproduced by ensemble-averaging over fully random kicks and interactions. Throughout this Section, we will consider infinite-temperature initial ensembles.

A. Kicked spin-1/2 Ising model

First, we will consider the case of spin-1/2, $q = 2$. We will choose the basis $|\sigma\rangle$ to be the eigenbasis of the z spin projection operator, such that $\sigma = \pm 1$. We will also employ the conventional Pauli matrix notations, $\hat{\sigma}_x, \hat{\sigma}_y, \hat{\sigma}_z$.

As the single-spin kick operator $\hat{W}$, we will choose a combination of a rotation around the z axis followed by a rotation around the x axis,

$$\hat{W} = e^{i\epsilon\hat{\sigma}_x} e^{ih\hat{\sigma}_z}. \quad (17)$$

Further, the two-spin term that depends on phases $\phi(\sigma, \sigma')$, reduces to the Ising interaction with a coupling strength J:

$$\phi(\sigma, \sigma') = J\sigma\sigma'. \quad (18)$$

Thus, for the $q = 2$ case, our model is equivalent to the much studied kicked Ising model (KIM), which is known to display a variety of dynamical regimes, depending on the values of parameters h, J, ϵ. In particular, for $h = 0$ this model becomes solvable by mapping onto free fermions via Jordan-Wigner transformation. In general, when all three parameters are non-zero, the model is non-integrable, and obeys the eigenstate thermalization hypothesis (ETH), and exhibits thermalizing dynamics [38].

Next, we assume that the influence matrix has a perfect dephaser (PD) form,

$$\mathcal{I}_{PD}(\{s, \bar{s}\}) = \prod_{\tau=0}^{t-1} \delta_{s^\tau \bar{s}^\tau}\,. \quad (19)$$

Let us plug this PD influence matrix (IM) into the self-consistency equation (14). We will see that for some special choices of the system's parameters ϵ, J, this IM indeed solves the equation. With this form of $\mathcal{I}$, the summation in the r.-h.s. of Eq. (14) is performed only over classical trajectories, so one has to keep track just of s^τ (since $\bar{s}^\tau = s^\tau$). Then, the r.-h.s. can be rewritten using a one-dimensional transfer-matrix, composed from the matrix elements of $\hat{W}$ and $e^{iJs^\tau\sigma^\tau}$. The field h

drops out and its value can be arbitrary. Then the self-consistency equation takes the following form:

$$\prod_{\tau=0}^{t-1}\delta_{\sigma^\tau\bar{\sigma}^\tau}=\frac{1}{2}(1\ \ 1)\left(\prod_{\tau=0}^{\overleftarrow{t-1}}B(\sigma^\tau,\bar{\sigma}^\tau)\,A\right)\begin{pmatrix}1\\1\end{pmatrix} \tag{20}$$

where

$$B(\sigma^\tau,\bar{\sigma}^\tau)=\begin{pmatrix}e^{iJ(\sigma^\tau-\bar{\sigma}^\tau)} & 0\\ 0 & e^{-iJ(\sigma^\tau-\bar{\sigma}^\tau)}\end{pmatrix} \tag{21}$$

$$A=\begin{pmatrix}\cos^2\epsilon & \sin^2\epsilon\\ \sin^2\epsilon & \cos^2\epsilon\end{pmatrix}, \tag{22}$$

and the arrow over the matrix product in Eq. (20) denotes time-ordering. The boundary vector in the r.-h.s. corresponds to the infinite-temperature averaging. For $\epsilon=\pm\pi/4$, $J=\pm\pi/4$, this equation is satisfied. To see this, note that the A matrix projects onto the vector $\frac{1}{\sqrt{2}}(1\ 1)^T$, while the expectation value of the matrix B on this vector equals $\cos(2J(\sigma^\tau-\bar{\sigma}^\tau))=\delta_{\sigma^\tau\bar{\sigma}^\tau}$. For any non-classical configuration, at least one of the factors will be zero. For classical configurations this expression gives 1, and therefore the self-consistency equation (20) is satisfied.

B. Higher spins

We now turn to the case $q>2$, and show that extensions of the kicked Ising model also become perfect dephasers for a suitable choice of parameters. We identify PD points using a generalization of the approach outlined in the previous Subsection. As a result, we obtain examples of PDs with $q>2$ which coincide with a family of dual-unitary models recently introduced by Gutkin *et al.* [36]. We emphasize that here our goal is to demonstrate that the IM approach allows one to construct examples of perfect dephasers, rather than to provide a complete classification of such solvable cases; this is left for future work.

Instead of a spin-1/2, we consider a clock variable $\sigma=1,2,\ldots,q$, and an Ising-like spin-spin interaction, $\phi(\sigma,s)=J\sigma s$. Let us assume the PD solution of the IM, and derive the suitable model parameters from the self-consistency equation. To that end, we can introduce the generalizations of the transfer matrices A,B from the previous Subsection, Eq. (21), which now become $q\times q$ matrices. The self-consistency equation will be satisfied by the PD IM, provided these transfer matrices satisfy the following properties:

$$\frac{1}{q}\sum_{\alpha}B_{\alpha\alpha}(\sigma^\tau,\bar{\sigma}^\tau)=\delta_{\sigma^\tau,\bar{\sigma}^\tau}\,, \tag{23}$$

$$A_{\alpha\beta}=A_{\alpha'\beta'}\quad\forall\alpha,\beta,\alpha',\beta'=1,\ldots,q. \tag{24}$$

These conditions indeed hold if we fix the parameter $J=\pi/2q$, and specify the single-qudit kick $\hat{W}$ to be of the following form, $\langle\sigma'|\hat{W}_q|\sigma\rangle=\frac{1}{\sqrt{q}}e^{i\epsilon\sigma\sigma'}\,e^{ih\sigma}$, with $\epsilon=\pi/2q$ and arbitrary h. Then, exactly the same mechanism as for the KIM with $q=2$ is effective at $q>2$, yielding the PD influence matrix $\mathcal{I}(\{\sigma,\bar{\sigma}\})=\prod_{\tau=0}^{t-1}\delta_{\sigma^\tau\bar{\sigma}^\tau}$.

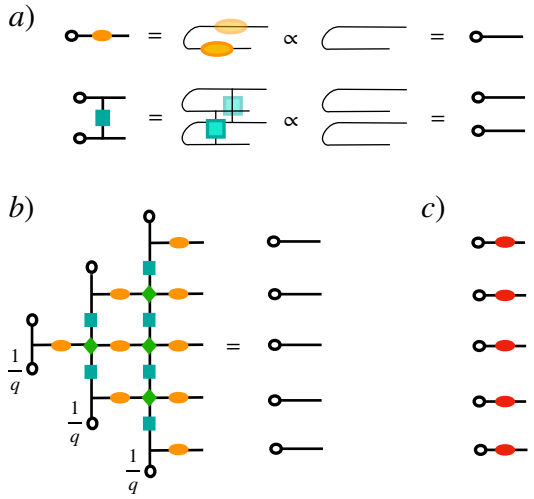

Figure 4. a) At the dual-unitary points of the Floquet model in Eq. (2), the depicted contractions in the space direction are allowed. b) In this case, the network contraction proceeds within the light-cone, and the influence matrix reduces to a perfect dephaser form, i.e., a projection on classical paths. The effect on the spins on the right is that of a Markovian bath, such that coherences are cancelled at each evolution step. c) The influence matrix acting on an impurity spin coupled to a perfect dephaser generates strictly Markovian dynamics with a dephasing strength that is tunable by changing the coupling to the spin (see Sec. III D).

C. Relation to dual-unitary and random circuits

The above examples of perfect dephasers fall into the wider class of dual-unitary circuits, as recently highlighted in Akila *et al.* [24] and further characterized in Refs. [25, 37, 39–41]. In fact, it is possible to show that the eigenvector of the dual transfer matrix has the perfect dephaser form in Eq. (19) whenever a circuit can be written in terms of alternating two-body unitary gates $U_{\gamma\delta,\alpha\beta}$ such that they maintain unitarity when reshaped to dual gates $\tilde{U}$ propagating along space direction, i.e., $\tilde{U}_{\beta\delta,\alpha\gamma}=U_{\gamma\delta,\alpha\beta}$ [25].

The proof of this statement can be graphically carried out by tensor contractions, as shown in Fig. 4 with tensor notations adapted to our setting. The parameter values of the perfect dephaser points found in previous Section allow the "horizontal" contractions shown in panel a), which express the dual-unitary property of the gates. The result of these iterative contractions is then shown in panel b), and is nothing but the graphical representation of the PD influence matrix in Eq. (19).

Interestingly, the above examples of perfect dephaser

circuits may be viewed as unitarily evolving systems which, in a certain sense, imitate the ensemble behavior of *random* unitary circuits, recently introduced as toy models to capture structural properties of quantum dynamics generated by local interactions [42]. In fact, perfect dephasing can be enforced by ensemble averaging over spatial or spatiotemporal randomness in the interactions and kicks. Similarly to the ensemble of initial states considered above, the influence matrix approach is naturally suited to incorporate averaging over randomness in the circuit elements, provided correlations between distinct spatial points are absent; furthermore, a self-consistency equation like Eq. (14) still holds provided the distribution of randomness is translationally invariant. In particular, the non-trivial eigenvector of the ensemble-averaged dual transfer matrix $\mathbb{E}(\tilde{T})$ represents the average influence of the random system on its local subsystem, and correctly generates the ensemble-averaged local observables and their temporal correlations [cf. Eq. (A7) in Appendix A].

To illustrate this, we show how the PD property appears in random circuit ensembles. We consider the fully random version of our model in Eq. (2), with random interactions $\phi^\tau_{j+1/2}(\sigma^\tau_j,\sigma^\tau_{j+1}) \in [0,2\pi)$ and random kicks $\hat{W}^\tau_j \in \mathcal{U}(q)$, independently distributed in space and time, uniformly with respect to the Haar measures. We denote by $\mathbb{E}(\cdot) \equiv \prod_{j,\tau}\int d\mu_{\rm Haar}(W^\tau_j)\int\prod_{\sigma,s}\frac{d\phi^\tau_{j+1/2}(\sigma,s)}{2\pi}(\,\cdot\,)$ the expectation value over this distribution. The self-consistency equation (14), which takes the form

$$\mathcal{I}(\{\sigma,\bar\sigma\}) = \sum_{\{s,\bar s\}}\mathcal{I}(\{s,\bar s\})\,\delta_{s^t\bar s^t}\,\mathbb{E}\left(\prod_{\tau=0}^{t-1} e^{i\phi^\tau_{j+1/2}(s^\tau,\sigma^\tau)-i\phi^\tau_{j+1/2}(\bar s^\tau,\bar\sigma^\tau)}\,\left[W^\tau_j\right]_{s^{\tau+1}s^\tau}\left[W^\tau_j\right]^*_{\bar s^{\tau+1}\bar s^\tau}\right)\frac{1}{q}\delta_{s^0\bar s^0}, \tag{25}$$

is satisfied by the perfect dephaser influence matrix $\mathcal{I}_{PD}(\{s,\bar s\}) = \prod_{\tau=0}^{t-1}\delta_{s^\tau\bar s^\tau}$. Since randomness is assumed uncorrelated in time, the expectation factorizes for different time steps. Hence, the equations

$$\mathbb{E}\Big([W^\tau_j]_{s,\sigma}[W^\tau_j]^*_{\bar s,\bar\sigma}\Big) = \frac{1}{q}\delta_{s,\bar s}\delta_{\sigma,\bar\sigma} \tag{26}$$

and

$$\mathbb{E}\Big(e^{i\phi^\tau_{j+1/2}(s,\sigma)-i\phi^\tau_{j+1/2}(\bar s,\bar\sigma)}\Big) = \delta_{s,\bar s}\delta_{\sigma,\bar\sigma} \tag{27}$$

lead to the solution $\mathcal{I}_{PD}$, as claimed. We note that these equations produce contractions analogous to those satisfied by dual-unitary circuit elements as in Fig. 4a of the manuscript, although the circuit elements themselves are (almost surely in the ensemble distribution) not dual-unitary. In this sense, dual-unitary perfect dephasers reproduce the noise of fully random models, i.e., classical white noise.

We further show that the perfect dephaser property also holds for a random *Floquet* version of the circuit, with interactions and kicks uncorrelated in space but constant in time, provided the local Hilbert space is large, $q\to\infty$. We note that this model is similar to one previously considered in Ref. [43], where random-matrix spectral correlations have been shown. The proof of perfect dephasing follows from the mathematical properties of integration over the Haar measure of the unitary group (the so-called Weingarten calculus) in the large-q limit. Let us consider again the self-consistency equation (25), but now we eliminate the τ-dependence of $\hat{W}$ and ϕ, such that the same two random objects appear multiple times in the equation. We want to show that the solution is again $\mathcal{I}_{PD}$. To verify that, let us substitute $\mathcal{I}_{PD}$ into the r.-h.s. of Eq. (25). We note that in the limit $q\to\infty$ the leading contribution in $1/q$ arises from trajectories where all the s^τ's are distinct. Upon averaging, the product of the kick operators yields $1/q^t$ (see, e.g., Ref. [44]). The remaining phase term exactly equals 1 if all $\sigma^\tau = \bar\sigma^\tau$. For trajectories such that $\sigma^\tau\neq\bar\sigma^\tau$ for some τ's, instead, the average over the random phases gives zero, unless the values of the corresponding s^τ's happen to be equal, producing the necessary phase cancellation; thus, the result is suppressed as $1/q$. In other words, we have proven that

$$\mathcal{I}[\{\sigma,\bar\sigma\}] = \prod_{\tau=0}^{t-1}\delta_{\sigma^\tau,\bar\sigma^\tau} + \mathcal{O}\left(\frac{1}{q}\right), \tag{28}$$

which is what we wanted to show. We finally remark that it can be shown that in both the random circuit and in the random Floquet circuit model, ensemble *fluctuations* around perfect dephaser average behavior are suppressed as $q\to\infty$, i.e., a random realization of the circuit is almost surely a perfect dephaser in this limit. This can be shown by evaluating $\mathbb{E}(\tilde{T}\otimes\tilde{T})$ using similar ideas as above (see also Ref. [43]).

D. A many-body system that is a Markovian bath

The knowledge of the influence matrix provides a complete characterization of a quantum bath and, in particular, gives a tool for describing its effect on dynamics of another quantum system coupled to it. In particular, one can analyze not just the dynamics of a translationally invariant system, but also the dynamics of an impurity immersed in the system. To illustrate this, we now study how a coupling to a perfect dephaser bath affects the evolution of a single spin.

We consider an impurity spin placed at site p, and coupled to its neighbors via a generic Ising coupling. We will see that the system acts on the impurity spin as a memoryless, *Markovian* bath. While the Markovian approximation is commonly employed in a range of problems, it normally relies on the separation of time scales between the system and the bath; in contrast, here it is *exact*, as a consequence of the PD property.

For simplicity, we focus on the kicked Ising model of spins 1/2, with an impurity spin at the edge, site p. We choose all couplings except those involving spin p to be $\epsilon = J = \pi/4$, while spin p is coupled to spin $p-1$ by an Ising coupling with possibly different strength $\tilde{J}$. The kick operator $\hat{W}_p$ may also be different from the $\pi/2$ rotation of the other spins. Then, using the PD property, we can derive the influence matrix for the impurity spin:

$$\mathcal{I}(\{\sigma,\bar{\sigma}\}) = \prod_{\tau=0}^{t-1} \cos\left(\tilde{J}(\sigma^\tau - \bar{\sigma}^\tau)\right). \tag{29}$$

This equation is most easily obtained graphically, noting that the last contraction on the right in Fig. 4b has now non-dual-unitary gates, producing a nontrivial but factorized IM. The latter is represented in Fig. 4c, where red tensors have a parameter $\tilde{J}$ that differs from that of the orange tensors.

The IM in Eq. (29) gives rise to a time-independent superoperator ("quantum map" or "channel") that evolves the local reduced single-spin density matrix,

$$\rho_p^{\tau+1} = \hat{W}_p\, \mathcal{D}\big(\rho_p^\tau\big)\, \hat{W}_p^\dagger\,, \tag{30}$$

where the dephasing superoperator $\mathcal{D}$ damps the off-diagonal entries by a factor $\cos(2\tilde{J})$:

$$\begin{aligned} \Big[\mathcal{D}\big(\rho_p^\tau\big)\Big]_{\sigma,\sigma} &= \big[\rho_p^\tau\big]_{\sigma,\sigma}\,, \\ \Big[\mathcal{D}\big(\rho_p^\tau\big)\Big]_{\sigma,-\sigma} &= \cos(2\tilde{J})\, \big[\rho_p^\tau\big]_{\sigma,-\sigma}\,. \end{aligned} \tag{31}$$

Unless the coupling $\tilde{J}$ equals 0 mod $\pi/2$, the damping is present.

The corresponding thermalization time is dictated by the leading nontrivial eigenvalue of the superoperator in Eq. (30), which depends on both the spin's autonomous dynamics $\hat{W}_p$ and on the coupling $\tilde{J}$. For instance, let us consider a kick operator $\hat{W}_p = \exp(i\tilde{\epsilon}\hat{\sigma}_x)$. We define the temporal correlation function

$$\mathcal{C}_{zz}(t) = \left\langle \hat{F}^{-t}\, \hat{\sigma}_p^z\, \hat{F}^t\, \hat{\sigma}_p^z \right\rangle_0, \tag{32}$$

where $\hat{F}$ is the Floquet operator of the "chain + impurity" and $\langle\cdot\rangle_0$ denotes infinite-temperature averaging. The polarization decay rate $\gamma_{\rm eff}$ of the impurity spin p, defined by the asymptotics

$$-\log|\mathcal{C}_{zz}(t)| \;\sim\; \gamma_{\rm eff}\, t, \tag{33}$$

depends on both $\tilde{\epsilon}$ and $\tilde{J}$. In particular, if $\tilde{J} = \pi/4$, we have $e^{-\gamma_{\rm eff}} = \cos(2\tilde{\epsilon})$, while if $\tilde{\epsilon} = \pi/4$, we have $e^{-\gamma_{\rm eff}} = \sqrt{\cos(2\tilde{J})}$.

The above discussion shows that the effects of perfectly dephasing baths can be computed for arbitrary times, and naturally raises the question about the structural properties of more general quantum ergodic baths possessing nontrivial temporal correlations. We tackle this intriguing question below.

IV. THERMALIZATION AWAY FROM PERFECT DEPHASER POINTS

The discussion above shows that certain fine-tuned Floquet systems can act as perfect dephasing baths for themselves. In other words, these systems can induce complete decoherence of the local degrees of freedom at each time step. The resulting thermalization dynamics is memoryless: i.e., it can be exactly described by a (discrete-time) Lindblad equation [45, 46].

This property is surprising, as the Born-Markov approach to open system dynamics typically requires neglecting the bath temporal correlations [47]. This approximation usually relies on a separation of timescales between the system and the bath. While this is suitable in many physical situations involving the interaction of a "slow" particle with distinct, "fast" degrees of freedom (phonons, electromagnetic fields, ...), it is generally inadequate for the local dynamics of *homogeneous* extended quantum many-body systems.

The factorized form of the influence matrix in Eq. (19) of perfect dephasers, remarkably, makes their local dynamics exactly Markovian. Such property is tied with a complete absence of *temporal entanglement* in the influence matrix. It is thus natural to investigate the structure of the influence matrix in systems detuned from perfect dephaser points. One may expect that such systems would provide more generic examples of thermalizing quantum systems. In this Section, we shall focus on this problem.

In Sec. IV A we will introduce the matrix-product state (MPS) approach, which we adopt as a computational tool throughout this Section. In Sec. IV B we unveil the underlying structure of the influence matrix of generic thermalizing systems away from PD points. We motivate and validate a description of the IM, reminiscent of the statistical mechanics of massive, weakly interacting particles in one dimension, where the role of particles is played by intervals of a Keldysh trajectory with $\sigma \neq \bar{\sigma}$. Finally, in Sec. IV C, we show that this approach can be successfully applied to compute the polarization decay rate of a slow impurity spin coupled to an ergodic chain. For the sake of definiteness, throughout this Section we will focus on the case of the spin-1/2 kicked Ising model described by Eq. (2) with the choice of operators (17) and (18).

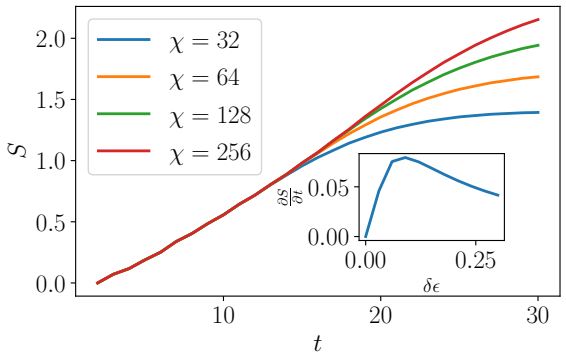

Figure 5. Growth of the maximal (half-time) bipartite temporal entanglement entropy $S(t)$ of the influence matrix viewed as a wave function in the folded space. It is plotted as a function of time, for a small detuning $\delta J = \delta\epsilon = 0.06$ from the PD point, and $h = 0.3$. Entropy growth is approximately linear in time but slow enough for the influence matrix with $t \lesssim 20$ to be accurately captured by an MPS with a bond dimensions $\chi \lesssim 256$. *Inset:* Slope of entanglement entropy $\frac{\partial S}{\partial t}$ as a function of detuning $\delta J = \delta\epsilon$. As the system approaches the PD point, this slope goes to zero. We note that the slope remains small in a broad range of detuning, enabling efficient MPS description.

A. Low temporal entanglement and matrix-product operator approach

It is convenient to "fold" the backwards and forwards contour, grouping together each spin σ^τ on the forward time branch and its equal-time counterpart $\bar{\sigma}^\tau$ on the backward branch, to form a composite four-dimensional local Hilbert space (cf. Fig. 2). The influence matrix can be interpreted as a "wavefunction" living on a chain of those four-dimensional qudits. In this picture, the influence matrix of perfect dephasers [Eq. (19)] is represented by an exact product state. It is natural to assume that for sufficiently small detuning $\delta J = \pi/4 - J$, $\delta\epsilon = \pi/4 - \epsilon$ from the PD point and arbitrary h, the influence matrix can be described in the folded picture by a matrix-product state (MPS) with a moderate bond dimension χ.

We set up a code based on the TeNPy library [48] which applies the dual transfer matrix $\tilde{T}$ repeatedly, starting from a product state. Due to the pseudoprojection property discussed in Sec. II B, it is sufficient to apply the dual transfer matrix t times in order to obtain the influence matrix in the thermodynamic limit. The dual transfer matrix can be expressed as a matrix-product operator (MPO) with bond dimension 4. After each step, the influence matrix MPS is compressed using conventional SVD truncation sweeps. Up to time $t = 2\log_2\chi$ the compression yields no truncation and the results from MPS match exact diagonalization to machine precision.

We take the convergence of the entanglement entropy S of this wavefunction upon increasing the bond dimension as a witness of the quality of our MPS representation. As shown in Fig. 5, the MPS approach allows us to explore the properties of the IMs for larger times t than those accessible via exact diagonalization, as $S(t)$ converges for generic values of the parameters at reasonably low bond dimensions. The results indicate that the initial growth of $S(t)$ is approximately linear in t with a slope decreasing to zero as the PD point is approached. Accordingly, in the following, we will use the MPS approach described here as a computational tool, with $\chi = 256$.

The occurrence of low entanglement entropy in the folded picture is supported by an intuitive argument similar to that in Ref. [49]: In the absence of a longitudinal field $h = 0$, the system can be described by quasiparticles which move to the left on the forward and to the right on the backward branch. In the unfolded picture, this leads to a strong entanglement between sites on the two branches. At the self dual point, those quasiparticles can only propagate along the light cone edges [25], which means that in the folded picture correlations can only exist between a forward site and its corresponding backward site. Thus, the entanglement entropy of the folded MPS is zero. Detuning from the self dual point introduces a small density of slower quasiparticles, which gives rise to a parametrically slow growth of entanglement between different folded lattice sites.

B. Statistical-mechanics description of the influence matrix

The influence matrix is expected to develop a complex structure in generic systems away from perfect dephaser points, corresponding to the appearance of memory effects, intricate decoherence dynamics and temporal entanglement. To analyze this, it is convenient to introduce some additional formalism. Within the previously introduced folding map (cf. Fig. 2), we perform a discrete Keldysh rotation: We denote the "classical" configurations as

$$|\sigma^\tau\bar{\sigma}^\tau\rangle = \begin{cases} |\uparrow\uparrow\rangle \equiv |c_\uparrow\rangle \\ |\downarrow\downarrow\rangle \equiv |c_\downarrow\rangle \end{cases}, \tag{34}$$

and the "quantum" configurations as

$$|\sigma^\tau\bar{\sigma}^\tau\rangle = \begin{cases} |\uparrow\downarrow\rangle \equiv |q_\uparrow\rangle \\ |\downarrow\uparrow\rangle \equiv |q_\downarrow\rangle \end{cases}. \tag{35}$$

We further introduce the states

$$|c_\pm\rangle = |c_\uparrow\rangle \pm |c_\downarrow\rangle\,, \qquad |q_\pm\rangle = |q_\uparrow\rangle \pm |q_\downarrow\rangle\,. \tag{36}$$

Note that these four basis states may be seen as the vectorization (via the folding map) of the four basis operators $\hat{\mathbb{1}}, \hat{\sigma}_z, \hat{\sigma}_x, i\hat{\sigma}_y$, respectively. With this notation, the initial infinite-temperature density matrices are represented as

$$\frac{1}{2}\mathbb{1} \to \frac{1}{2}|c_+\rangle \tag{37}$$

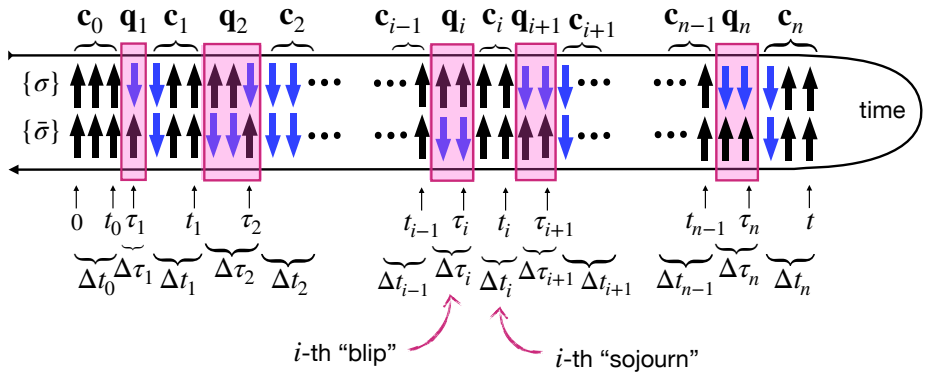

Figure 6. Illustration of the "sojourn-blip" parametrization in Eq. (42) of a generic spin trajectory on the Keldysh contour.

and the perfect dephaser influence matrix assumes the following simple form:

$$|\mathcal{I}_{PD}\rangle = \bigotimes_{\tau=1}^{t-1} |c_+\rangle = |c_+ c_+ \dots c_+\rangle \,. \tag{38}$$

General properties of the influence matrix (see Appendix A for details) dictate that $|\mathcal{I}(\{\sigma,\bar\sigma\})| \leq 1$, and $\mathcal{I}(\{\sigma,\bar\sigma\}) = 1$ for all classical trajectories, i.e.,

$$\mathcal{I}(c_{\uparrow,\downarrow} c_{\uparrow,\downarrow} \dots c_{\uparrow,\downarrow}) = 1 \quad \text{or} \quad \mathcal{I}(\{\sigma = \bar\sigma\}) = 1. \tag{39}$$

More generally, as discussed in the Appendix [see in particular Eq. (A5)], the value of $\mathcal{I}$ on mixed classical/quantum trajectories depends only on the configuration extending between the first and the last quantum site [50]

$$\mathcal{I}\big(c_{\uparrow,\downarrow} \dots c_{\uparrow,\downarrow} (q_{\alpha_\tau} \dots q_{\alpha_{\tau'}}) c_{\uparrow,\downarrow} \dots c_{\uparrow,\downarrow}\big) = \mathcal{I}(q_{\alpha_\tau} \dots q_{\alpha_{\tau'}}). \tag{40}$$

This property motivates us to view classical Keldysh paths as "vacuum", and to interpret the quantum excursions $(\sigma^\tau \bar\sigma^\tau) = q_{\uparrow,\downarrow} = (\uparrow\downarrow)$ or $(\downarrow\uparrow)$ of a path $\{\sigma,\bar\sigma\}$ as "particles". In this description, the influence matrix is regarded as a *complex* statistical weight for a particle configuration,

$$\mathcal{I}(\{\sigma,\bar\sigma\}) = e^{-\mathcal{S}(\{\sigma,\bar\sigma\})} \,. \tag{41}$$

where we refer to $\mathcal{S}$ as the *influence action*. Note that $\mathfrak{Re}\,\mathcal{S} \geq 0$. In the limit of vanishing coupling to the bath, one trivially obtains $\mathcal{S}(\{\sigma,\bar\sigma\}) = 0$ for all trajectories, irrespective of their particle content. In the opposite limit of a perfect dephaser, one has $\mathcal{I}(\{\sigma,\bar\sigma\}) = 0$ [i.e., $\mathfrak{Re}\,\mathcal{S}(\{\sigma,\bar\sigma\}) = \infty$] whenever a trajectory has some particles [see Eq. (19)]. In the generic case, a particle configuration will be penalized by a non-zero value of the action, with $\mathfrak{Re}\,\mathcal{S}(\{\sigma,\bar\sigma\}) > 0$. Since the influence matrix contains all possible information on the dynamical effects of a part of the spin chain on the spins coupled to it, it is clear that the "interactions" encoded in the action $\mathcal{S}$ characterize the ergodicity of the quantum dynamics, or lack thereof.

Our goal in the following is to characterize the influence matrix of generic ergodic quantum systems. To this end, we describe Keldysh trajectories in terms of alternating classical and quantum intervals. Following the seminal work by Leggett *et al.* [28], we refer to classical intervals (where $\{\sigma,\bar\sigma\} = \{\sigma,\sigma\}$) as "sojourns" and to quantum intervals (for which $\{\sigma,\bar\sigma\} = \{\sigma,-\sigma\}$) as "blips". We can parametrize a trajectory as an alternating sequence of $n+1$ sojourns and n blips,

$$\{\sigma,\bar\sigma\} \leftrightarrow \big(\mathbf{c}_0, \mathbf{q}_1, \mathbf{c}_1, \dots, \mathbf{q}_n, \mathbf{c}_n\big) \,, \tag{42}$$

with

$$\mathbf{c}_j = (\underbrace{c_{\uparrow,\downarrow}, \dots, c_{\uparrow,\downarrow}}_{\Delta t_j \text{ times}}), \qquad \mathbf{q}_i = (\underbrace{q_{\uparrow,\downarrow}, \dots, q_{\uparrow,\downarrow}}_{\Delta\tau_i \text{ times}}), \tag{43}$$

and whose durations sum up to the total trajectory time:

$$\Delta t_0 + \Delta\tau_1 + \Delta t_1 + \dots + \Delta\tau_n + \Delta t_n = t + 1. \tag{44}$$

This parameterization is illustrated in Fig. 6. (Here we assumed for simplicity that the initial density matrix is diagonal.)

In the following, we will use a combination of analytical insights and numerical computations to show that in quantum ergodic many-body systems, blips behave as a "gas" of massive, short-range interacting particles.

1. *Blip weights*

Paths without blips, $n = 0$, are entirely classical, and correspond to the influence matrix $\mathcal{I} = 1$. The simplest nontrivial configurations have $n = 1$, i.e., a single blip. Their influence matrix elements, hereby called influence *weights*, only depend on the internal blip structure, and not on the external sojourns.

To develop some intuition regarding the blip weights, let us first consider a constant blip,

$$\{\sigma,\bar\sigma\} = \{\sigma,-\sigma\} = (\underbrace{q_\uparrow q_\uparrow \dots q_\uparrow}_{\Delta\tau \text{ times}}) \tag{45}$$

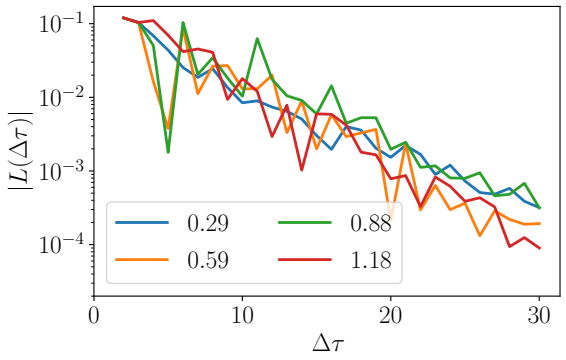

Figure 7. Absolute value of the Loschmidt echo $L(\Delta\tau)$, equivalent to a weight of a single blip, plotted as a function of blip duration, $\Delta\tau$, near the PD point $\delta J = \delta\epsilon = 0.06$ for different values of h reported in the legend. A constant blip that consists of $q_\uparrow$ spin configurations is considered. The decay is approximately exponential, with a rate that is nearly independent of h, and exhibits pronounced time-dependent fluctuations around an exponential envelope.

(a blip with constant $q_\downarrow$ can be described in an analogous manner). In this case, it follows from the definition (16) [or, more generally, (A5)] that the influence matrix $\mathcal{I}$ reduces to the discrete-time, infinite-temperature version of the so-called *Loschmidt echo*, i.e., the overlap between two wavefunctions evolved from the same initial state with two slightly different Hamiltonians (see, e.g. Refs. [51, 52] for reviews). Denoting by a subscript E the "environment" spins at positions $0 \le k < p$, we have

$$\mathcal{I}(\underbrace{q_\uparrow \dots q_\uparrow}_{\Delta\tau-1 \text{ times}}) = \mathrm{Tr}\left[\left(\hat{U}_E^+\right)^{\Delta\tau} \frac{\mathbb{1}}{2^p} \left(\hat{U}_E^{-\,\dagger}\right)^{\Delta\tau}\right] \equiv L(\Delta\tau). \quad (46)$$

The two evolution operators $\hat{U}_E^+$ and $\hat{U}_E^-$ differ by a classical "field" $e^{i\phi(\sigma_{p-1},\pm1)} = e^{\pm iJ\sigma_{p-1}}$ acting on the boundary spin of the environment, due to the spin σ_p being $\uparrow$ in the forward and $\downarrow$ in the backward evolution.

In the limit of weak coupling $J \to 0$ between spins $p-1$ and p, the two time evolutions in Eq. (46) differ only slightly, and it makes sense to consider L as a measure of the sensitivity of the time-evolution to small perturbations in the Floquet operator. In fact, the continuous-time Loschmidt echo has been introduced as a quantifier of chaotic behavior in quantum systems [53, 54]. It has been found that Loschmidt echoes generically exhibit an exponential decay in ergodic systems [55], while in MBL systems it displays a power-law behavior [56].

We are generally interested in the case of a finite, rather than weak, coupling strength J. Nevertheless, it is natural to expect that in ergodic systems weights of constant blips should decay exponentially upon increasing the blip size, similar to the Loschmidt echo. In Fig. 7 we report the results of numerical computations of the influence weight of individual blips with constant $q_\uparrow$ in the kicked Ising chain, for a range of parameters in a neighborhood of the perfect-dephaser point. In all cases, a clear exponential decay is evident, consistent with our expectations.

Furthermore, the influence weight of non-constant blips may be viewed as a generalized time-dependent Loschmidt echo of the environment, formed by the overlap of two time-evolutions subject to a classical boundary field that differs at all times. It is natural to expect the influence weight of all blips to decay exponentially as a function of the blip duration in generic ergodic models. To show that this exponential decay is a generic feature of long blips, we next prove that the average weight $\bar{I}(\mathbf{q})$ of all blips of duration $\Delta\tau$ also decays exponentially as $(\cos(2J))^{\Delta\tau}$. We start with the self-consistency equation (14) for the IM, summing over all internal configurations of a blip of length $\Delta\tau$, which yields:

$$\frac{1}{2^{\Delta\tau}} \sum_{\mathbf{q}:|\mathbf{q}|=\Delta\tau} \mathcal{I}(c_\uparrow, \mathbf{q}, c_\uparrow) = \sum_{\{\sigma,\bar{\sigma}\}} \mathcal{I}(\{\sigma,\bar{\sigma}\}) \prod_{\tau=0}^{t-1} [\mathcal{W}]_{\sigma^\tau \bar{\sigma}^\tau}^{\sigma^{\tau+1}\bar{\sigma}^{\tau+1}} \prod_{\kappa=t_0+1}^{t_0+\Delta\tau} \cos(J(\sigma^\kappa + \bar{\sigma}^\kappa)) \,. \quad (47)$$

The $\mathcal{W}$ transition amplitudes are antisymmetric with respect to the change of sign of the first sojourn. Since such a change does not affect the value of the influence matrix, the contributions of configurations with at least one blip cancel out in the average. This leaves just the contributions from purely classical trajectories, without blips (as in Sec. III D). For those trajectories, the influence matrix is always $\mathcal{I}(\{\sigma,\sigma\}) = 1$. Further, note that for all classical trajectories of σ the J dependent term in Eq. (47) is the same and equal $(\cos(2J))^{\Delta\tau}$. Thus, the $\mathcal{W}$ transition amplitudes can be summed separately, which yields one. As a result, we get

$$\frac{1}{2^{\Delta\tau}} \sum_{\mathbf{q}:|\mathbf{q}|=\Delta\tau} \mathcal{I}(\{c_\uparrow, \mathbf{q}, c_\downarrow\}) = (\cos(2J))^{\Delta\tau} \,. \quad (48)$$

We have numerically verified this relation for various values of the model parameters, confirming that average weight of a single blip decays exponentially with its duration. Interestingly, as is evident in Fig. 7, the weight of a blip with a fixed internal structure, exhibits fluctuations around the approximate exponential decay.

2. *Blip interactions*

Within the above suggestive analogy between an IM and a statistical-mechanical complex "action" for blips, a long blip $\mathbf{q}$ may be pictured as a structured aggregate of particles, the "mass" $\mathcal{S}(\mathbf{q})$ of which increases approximately proportionally to its length.

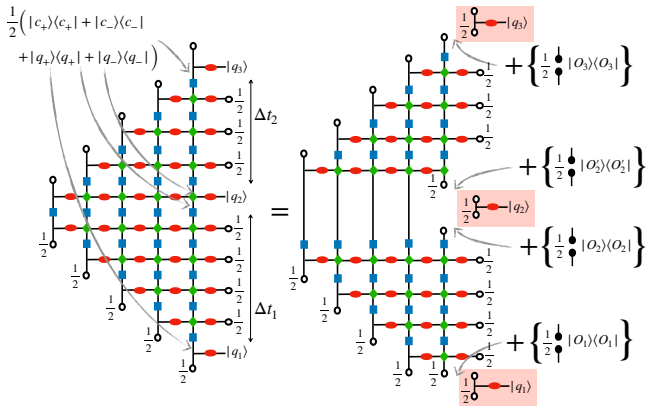

Figure 8. Illustration of the decomposition of the influence weight of a multiple-blip configuration into cluster contributions, cf. Eq. (50). *Left-hand side:* graphical representation of the influence matrix element $\mathcal{I}(q_1, \mathbf{c}_1, q_2, \mathbf{c}_2, q_3)$ of a configuration with $n = 3$ blips of duration $\Delta\tau = 1$, averaged over the intermediate sojourns $\mathbf{c}_1, \mathbf{c}_2$. We insert spectral resolutions of the identity on each tensor leg connecting a blip with the rest of the network, as indicated by the arrows, obtaining $\mathcal{O}(4^n)$ contributions. Each of them consists of the product of n disconnected networks including individual blips and the exterior network including all sojourns. *Right-hand side:* The disconnected-blip contribution is isolated by choosing the identity state $\frac{1}{2}\,|c_+\rangle\,\langle c_+|$ in the resolution of the identity on every leg, and is highlighted by the red shading. In this case the exterior network equals 1, as it can be completely contracted via the rules in Fig. 3a. In contrast, for all the other contributions, the exterior network is equivalent to a temporal correlation function of traceless local operators, corresponding to states $|c_-\rangle$, $|q_+\rangle$, $|q_-\rangle$, denoted O_i here. In ergodic dynamics, these correlations generically decay as the temporal separation Δt_1 or Δt_2 increase.

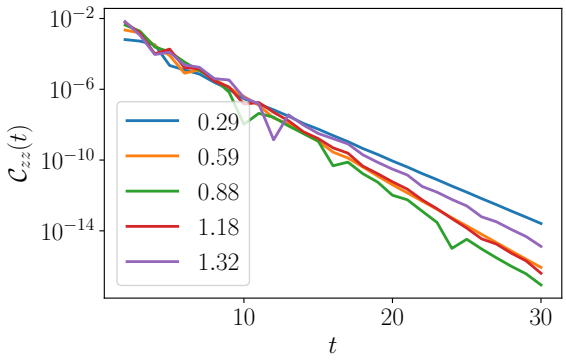

Figure 9. Decay of the polarization autocorrelation $\mathcal{C}_{zz}(t)$ defined in Eq. (32) vs time close to the PD point ($\delta J = \delta\epsilon = 0.06$) for different values of h. The drop is exponential with a decay rate that depends on h.

While the weight of long blips is strongly suppressed, this need not be the case for configurations with multiple blips separated by long sojourns. It is natural to define the *interaction* influence weight of a multiple-blip configuration as the excess influence weight compared to the product of the influence weights of the individual blips:

$$e^{-\mathcal{S}_{\rm int}(\mathbf{q}_1,\mathbf{c}_1,\mathbf{q}_2,\mathbf{c}_2,\ldots,\mathbf{q}_n)} = e^{-\mathcal{S}(\mathbf{q}_1,\mathbf{c}_1,\mathbf{q}_2,\mathbf{c}_2,\ldots,\mathbf{q}_n)+\sum_{i=1}^{n}\mathcal{S}(\mathbf{q}_i)} \quad (49)$$

Note that $\mathcal{S}_{\rm int}$ depends on the specific configuration of the sojourns $\mathbf{c}_j$ between the blips. The question of the range of the blip interactions is intimately related to the memory time of the system. It is expected that a weak non-Markovianity of the reduced dynamics can be translated into a fast decay of interactions.

In fact, the decay of the blip interactions may be precisely related to the temporal decay of the correlations of certain local operators, via the following argument. Let us consider a spin trajectory with n blips, $\{|\mathbf{q}_i\rangle\}_{i=1,\ldots,n}$, and let us evaluate its IM element by contracting the corresponding tensor network, as shown in the example in Fig. 8 for $n = 3$ and blips of duration $\Delta\tau_i = 1$. (In the Figure we average over the configurations of the intermediate sojourns, although this is not necessary for the argument that follows.) To isolate the disconnected blip contributions, we insert a spectral resolution of the identity formed by the states $|c_+\rangle$, $|c_-\rangle$, $|q_+\rangle$, $|q_-\rangle$ defined in Eqs. (34), (35), on each four-dimensional tensor leg connecting a blip with the rest of the network, as indicated by the arrows in the Figure. In this way, we have formally decomposed the IM element as a sum of $\mathcal{O}(4^n)$ contributions, each given by the product of $n+1$ disconnected network contractions: that is, n "small" single-blip networks including $|\mathbf{q}_1\rangle, \ldots, |\mathbf{q}_n\rangle$ respectively, and the remaining "large" exterior network comprising all sojourns. In this sum, the term where we choose $\frac{1}{2}\,|c_+\rangle\,\langle c_+|$ on every leg (which is explicitly represented in the Figure) yields exactly the product of the individual blip weights (red shaded), because the exterior network is equivalent to the influence weight of a classical trajectory and thus evaluates to 1 (using the contraction rules in Fig. 3a). For all the other contributions, the large exterior network may be viewed as a (possibly complicated) temporal correlation function of local operators $\hat{O}_1, \ldots, \hat{O}_n$, all with spatial support near the boundary of the chain, and with temporal support near the respective blips. In quantum ergodic systems, such temporal correlations are expected to decay rapidly upon increasing the time separations $\Delta t_1, \ldots, \Delta t_{n-1}$ between the operators (i.e., the duration of the intermediate sojourns). Thus, in general, one expects the interaction strength between clusters of blips to vanish for sufficiently long sojourns in between: i.e., if $\Delta t_m \to \infty$,

$$e^{-\mathcal{S}(\mathbf{q}_1,\mathbf{c}_1,\mathbf{q}_2,\mathbf{c}_2,\ldots,\mathbf{q}_n)} \simeq e^{-\mathcal{S}(\mathbf{q}_1,\mathbf{c}_1,\ldots,\mathbf{q}_m)} \times e^{-\mathcal{S}(\mathbf{q}_{m+1},\mathbf{c}_{m+1},\ldots,\mathbf{q}_n)}. \quad (50)$$

This scenario is supported by our numerical computations. First, we verify that temporal correlations of local operators decay upon increasing the time separation. For

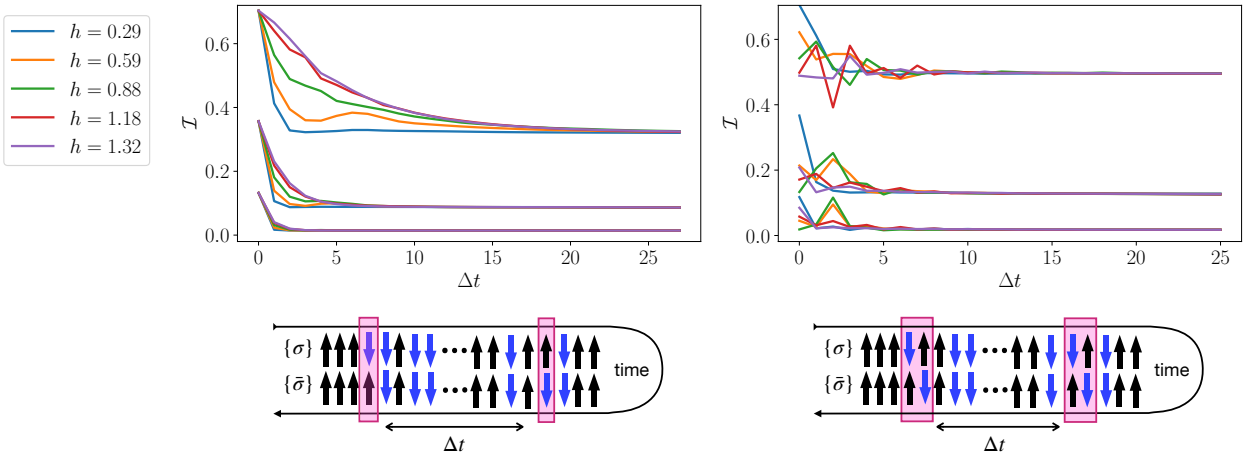

Figure 10. Influence matrix elements of two blips. *Left (Right)*: Blips of length one (two) separated by sojourns of duration Δt. Detuning from the PD points, $\delta J = \delta\epsilon = 0.06, 0.15, 0.3$, increasing from bottom to top. Different values of h are reported in the legend. In both cases, $\mathcal{I}(\mathbf{q}_1, \mathbf{c}, \mathbf{q}_2)$ decays to the product $\mathcal{I}(\mathbf{q}_1)\mathcal{I}(\mathbf{q}_2)$ of the values of individual blips, with $\mathcal{I}(q_\uparrow) = \mathcal{I}(q_\downarrow) = \cos(2J)$ and $\mathcal{I}(q_\uparrow q_\downarrow) = \mathcal{I}(q_\downarrow q_\uparrow) = \cos^2(2J) + \sin^2(2J)\cos(2\epsilon)$.

the sake of illustration, we report in Fig. 9 the dynamics of the spin polarization autocorrelation $\mathcal{C}_{zz}$, defined in Eq. (32). The decay occurs for all values of the parameters, as expected in generic ergodic systems. By the above arguments, the generic decay of temporal correlations such as the ones we reported in Fig. 9 justifies the cluster approximation of the blip action. We further verify this directly by inspecting the IM elements. In Fig. 10 we report the influence weight of a pair of blips for the kicked Ising chain, averaged over the configurations of the intermediate sojourns, as a function of their temporal separation, for two examples of blip structures, and for a range of parameters in a neighborhood of the perfect-dephaser point. As the plots clearly show, in all cases the IM approaches a constant plateau equal to the product of the disconnected blip weights.

C. Decay rate of a slow impurity

In the previous Subsection, we analyzed the influence action, finding that blips have a finite range of interactions, which is related to the relaxation time of the system. Next, we analyze the effect of a many-body bath on a "probe" spin embedded a spin chain, whose own dynamics is slower than that of the environment. In this case, thanks to the separation of time scales, the blip "gas" is effectively dilute and can be treated as non-interacting. This will enable us to predict the relaxation rate of the impurity spin.

To make this intuition quantitative, we compute the polarization decay rate of an impurity spin at the edge of a kicked Ising spin chain defined by Eqs. (2), (17), (18), with parameters $\epsilon = \pi/4 - \delta\epsilon$, $J = \pi/4 - \delta J$ detuned from a perfect dephaser point. This impurity spin differs from the other spins of the chain by the smaller strength $\tilde{\epsilon}$ of its kicks,

$$|\tilde{\epsilon}| \ll \epsilon\,. \tag{51}$$

Our aim is to compute the persistence of the impurity spin polarization,

$$P_{\sigma^0=\uparrow\,\to\,\sigma^t=\uparrow} \equiv P_{\uparrow\uparrow}(t) = \frac{1+\mathcal{C}_{zz}(t)}{2}, \tag{52}$$

where the autocorrelation function $\mathcal{C}_{zz}(t)$ has been previously defined in Eq. (32).

We can express this transition probability as a sum over Keldysh trajectories of the impurity spin. Denoting the path variables by $\sigma, \bar{\sigma}$, we can write the above equation as follows,

$$P_{\uparrow\uparrow}(t) = \sum_{\substack{\{\sigma^1=\uparrow,\downarrow,\,...,\,\sigma^{t-1}=\uparrow,\downarrow\}\\ \{\bar{\sigma}^1=\uparrow,\downarrow,\,...,\,\bar{\sigma}^{t-1}=\uparrow,\downarrow\}}} \prod_{\tau=0}^{t-1} \langle\sigma^{\tau+1}|\exp(i\tilde{\epsilon}\hat{\sigma}_x)|\sigma^\tau\rangle\,\langle\bar{\sigma}^{\tau+1}|\exp(-i\tilde{\epsilon}\hat{\sigma}_x)|\bar{\sigma}^\tau\rangle\; e^{ih(\sigma^\tau-\bar{\sigma}^\tau)} \;\times\; \mathcal{I}(\{\sigma,\bar{\sigma}\})\,. \tag{53}$$

Switching to the sojourn-blip parameterization in Eq. (42), see Fig. 6, we can rewrite Eq. (53) as follows:

$$P_{\uparrow\uparrow}(t) \;=\; \sum_{n\geq 0} (-)^n (\cos\tilde{\epsilon}\sin\tilde{\epsilon})^{2n} \;\times \sum_{0\leq t_0<\cdots<\tau_n<t} \;\sum_{\mathbf{c}_0,\mathbf{q}_1,\mathbf{c}_1,\ldots,\mathbf{c}_{n-1},\mathbf{q}_n,\mathbf{c}_n} \left(\prod_{j=0}^{n} \widetilde{\mathcal{W}}[\mathbf{c}_j]\right) \left(\prod_{i=1}^{n} \widetilde{\mathcal{W}}[\mathbf{q}_i]\, e^{2ih\mathcal{M}[\mathbf{q}_i]}\right) \times \mathcal{I}[\mathbf{q}_1,\mathbf{c}_1,\ldots,\mathbf{c}_{n-1},\mathbf{q}_n]\,. \quad (54)$$

Now the sum over paths is arranged as a summation over the number of blips, over their positions in time, and over the internal configurations of individual sojourns and blips. In this equation, we have combined the intra-sojourn and intra-blip kick transition amplitudes into the terms

$$\widetilde{W}[\mathbf{c}] \;=(\cos^2\tilde{\epsilon})^{\Delta t-1-K[\mathbf{c}]}\;(-\sin^2\tilde{\epsilon})^{K[\mathbf{c}]} \quad (55)$$

$$\widetilde{W}[\mathbf{q}] =(\cos^2\tilde{\epsilon})^{\Delta\tau-1-K[\mathbf{q}]}\;(-\sin^2\tilde{\epsilon})^{K[\mathbf{q}]} \quad (56)$$

where $K[\mathbf{c}]$ ($K[\mathbf{q}]$) is the number of domain walls in the sojourn or blip configuration, and we have defined the total magnetization a blip,

$$\mathcal{M}[\mathbf{q}]=\sum_{\tau=1}^{\Delta\tau} m[q^\tau], \quad \text{with } m[q_\uparrow]=+1,\; m[q_\downarrow]=-1. \quad (57)$$

The above equations show that for weak kicks $|\tilde{\epsilon}|\ll 1$ of the impurity spin, the sum over trajectories will be dominated by terms with a low density of blips. In fact, the kick strength $\tilde{\epsilon}$ acts as a "chemical potential" for blips. Thus, in most of the relevant blip configurations, we may treat the blips as noninteracting, i.e., substitute

$$\mathcal{I}[\mathbf{q}_1,\mathbf{c}_1,\mathbf{q}_2,\mathbf{c}_2,\ldots,\mathbf{c}_{n-1},\mathbf{q}_n] \;\simeq\; \mathcal{I}[\mathbf{q}_1]\,\mathcal{I}[\mathbf{q}_2]\,\ldots\,\mathcal{I}[\mathbf{q}_n]\,. \quad (58)$$

The success of this non-interacting blip approximation (NIBA), discussed at length by Leggett *et al.* in the context of a two-level system coupled to a bath of independent harmonic oscillators [28], relies on the typical interblip distance being larger than the blip interaction range.

The factorized form of the IM in Eq. (58) allows us to analytically compute the polarization decay rate of the impurity. After this simplification, the influence matrix in Eq. (54) does not depend on the sojourns' internal structure. The summation over all configurations of one sojourn yields

$$\sum_{\mathbf{c}:|\mathbf{c}|=\Delta t} \widetilde{W}[\mathbf{c}] = 2\,(\cos(2\tilde{\epsilon}))^{\Delta t-1}\,. \quad (59)$$

Note that the first and last spin are restricted to being $\sigma^0=\sigma^t=\uparrow$, which gives an extra overall factor of $1/4$; moreover, the term $n=0$ has both ends fixed and gives $\frac{1}{2}[1+\cos^t(2\tilde{\epsilon})]$. For blips, instead, we define the "dressed" single-blip weight

$$\widetilde{\mathcal{I}}(\Delta\tau)\equiv \sum_{\mathbf{q}:|\mathbf{q}|=\Delta\tau} \widetilde{W}[\mathbf{q}]\, e^{2ih\mathcal{M}[\mathbf{q}]}\,\mathcal{I}[\mathbf{q}]\,. \quad (60)$$

This quantity depends on how the environment suppresses individual blips, and should be considered as an input for the computation of the polarization decay. Note that the identities $\mathcal{M}[-\mathbf{q}]=-\mathcal{M}[\mathbf{q}]$, $\mathcal{I}[-\mathbf{q}]=\mathcal{I}[\mathbf{q}]^*$ imply that $\widetilde{\mathcal{I}}(\Delta\tau)$ is real.

Since we are interested in the asymptotic decay rate of $P_{\uparrow\uparrow}(t)$, it is convenient to compute its generating function (or a discrete Laplace transform),

$$\bar{P}_{\uparrow\uparrow}(\lambda)=\sum_{t=0}^{\infty} e^{-\lambda t} P_{\uparrow\uparrow}(t). \quad (61)$$

We split t into intervals according to Eq. (44), and, for each n, we perform the sums over the durations of blips and sojourns. For the blips, we define

$$\sum_{\Delta\tau=1}^{\infty} e^{-\lambda\Delta\tau}\widetilde{\mathcal{I}}(\Delta\tau)\equiv\bar{\mathcal{I}}(\lambda). \quad (62)$$

Putting everything together, we find

$$\bar{P}_{\uparrow\uparrow}(\lambda)=\frac{1}{2}\left\{\frac{1}{1-e^{-\lambda}}+\frac{1}{1-e^{-\lambda}\big[\cos(2\tilde{\epsilon})-2\cos^2(\tilde{\epsilon})\sin^2(\tilde{\epsilon})\,\bar{\mathcal{I}}(\lambda)\big]}\right\} \quad (63)$$

The long-time behavior of the polarization is governed by the asymptotics of $\bar{P}_{\uparrow\uparrow}(\lambda)$ for small argument. In particular, an exponential decay of the correlation function $\mathcal{C}_{zz}(t)$ in Eq. (32) with a rate $\gamma_{\rm eff}$ gives:

$$\bar{P}_{\uparrow\uparrow}(\lambda) \underset{\lambda\to 0}{\sim} \frac{P_{\rm av}}{\lambda}+\frac{1}{1-e^{-\gamma_{\rm eff}}}+\mathcal{O}(\lambda), \quad (64)$$

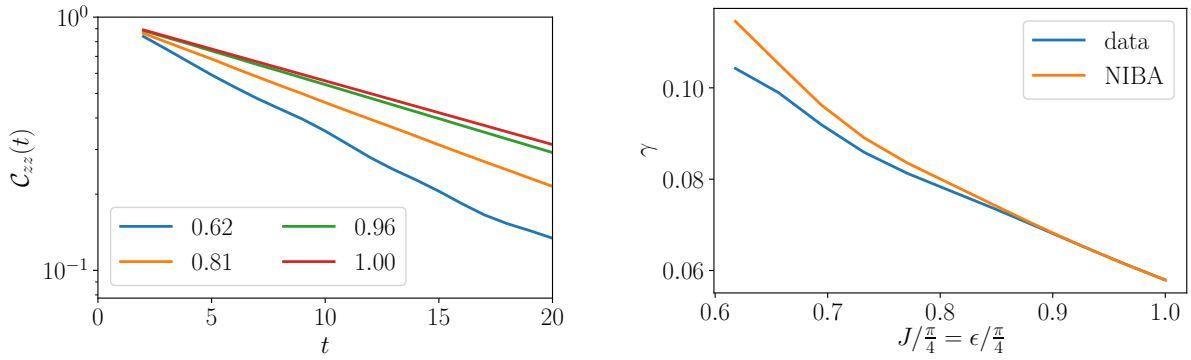

Figure 11. Left panel: dynamics of the polarization autocorrelation $\mathcal{C}_{zz}(t)$ defined in Eq. (32) of a slow spin, for $h = 0.29; \tilde{\epsilon} = 0.17$ and a range of values of $\epsilon = J$, in units of $\pi/4$ (reported in the legend). Right panel: comparison between the numerical (blue) and the theoretically predicted (orange) decay rates vs detuning from the PD point. The former is extracted by fitting the decay curves such as those in the left panel, while the latter is described by Eq. (66).

with

$$P_{\rm av} = \lim_{t\to\infty} P_{\uparrow\uparrow}(t) = \frac{1}{2}. \tag{65}$$

Comparing with the result in Eq. (63), we find

$$e^{-\gamma_{\rm eff}} = \cos(2\tilde{\epsilon}) - 2\cos^2(\tilde{\epsilon})\sin^2(\tilde{\epsilon}) \left(\sum_{\Delta\tau} \widetilde{\mathcal{I}}(\Delta\tau)\right). \tag{66}$$

For small $\tilde{\epsilon}$, this reduces, in the lowest non-vanishing order in $\tilde{\epsilon}$, to

$$\gamma_{\rm eff} \simeq 2\,\tilde{\epsilon}^2 \left[1 + \sum_{\Delta\tau} \widetilde{\mathcal{I}}(\Delta\tau)\right]. \tag{67}$$

This equation expresses the decay rate of a slow impurity spin coupled to a spin chain detuned from the PD point, which is a non-Markovian bath. In the limit of a perfect dephasing bath with $|\epsilon| = |J| = \pi/4$, where the blips are completely suppressed, the above equation reduces to the Markovian dynamics, as in Eq. (33). In fact, the first term in Eq. (67) represents the decay rate in this limit. This contribution is purely classical, as the environment completely suppresses interference between all pairs of quantum trajectories. The second term represents instead the noninteracting-blip contribution. This correction can be of either sign, due to the complex blip weights.

Blip interactions generate higher-order corrections to $\gamma_{\rm eff}$. Leaving their detailed analysis for future work, we note that such corrections can be systematically taken into account via a renormalization procedure, in which one progressively includes *connected* contributions of clusters of two, three, etc blips into $\widetilde{\mathcal{I}}(\Delta\tau)$. Such a scheme can be truncated as long as the series (54) is dominated by terms with a low density n/t of blips. For small $\tilde{\epsilon}$, this holds, since the blip density scales as $\mathcal{O}(\tilde{\epsilon}^2)$. The first correction arising from blip interactions is suppressed as $r\tilde{\epsilon}^2$, where r is an effective parameter describing the range of two-blip interactions. Note that the value of r may depend on the structure of the blips involved and model parameters, see e.g. Fig. 10. This will lead to a correction of the order $\mathcal{O}(r\tilde{\epsilon}^4)$ to the relaxation rate $\gamma_{\rm eff}$ in Eq. (67). For fixed $\tilde{\epsilon}$, this correction becomes increasingly important as one detunes the system from a perfect dephaser point, effectively enhancing the blip interaction range r.

We tested the predictions of Eq. (67) against our numerical computations, finding a good agreement in a broad range of model parameters. The comparison is shown in Fig. 11. In the left panel, the dynamics of the probe spin polarization autocorrelation $\mathcal{C}_{zz}(t)$ is plotted for increasing detuning $\delta\epsilon = \delta J$ of the chain from the perfect dephaser point, where the behavior is exactly exponential, $\mathcal{C}_{zz}(t) = \cos^t(2\tilde{\epsilon})$. As shown, the decay of $\mathcal{C}_{zz}(t)$ remains approximately exponential even for sizeable detunings. In the right panel, we compare the measured decay rate γ with the prediction of the NIBA in Eq. (66). For small detunings the approximation is excellent. A small discrepancy appears for larger detunings, which we attribute to the neglected contribution of blip interactions. The latter could be accounted for via the renormalization procedure briefly sketched above. We note that we found the range of quantitative validity of the NIBA to be sensitive to the value of the integrability-breaking parameter h. This can be attributed to the fact that, as we saw in the previous subsection, changing h tunes the range of blip interactions.

We conclude this section with some remarks. First, the blip gas approach presented above can be straightforwardly applied to more general systems than discussed here; for example, we expect that it works similarly for the class of random models introduced in Sec. III C upon detuning from the perfect dephaser limit, e.g., by decreasing the amount of randomness or the local Hilbert space dimension q.

Second, it is instructive to contrast this approach to the perturbation theory scheme set up in Ref. [57]. The

latter work expresses space-time correlators perturbatively in the detuning from the dual-unitary points of brickwork quantum circuits, and relies on a small space-time density of perturbed gates. In contrast, the influence matrix approach discussed here is non-perturbative at its core. While we found it convenient to focus here on a neighborhood of a dual-unitary point for conceptual clarity and clear numerical advantage, this is not at all a crucial ingredient; for instance, an MPS representation of the IM can also be efficient in very different regimes, e.g., when either parameter value J, ϵ or h is small [58], or in the presence of strong disorder [59]. Similarly, the blip gas analysis presented above is perturbative in the impurity's internal frequency scale, but not necessarily in the detuning from PD points, which enters non-perturbatively via the blip weights and interactions. The latter can be computed analytically or extracted numerically for general ergodic quantum circuits.

We finally briefly comment on the difference between the discrete spin dynamics studied above, and continuous evolution of a two-level system coupled to a bath of harmonic oscillators [28]. In the"strong decoherence limit", when blips are completely suppressed, the dynamics in the two cases is qualitatively different. In the continuous setting, a complete suppression of quantum interference resulting from strong interaction with the environment freezes the spin state and it cannot relax to equilibrium. This phenomenon is known as the quantum Zeno effect [60]. In the discrete case, blips are suppressed for $\tilde{\epsilon} = \pi/4$. Then, in contrast, the spin thermalizes over just one time step, as discussed in Sec. III D.

V. SUMMARY AND OUTLOOK

We have developed an approach to analyzing highly non-equilibrium dynamics of isolated many-body systems, inspired by the Feynman-Vernon influence functional formalism [27]. Focusing on a class of interacting Floquet models, we formulated the self-consistency equation for the influence matrix, and demonstrated that it can be analyzed using complementary analytical and numerical considerations in a whole range of model parameters. Therefore, both "solvable" perfect dephaser baths that are Markovian, and more generic non-Markovian models can be characterized within the IM approach. As an example, we analyzed the effect of a generic many-body system on an impurity spin coupled to it.

The influence matrix provides a novel probe for characterizing quantum chaos and its absence in many-body systems. Compared to spectral probes, such as level statistics, the advantage of the IM is that it provides detailed information regarding the memory time scales and temporal correlation functions. IMs also contain the information expressed by other previously studied dynamical probes, such as the Loschmidt echo, and the statistics of matrix elements of local operators. In future work, it will be interesting to develop a connection between the properties of the IM and the eigenstate thermalization hypothesis.

We have found a family of ergodic models (in particular, in the vicinity of the perfect dephaser points), where MPS-based methods are efficient for computing the IM. This stems from viewing the IM as a "wavefunction", whose "temporal entanglement" scales slowly with the evolution time. Interestingly, conventional methods relying on the smallness of spatial entanglement would not recognize such models as "easy". As a matter of fact, this represents the key distinction from conventional time-evolution methods based on tensor contractions sequentially in time. While these rely on truncating long-distance spatial correlations built up in the course of evolution, the IM approach relies instead on long-range correlations *in time* remaining low. This scheme could be expected to be suited to strongly chaotic quantum systems, which induce a rapid thermalization of subsystems initially out of equilibrium, thus quickly erasing local memory of the past. Presumably, this different principle of efficiency leads to a new "corner of solvability" in quantum many-body systems out of equilibrium, as we illustrated with the perfect dephaser family, where temporal entanglement is low and spatial entanglement is high. This insight complements previous works on Hamiltonian systems [19, 49, 61]. Interestingly, better compression schemes than conventional singular value truncations are conceivable, which could make the influence matrix approach even more numerically efficient and broaden its range of applicability. A possible idea draws on memory kernel approximations inspired by the theory of open quantum systems [62].

Our work also suggests several promising future directions. First, it appears that PD circuits can be found in higher dimensions. Second, it would be interesting to analyze the precise relation between PD and dual-unitary circuits. As we discussed (see also Refs. [25, 37]), dual-unitarity implies that a system is a PD, but we do not know whether the converse generally holds. Other promising generalizations of our approach include Hamiltonian systems and their dynamics at a finite, rather than infinite, temperature.

In future work, we plan to further analyze the interacting blip gas, and the effects of blip interactions on the impurity spin dynamics, as briefly discussed in the last Section. We envision that, detuning from PD points, the self-consistency equation for the IM may be solved perturbatively in the detuning. This, along with applying the IM approach to non-ergodic systems [59], will likely lead to a more complete characterization of non-equilibrium quantum matter.

VI. ACKNOWLEDGMENTS

This work was supported by the Swiss National Science Foundation. We thank Soonwon Choi and Ehud Altman for inspiring discussions. Computations were performed

at the University of Geneva on the "Baobab" HPC cluster.

Appendix A: General properties of influence matrices

In this Appendix we review the basic properties of Feynman-Vernon's influence functional, adapted from Ref. [27] to our discrete-time dynamics. For simplicity, we focus on two-level systems ($q = 2$); the generalization to the case of $q > 2$ is straightforward.

We consider a quantum spin (S) interacting with an environment (E). In the main text discussion, S is a spin at position p in a spin chain, and E is formed by all spins on previous positions $k < p$; here, however, for the sake of generality we keep the discussion more abstract. We assume the spin-environment interaction to be of the form $\hat{V}_{\rm int} = \hat{V}_S \otimes \hat{V}_E$. Without loss of generality, we take $\hat{V}_S = J\hat{\sigma}^z$, such that

$$\hat{U}_{\rm int} = e^{i(J\hat{\sigma}^z \otimes \hat{V}_E)}. \tag{A1}$$

The global Floquet operator has thus the form

$$\hat{F} = e^{iJ\hat{\sigma}^z \otimes \hat{V}_{\rm E}}\, \hat{U}_S \otimes \hat{U}_E, \tag{A2}$$

where $\hat{U}_S, \hat{U}_E$ are the parts of the Floquet operator acting on the spin and environment separately. We further assume that in the initial state

$$\rho = \rho_S \otimes \rho_E, \tag{A3}$$

such that the spin and environment are uncorrelated.

According to the standard laws of quantum mechanics, the transition probability $P_{\sigma^0 \to \sigma^t}$ for the spin S can be expressed as a discrete path integral [63]:

$$P_{\sigma^0\to\sigma^t} = \sum_{\{\sigma^1=\uparrow,\downarrow,\,\ldots,\,\sigma^{t-1}=\uparrow,\downarrow\}} \sum_{\{\bar\sigma^1=\uparrow,\downarrow,\,\ldots,\,\bar\sigma^{t-1}=\uparrow,\downarrow\}} \prod_{\tau=0}^{t-1} \langle\sigma^{\tau+1}|\hat{U}_S|\sigma^\tau\rangle \left\langle\bar\sigma^{\tau+1}|\hat{U}_S|\bar\sigma^\tau\right\rangle^* \times \mathcal{I}(\{\sigma,\bar\sigma\}), \tag{A4}$$

where we have collected the partial trace over the environment degrees of freedom into the *influence matrix*

$$\begin{aligned}\mathcal{I}(\{\sigma,\bar\sigma\}) &= {\rm Tr}_E\left(\hat{U}_E[\{\sigma\}]\;\hat\rho_E\;\hat{U}_E^\dagger[\{\bar\sigma\}]\right)\\ &= {\rm Tr}_E\Big(\big(\underbrace{e^{\pm iJ\hat{V}_{\rm E}}}_{\sigma^{t-1}=\pm}\hat{U}_E\big)\;\ldots\;\big(\underbrace{e^{\pm iJ\hat{V}_{\rm E}}}_{\sigma^{1}=\pm}\hat{U}_E\big)\;\hat\rho_E\;\big(\hat{U}_E^\dagger\underbrace{e^{\mp iJ\hat{V}_{\rm E}}}_{\bar\sigma^{1}=\pm}\big)\;\ldots\;\big(\hat{U}_E^\dagger\underbrace{e^{\mp iJ\hat{V}_{\rm E}}}_{\bar\sigma^{t-1}=\pm}\big)\Big).\end{aligned} \tag{A5}$$

In this expression, the modified environment evolution operator takes the form

$$\hat{U}_E[\{\sigma\}] = \prod_{\tau=1}^{\overleftarrow{t-1}} \hat{U}_E[\sigma^\tau = \pm] = \prod_{\tau=1}^{\overleftarrow{t-1}} e^{\pm iJ\hat{V}_{\rm E}}\,\hat{U}_E \tag{A6}$$

where the arrow denotes time-ordering of the matrix product and now the c-numbers $\{\sigma^\tau = \pm 1\}$ are given by the considered trajectory of the spin S. Inserting this expression into Eq. (A4) we reconstruct the full summation over Feynman histories of the composite system.

From expression (A5) for the influence matrix, it follows that $|\mathcal{I}| \le 1$. In particular, it is evident that the absolute value of the influence matrix may be smaller than 1 if the forward and backward trajectories differ. Indeed, when $\sigma^\tau = \bar\sigma^\tau$ for all τ's, the resulting "standard" time-evolution of the density matrix preserves its trace, giving $\mathcal{I}(\{\sigma,\sigma\}) = 1$.

More generally, if $\sigma^\tau = \bar\sigma^\tau$ for all $\tau > \tau_f$, the forward and backward evolution after τ_f cancel out. For this reason, we may always think of the Keldysh contour as extending up to time $+\infty$. Similarly, when the initial state is the infinite-temperature density matrix, the evolution up to τ_i cancels out if $\sigma^\tau = \bar\sigma^\tau$ for all $\tau < \tau_i$, and the Keldysh contour can be thought as extended from time $-\infty$.

The influence matrix is generally a complicated, nonlocal functional of the spin trajectory. As explained in Sec. IV B, we can parametrize a trajectory in terms of alternating classical ($\sigma^\tau = \bar\sigma^\tau$) and quantum ($\sigma^\tau \ne \bar\sigma^\tau$) intervals, referred to as "sojourns" and "blips", see Fig. 6.

We finally recall two simple and useful properties of influence functionals [27]. First, if the environment contains some degree of randomness, either in its Hamiltonian parameters (e.g., disorder or noisy couplings) or in its initial state (statistical mixture), the ensemble-averaged influence functional correctly describes the ensemble-averaged time-dependent observables:

$$\mathbb{E}\big(\mathcal{I}(\{\sigma,\bar\sigma\})\big) \quad\rightsquigarrow\quad \mathbb{E}\big(\hat{O}_S(\tau)\hat{O}_S(\tau')\big), \tag{A7}$$

where $\mathbb{E}(\,\cdot\,)$ denotes the ensemble-averaging over randomness. Second, if the system is coupled to multiple uncorrelated environments, the composite functional describing the simultaneous influence of all of them is the

product of the individual influence functionals:

$$S \cup E_1 \cup \cdots \cup E_n \quad \Longrightarrow \quad \mathcal{I}(\{\sigma, \bar{\sigma}\}) = \prod_{i=1}^{N} \mathcal{I}_{E_i}(\{\sigma, \bar{\sigma}\})\,. \tag{A8}$$

[1] Immanuel Bloch, Jean Dalibard, and Wilhelm Zwerger, "Many-body physics with ultracold gases," Rev. Mod. Phys. **80**, 885–964 (2008).

[2] Tim Langen, Remi Geiger, and Jörg Schmiedmayer, "Ultracold atoms out of equilibrium," Annual Review of Condensed Matter Physics **6**, 201–217 (2015).

[3] Luca D'Alessio, Yariv Kafri, Anatoli Polkovnikov, and Marcos Rigol, "From quantum chaos and eigenstate thermalization to statistical mechanics and thermodynamics," Advances in Physics **65**, 239–362 (2016).

[4] Rahul Nandkishore and David A. Huse, "Many-body localization and thermalization in quantum statistical mechanics," Annual Review of Condensed Matter Physics **6**, 15–38 (2015).

[5] Dmitry A. Abanin, Ehud Altman, Immanuel Bloch, and Maksym Serbyn, "Colloquium: Many-body localization, thermalization, and entanglement," Rev. Mod. Phys. **91**, 021001 (2019).

[6] Ehud Altman and Ronen Vosk, "Universal dynamics and renormalization in many-body-localized systems," Annual Review of Condensed Matter Physics **6**, 383–409 (2015).

[7] Fabien Alet and Nicolas Laflorencie, "Many-body localization: An introduction and selected topics," Comptes Rendus Physique **19**, 498 – 525 (2018).

[8] Anatole Abragam, *The principles of nuclear magnetism; Reprint with corrections*, International series of monographs on physics (Clarendon Press, Oxford, 1989).

[9] Mark S. Rudner, Netanel H. Lindner, Erez Berg, and Michael Levin, "Anomalous edge states and the bulk-edge correspondence for periodically driven two-dimensional systems," Phys. Rev. X **3**, 031005 (2013).

[10] Pedro Ponte, Z. Papić, François Huveneers, and Dmitry A. Abanin, "Many-body localization in periodically driven systems," Phys. Rev. Lett. **114**, 140401 (2015).

[11] Achilleas Lazarides, Arnab Das, and Roderich Moessner, "Fate of many-body localization under periodic driving," Phys. Rev. Lett. **115**, 030402 (2015).

[12] Dmitry A. Abanin, Wojciech De Roeck, and François Huveneers, "Theory of many-body localization in periodically driven systems," Annals of Physics **372**, 1 – 11 (2016).

[13] Vedika Khemani, Achilleas Lazarides, Roderich Moessner, and S. L. Sondhi, "Phase structure of driven quantum systems," Phys. Rev. Lett. **116**, 250401 (2016).

[14] Dominic V. Else, Bela Bauer, and Chetan Nayak, "Floquet time crystals," Phys. Rev. Lett. **117**, 090402 (2016).

[15] Frederik Nathan, Dmitry Abanin, Erez Berg, Netanel H. Lindner, and Mark S. Rudner, "Anomalous floquet insulators," Phys. Rev. B **99**, 195133 (2019).

[16] Soonwon Choi, Joonhee Choi, Renate Landig, Georg Kucsko, Hengyun Zhou, Junichi Isoya, Fedor Jelezko, Shinobu Onoda, Hitoshi Sumiya, Vedika Khemani, Curt von Keyserlingk, Norman Y. Yao, Eugene Demler, and Mikhail D. Lukin, "Observation of discrete time-crystalline order in a disordered dipolar many-body system," Nature **543**, 221–225 (2017).

[17] J. Zhang, P. W. Hess, A. Kyprianidis, P. Becker, A. Lee, J. Smith, G. Pagano, I. D. Potirniche, A. C. Potter, A. Vishwanath, N. Y. Yao, and C. Monroe, "Observation of a discrete time crystal," Nature **543**, 217–220 (2017).

[18] Guifré Vidal, "Efficient classical simulation of slightly entangled quantum computations," Phys. Rev. Lett. **91**, 147902 (2003).

[19] M. C. Bañuls, M. B. Hastings, F. Verstraete, and J. I. Cirac, "Matrix product states for dynamical simulation of infinite chains," Phys. Rev. Lett. **102**, 240603 (2009).

[20] Sebastian Paeckel, Thomas Köhler, Andreas Swoboda, Salvatore R. Manmana, Ulrich Schollwöck, and Claudius Hubig, "Time-evolution methods for matrix-product states," Annals of Physics **411**, 167998 (2019).

[21] Laurens Vanderstraeten, Jutho Haegeman, and Frank Verstraete, "Tangent-space methods for uniform matrix product states," SciPost Phys. Lect. Notes , 7 (2019).

[22] Vladimir Gritsev and Anatoli Polkovnikov, "Integrable Floquet dynamics," SciPost Phys. **2**, 021 (2017).

[23] Amos Chan, Andrea De Luca, and J. T. Chalker, "Solution of a minimal model for many-body quantum chaos," Phys. Rev. X **8**, 041019 (2018).

[24] M Akila, D Waltner, B Gutkin, and T Guhr, "Particle-time duality in the kicked ising spin chain," Journal of Physics A: Mathematical and Theoretical **49**, 375101 (2016).

[25] Bruno Bertini, Pavel Kos, and Toma ž Prosen, "Exact correlation functions for dual-unitary lattice models in $1+1$ dimensions," Phys. Rev. Lett. **123**, 210601 (2019).

[26] S. J. Garratt and J. T. Chalker, "Many-body quantum chaos and the local pairing of feynman histories," arxiv:2008.01697 (2020).

[27] R.P Feynman and F.L Vernon, "The theory of a general quantum system interacting with a linear dissipative system," Annals of Physics **24**, 118 – 173 (1963).

[28] A. J. Leggett, S. Chakravarty, A. T. Dorsey, Matthew P. A. Fisher, Anupam Garg, and W. Zwerger, "Dynamics of the dissipative two-state system," Rev. Mod. Phys. **59**, 1–85 (1987).

[29] A. Strathearn, P. Kirton, D. Kilda, J. Keeling, and B. W. Lovett, "Efficient non-Markovian quantum dynamics using time-evolving matrix product operators," Nature Communications **9**, 3322 (2018).

[30] Jinshuang Jin, Matisse Wei-Yuan Tu, Wei-Min Zhang, and YiJing Yan, "Non-equilibrium quantum theory for nanodevices based on the Feynman-Vernon influence functional," New Journal of Physics **12**, 083013 (2010).

[31] Shmuel Fishman, D. R. Grempel, and R. E. Prange, "Chaos, quantum recurrences, and anderson localization," Phys. Rev. Lett. **49**, 509–512 (1982).

[32] Maksym Serbyn, Z. Papić, and Dmitry A. Abanin, "Thouless energy and multifractality across the many-body localization transition," Phys. Rev. B **96**, 104201 (2017).

[33] For open chains, the trace is replaced by boundary vectors with uniform unit components.

[34] In our model, there is a strictly linear light cone. Therefore, a system of size $L > 2t$, effectively, is free of finite-size effects, and its dynamics at times $\tau \leq t$ is equivalent to that of an infinite system.

[35] B. Gutkin, P. Braun, M. Akila, D. Waltner, and T. Guhr, "Exact local correlations in kicked chains at light cone edges," arXiv:2004.08386 (2020).

[36] Boris Gutkin, Petr Braun, Maram Akila, Daniel Waltner, and Thomas Guhr, "Local correlations in dual-unitary kicked chains," arXiv:2001.01298 (2020).

[37] Lorenzo Piroli, Bruno Bertini, J. Ignacio Cirac, and Toma ž Prosen, "Exact dynamics in dual-unitary quantum circuits," Phys. Rev. B **101**, 094304 (2020).

[38] Hyungwon Kim, Tatsuhiko N. Ikeda, and David A. Huse, "Testing whether all eigenstates obey the eigenstate thermalization hypothesis," Phys. Rev. E **90**, 052105 (2014).

[39] Suhail Ahmad Rather, S. Aravinda, and Arul Lakshminarayan, "Creating ensembles of dual unitary and maximally entangling quantum evolutions," Phys. Rev. Lett. **125**, 070501 (2020).

[40] Pieter W. Claeys and Austen Lamacraft, "Maximum velocity quantum circuits," Phys. Rev. Research **2**, 033032 (2020).

[41] Pieter W. Claeys and Austen Lamacraft, "Ergodic and non-ergodic dual-unitary quantum circuits with arbitrary local Hilbert space dimension," arXiv:2009.03791 (2020).

[42] Adam Nahum, Sagar Vijay, and Jeongwan Haah, "Operator spreading in random unitary circuits," Phys. Rev. X **8**, 021014 (2018).

[43] Amos Chan, Andrea De Luca, and J. T. Chalker, "Spectral statistics in spatially extended chaotic quantum many-body systems," Phys. Rev. Lett. **121**, 060601 (2018).

[44] P. W. Brouwer and C. W. J. Beenakker, "Diagrammatic method of integration over the unitary group, with applications to quantum transport in mesoscopic systems," Journal of Mathematical Physics **37**, 4904–4934 (1996), https://doi.org/10.1063/1.531667.

[45] Vittorio Gorini, Andrzej Kossakowski, and E. C. G. Sudarshan, "Completely positive dynamical semigroups of N-level systems," Journal of Mathematical Physics **17**, 821–825 (1976).

[46] G. Lindblad, "On the generators of quantum dynamical semigroups," Communications in Mathematical Physics **48**, 119–130 (1976).

[47] H.-P. Breuer and F. Petruccione, *The theory of open quantum systems* (Oxford University Press, 2007).

[48] Johannes Hauschild and Frank Pollmann, "Efficient numerical simulations with Tensor Networks: Tensor Network Python (TeNPy)," SciPost Phys. Lect. Notes **5** (2018), 10.21468/SciPostPhysLectNotes.5, code available from `https://github.com/tenpy/tenpy`, arXiv:1805.00055.

[49] Alexander Müller-Hermes, J Ignacio Cirac, and Mari Carmen Banuls, "Tensor network techniques for the computation of dynamical observables in one-dimensional quantum spin systems," New Journal of Physics **14**, 075003 (2012).

[50] This is true for infinite-temperature ensembles. For general initial states, however, the influence matrix may depend nontrivially on the entire trajectory up to the last quantum state.

[51] Thomas Gorin, Tomaž Prosen, Thomas H. Seligman, and Marko Žnidarič, "Dynamics of loschmidt echoes and fidelity decay," Physics Reports **435**, 33 – 156 (2006).

[52] Pablo R Zangara and Horacio M Pastawski, "Loschmidt echo in many-spin systems: a quest for intrinsic decoherence and emergent irreversibility," Physica Scripta **92**, 033001 (2017).

[53] Asher Peres, "Stability of quantum motion in chaotic and regular systems," Phys. Rev. A **30**, 1610–1615 (1984).

[54] H.M Pastawski, P.R Levstein, G Usaj, J Raya, and J Hirschinger, "A nuclear magnetic resonance answer to the boltzmann–loschmidt controversy?" Physica A: Statistical Mechanics and its Applications **283**, 166 – 170 (2000).

[55] Toma ž Prosen, "General relation between quantum ergodicity and fidelity of quantum dynamics," Phys. Rev. E **65**, 036208 (2002).

[56] Maksym Serbyn and Dmitry A. Abanin, "Loschmidt echo in many-body localized phases," Phys. Rev. B **96**, 014202 (2017).

[57] Pavel Kos, Bruno Bertini, and Toma ž Prosen, "Correlations in perturbed dual-unitary circuits: Efficient path-integral formula," Phys. Rev. X **11**, 011022 (2021).

[58] Alessio Lerose, Michael Sonner, and Dmitry A. Abanin, "to appear," arXiv e-prints (2021).

[59] Michael Sonner, Alessio Lerose, and Dmitry A. Abanin, "Characterizing many-body localization via exact disorder-averaged quantum noise," arXiv e-prints , arXiv:2012.00777 (2020), arXiv:2012.00777 [cond-mat.dis-nn].

[60] B. Misra and E. C. G. Sudarshan, "The zeno's paradox in quantum theory," Journal of Mathematical Physics **18**, 756–763 (1977).

[61] M. B. Hastings and R. Mahajan, "Connecting entanglement in time and space: Improving the folding algorithm," Phys. Rev. A **91**, 032306 (2015).

[62] Dmitrii E. Makarov and Nancy Makri, "Path integrals for dissipative systems by tensor multiplication. Condensed phase quantum dynamics for arbitrarily long time," Chemical Physics Letters **221**, 482–491 (1994).

[63] R.P. Feynman, A.R. Hibbs, and D.F. Styer, *Quantum Mechanics and Path Integrals*, Dover Books on Physics (Dover Publications, 2010).

5 Exact disorder averaging and Many-Body localization

5.1 Introduction

Many-Body Localized (MBL) systems are interacting quantum systems which fail to thermalize due to strong disorder. Those quantum systems can stay coherent and are protected from heating, even in the presence of driving and in the absence of fine-tuning. This enables the realization of novel physical phases [137] such as time-crystals [19–22]. The lack of thermalization can be understood as the failure of MBL systems to act as thermal environments for their subsystems. For more details on thermalization and localization, I refer to Sec. 1.3 of this thesis. In this chapter we explore the structure of the IM across the MBL transition and leverage these results to provide an efficient numerical method to simulate disorder-averaged dynamics in MBL systems.

In the MBL phase, spatial entanglement entropy grows logarithmically in time [68], allowing in principle the use of MPS time evolution methods like TEBD to simulate dynamics for each disorder configuration [138]. However, the averaging of observables over disorder configurations can be challenging: Rare rare regions [139–142] can be impactful. Furthermore the effect of finite system sizes can be difficult to estimate [143].

Computing observables from the IM, using Eq. (2.5) is *linear* in the IM. We can therefore obtain the dynamics of the disorder-averaged observable by simply using the disorder-averaged IM. This is analogous of how the Keldysh path integral allows for disorder averaging [144, 145]. In one dimensional systems, if the disorder on the coupling is chosen independently for each site, we can use the algorithms described in Chap. 3 together with the disorder averaged transfer matrix to obtain the disorder-averaged IM. It should be noted that for discrete disorder, there are alternative methods to compute exactly disorder averaged observables using ancillary qubits[146].

Here we study the kicked Ising chain (KIC) with disordered longitudinal field [7, 147], which can be tuned from a fully localized MBL phase to the maximally chaotic dual unitary point [112] as well as Chap. 4. In this model, we find that the TE is low in both the strongly localized as well as in the strongly delocalized phase, which is due to the proximity to the dual unitary point and has been discussed in the previous chapter. Close to the MBL transition on the other hand TE increases rapidly, rendering MPS techniques inefficient. For those points in phase space, we defer to *exact diagonalization* computation which are accelerated by the use of the *Fast Walsh-Hadamard transformation*[148]. We use these IM to compute the *remanent magnetization* which can be seen as a dynamical order parameter for MBL [149], as well as study the IM structure.

Apart from being an efficient numerical tool, the IM formalism can serve as a starting

point for analytical studies of the MBL transition. We find that the MBL transition is reflected in a symmetry breaking on the space of trajectories. This is analogous to the symmetry breaking observed in the spectral form factor [150].

The MBL transition can further also be observed in the entanglement structure of the IM. While TE is low on both far ends of the transition in the KIC model, it is low due to different reasons. In localized phase, TE is low since the environment is effectively small, where as near the dual unitary point TE is low since information is dissipated quickly. This difference is reflected in the in the "unfolded" entanglement entropy, the entanglement entropy of the IM if the legs are ordered along the Keldysh contour as opposed to the "folded" entanglement entropy which we call TE, where the corresponding legs of the forward and backward contour are paired up [97–99]. The unfolded entanglement entropy in the localized phase is low, while it becomes volume law at the dual unitary point.

Characterizing many-body localization via exact disorder-averaged quantum noise

Michael Sonner,[1,*] Alessio Lerose,[1,*] and Dmitry A. Abanin[1]

[1] *Department of Theoretical Physics, University of Geneva, Quai Ernest-Ansermet 24, 1205 Geneva, Switzerland*

(Dated: 3rd January 2022)

Many-body localized (MBL) phases of disordered quantum many-particle systems have a number of unique properties, including failure to act as a thermal bath and protection of quantum coherence. Studying MBL is complicated by the effects of rare ergodic regions, necessitating large system sizes and averaging over many disorder configurations. Here, building on the Feynman-Vernon theory of quantum baths, we characterize the quantum noise that a disordered spin system exerts on its parts via an influence matrix (IM). In this approach, disorder averaging is implemented exactly, and the thermodynamic-limit IM obeys a self-consistency equation. Viewed as a wavefunction in the space of trajectories of an individual spin, the IM exhibits slow scaling of temporal entanglement in the MBL phase. This enables efficient matrix-product-states computations to obtain temporal correlations, providing a benchmark for quantum simulations of non-equilibrium matter. The IM quantum noise formulation provides an alternative starting point for novel rigorous studies of MBL.

Introduction — Many-body localization (MBL) in strongly disordered interacting quantum systems represents one of the rare known examples of a genuinely non-ergodic phase of quantum matter [1–3]. The phenomenology of the MBL phase [4–7], its persistence in periodically driven systems [8–10], and new phases of matter enabled by MBL [11] are being intensely investigated.

Unlike in conventional phase transitions, thermal ensembles bear no signatures of the MBL transition. Localization effects instead manifest themselves in the properties of individual highly-excited energy eigenstates, as well as in the coherent, far-from-equilibrium dynamics, which differ drastically from those in the thermalizing phase. In particular, MBL eigenstates exhibit boundary-law entanglement scaling [4, 12], similar to ground states of gapped systems [13]. Local memory of the initial state is preserved, owing to the emergence of local integrals of motion [4–7] – a signature that has been widely used to diagnose MBL in quantum quench experiments with ultracold atoms [14–16], trapped ions [17], and superconducting qubits [18].

The simultaneous presence of disorder and interactions, combined with a necessity to describe highly excited eigenstates, poses a major challenge for the theoretical description of MBL. Rigorous perturbative approaches are difficult, as they require treating disorder probabilistically [7] and incorporating the effects of rare regions [19]. Exact diagonalization (ED) studies [20–23] give access to excited eigenstates, but are limited in system size. Tensor-network approaches to MBL, relying on low real-space entanglement of MBL states, have been used to approximately construct eigenstates [24–27] and simulate non-equilibrium dynamics [28] beyond the reach of ED. While such investigations gave insights into MBL physics, their power is limited by finite-size and/or -time effects, and by the practical cost of sampling disorder configurations.

In this Article, we introduce a method for describing *disorder-averaged* dynamical properties of many-body systems, and apply it to a periodically driven (Floquet) spin model of MBL. We characterize the system's dynamics by its *influence matrix* (IM) [29], inspired by the Feynman-Vernon theory of a quantum particle interacting with a bath of harmonic oscillators [30, 31]. We use the IM to characterize how a quantum many-body system affects the time evolution of its local subsystems, i.e., how it acts as a "bath" on itself. An IM contains full information on temporal correlations of local operators, and can be viewed as a kind of generating functional of the system's self-induced quantum noise. This formalism is advantageous for MBL, as it naturally accommodates the thermodynamic limit and *exact* disorder averaging.

In one-dimensional homogeneous systems, the IM can be found from a linear self-consistency equation [29, 32]. While individual realizations of disordered systems have IMs that depend on position, averaging over a translationally invariant disorder distribution leads to a translationally invariant IM. Disorder-averaging, however, leads to terms which are non-local in time in the self-consistency equation. Below we argue that, in spite of this nonlocality, the disorder-averaged IM of a MBL system is characterized by low *temporal entanglement*. This opens the door to efficient matrix-product states (MPS) methods for computing disorder-averaged dynam-

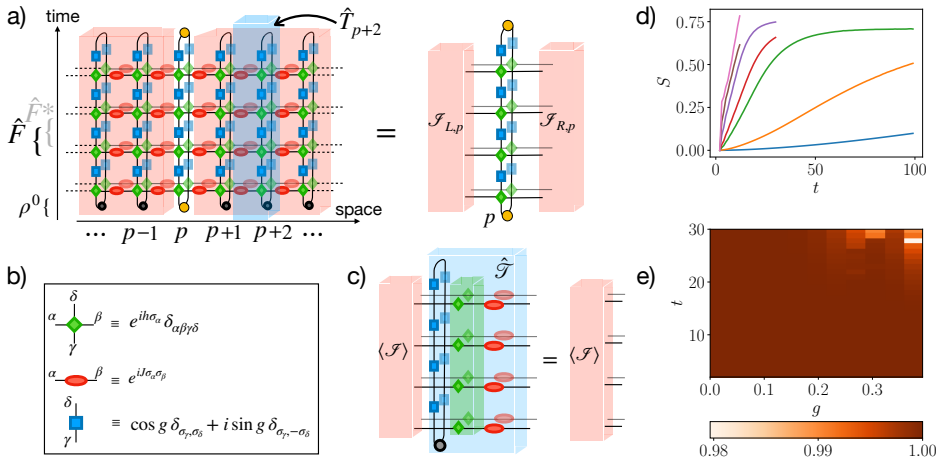

Figure 1. a) Circuit representation of a local temporal correlation function in the Keldysh path integral representation, Eq. (2), with circuit elements for model (1) defined in panel b). The two layers reflect forward and backward propagation of the system. Panel a) pictures Eq. (3). The blue shaded tensor represents the transfer matrix, defined in Eq. (4). Panel c) illustrates Eq. (5) (self-consistency equation). The green shaded tensor corresponds to non-local in time "interactions" arising from exact disorder averaging. d) Scaling of temporal entanglement of the IM for $J = g = 0.04, 0.08, 0.16, 0.20, 0.27$ (DMRG) and $J = g = 0.35, 0.51$ (ED), bottom to top. e) Expectation value of the transfer matrix applied to the MPS with bond dimension $\chi = 128$ obtained from DMRG.

ical properties. As a first application of the method, we compute the dynamical correlation functions of a MBL system up to long times.

The IM undergoes a drastic change when the system transitions from the ergodic to the MBL phase; MBL IMs are characterized by persistent quantum-interference effects, which express the fact that MBL systems are not efficient thermal baths. This can be viewed as the emergence of *temporal long-range order* in the statistical ensemble of local trajectories governed by the IM. Below, we will use an MPS approach to demonstrate this phenomenon [33].

Model — For concreteness, in this Article we will focus on the disordered kicked Ising chain (KIC), which provides a Floquet model of MBL [34, 35]. Time evolution of this system is governed by repeated applications of the Floquet operator,

$$\hat{F} = \exp\left(i\sum_j g\hat{\sigma}_j^x\right)\exp\left(i\sum_j J\hat{\sigma}_j^z\hat{\sigma}_{j+1}^z + h_j\hat{\sigma}_j^z\right), \tag{1}$$

where $\hat{\sigma}_j^\alpha$, $\alpha = x, y, z$, are Pauli matrices acting on site $j \in \mathbb{Z}$ of a linear chain. The phases h_j are independently drawn from a uniform distribution in $[-\pi, \pi)$. The Hamiltonian version of this model, obtained by substituting $J, g, h_j \mapsto \tau J, \tau g, \tau h_j$ in Eq. (1) and taking the continuous-time limit $\tau \to 0$, is similar to the model where MBL was rigorously established in the regime $g \ll 1$ [7]. MBL behavior is known to persist in the same regime for finite driving period $\tau > 0$ [8, 9, 34, 36, 37]. Setting $J = g$ in Eq. (1), ED studies indicate that the MBL phase extends to $|g| < g_* \approx 0.4$ [35]. For weaker disorder strength $|J| = |g| > g_*$ the disordered KIC is ergodic. In particular, at the self dual points $|J| = |g| = \pi/4$ signatures of chaotic behavior in spectral correlations have been obtained [38]. We note that other kicked Floquet models of MBL have been investigated [8, 37, 39].

Disorder-averaged influence matrix — The influence matrix encodes the full set of temporal correlations of local operators [29, 30]. To illustrate this, we consider the dynamical structure factor $\langle O_p(t)O_p(0)\rangle = \mathrm{Tr}(\hat{F}^{-t}O_p\hat{F}^t O_p\rho^0)$ of a local observable $O_p = \mathbb{1}\otimes\cdots\otimes\mathbb{1}\otimes O\otimes\mathbb{1}\otimes\cdots\otimes\mathbb{1}$ acting on spin p, using Keldysh path integral representation, graphically illustrated in Fig. 1(a,b),

$$\langle O_p(t)O_p(0)\rangle = \sum_{\{\sigma_j^\tau\},\{\bar{\sigma}_j^\tau\}} [O_p]_{\{\bar{\sigma}^t\},\{\sigma^t\}} \left[O_p\rho^0\right]_{\{\sigma^0\},\{\bar{\sigma}^0\}} \prod_j \prod_{\tau=0}^{t-1} W_{\sigma_j^{\tau+1}\sigma_j^\tau} W^*_{\bar{\sigma}_j^{\tau+1}\bar{\sigma}_j^\tau}\, e^{iJ\left(\sigma_j^\tau\sigma_{j+1}^\tau - \bar{\sigma}_j^\tau\bar{\sigma}_{j+1}^\tau\right) + ih_j\left(\sigma_j^\tau - \bar{\sigma}_j^\tau\right)} \tag{2}$$

where $W_{\sigma'\sigma} = \langle\sigma'|e^{ig\hat{\sigma}^x}|\sigma\rangle$. We say that configurations σ_j^τ associated with the operator $\hat{F}^t$ are on the *forward* time path and those $\bar{\sigma}_j^\tau$ associated with $\hat{F}^{-t}$ on the *backward* path. The summation is over all spin trajectories $\{\sigma_j^\tau = \pm 1\}, \{\bar{\sigma}_j^\tau = \pm 1\}$ extending from time $\tau = 0$ to $\tau = t$. Assuming that the initial density matrix $\rho^0 = \otimes_j \rho_j^0$ is a product operator, we formally perform the summation over trajectories of all spins on the left $\{\sigma_{j<p}^\tau\}, \{\bar{\sigma}_{j<p}^\tau\}$ and on the right $\{\sigma_{j>p}^\tau\}, \{\bar{\sigma}_{j>p}^\tau\}$ of spin p in Eq. (2), obtaining

$$\langle O_p(t)O_p(0)\rangle = \sum_{\{\sigma^\tau\},\{\bar{\sigma}^\tau\}} \mathscr{I}_{L,p}[\{\sigma^\tau,\bar{\sigma}^\tau\}]\Big([O]_{\bar{\sigma}^t\sigma^t} \prod_{\tau=0}^{t-1} W_{\sigma^{\tau+1}\sigma^\tau} W^*_{\bar{\sigma}^{\tau+1}\bar{\sigma}^\tau} e^{ih_p(\sigma^\tau-\bar{\sigma}^\tau)} \left[O\rho_p^0\right]_{\sigma^0\bar{\sigma}^0} \Big) \mathscr{I}_{R,p}[\{\sigma^\tau,\bar{\sigma}^\tau\}] \tag{3}$$

where we have denoted the result of the summation over spins on the left (right) as the left (right) *influence matrix* $\mathscr{I}_{L(R),p}$ acting on the forward and backward trajectories $\{\sigma^\tau\}, \{\bar{\sigma}^\tau\}$, $0 \le \tau \le t-1$ of spin p only. These objects, graphically represented in Fig. 1(a), capture the influence the rest of the system has on the dynamics of spin p. Clearly, expression (3) can be straightforwardly generalized to arbitrary time-ordered temporal correlations of local operators $\langle O_p^{(n)}(t_n)\cdots O_p^{(1)}(t_1)\rangle$.

In a chain (or, more generally, in loop-free geometries), an influence matrix can be recursively computed from influence matrices of smaller subsystems, as illustrated from in Fig. 1(a,c). For a finite system of N spins, this can be concisely expressed by introducing transfer matrices $\hat{T}_j$ acting along the space direction, i.e., $\mathscr{I}_{L,p} = \left(\prod_{j=1}^{p-1} \hat{T}_j\right) \mathscr{I}_0$ and $\mathscr{I}_{R,p} = \left(\prod_{j=N}^{p+1} \hat{T}_j\right) \mathscr{I}_0$, with

$$[T_j]_{\{\sigma,\bar{\sigma}\},\{s,\bar{s}\}} = \left(\prod_{\tau=0}^{t-1} e^{iJ(\sigma^\tau s^\tau - \bar{\sigma}^\tau \bar{s}^\tau)}\right) e^{ih_j \sum_{\tau=0}^{t-1}(s^\tau - \bar{s}^\tau)} \left(\delta_{s^t\bar{s}^t} \prod_{\tau=0}^{t-1} W_{s^{\tau+1}s^\tau} W^*_{\bar{s}^{\tau+1}\bar{s}^\tau} \left[\rho_j^0\right]_{s^0\bar{s}^0}\right), \tag{4}$$

and open boundary condition $\mathscr{I}_0[\{s,\bar{s}\}] \equiv 1$.

We are interested in disorder-averaged temporal correlations such as $\langle\langle O_p(t)O_p(0)\rangle\rangle$. Since the random field h_j is uncorrelated and equally distributed at each lattice site, the averaged transfer matrices $\langle\hat{T}_j\rangle = \hat{\mathcal{T}}$ are translationally invariant, provided the initial density matrices ρ_j^0 are the same. Unitarity of time evolution for a periodic chain of arbitrary size N gives $\mathrm{Tr}(\hat{\mathcal{T}}^N) \equiv \langle\langle \mathbb{1}\rangle\rangle = 1$; hence, $\hat{\mathcal{T}}$ has a single non-vanishing and non-degenerate eigenvalue equal to 1. The "bulk" disorder-averaged influence matrix $\langle\mathscr{I}\rangle = \hat{\mathcal{T}}^\ell \mathscr{I}_0$, with $\ell > t$, is thus real [40], and can be identified with the single eigenvector of $\hat{\mathcal{T}}$, i.e., by the characteristic *self-consistency equation*

$$\hat{\mathcal{T}}\langle\mathscr{I}\rangle = \langle\mathscr{I}\rangle. \tag{5}$$

Due to the absence of correlations in the initial state and the strictly linear light-cone effect in this Floquet model, finite-size effects are present only at a distance $\ell \le t$ from the boundaries [41].

Disorder averaging in model (1) can be carried out explicitly [38]: since disorder is random in space but uniform in time, averaging introduces non-local in time "interactions". Indeed, integrating over h_j in Eq. (4) transforms the corresponding phase term into a constraint $\delta\big(\sum_{\tau=0}^{t-1}(s^\tau - \bar{s}^\tau)\big) \equiv \delta_{M,\overline{M}}$, which couples the configurations of the considered spin between all times. Such a term cancels interference between forward and backward trajectories with different total magnetization $M \neq \overline{M}$, and is responsible for the development of long-range temporal correlations in the MBL phase.

MPS approach and temporal entanglement — To gain an insight into the structure of the IM in the MBL phase, we approximate the solution of the self-consistency equation (5) by an MPS ansatz with a maximal bond dimension χ. The reliability of this approximation depends on the amount of "bipartite entanglement" in the IM interpreted as a many-body "wavefunction" in the 4^t-dimensional space of forward/backward spin trajectories. This *temporal entanglement* (TE) may be considered as a quantifier of the system's dynamics computational complexity.

Previously, we have shown [29] that the maximal (half-chain) von Neumann entanglement entropy $S(t/2)$ of the infinite-temperature folded IM —

obtained by considering $\sigma^\tau, \bar{\sigma}^\tau$ as a single 4-dit, cf. Fig. 1(a-c) — is exactly zero when $|J| = |g| = \pi/4$ for any h_j [42] thanks to the fact that the system acts as a perfectly dephasing (PD) Markovian bath. However, detuning away from these PD points, the entanglement $S(t/2)$ acquires "volume-law" scaling with t, albeit with a prefactor that vanishes as those points are approached. This scaling is expected to be a generic feature of thermalizing phases, and generally prevents MPS description from being efficient at long times, except near "special" points [29].

In contrast, we find that MPS methods remain efficient in the MBL phase up to long times, thanks to the slow scaling of TE. To implement MPS algorithms, we work in the folded picture [29, 32, 43]. The disorder-averaged transfer matrix $\hat{\mathcal{T}}$ is represented as a matrix product operator (MPO), which consists of the diagonal two-site matrices W, the global projection operator $\delta_{M,\overline{M}}$ originating from averaging over the random phase h, and the factorized operator dependent on the interaction strength J [see Eq. (4)]. The first and last operators can be expressed as MPOs with bond dimension 4 and 1, respectively. The projection operator can be expressed as a MPO with maximal bond dimension t [44]. Thus, the maximal bond dimension of $\hat{\mathcal{T}}$ is $4t$.

To find the IM one can iteratively apply the transfer matrix to the boundary vector $\mathscr{I}_0$. This approach was used to obtain the ED results, but it does not yield a good approximation of the optimal MPS at a fixed bond dimension, mainly due to the relatively large bond dimension of the MPO. To mitigate this problem we refine the MPS afterwards by using the density matrix renormalization group (DMRG) algorithm [45]. We estimated the quality of the MPS representation using several metrics [44], including the proximity of the eigenvalue obtained from DMRG to the exact value 1 (see Fig. 1(e)).

We have used a combination of the MPS method and ED to analyze the infinite-temperature IM's TE across the MBL transition in model (1), see Fig. 1(d). In the ergodic phase, TE increases fast with t, similarly to generic non-disordered thermal systems [29], which restricts us to the ED approach and thus limited time. However, this behavior drastically changes in the MBL phase, where TE exhibits an initial rise followed by a crossover to a very slow growth. Interestingly, the crossover occurs at longer times at smaller values of g. We remark that the TE patterns in the MBL phase and near PD points are qualitatively different: in [44], we show that TE of unfolded IM remains low in the former case, and is high in the latter case.

MBL and temporal long-range order — The IM contains information about the full *disorder-averaged* quantum noise spectrum of a system, allowing for a computation of time-dependent correlation functions. Here we consider the infinite temperature correlator of the local magnetization, $\langle\langle \hat{\sigma}^z_p(t)\hat{\sigma}^z_p(0)\rangle\rangle$, whose long-time behavior provides a direct probe of ergodicity breakdown in the MBL phase, widely used in experiments [14]; in this case, this correlator does not decay to zero as $t \to \infty$, indicating remanent magnetization. From a theory standpoint, the time-averaged remanent magnetization is of key importance, since it reflects the emergence of LIOMs, providing a dynamical order parameter of MBL [46]. Analysis of this quantity [47] is challenging due to inevitable presence of rare resonances, which have to be treated non-perturbatively [7]. In contrast, disorder-averaged IM contains the contribution of all resonances that are effective up to time t. Using formula (3) and the MPS representation of the IM obtained by DMRG, we calculate the disorder-averaged correlator $\langle\langle \hat{\sigma}^z(t)\hat{\sigma}^z(0)\rangle\rangle$ [Fig. 2(a)]. We observe that at strong disorder the magnetization saturates to a finite value, signalling MBL, while in the critical region it continues decaying at accessible time scales. Note that increasing bond dimension from $\chi = 128$ to $\chi = 256$ gives rise to a slower decay of magnetization. This indicates that $\chi = 128$ is not sufficient to faithfully capture the IM in the critical region, where, as seen in Fig. 1(d), TE is relatively high.

Next, we inquire into the difference of the IM between the MBL and the ergodic phase. The general structure of the IM of a thermalizing bath has been studied for an ensemble of non-interacting harmonic oscillators [30, 31], and more recently for quantum spin chains [29]. In this case the IM strongly suppresses "quantum" trajectories where $\sigma^\tau \neq \bar{\sigma}^\tau$, behaving similarly to a source of classical noise. This causes the system to damp local quantum-interference effects and dephase its spins, thus erasing local memory after a finite correlation time. An MBL system, in contrast, does not act as an efficient bath upon itself, producing quantum noise that does not fully erase local memory of initial states. We find that here the quantum trajectories are only weakly suppressed, reflecting the key role of persistent interference processes.

The onset of remanent magnetization can be linked to the appearance of temporal long-range order in the IM. To that end, we write $\langle\langle Z\rangle\rangle \equiv$

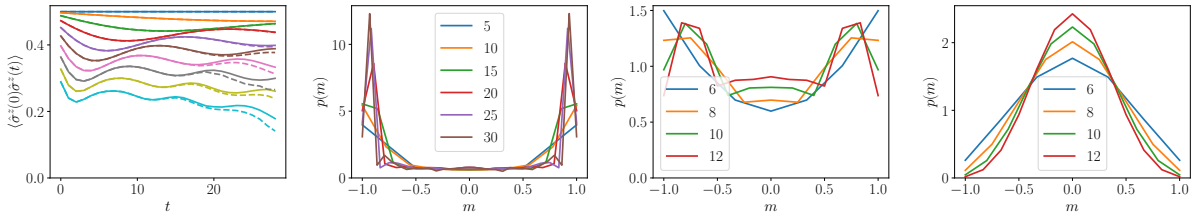

Figure 2. (a) Remanent magnetization $\langle\langle\hat{\sigma}^z(0)\hat{\sigma}^z(t)\rangle\rangle$ for different disorder strength equally spaced along the line $J = g = 0.04\ldots0.35$ (top to bottom curves). These computations were performed at bond dimensions $\chi = 256$ (solid) and $\chi = 128$ (dashed). Note that the computations are well-converged at stronger disorder, while in the critical regime ($g = 0.35$) increasing bond dimension slows down the magnetization decay, indicating that there $\chi = 128$ is not sufficient to faithfully approximate IM. (b-d) Probability density $p(m)$ of time-averaged magnetization sectors in the ensemble of local spin trajectories defined by the IM: in the MBL phase ($J = g = 0.27$) (b), in the transition region ($J = g = 0.47$)(c), and in the ergodic phase ($J = g = 0.71$) (d). Different curves correspond to different evolution times, specified in the legend.

$\lim_{t\to\infty}\frac{1}{t}\sum_{\tau=1}^{t}\langle\langle\hat{\sigma}_j^z(\tau)\hat{\sigma}_j^z(0)\rangle\rangle$ as follows:

$$\langle\langle Z\rangle\rangle = \lim_{t\to\infty}\frac{1}{2t^2}\sum_{\tau,\tau'=0}^{t}\sum_{\{\sigma^s\},\{\bar{\sigma}^s\}}\sigma^\tau\sigma^{\tau'} \times\delta\Big(\sum_s(\sigma^s-\bar{\sigma}^s)\Big)\prod_s W_{\sigma^{s+1},\sigma^s}\,W^*_{\bar{\sigma}^{s+1},\bar{\sigma}^s}\,\langle\mathscr{I}\rangle^2[\{\sigma,\bar{\sigma}\}],$$

[cf. Eq. (3)] where we took into account that left and right IM are equal to $\langle\mathscr{I}\rangle$. Next, we represent the r.-h.s. of Eq. (6) as a sum over sets of trajectories with fixed magnetization $M = \sum_s\sigma^s = \sum_s\bar{\sigma}^s$ [48]. That enables us to take the sum over τ,τ', which, within a given magnetization sector, yields M^2. Thus,

$$\langle\langle Z\rangle\rangle = \lim_{t\to\infty}\sum_{M=-t}^{t}(M/t)^2P(M) = \int_{-1}^{1}dm\,m^2p(m), \tag{7}$$

where

$$P(M) = \lim_{t\to\infty}\frac{1}{2}\sum_{\{\sigma^s\},\{\bar{\sigma}^s\}}\delta\left(\sum_s\bar{\sigma}^s - M\right)\delta\left(\sum_s\sigma^s - M\right)\prod_s W_{\sigma^{s+1},\sigma^s}\,W^*_{\bar{\sigma}^{s+1},\bar{\sigma}^s}\,\langle\mathscr{I}\rangle^2[\{\sigma,\bar{\sigma}\}], \tag{8}$$

is a positive "weight" representing the sum over trajectories in the sector with magnetization M. If the influence matrix is given as MPS, $P(M)$ can be expressed as a contraction with another MPS that implements the constraint $\delta\left(\sum_s\bar{\sigma}^s - M\right)\delta\left(\sum_s\sigma^s - M\right)$. Unitarity dictates that $\sum_M P(M) = 1$, and therefore $P(M)$ may be viewed as a probability. For convenience, we switch to the magnetization density $m = M/t$ in time and rescaled the probability density $p(m) = t\,P(M)$.

Expression (7) gives a necessary and sufficient criterion for MBL: ergodicity is broken, and local integrals of motion exist, if the probability distribution $p(m)$ for the time-averaged magnetization of individual-spin trajectories has a finite width in the infinite-time limit. In the ergodic phase, the width of $p(m)$ shrinks around its average $m = 0$ as $1/t$, satisfying central limit theorem scaling. We confirmed this by an exact computation at the self-dual points, which gives a binomial distribution $P(M) = 2^{-t}\binom{(t+M)/2}{t}$. However, as the MBL phase is approached, $p(m)$ develops two symmetric peaks at finite values $\pm m^*$. This highlights that the MBL phase dynamically breaks the $\mathbb{Z}_2$-symmetry of the disorder-averaged chain: Selecting "up" or "down" boundary conditions for the trajectory (i.e., initial and final state of spin p) produces a finite bias in the average magnetization towards the positive or negative side, respectively.

In Fig. 2(b-d) we report the results for the distribution $p(m)$ obtained with MPS for the MBL phase, and by ED at the transition and in the ergodic phase. It is apparent that $p(m)$ follows the above expectations, developing increasingly sharp peaks close to

$m = \pm 1$ in the MBL phase as the observation time window t is enlarged [panel (b)]; in contrast, in the ergodic phase [panel (d)], the distribution is single-peaked at $m = 0$ and narrows as t is increased. In the critical region between them [panel (c)], a peak at $m = 0$ is observed which slowly develops upon increasing t, reflecting the tendency to restoring thermal behavior at long times.

Summary and outlook — We have characterized a many-body, disordered system via its influence matrix, which fully describes its properties as a quantum bath. This approach allows for exact disorder averaging, therefore incorporating effects of rare regions on MBL. The slow increase of temporal entanglement in the MBL phase reflects that the system fails to act as a thermal bath on itself, and opens the door to efficient tensor-network approaches. We have implemented a proof-of-principle MPS algorithm and used it to extract time-dependent correlation functions that provide a benchmark for current quantum simulation experiments.

Looking forward, the slow entanglement scaling of IM in the MBL phase paves the way to constructing variational, and possibly exact, solutions for the self-consistency equation (5) in the limit $t \to \infty$. Such a solution, and its breakdown at weaker disorder due to proliferating resonances, will shed new light on MBL and the MBL-thermal transition. Finally, further applications of the IM approach may include other form of ergodicity breaking such as quantum scars, time crystals as well as circuits that combine unitary evolution with measurements or dissipation. Preliminary results [49] indicate that the temporal entanglement decreases when dissipation is added, broadening the applicability of our method.

Acknowledgments — We thank S. Choi, S. Garratt and L. Piroli for insightful discussions. A.L. acknowledges valuable discussions with G. Giudici and F. M. Surace on tensor-network implementations. The MPS computations in this work were performed using TeNPy [50]. This work is supported by the Swiss National Science Foundation nd by the European Research Council (ERC) under the European Union's Horizon 2020 research and innovation program (Grant Agreement No. 864597).

---

* These two authors contributed equally to this work

[1] R. Nandkishore and D. A. Huse, Annual Review of Condensed Matter Physics **6**, 15 (2015).
[2] D. A. Abanin, E. Altman, I. Bloch, and M. Serbyn, Rev. Mod. Phys. **91**, 021001 (2019).
[3] E. Altman, Nature Physics **14**, 979 (2018).
[4] M. Serbyn, Z. Papić, and D. A. Abanin, Phys. Rev. Lett. **111**, 127201 (2013).
[5] D. A. Huse, R. Nandkishore, and V. Oganesyan, Phys. Rev. B **90**, 174202 (2014).
[6] V. Ros, M. Müller, and A. Scardicchio, Nuclear Physics B **891**, 420 (2015).
[7] J. Z. Imbrie, Journal of Statistical Physics **163**, 998 (2016).
[8] P. Ponte, Z. Papić, F. Huveneers, and D. A. Abanin, Phys. Rev. Lett. **114**, 140401 (2015).
[9] A. Lazarides, A. Das, and R. Moessner, Phys. Rev. Lett. **115**, 030402 (2015).
[10] P. Bordia, H. Lüschen, U. Schneider, M. Knap, and I. Bloch, Nature Physics **13**, 460 (2017).
[11] R. Moessner and S. L. Sondhi, Nature Physics **13**, 424 (2017).
[12] B. Bauer and C. Nayak, Journal of Statistical Mechanics: Theory and Experiment **2013**, P09005 (2013).
[13] J. Eisert, M. Cramer, and M. B. Plenio, Rev. Mod. Phys. **82**, 277 (2010).
[14] M. Schreiber, S. S. Hodgman, P. Bordia, H. P. Lüschen, M. H. Fischer, R. Vosk, E. Altman, U. Schneider, and I. Bloch, Science **349**, 842 (2015).
[15] J.-y. Choi, S. Hild, J. Zeiher, P. Schauß, A. Rubio-Abadal, T. Yefsah, V. Khemani, D. A. Huse, I. Bloch, and C. Gross, Science **352**, 1547 (2016).
[16] A. Lukin, M. Rispoli, R. Schittko, M. E. Tai, A. M. Kaufman, S. Choi, V. Khemani, J. Léonard, and M. Greiner, Science **364**, 256 (2019).
[17] J. Smith, A. Lee, P. Richerme, B. Neyenhuis, P. W. Hess, P. Hauke, M. Heyl, D. A. Huse, and C. Monroe, Nat. Phys. **12**, 907 (2016).
[18] B. Chiaro, C. Neill, A. Bohrdt, M. Filippone, F. Arute, K. Arya, R. Babbush, D. Bacon, J. Bardin, R. Barends, S. Boixo, D. Buell, B. Burkett, Y. Chen, Z. Chen, R. Collins, A. Dunsworth, E. Farhi, A. Fowler, B. Foxen, C. Gidney, M. Giustina, M. Harrigan, T. Huang, S. Isakov, E. Jeffrey, Z. Jiang, D. Kafri, K. Kechedzhi, J. Kelly, P. Klimov, A. Korotkov, F. Kostritsa, D. Landhuis, E. Lucero, J. McClean, X. Mi, A. Megrant, M. Mohseni, J. Mutus, M. McEwen, O. Naaman, M. Neeley, M. Niu, A. Petukhov, C. Quintana, N. Rubin, D. Sank, K. Satzinger, A. Vainsencher, T. White, Z. Yao, P. Yeh, A. Zalcman, V. Smelyanskiy, H. Neven, S. Gopalakrishnan, D. Abanin, M. Knap, J. Martinis, and P. Roushan, "Direct measurement of non-local interactions in the many-body localized phase," (2020), arXiv:1910.06024 [cond-mat.dis-nn].
[19] W. De Roeck and F. m. c. Huveneers, Phys. Rev. B **95**, 155129 (2017).
[20] A. Pal and D. A. Huse, Phys. Rev. B **82**, 174411 (2010).
[21] D. J. Luitz, N. Laflorencie, and F. Alet, Phys. Rev. B **91**, 081103 (2015).
[22] X. Yu, D. J. Luitz, and B. K. Clark, Phys. Rev. B **94**, 184202 (2016).
[23] M. Serbyn, Z. Papić, and D. A. Abanin, Phys. Rev. B **96**, 104201 (2017).

[24] A. Chandran, J. Carrasquilla, I. H. Kim, D. A. Abanin, and G. Vidal, Phys. Rev. B **92**, 024201 (2015).

[25] M. Serbyn, A. A. Michailidis, D. A. Abanin, and Z. Papić, Phys. Rev. Lett. **117**, 160601 (2016).

[26] F. Pollmann, V. Khemani, J. I. Cirac, and S. L. Sondhi, Phys. Rev. B **94**, 041116 (2016).

[27] T. B. Wahl, A. Pal, and S. H. Simon, Phys. Rev. X **7**, 021018 (2017).

[28] M. C. Bañuls, N. Y. Yao, S. Choi, M. D. Lukin, and J. I. Cirac, Phys. Rev. B **96**, 174201 (2017).

[29] A. Lerose, M. Sonner, and D. A. Abanin, "Influence matrix approach to many-body floquet dynamics," (2020), arXiv:2009.10105 [cond-mat.str-el].

[30] R. Feynman and F. Vernon, Annals of Physics **24**, 118 (1963).

[31] A. J. Leggett, S. Chakravarty, A. T. Dorsey, M. P. A. Fisher, A. Garg, and W. Zwerger, Rev. Mod. Phys. **59**, 1 (1987).

[32] M. C. Bañuls, M. B. Hastings, F. Verstraete, and J. I. Cirac, Phys. Rev. Lett. **102**, 240603 (2009).

[33] We note that for problems with discrete disorder potential, an alternative tensor-network approach to disorder averaging exists [51].

[34] L. Zhang, V. Khemani, and D. A. Huse, Phys. Rev. B **94**, 224202 (2016).

[35] M. Sonner, M. Serbyn, Z. Papic, and D. A. Abanin, "Thouless energy in a floquet model of many-body localization," (2020), to appear.

[36] D. A. Abanin, W. D. Roeck, and F. Huveneers, Annals of Physics **372**, 1 (2016).

[37] C. Sünderhauf, D. Pérez-García, D. A. Huse, N. Schuch, and J. I. Cirac, Phys. Rev. B **98**, 134204 (2018).

[38] B. Bertini, P. Kos, and T. c. v. Prosen, Phys. Rev. Lett. **121**, 264101 (2018).

[39] A. Chan, A. De Luca, and J. T. Chalker, Phys. Rev. Lett. **121**, 060601 (2018).

[40] By virtue of the $\mathbb{Z}_2$ symmetry of the model.

[41] Mathematically, this means that the null subspace of $\hat{\mathcal{T}}$ fractures into nilpotent Jordan blocks of size $\leq t$.

[42] L. Piroli, B. Bertini, J. I. Cirac, and T. c. v. Prosen, Phys. Rev. B **101**, 094304 (2020).

[43] A. Müller-Hermes, J. I. Cirac, and M. C. Banuls, New Journal of Physics **14**, 075003 (2012).

[44] See Suplemental online material for details on the numerical methods used in the main text. Contains references [52, 53].

[45] U. Schollwöck, Annals of physics **326**, 96 (2011).

[46] A. Chandran, I. H. Kim, G. Vidal, and D. A. Abanin, Phys. Rev. B **91**, 085425 (2015).

[47] V. Ros and M. Müller, Phys. Rev. Lett. **118**, 237202 (2017).

[48] We remind that the delta-function there originates from disorder-averaging, which effectively cancels out interference terms between sectors with different magnetization.

[49] M. Sonner, A. Lerose, and D. A. Abanin, in preparation.

[50] J. Hauschild and F. Pollmann, SciPost Phys. Lect. Notes , 5 (2018), code available from `https://github.com/tenpy/tenpy`, arXiv:1805.00055.

[51] B. Paredes, F. Verstraete, and J. I. Cirac, Phys. Rev. Lett. **95**, 140501 (2005).

[52] T. L. Lezama, S. Bera, and J. H. Bardarson, Physical Review B **99**, 161106 (2019).

[53] E. Stoudenmire and S. R. White, New Journal of Physics **12**, 055026 (2010).

Supplemental Material
Characterizing many-body localization via exact disorder-averaged quantum noise

Michael Sonner,[1,*] Alessio Lerose,[1,*] and Dmitry A. Abanin[1]

[1] *Department of Theoretical Physics, University of Geneva, Quai Ernest-Ansermet 24, 1205 Geneva, Switzerland*

(Dated: January 3, 2022)

In this Supplemental Material, we provide additional details on the numerical calculations used in the main text.

EXACT DIAGONALIZATION

As a benchmark for MPS calculations and to explore the ergodic side of the MBL transition, we employ an exact diagonalization (ED) code. To this end, we interpret the influence matrix (IM) $\mathscr{I}[\{\sigma,\bar\sigma\}]$ as a "wavefunction" in the 2^{2t}-dimensional vector space spanned by the basis $\{|\sigma_0=\pm,\dots,\sigma_{t-1}=\pm,\bar\sigma_{t-1}=\pm,\dots,\bar\sigma_0=\pm\rangle\}$. Accordingly, we express the transfer matrix $[\mathcal{T}]_{\{\sigma,\bar\sigma\},\{s,\bar s\}}$ in Eq. (5) of the main text [obtained by taking the average of Eq. (4) of the main text over the random phase h_j] as a product of three operators,

$$\hat{\mathcal{T}} = \hat{\mathcal{V}}\hat{\mathcal{P}}\hat{\mathcal{W}}\,, \tag{S1a}$$

$$[\mathcal{V}]_{\{\sigma,\bar\sigma\},\{s,\bar s\}} = \prod_{\tau=0}^{t-1}\exp\left(iJ\sigma^\tau s^\tau\right)\prod_{\tau=0}^{t-1}\exp\left(-iJ\bar\sigma^\tau\bar s^\tau\right)\,, \tag{S1b}$$

$$[\mathcal{P}]_{\{\sigma,\bar\sigma\},\{s,\bar s\}} = \prod_{\tau=0}^{t-1}\delta_{\sigma^\tau s^\tau}\prod_{\tau=0}^{t-1}\delta_{\bar\sigma^\tau\bar s^\tau}\left(\delta_{\sum_{\tau=0}^{t-2}s^\tau,\sum_{\tau=0}^{t-2}\bar s^\tau}\right)\,, \tag{S1c}$$

$$[\mathcal{W}]_{\{\sigma,\bar\sigma\},\{s,\bar s\}} = \prod_{\tau=0}^{t-1}\delta_{\sigma^\tau s^\tau}\prod_{\tau=0}^{t-1}\delta_{\bar\sigma^\tau\bar s^\tau}\left(\delta_{s_{t-1}\bar s_{t-1}}\prod_{\tau=0}^{t-2}W_{s^{\tau+1}s^\tau}W^*_{\bar s^{\tau+1}\bar s^\tau}\,\rho^0_{s^0\bar s^0}\right)\,, \tag{S1d}$$

where $W_{\sigma'\sigma}=\langle\sigma'|e^{ig\hat\sigma^x}|\sigma\rangle\equiv\cos g\,\delta_{\sigma',\sigma}+i\sin g\,\delta_{\sigma',-\sigma}$. This representation is illustrated in Fig. S1-(a,b). We note that the last kick has been erased compared to Fig. 1-(c) of the main text, exploiting its unitarity; a further simplification can be done to the first longitudinal field when $\rho^0=\mathbb{1}/2$ (infinite-temperature ensemble), imposing $s^0=\bar s^0$ in $\hat{\mathcal{P}}$. The combination of these two operations decreases the total dimensionality of the input and output vector space by a factor 4.

The matrices $\hat{\mathcal{W}}$ and $\hat{\mathcal{P}}$ are diagonal in the computational basis, which we can interpret as the $\hat\sigma^z$ product basis for our chain of $2t$ spins-1/2. Within this interpretation, the operator $\hat{\mathcal{V}}$ is diagonal in the $\hat\sigma^x$ product basis. We exploit this fact for an efficient implementation of the applications of $\hat{\mathcal{T}}$ via the Fast Walsh Hadamard transformation (FWHT)[S1], which can be used to convert between these two bases with $\mathcal{O}(t2^{2t-1})$ basic operations. Note that the FWHT is an involution. The algorithm to apply $\hat{\mathcal{T}}$ to an arbitrary vector thus reads:

1. multiply its components by the diagonal components of $\hat{\mathcal{P}}$ and $\hat{\mathcal{W}}$;
2. apply FWHT;
3. multiply the vector's components by the (now diagonal) components of $\hat{\mathcal{V}}$;
4. apply FWTH again.

To find the thermodynamic-limit IM we simply use this procedure t times starting from the boundary vector $\mathscr{I}_0[\{s,\bar s\}]\equiv 1$. For the infinite-temperature initial ensemble, $t/2$ iterations suffice. This algorithm spares us from constructing and diagonalizing $\hat{\mathcal{T}}$, thus allowing us to push our ED results up to $t=12$ with modest resources.

MATRIX PRODUCT STATES

For the matrix product state (MPS) method, we choose to work in the folded picture where each spin on the forward trajectory is paired up with its corresponding spin on the backward trajectory such that they form a 4-dimensional local space[S2]. This gives an open chain geometry, thus avoiding complications arising from periodic

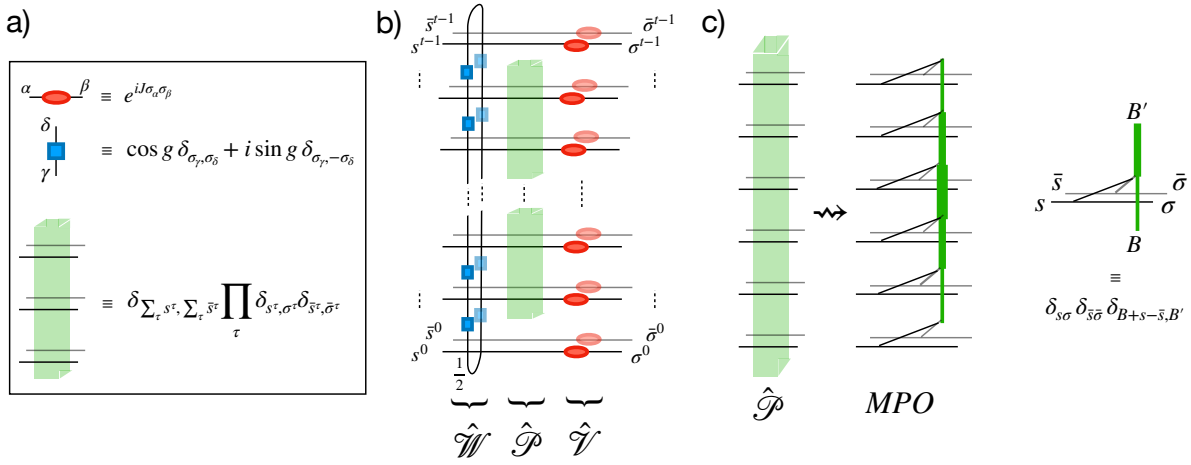

FIG. S1. Panels a), b): Graphical representation of Eqs. (S1). Panel c): Graphical illustration of the MPO representation of $\hat{\mathcal{P}}$ in Eq. (S4)

boundary conditions of the closed Keldysh contour, present in the unfolded representation. We label and order the basis vectors of this local space by $S = (s, \bar{s}) = (\uparrow,\uparrow), (\downarrow,\downarrow), (\uparrow,\downarrow), (\downarrow,\uparrow)$. It is straightforward to write the factors $\hat{\mathcal{V}}$ and $\hat{\mathcal{W}}$ in the transfer matrix decomposition in Eq. (S1) as matrix product operators (MPOs) of bond dimensions 1 and 4, respectively:

$$[\mathcal{V}]_{\{S^\tau\},\{\Sigma^\tau\}} = \prod_{\tau=0}^{t-1} \begin{pmatrix} 1 & 1 & e^{-2iJ} & e^{2iJ} \\ 1 & 1 & e^{2iJ} & e^{-2iJ} \\ e^{-2iJ} & e^{2iJ} & 1 & 1 \\ e^{2iJ} & e^{-2iJ} & 1 & 1 \end{pmatrix}_{S^\tau,\Sigma^\tau} \tag{S2}$$

$$[\mathcal{W}]_{\{S^\tau\},\{\Sigma^\tau\}} = \sum_{\{A^\tau\}} \mathbb{1}_{A^t} \prod_{\tau=0}^{t-1} \begin{pmatrix} \cos^2 g & \sin^2 g & i\sin g\cos g & -i\sin g\cos g \\ \sin^2 g & \cos^2 g & -i\sin g\cos g & i\sin g\cos g \\ i\sin g\cos g & -i\sin g\cos g & \cos^2 g & \sin^2 g \\ -i\sin g\cos g & i\sin g\cos g & \sin^2 g & \cos^2 g \end{pmatrix}_{A^{\tau+1},A^\tau} \delta_{A^\tau,S^\tau}\,\delta_{S^\tau,\Sigma^\tau}\,\rho^0_{A^0} \tag{S3}$$

In the second equation, the labels $\{A^\tau = (a^\tau, \bar{a}^\tau)\}$ of virtual bonds run over the bases of four-dimensional ancillary spaces isomorphic to the local folded spin spaces. The projection operator $\hat{\mathcal{P}}$ which arises from disorder averaging can be represented as a MPO with maximum bond dimension t. Here the virtual index B^T on each bond $(T, T+1)$ represents the difference in magnetization $\sum_{\tau=0}^{T} s^\tau - \bar{s}^\tau$ between the portions of forward and backward paths to the left of this bond. In other words, the local matrices

$$P^{S^\tau,\Sigma^\tau}_{B^\tau,B^{\tau+1}} = \delta_{S^\tau,\Sigma^\tau}\delta_{B^\tau+s^\tau-\bar{s}^\tau,B^{\tau+1}} \tag{S4}$$

composing the MPO, read the incoming virtual index B^τ and add the local magnetization difference $s^\tau - \bar{s}^\tau$ to it to produce the outgoing virtual index $B^{\tau+1}$. The value of the virtual index B^τ can thus remain unchanged, increase by one or decrease by one when proceeding to $B^{\tau+1}$, making the local bond dimension $\chi_\tau = 2\tau + 1$. Since $\hat{\mathcal{P}}$ globally projects onto the zero magnetization sector $\sum_\tau (s^\tau - \bar{s}^\tau) = 0$, we only need to carry virtual indices which are consistent with this sector. Thus the maximal bond dimension is t at the central bond(s) of the chain. This MPO is represented in Fig. S1-(c).

Due to the large bond dimension it is not possible to iteratively apply the transfer matrix MPO for $\hat{\mathcal{T}}$ to an MPS at once and compress the result. Instead the MPS needs to be compressed during the application of the MPO, using the zip-up method[S3]. We can improve the iterative MPS by feeding it into a two-site DMRG code where we target the eigenvector with largest absolute eigenvalue. As this method is variational, it avoids compounding errors in contrast to the iterative method[S4].

Different metrics of the quality of the MPS are displayed in Fig. S2. The role of energy in conventional DMRG is taken by the eigenvalue of the transfer matrix MPO in the last DMRG step. Due to the pseudo-projection property of $\hat{\mathcal{T}}$ (see the main text), the exact eigenvalue is 1. We can also inspect the discrepancy of the IM entry on classical

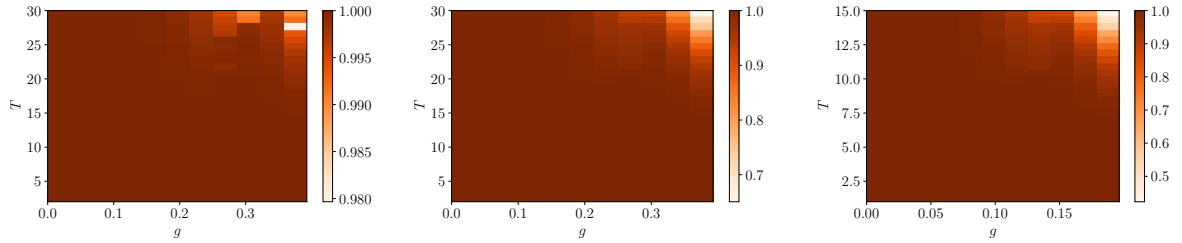

FIG. S2. Different metrics to assess the quality of the MPS representation of the IM, as a function of the model parameter $g = J$ and of the evolution time T. Left panel: DMRG eigenvalue of the transfer matrix; the exact value is 1 (see the main text). Middle panel: average IM elements of classical trajectories $\{\sigma = \bar{\sigma}\}$; the exact value of each of them is 1 (see Ref. S2). Right panel: expectation value of the identity matrix $\langle\langle \mathbb{1}(t)\mathbb{1}(0)\rangle\rangle$ [cf. Fig. 1-(a) of the main text] computed using the DMRG IM. For all the three metrics, depletion from the exact result is consistently observed for large T and large $J = g$.

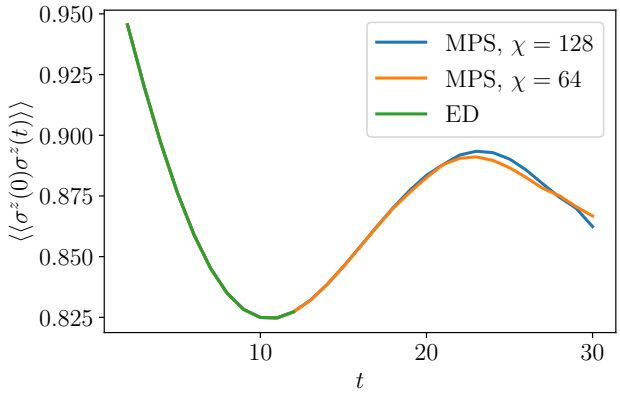

FIG. S3. Comparison between the evolution of the dynamical structure factor $\langle\langle\hat{\sigma}^z(t)\hat{\sigma}^z(0)\rangle\rangle$ computed with ED and MPS methods, for $J = g = 0.12$.

trajectories $\{\sigma = \bar{\sigma}\}$ from the exact value 1 (see Ref. S2). Last, we can compute the full path-integral of Fig. 1-(a) of the main text, with all observables of spin p set to identity, using the DMRG IMs. The exact value of this quantity is 1. We observe consistent deviations of the three metrics from their exact values for intermediate coupling strength (i.e., towards the MBL transition) and large times beyond the reach of ED, the last metric being the most sensitive. Furthermore, Fig. S3 shows the agreement between converged MPS data and ED data for the dynamical structure factor $\langle\langle\hat{\sigma}^z(t)\hat{\sigma}^z(0)\rangle\rangle$.

Lastly, we elucidate the differences in entanglement patterns between the MBL phase and the vicinity of PD points. Since both regions show low temporal entanglement (albeit scaling differently with the evolution time), it is legitimate to question the nature of this apparent similarity. The latter, however, disappears upon unfolding the IM wavefunction, as illustrated in Fig. S4. Here, we have the possibility to consider a bipartition separating forward and backward spins. The entanglement entropy $S_{f/b}(t)$ associated with such a bipartition is only low in the MBL phase, whereas it is large in the ergodic phase. At the self-dual point, in particular, we have $S_{f/b}(t) = (t+1)\log 2$, because the IM wavefunction is a product state of $t+1$ maximally entangled Bell pairs between each spin on the forward branch and its equal-time partner on the backward branch. This occurrence is interpreted as follows. In the MBL phase, there exist as much correlations between spins on the same time branch as between spins on opposite time branches. Conversely, ergodicity produces strong correlations between forward and backward trajectories: a manifestation of the suppression of quantum interference.

---

* These two authors contributed equally to this work

[S1] T. L. Lezama, S. Bera, and J. H. Bardarson, Physical Review B **99**, 161106 (2019).

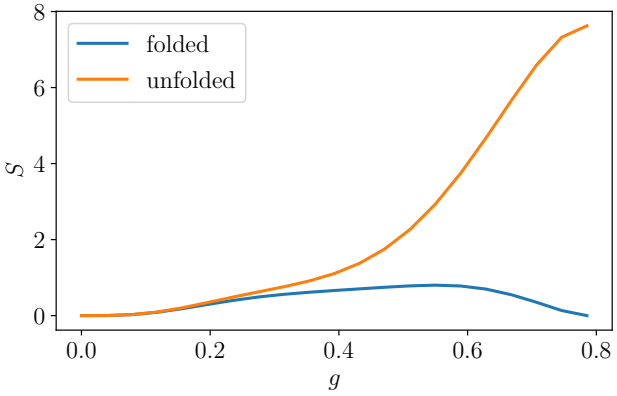

FIG. S4. Entanglement pattern across the MBL transition. Data are obtained from ED computations of the IMs for $t = 12$. The two curves show the bipartite entanglement entropy of the IM wavefunction corresponding to two structurally different bipartitions. The "folded" curve shows $S(t/2)$ of the folded IM, as in the main text; this quantity is low both near the fully decoupled line $J = 0$ and near the self-dual point $J = g = \pi/4$. The "unfolded" curve $S_{f/b}(t)$ corresponds instead to bipartitioning the chain into forward and backward spins; this quantity is only low in the MBL phase, but is very large in the ergodic phase.

[S2] A. Lerose, M. Sonner, and D. A. Abanin, "Influence matrix approach to many-body floquet dynamics," (2020), arXiv:2009.10105 [cond-mat.str-el].
[S3] E. Stoudenmire and S. R. White, New Journal of Physics **12**, 055026 (2010).
[S4] U. Schollwöck, Annals of physics **326**, 96 (2011).

6 Influence matrices of fermionic baths and Quantum Impurity problems

6.1 Introduction

Quantum impurity models (QIM) are models where an interacting impurity is coupled to environments consisting of non-interacting fermions. Even though only a small part of such systems is interacting, they still exhibit a wide variety of phenomena[151–154]. Experimentally such models can be realized on different platforms such as mesoscopic systems consisting of quantum dots coupled to leads [152, 155, 156], or more recently, ultra-cold atom experiments [157–159].

Apart from having rich physics their own, quantum impurity problems are also central to various numerical approaches to correlated matter. In dynamical mean field theory (DMFT)[160] and its non-equilibrium extensions [161], the local environment of an interacting site is approximated as being non-interacting. The hybridization function which characterizes these local environments is calculated self-consistently by solving the local QIM.

Given the ubiquity and importance of QIM, numerous approaches to solve them numerically have been proposed over the years. In equilibrium, various quantum monte-carlo methods (QMC) [162–164] and numerical renormalization group (NRG)[165, 166] have been shown to to be efficient in finding the imaginary time green's function of the impurity. Both methods are routinely used in state of the art DMFT codes[167–169].

Describing out-of-equilibrium systems like quenched systems or stationary currents remains a major challenge. While QMC approaches are widely successful for the equilibrium problem, in out-of-equilibrium problems, these approaches often suffer from the dynamical fermionic sign problem, fundamentally due to the complex phases in the time evolution operator. However, there is remarkable progress in mitigating this issue in QMC approaches [170–176]. Another common class of approaches works by mapping the fermionic environment to a chain via Wilson's NRG method[165, 177–181] or orthogonal polynomials[182, 183] and using conventional MPS methods to compute time evolution. NRG approaches have been extended to real-time problems as well[184, 185].

The IM formalism is particularly well suited to study out-of-equilibrium problems involving environments consisting of non-interacting fermions, since those environments have low TE[5, 6, 10, 119]. A qualitative argument for low TE in free fermion systems is given in Sec. 3.3 of this thesis.

In principle, one could map any fermionic bath to a fermionic chain using methods like Wilson's NRG approach[165] or orthogonal polynomials[182, 186]. This chain could then be discretized in time and the IM can be computed using the light-cone growth

algorithm laid out in Chap. 3.4 to contract the resulting tensor network. Since chain mappings generically are non-homogeneous, the guarantee that no intermediate IM has high TE do not apply. Furthermore, the amount of individual tensor contractions and compressions scales with the square of the number of time steps making this approach relatively expensive.

Instead, we start with the Keldysh path integral representation of the IM described in Sec.2.5. For non-interacting environments, the IM can be written as a Gaussian state using the spectral density. The Gaussian state corresponding to the IM is generically not particle number conserving, independently of the physical particle number conservation of the environment itself. We can hence write it as a Bardeen-Cooper-Schrieffer (BCS)-like [187] wavefunction in the time domain. This BCS wavefunction is then converted into a matrix product state using an algorithm developed by Fishmann and White [188] which we extended to support Gaussian states without particle number conservation. Following this algorithm, we first construct a quantum circuit which results in the target state if applied to the vacuum state. The quantum circuit is constructed by identifying modes which are up to a given cutoff localized within a subsystem. The size of the subsystem necessary to find such a mode is the *window size*. The Fishmann-White quantum circuit is then applied to a MPS representation of the vacuum state, keeping the bond dimension constant by using SVD compression. This results in an approximate MPS representation of the IM. The number of expensive SVD compressions is determined by the product of evolution time and window size. The errors compared to the exact IM stem from time discretization, the Fishmann-White cutoff and the SVD-truncation.

It was shown[119], that the window size for a given cutoff scales logarithmically in the evolution time. This results in a polynomial bound on the IM bond dimension, guaranteeing *polynomial-time* algorithm to solve any QIM. The numerical experiments below demonstrate that this bound is in fact pessimistic and that SVD compression during the application of the Fishmann-White circuit to the MPS representation of the vacuum allows for significantly lower bond dimension.

Once the IM representation of the non-interacting environment has been obtained, QIMs with arbitrary local impurity time evolution can be solved using the contraction algorithm laid out in Sec. 2.4. In this work, we focus on the Anderson Impurity model [189], where a single impurity site with a local Hubbard interaction is coupled to a non-interacting bath of free, spin-$\frac{1}{2}$ fermions. In the high U limit at half-filling and at low temperatures this model is governed by the Kondo effect[190]. In this regime, the effective impurity spin forms a singlet with the itinerant fermions in the environment. Dynamically this regime is characterized by a fast charge dynamics and a slow relaxation of the spin degree of freedom.

We start by computing the time evolution of the impurity density matrix after a quantum quench. The impurity is initialized in a spin polarized state and coupled to a non-interacting environment defined by a smoothened wide-band spectral density with the same parameters as Ref. [176]. Compared to Ref. [176], the time evolution of the population of the four impurity states stays accurate for longer times. Remarkably the trace and positivity of the impurity matrix are well preserved, even though this is not imposed by the method. Together with convergence with respect to bond dimension and

time-step this indicates accuracy for long times.

Stationary currents between reservoirs with a voltage bias are another important example of out-of-equilibrium systems. Here we compute currents between two leads represented by two semi-infinite homogeneous chain. By counting the charge on the impurity after each half-step of the discretized time evolution (c.f. Sec. 2.4) we can compute the instantaneous current between the leads and the impurity. The result compare well to Ref. [191], which used different environments, hence deviates for larger biases. Since the current becomes stationary on short time scales, the computation is accurate even for very low bond dimensions.

Finally we estimate the dependence of the error on bond dimension and time. By considering equal error lines we find that a moderate increase in bond dimension with evolution time is sufficient.

6.2 Reprint

An efficient method for quantum impurity problems out of equilibrium

Julian Thoenniss,[1,*] Michael Sonner,[1,*] Alessio Lerose,[1] and Dmitry A. Abanin[1]

[1] *Department of Theoretical Physics, University of Geneva, Quai Ernest-Ansermet 30, 1205 Geneva, Switzerland*

(Dated: 22nd November 2022)

We introduce an efficient method to simulate dynamics of an interacting quantum impurity coupled to non-interacting fermionic reservoirs. Viewing the impurity as an open quantum system, we describe the reservoirs by their Feynman-Vernon influence functionals (IF). The IF are represented as matrix-product states in the temporal domain, which enables an efficient computation of dynamics for arbitrary interactions. We apply our method to study quantum quenches and transport in an Anderson impurity model, including highly non-equilibrium setups, and find favorable performance compared to state-of-the-art methods. The computational resources required for an accurate computation of dynamics scale polynomially with evolution time, indicating that a broad class of out-of-equilibrium quantum impurity problems are efficiently solvable. This approach will provide new insights into dynamical properties of mesoscopic devices and correlated materials.

Introduction. Non-equilibrium many-body dynamics is actively investigated in condensed matter and synthetic quantum systems such as ultracold atoms [1]. The aim of the ongoing quest is to find regimes where a non-equilibrium system exhibits desired physical properties, which may be qualitatively different compared to equilibrium. Theoretically, out-of-equilibrium many-body problems are extremely challenging, both for analytical and numerical methods [2, 3].

Quantum impurity models (QIM), where a small quantum system such as a quantum dot is coupled to reservoir(s) of itinerant electrons, naturally arise in a variety of systems, including mesoscopic conductors [4] and ultracold atoms [5, 6]. Even relatively simple QIM such as the celebrated Anderson impurity model (AIM) [7], exhibit rich many-body physics including the Kondo effect whereby the impurity spin is screened by itinerant electrons [8]. Fermionic QIM, including the Anderson models, also play a central role in state-of-the-art methods for strongly correlated materials such as dynamical mean-field theory (DMFT), where the material properties are expressed via a self-consistent QIM [3, 9].

A large number of methods for non-equilibrium QIM, and in particular for the AIM, have been developed in recent years. These include iterative path-integral approximations [10–12], non-Markovian [13, 14] or auxiliary master equations (AME) [15, 16], hierarchical equations of motion (HEOM) [17–19], time-dependent numerical renormalization group (NRG) [20–22] and density matrix renormalization group (tDMRG) [23–28], various variants of Quantum Monte Carlo (QMC) [29–34], as well as variational [35, 36] techniques. Recent advances including inchworm algorithm [37] and increasingly sophisticated high-order diagrammatic calculations [38, 39] ameliorated the sign problem of QMC, thereby giving access to longer evolution times. However, despite recent developments, the current methods cannot provide guarantees of computational efficiency for out-of-equilibrium QIM, which remain a subject of active research.

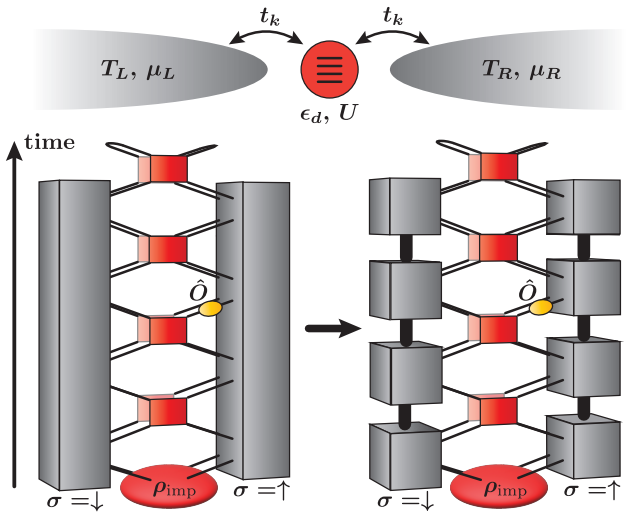

Figure 1. Top: Illustration of single impurity Anderson model [Eq. (1)] with an impurity (red) tunnel-coupled to two reservoirs (gray). Bottom: Tensor-network representation of a time-dependent observable $\langle\hat{O}(t)\rangle$. The dynamical influence of the environment is encoded in a single IF per orbital degree of freedom (here, two gray tensors for $\sigma=\uparrow,\downarrow$, left) which can be efficiently represented as MPS in the temporal domain (right) and hence contracted with the local impurity evolution (product of red tensors). Foreground [background] layer represents forward [backward] branch of the Keldysh contour.

In this Article, we present a conceptually simple and efficient method for fermionic QIM, building on recent developments in describing interacting [40–50] and non-interacting [51–53] quantum baths using temporal tensor networks. The starting point of our approach is to treat the impurity as an open quantum system coupled to the

* These authors contributed equally to this work.

"bath" that consists of fermionic leads (Fig. 1). The effect of the leads is then represented by the fermionic extension of the Feynman-Vernon influence functional (IF) [54], which can be obtained in closed form for arbitrary non-interacting reservoirs [3, 14, 52]. As a key ingredient of our approach, the IF can be efficiently represented as a matrix-product state (MPS) in the temporal domain with controlled bond dimension, thanks to the favorable scaling of temporal entanglement of the IF [43, 52]. This enables an efficient computation of time-dependent observables at the impurity location (e.g. charge, spin, currents) via straightforward tensor contraction.

We demonstrate the efficiency of our method for paradigmatic non-equilibrium QIM setups, including (i) a quantum quench, where impurity site is connected to equilibrium leads at time $t = 0$ and (ii) a biased AIM with two imbalanced leads. In all cases, our method is capable of reproducing and going beyond the state-of-the-art results obtained by inchworm and diagrammatic QMC.

Besides conceptual simplicity, the method presented here has a number of advantages. First and foremost, required resources grow polynomially in evolution time. In terms of computational complexity [55, 56], this implies that QIM are efficiently solvable even far away from equilibrium. Furthermore, the method is non-perturbative, in contrast e.g. to QMC, which involves perturbative expansions either in the impurity-reservoirs hybridization or in the on-site Coulomb interaction. In addition, from a practical viewpoint, once an efficient MPS representation of the reservoirs' IF is found, dynamics of impurities with an arbitrary choice of time-dependent local Hamiltonian can be subsequently computed with modest effort.

Description of the method. We consider the single-impurity Anderson model, described by the Hamiltonian

$$H = \sum_{\substack{k\\ \sigma=\uparrow,\downarrow\\ \alpha=L,R}} \Big[\big(t_k d_\sigma^\dagger c_{k,\alpha,\sigma} + h.c.\big) + \epsilon_k c_{k,\alpha,\sigma}^\dagger c_{k,\alpha,\sigma}\Big] + H_{\rm imp}, \tag{1}$$

with $H_{\rm imp} = (\epsilon_d - U/2)\sum_\sigma \hat{d}_\sigma^\dagger \hat{d}_\sigma + U\hat{d}_\uparrow^\dagger \hat{d}_\uparrow \hat{d}_\downarrow^\dagger \hat{d}_\downarrow$. The impurity level described by fermions d_σ is coupled to two baths ($\alpha = L, R$) of free fermions $c_{k,\alpha,\sigma}$ with identical dispersion ϵ_k and tunnel couplings t_k, initially in thermal equilibrium (see top illustration in Fig. 1). Coulomb interaction $U \neq 0$ in $H_{\rm imp}$ gives rise to strong correlations in and out of equilibrium.

We are primarily interested in the real-time evolution of an impurity observable $\langle \hat{O}(t)\rangle$ starting from a factorized initial state $\rho(0) = \rho_L \otimes \rho_{\rm imp} \otimes \rho_R$, with $\rho_{L,R}$ equilibrium states at inverse temperatures $\beta_{L,R}$ and chemical potentials $\mu_{L,R}$. While conventional tensor-network approaches attempt to compactly represent $\rho(t)$ [2], we instead express $\langle \hat{O}(t)\rangle$ as a Keldysh path integral over Grassmann trajectories of impurity and baths. Gaussian integration over the bath trajectories gives

$$\begin{aligned}\langle \hat{O}(t)\rangle \;\propto\; & \int \Big(\prod_{\sigma,\tau} d\bar{\eta}_{\sigma,\tau} d\eta_{\sigma,\tau}\Big)\mathcal{O}(\bar{\boldsymbol{\eta}}_t, \boldsymbol{\eta}_t)\\ & \times \exp\Big\{\int_{\mathcal{C}} d\tau \Big[\sum_\sigma \bar{\eta}_{\sigma,\tau}\partial_\tau \eta_{\sigma,\tau} - i\mathcal{H}_{\rm imp}(\bar{\boldsymbol{\eta}}_\tau, \boldsymbol{\eta}_\tau)\Big]\Big\}\\ \times \rho_{\rm imp}[\bar{\boldsymbol{\eta}}_0, \boldsymbol{\eta}_0] & \prod_{\sigma=\uparrow,\downarrow} \exp\Big(\int_{\mathcal{C}} d\tau \int_{\mathcal{C}} d\tau' \bar{\eta}_{\sigma,\tau}\Delta(\tau,\tau')\eta_{\sigma,\tau'}\Big).\end{aligned} \tag{2}$$

Here $\bar{\boldsymbol{\eta}}_\tau = (\bar{\eta}_{\uparrow,\tau}, \bar{\eta}_{\downarrow,\tau})$ and $\boldsymbol{\eta}_\tau = (\eta_{\uparrow,\tau}, \eta_{\downarrow,\tau})$ parametrize the impurity trajectory. The IF is the last exponential in Eq. (2), defined by the hybridization function $\Delta(\tau,\tau') = \sum_\alpha \Delta^\alpha(\tau,\tau')$, where Δ^α fully encodes the dynamical influence of the bath α,

$$\Delta^\alpha(\tau,\tau') = \int \frac{d\omega}{2\pi}\Gamma(\omega) g^\alpha_{\tau,\tau'}(\omega). \tag{3}$$

The latter is determined by the bath's spectral density $\Gamma(\omega) = 2\pi\sum_k |t_k|^2\delta(\omega-\epsilon_k)$ and non-interacting Green's function $g^\alpha_{\tau,\tau'}(\omega) = \big(n^\alpha_{\rm F}(\omega) - \Theta_{\mathcal{C}}(\tau,\tau')\big)e^{-i\omega(\tau-\tau')}$, where $n^\alpha_{\rm F}$ is the Fermi distribution at inverse temperature β_α and chemical potential μ_α and $\Theta_{\mathcal{C}}$ is the Heaviside step function on the Keldysh contour $\mathcal{C}$ (see e.g. Ref. [3]). Equation (2) is the starting point of advanced techniques for impurity dynamics such as AME, HEOM or QMC.

The difficulty in evaluating the path integral arises from the combination of non-Gaussianity (in $\mathcal{H}_{\rm imp}$) and time-non-locality (in $\Delta(\tau,\tau')$). The key idea of our method is to interpret Eq. (2) as a scalar product of fictitious states and operators defined in a fermionic Fock space on a temporal lattice. To that end, we note that the textbook expression in Eq. (2) is defined as the limit $M \to \infty$ of a discrete-time expression, obtained by dividing the full time evolution window $[0, T]$ into M steps of size $\delta t = T/M$; we fix a sufficiently large M. For our purpose, it is convenient to use a Trotter scheme that further splits the Trotter step into impurity and hybrization, leading to $8M$ trajectory variables per spin species along the discretized Keldysh contour, see Supplemental Material (SM) for details. We arrange these in two arrays, $\boldsymbol{\eta}_\sigma = (\eta_{\sigma,0^+}, \eta_{\sigma,0^-}, \ldots, \eta_{\sigma,(2M-1)^+}, \eta_{\sigma,(2M-1)^-})$ and analogously $\bar{\boldsymbol{\eta}}_\sigma$, with degrees of freedom alternating on the forward (+) and backward (−) branch of the Keldysh contour. A series of manipulations with the discrete-time path integral, including partial "particle-hole transformations" $\eta \leftrightarrow \bar{\eta}$, allows us to rewrite Eq. (2) in a scalar product form (see SM for details):

$$\begin{aligned}\langle \hat{O}(t)\rangle \;\propto\; & \int \Big(\prod_\sigma d\bar{\boldsymbol{\eta}}_\sigma d\boldsymbol{\eta}_\sigma\Big)\\ & \times \mathcal{I}[\boldsymbol{\eta}_\downarrow] e^{-\bar{\boldsymbol{\eta}}_\downarrow \boldsymbol{\eta}_\downarrow}\mathcal{D}_{\mathcal{O},t}[\bar{\boldsymbol{\eta}}_\downarrow, \boldsymbol{\eta}_\uparrow]\, e^{-\bar{\boldsymbol{\eta}}_\uparrow \boldsymbol{\eta}_\uparrow}\mathcal{I}[\bar{\boldsymbol{\eta}}_\uparrow]\\ \equiv\; & \langle I|\, \hat{D}_{\hat{O},t}\, |I\rangle\,.\end{aligned} \tag{4}$$

Here, the kernel $\mathcal{D}_{\mathcal{O},t}[\bar{\boldsymbol{\eta}}_\downarrow, \boldsymbol{\eta}_\uparrow]$, which is non-Gaussian, describes impurity's own dynamics, and has a simple

product form due to time locality. This gives rise to a product operator $\hat{D}_{\hat{O},t} = \hat{D}_1 \otimes \cdots \otimes \hat{D}_M$, where each $\hat{D}_m$ is a 16×16 matrix (except the first and last: see superimposed red tensors in Fig. 1) and $\hat{D}_{m^*=t/\delta t}$ contains $\hat{O}$. The discrete-time IF has a Gaussian form, $\mathcal{I}[\boldsymbol{\eta}_\sigma] = \exp\left(\boldsymbol{\eta}_\sigma^T \mathbf{B}\, \boldsymbol{\eta}_\sigma\right)$, where the antisymmetric matrix $\mathbf{B}$ is related to the time-discretization of $\Delta(\tau, \tau')$ (see SM). The Gaussian many-body wave function $|I\rangle$ associated with $\mathcal{I}$ (gray tensors in Fig. 1 bottom left) is obtained by replacing Grassmann variables by corresponding creation operators acting on the Fock space vacuum, $\boldsymbol{c}^\dagger \equiv (c^\dagger_{0^+}, c^\dagger_{0^-}, \ldots, c^\dagger_{(2M-1)^+}, c^\dagger_{(2M-1)^-})$,

$$|I\rangle = \exp\left(\mathbf{c}^{\dagger T} \mathbf{B}\, \mathbf{c}^\dagger\right) |\emptyset\rangle\,. \tag{5}$$

Such a state formally has a Bardeen-Cooper-Schrieffer form, regardless of the fermion-number conservation of the original problem, cf. Eq. (2); this is related to the "particle-hole transformations" performed to arrive at Eq. (4). We note that particle number conservation shows up as a sublattice symmetry in Eq. (5).

Next, we aim to represent the state $|I\rangle$ as a MPS. Correlations of this state, described by the function $\Delta(\tau, \tau')$, reflect non-Markovianity of the bath. The possibility of a compact MPS representation is determined by the entanglement properties of a wave function; we previously showed [52] that Gaussian IF wave functions arising in QIM exhibit at most logarithmic scaling of temporal entanglement with evolution time for both equilibrium and certain non-equilibrium initial states of the reservoirs. This suggests that such wave functions can be described by a polynomial-in-T number of parameters.

Previous works [57, 58] proposed algorithms for representing a fermionic Gaussian wave function as a MPS. Here we apply the Fishman-White (FW) algorithm [57], extended to BCS-like wave functions [52]. We first approximately represent the Gaussian state determined by $\mathbf{B}$ [Eq. (5)] as a quantum circuit of nearest-neighbor Gaussian unitary gates applied to the vacuum (a product state in a temporal chain of $4M$ spins). The approximation is controlled by a threshold parameter ϵ of the algorithm [52, 57], which determines the maximum number D of gates acting on a given site in this circuit (which we refer to as "local depth" below). Second, we compress the circuit with standard singular-value truncations to produce a MPS approximation of $|I\rangle$ with bond dimension $\chi \leq 2^D$. Once the MPS is obtained (gray tensors in Fig. 1 bottom right), the impurity's reduced density matrix time evolved with an arbitrary (possibly time-dependent) impurity Hamiltonian $H_{\rm imp}$ can be efficiently computed by tensor contraction in the time direction. This method is straightforwardly applicable to the computation of multi-time observables, e.g. the impurity Green's function, as well as currents (see below).

A quantum quench. As a first application of our method, we study a local quantum quench, where tunneling between impurity and the bath – initially in equilibrium at equal β and μ – is turned on at time $t = 0$. We monitor the real-time evolution of the impurity level population at $t > 0$. In the Kondo regime (strong interaction and low temperature), strong correlations develop in real time between the impurity and the bath, corresponding to the formation of a local screening cloud over a non-perturbatively long timescale – a real-time manifestation of the Kondo effect, which was previously investigated with other methods [20, 21, 24, 35, 59].

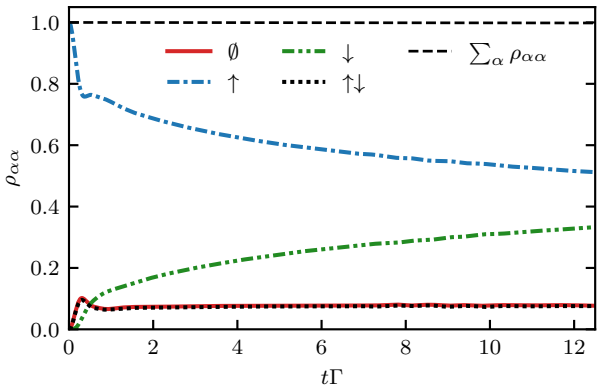

Figure 2. Real-time evolution of the impurity density matrix after a quench. The plot reports diagonal entries $\rho_{\alpha\alpha}$, with $\alpha = \emptyset, \uparrow, \downarrow, \uparrow\downarrow$ as a function of time. The environment is modelled as in Ref. [37] (see main text), with $\beta = 50/\Gamma$ and $\mu = 0$. Simulation parameters: Bond dimension $\chi = 256$ per spin species, FW threshold $\epsilon = 5 \cdot 10^{-13}$, Trotter step $\delta t = 0.02/\Gamma$.

Here we benchmark the state-of-the-art results of inchworm QMC in Ref. [37]: We consider a bath defined by a flat band with smooth edges, $\Gamma(\omega) = \Gamma/\left[(1 + e^{\nu(\omega-\omega_c)})(1 + e^{-\nu(\omega+\omega_c)})\right]$ with $\omega_c = 10\Gamma$ and $\nu = 10/\Gamma$. Moreover, we set $\beta = 50/\Gamma$, $\mu = 0$. We prepare the impurity in a singly occupied state $\rho_{\rm imp} = |\uparrow\rangle\langle\uparrow|$, with $\epsilon_d = 0$ and $U = 8\Gamma$, and couple it to the bath at time $t = 0$. In Fig. 2 we report our results for the evolution of the diagonal components of the impurity's reduced density matrix. Data are converged with respect to all simulation parameters (see caption), demonstrating accuracy beyond the data of Ref. [37]. These results showcase the ability of our method to capture the slow dynamical formation of a spin singlet in the Kondo regime, which will be further investigated elsewhere.

Non-equilibrium transport. The system described by Eq. (1) with a temperature or chemical potential bias between L and R reservoirs models paradigmatic non-equilibrium setups with correlated nanodevices. Capturing the full transient charge and spin dynamics after a quench (either of tunnel-couplings or of interactions) toward the non-equilibrium stationary state is a recurrent challenging test for novel advanced numerical techniques [22, 38, 60–62].

Here we benchmark the state-of-the-art computation of the system's current-voltage characteristics in Ref. [38].

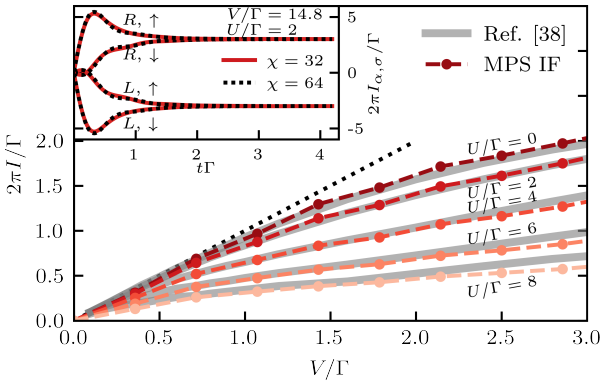

Figure 3. Current-voltage characteristics of an AIM. Reservoirs L and R are tight-binding chains as in Refs. [24, 38] (see main text), of $L = 600$ sites each, at zero temperature and chemical potentials $\pm V/2$. Simulation parameters: Bond dimension $\chi = 32$ per reservoir per spin species, FW threshold $\epsilon = 1 \cdot 10^{-12}$, Trotter step $\delta t = 0.007/\Gamma$. For all values of V and U we evolve until time $T = 4.2/\Gamma$ and verify that at this time stationary state is reached. Inset: At fixed $V/\Gamma = 14.8$ and $U/\Gamma = 2$, we demonstrate convergence in bond dimension for all four components of the transient current, $\langle I_{\alpha,\sigma}(t)\rangle$ with $\alpha = L, R$ and $\sigma = \uparrow, \downarrow$.

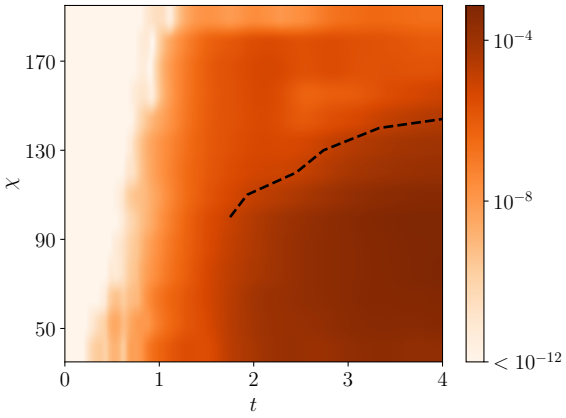

Figure 4. Error $e(t, \chi)$ of the time-evolved impurity density matrix as a function of bond dimension and evolution time (see main text for a precise definition), for an impurity starting from $\rho_{\mathrm{imp}}(0) = |\uparrow\rangle\langle\uparrow|$ and coupled with tunneling amplitude $t'_{\mathrm{hop}} = 0.3162$ to a single tight-binding chain of $L = 400$ sites with homogeneous nearest-neighbor hopping $t_{\mathrm{hop}} = 1$, initially at zero temperature and half filling (cf. Ref. [24]). The constant-error $e = 10^{-5}$ dashed line indicates that the required bond dimension grows slowly with simulation time. Here we fixed $T = 4$, $\delta t = 0.01$, $\epsilon = 10^{-12}$.

We model the reservoirs as two homogenous tight-binding chains with nearest-neighbor hopping $t_{\mathrm{hop}} = 1$, coupled to the impurity with tunneling amplitude $t'_{\mathrm{hop}} = 0.3162$, corresponding to a resonance width $\Gamma(\epsilon_d = 0) = 0.1$ (cf. Ref. [24]). We initialize the two reservoirs at zero temperature and chemical potentials $\pm V/2$, and monitor the time-dependent current flowing through the impurity for several values of U, until the stationary state is reached.

Unlike the contraction illustrated in Fig. 1 and used above for the quench simulation, computing the current into either reservoir requires one to keep track of the separate influence of reservoirs L and R. A suitable Trotter decomposition (see Ref. [52] and SM) allows us to couple the two reservoirs with the impurity alternatively in discrete time steps δt. The current of spin σ electrons flowing into reservoir α, can then be computed as $\langle I_{\alpha,\sigma}(t)\rangle = \frac{1}{\delta t}\left[\langle d^\dagger_\sigma(t+\delta t) d_\sigma(t+\delta t)\rangle - \langle d^\dagger_\sigma(t) d_\sigma(t)\rangle\right]$, where the impurity interacts only with reservoir α during the time step from t to $t + \delta t$.

Keeping track of L and R separately results in a tensor contraction with four IF MPS. This considerably limits the bond dimension we can afford for each IF, as the final impurity evolution entails storing matrices acting on a $16\chi^4$-dimensional space (while it was $16\chi^2$ before). Nonetheless, we found that the value of the current is converged over the full transient to the stationary state for bond dimension as low as $\chi = 32$ (see inset of Fig. 3).

Figure 3 shows the results of our computations, as well as the corresponding data from Fig. 15 of Ref. [38]. We find a fairly good agreement throughout the wide explored parameter regime. The unit slope of the dotted line represents the universal Landauer linear-response conductance, $I = (e^2/h)V$ (recall $e = \hbar = 1$ in our units). We note that small discrepancies are to be expected at large biases $V \gg \Gamma$ due to non-universal effects of finite bath bandwidth ($t_{\mathrm{hop}} = 10\Gamma$ here). We further remark that for small bias and large interaction the non-equilibrium Kondo regime is approached, characterized by slow relaxation. Accordingly, in the computation with smallest bias $V = 0.36\Gamma$ and largest interaction $U = 8\Gamma$ in Fig. 3, the time-dependent current has not yet fully reached its stationary value at time T.

Computational efficiency. Finally, we report on the computational efficiency of our method. Previous works found that for Gaussian ground states [57] and IFs [52] (including states with algebraic correlations), the FW algorithm produces a quantum circuit of "local depth" $D = D(T)$ that scales at most logarithmically with evolution time T. We note that the FW control parameter ϵ affects the prefactor of $\log T$ scaling of D. In turn, D puts an exact upper bound on the bond dimension of the corresponding MPS as $\chi \leq 2^D$ [52, 57], indicating that computational complexity of the algorithm scales at most polynomially with evolution time.

We found that compression of the FW circuit using conventional singular-value truncation typically leads to a further significant reduction of the required computational resources. For example, for the data shown in Fig. 2, we find a maximum "local depth" $D = 28$ which sets the hard upper bound $\chi \leq 2^{28}$. However, this circuit could be accurately approximated by a MPS with a much smaller bond dimension $\chi = 256 = 2^8$.

We finally investigated how this MPS compression affects the *a posteriori* error of observables. To this end, we considered an environment that consists of a single tight-binding chain [63]. Having fixed an extremely low FW threshold ϵ (which makes this source of error negligible), we estimated the residual error of time-dependent observables in $t \in [0, T]$ due to the truncated bond dimension, as the trace distance $e(t, \chi) = \left|\left|\rho_{\rm imp}^{(\chi)}(t) - \rho_{\rm imp}^{(\infty)}(t)\right|\right|_1$ between the reduced density matrix computed with a cutoff χ on the IF MPS and the fully converged result (computed using a much higher $\chi = 512$).

The behavior of the error e as a function of t and χ is illustrated in Fig. 4. We observe that the bond dimension $\chi = \chi(t)$ required to achieve a fixed error e grows approximately linearly with t, indicating the efficiency of the approach. We similarly found in other examples we studied, that representing IF with an MPS with a moderate bond dimension is sufficient to accurately compute impurity observables. Thus, we conclude that our approach indeed has a polynomial complexity [43, 52], allowing one to access long-time impurity dynamics using resources available in present-day computers.

Summary and outlook. To summarize, we introduced a method for studying dynamics of QIM, based on a tensor-network representation of reservoir's IF. We applied this approach to paradigmatic quantum quenches in AIM, demonstrating that it compares favorably to state-of-the art QMC computations. The approach is non-perturbative and offers several other advantages: in particular, it applies to both equilibrium and highly non-equilibrium QIM setups. Moreover, once a MPS form of the IF is obtained, arbitrary choices of impurity interactions can be analyzed with modest extra effort.

We showed that the required computational resources scale polynomially with the evolution time. Combined with previous results on temporal entanglement scaling [52], this demonstrates that a broad range of non-equilibrium QIM problems are efficiently solvable using our approach. While here we focused on quenches of the impurity-reservoir tunnel-coupling in the single-impurity Anderson model, the approach can be extended to a number of other setups, including multi-orbital impurities and initial states where entanglement between impurity and reservoirs is present. Another promising application is to DMFT, which will require imaginary-time extension of the technique introduced here. We expect the computational efficiency of the approach to enable long-time simulations of dynamics in such setups as well, opening the door to analyzing non-equilibrium behavior of mesoscopic devices and quantum materials.

Acknowledgements. We thank E. Arrigoni, G. Cohen, M. Eckstein, S. Florens, Y. Ke, M. Stoudenmire, X. Waintal for discussions. Support by the European Research Council (ERC) under the European Union's Horizon 2020 research and innovation programme (grant agreement No. 864597) and by the Swiss National Science Foundation is gratefully acknowledged.

While finishing this manuscript, we became aware of a related work by Ng *et al.*, which appeared simultaneously [64].

[1] I. Bloch, J. Dalibard, and W. Zwerger, Many-body physics with ultracold gases, Rev. Mod. Phys. **80**, 885 (2008).
[2] S. Paeckel, T. Köhler, A. Swoboda, S. R. Manmana, U. Schollwöck, and C. Hubig, Time-evolution methods for matrix-product states, Annals of Physics **411**, 167998 (2019).
[3] H. Aoki, N. Tsuji, M. Eckstein, M. Kollar, T. Oka, and P. Werner, Nonequilibrium dynamical mean-field theory and its applications, Rev. Mod. Phys. **86**, 779 (2014).
[4] M. Pustilnik and L. Glazman, TOPICAL REVIEW: Kondo effect in quantum dots, Journal of Physics Condensed Matter **16**, R513 (2004), arXiv:cond-mat/0401517 [cond-mat.mes-hall].
[5] M. Kanász-Nagy, Y. Ashida, T. Shi, C. Moca, T. N. Ikeda, S. Fölling, J. I. Cirac, G. Zaránd, and E. A. Demler, Exploring the anisotropic kondo model in and out of equilibrium with alkaline-earth atoms, Phys. Rev. B **97**, 155156 (2018).
[6] L. Riegger, N. Darkwah Oppong, M. Höfer, D. R. Fernandes, I. Bloch, and S. Fölling, Localized magnetic moments with tunable spin exchange in a gas of ultracold fermions, Phys. Rev. Lett. **120**, 143601 (2018).
[7] P. W. Anderson, Localized magnetic states in metals, Phys. Rev. **124**, 41 (1961).
[8] A. C. Hewson, *The Kondo Problem to Heavy Fermions*, Cambridge Studies in Magnetism (Cambridge University Press, 1993).
[9] A. Georges, G. Kotliar, W. Krauth, and M. J. Rozenberg, Dynamical mean-field theory of strongly correlated fermion systems and the limit of infinite dimensions, Rev. Mod. Phys. **68**, 13 (1996).
[10] D. E. Makarov and N. Makri, Path integrals for dissipative systems by tensor multiplication. Condensed phase quantum dynamics for arbitrarily long time, Chemical Physics Letters **221**, 482 (1994).
[11] S. Weiss, J. Eckel, M. Thorwart, and R. Egger, Iterative real-time path integral approach to nonequilibrium quantum transport, Phys. Rev. B **77**, 195316 (2008).
[12] D. Segal, A. J. Millis, and D. R. Reichman, Numerically exact path-integral simulation of nonequilibrium quantum transport and dissipation, Phys. Rev. B **82**, 205323 (2010).
[13] M. W. Y. Tu and W.-M. Zhang, Non-markovian decoherence theory for a double-dot charge qubit, Phys. Rev. B **78**, 235311 (2008).
[14] J. Jin, M. Wei-Yuan Tu, W.-M. Zhang, and Y. Yan, Non-equilibrium quantum theory for nanodevices based on the Feynman-Vernon influence functional, New Journal of Physics **12**, 083013 (2010).
[15] A. Dorda, M. Nuss, W. von der Linden, and E. Arrigoni, Auxiliary master equation approach to nonequilibrium correlated impurities, Phys. Rev. B **89**, 165105 (2014).

[16] M. Lotem, A. Weichselbaum, J. von Delft, and M. Goldstein, Renormalized lindblad driving: A numerically exact nonequilibrium quantum impurity solver, Phys. Rev. Research **2**, 043052 (2020).

[17] Y. Tanimura and R. Kubo, Time evolution of a quantum system in contact with a nearly gaussian-markoffian noise bath, Journal of the Physical Society of Japan **58**, 101 (1989), https://doi.org/10.1143/JPSJ.58.101.

[18] J. Jin, X. Zheng, and Y. Yan, Exact dynamics of dissipative electronic systems and quantum transport: Hierarchical equations of motion approach, The Journal of Chemical Physics **128**, 234703 (2008), https://doi.org/10.1063/1.2938087.

[19] X. Dan, J. T. Xu, Meng Stockburger, J. Ankerhold, and Q. Shi, Efficient low temperature simulations for fermionic reservoirs with the hierarchical equations of motion method: Application to the anderson impurity model 10.48550/arXiv.2211.04089 (2022).

[20] F. B. Anders and A. Schiller, Real-time dynamics in quantum-impurity systems: A time-dependent numerical renormalization-group approach, Phys. Rev. Lett. **95**, 196801 (2005).

[21] H. T. M. Nghiem and T. A. Costi, Time evolution of the kondo resonance in response to a quench, Phys. Rev. Lett. **119**, 156601 (2017).

[22] F. Schwarz, I. Weymann, J. von Delft, and A. Weichselbaum, Nonequilibrium steady-state transport in quantum impurity models: A thermofield and quantum quench approach using matrix product states, Phys. Rev. Lett. **121**, 137702 (2018).

[23] J. Prior, A. W. Chin, S. F. Huelga, and M. B. Plenio, Efficient simulation of strong system-environment interactions, Phys. Rev. Lett. **105**, 050404 (2010).

[24] M. Nuss, M. Ganahl, E. Arrigoni, W. von der Linden, and H. G. Evertz, Nonequilibrium spatiotemporal formation of the kondo screening cloud on a lattice, Phys. Rev. B **91**, 085127 (2015).

[25] F. A. Wolf, I. P. McCulloch, and U. Schollwöck, Solving nonequilibrium dynamical mean-field theory using matrix product states, Phys. Rev. B **90**, 235131 (2014).

[26] A. Nüßeler, I. Dhand, S. F. Huelga, and M. B. Plenio, Efficient simulation of open quantum systems coupled to a fermionic bath, Phys. Rev. B **101**, 155134 (2020).

[27] G. Wójtowicz, J. E. Elenewski, M. M. Rams, and M. Zwolak, Open-system tensor networks and kramers' crossover for quantum transport, Phys. Rev. A **101**, 050301 (2020).

[28] L. Kohn and G. E. Santoro, Quench dynamics of the anderson impurity model at finite temperature using matrix product states: entanglement and bath dynamics, Journal of Statistical Mechanics: Theory and Experiment **2022**, 063102 (2022).

[29] L. Mühlbacher and E. Rabani, Real-time path integral approach to nonequilibrium many-body quantum systems, Phys. Rev. Lett. **100**, 176403 (2008).

[30] M. Schiró and M. Fabrizio, Real-time diagrammatic monte carlo for nonequilibrium quantum transport, Phys. Rev. B **79**, 153302 (2009).

[31] P. Werner, T. Oka, and A. J. Millis, Diagrammatic monte carlo simulation of nonequilibrium systems, Phys. Rev. B **79**, 035320 (2009).

[32] E. Gull, D. R. Reichman, and A. J. Millis, Numerically exact long-time behavior of nonequilibrium quantum impurity models, Phys. Rev. B **84**, 085134 (2011).

[33] G. Cohen and E. Rabani, Memory effects in nonequilibrium quantum impurity models, Phys. Rev. B **84**, 075150 (2011).

[34] G. Cohen, E. Gull, D. R. Reichman, A. J. Millis, and E. Rabani, Numerically exact long-time magnetization dynamics at the nonequilibrium kondo crossover of the anderson impurity model, Phys. Rev. B **87**, 195108 (2013).

[35] Y. Ashida, T. Shi, M. C. Bañuls, J. I. Cirac, and E. Demler, Solving quantum impurity problems in and out of equilibrium with the variational approach, Phys. Rev. Lett. **121**, 026805 (2018).

[36] T. Shi, E. Demler, and J. Ignacio Cirac, Variational study of fermionic and bosonic systems with non-gaussian states: Theory and applications, Annals of Physics **390**, 245 (2018).

[37] G. Cohen, E. Gull, D. R. Reichman, and A. J. Millis, Taming the dynamical sign problem in real-time evolution of quantum many-body problems, Phys. Rev. Lett. **115**, 266802 (2015).

[38] C. Bertrand, S. Florens, O. Parcollet, and X. Waintal, Reconstructing nonequilibrium regimes of quantum many-body systems from the analytical structure of perturbative expansions, Phys. Rev. X **9**, 041008 (2019).

[39] M. Maček, P. T. Dumitrescu, C. Bertrand, B. Triggs, O. Parcollet, and X. Waintal, Quantum quasi-monte carlo technique for many-body perturbative expansions, Phys. Rev. Lett. **125**, 047702 (2020).

[40] M. C. Bañuls, M. B. Hastings, F. Verstraete, and J. I. Cirac, Matrix product states for dynamical simulation of infinite chains, Phys. Rev. Lett. **102**, 240603 (2009).

[41] Y.-K. Huang, P. Chen, Y.-J. Kao, and T. Xiang, Long-time dynamics of quantum chains: Transfer-matrix renormalization group and entanglement of the maximal eigenvector, Phys. Rev. B **89**, 201102 (2014).

[42] A. Lerose, M. Sonner, and D. A. Abanin, Influence matrix approach to many-body floquet dynamics, Phys. Rev. X **11**, 021040 (2021).

[43] A. Lerose, M. Sonner, and D. A. Abanin, Scaling of temporal entanglement in proximity to integrability, Phys. Rev. B **104**, 035137 (2021).

[44] E. Ye and G. K.-L. Chan, Constructing tensor network influence functionals for general quantum dynamics, The Journal of Chemical Physics **155**, 044104 (2021), https://doi.org/10.1063/5.0047260.

[45] M. Sonner, A. Lerose, and D. A. Abanin, Influence functional of many-body systems: Temporal entanglement and matrix-product state representation, Annals of Physics **435**, 168677 (2021).

[46] M. Sonner, A. Lerose, and D. A. Abanin, Characterizing many-body localization via exact disorder-averaged quantum noise, Phys. Rev. B **105**, L020203 (2022).

[47] L. Piroli, B. Bertini, J. I. Cirac, and T. c. v. Prosen, Exact dynamics in dual-unitary quantum circuits, Phys. Rev. B **101**, 094304 (2020).

[48] K. Klobas, B. Bertini, and L. Piroli, Exact thermalization dynamics in the "rule 54" quantum cellular automaton, Physical Review Letters **126**, 160602 (2021).

[49] G. Giudice, G. Giudici, M. Sonner, J. Thoenniss, A. Lerose, D. A. Abanin, and L. Piroli, Temporal entanglement, quasiparticles, and the role of interactions, Phys. Rev. Lett. **128**, 220401 (2022).

[50] A. Lerose, M. Sonner, and D. A. Abanin, Overcoming the entanglement barrier in quantum many-body dynamics

via space-time duality, arXiv preprint arXiv:2201.04150 (2022).
[51] A. Strathearn, P. Kirton, D. Kilda, J. Keeling, and B. W. Lovett, Efficient non-Markovian quantum dynamics using time-evolving matrix product operators, Nature Communications **9**, 3322 (2018).
[52] J. Thoenniss, A. Lerose, and D. A. Abanin, Non-equilibrium quantum impurity problems via matrix-product states in the temporal domain 10.48550/ARXIV.2205.04995 (2022).
[53] A. Bose and P. L. Walters, A tensor network representation of path integrals: Implementation and analysis, arXiv preprint arXiv:2106.12523 (2021).
[54] R. Feynman and F. Vernon, The theory of a general quantum system interacting with a linear dissipative system, Annals of Physics **24**, 118 (1963).
[55] S. Bravyi and D. Gosset, Complexity of quantum impurity problems, Communications in Mathematical Physics **356**, 451 (2017).
[56] M. Debertolis, S. Florens, and I. Snyman, Few-body nature of kondo correlated ground states, Phys. Rev. B **103**, 235166 (2021).
[57] M. T. Fishman and S. R. White, Compression of correlation matrices and an efficient method for forming matrix product states of fermionic gaussian states, Phys. Rev. B **92**, 075132 (2015).
[58] N. Schuch and B. Bauer, Matrix product state algorithms for gaussian fermionic states, Phys. Rev. B **100**, 245121 (2019).
[59] M. Medvedyeva, A. Hoffmann, and S. Kehrein, Spatiotemporal buildup of the kondo screening cloud, Phys. Rev. B **88**, 094306 (2013).
[60] T. L. Schmidt, P. Werner, L. Mühlbacher, and A. Komnik, Transient dynamics of the anderson impurity model out of equilibrium, Phys. Rev. B **78**, 235110 (2008).
[61] P. Werner, T. Oka, M. Eckstein, and A. J. Millis, Weak-coupling quantum monte carlo calculations on the keldysh contour: Theory and application to the current-voltage characteristics of the anderson model, Phys. Rev. B **81**, 035108 (2010).
[62] D. M. Fugger, A. Dorda, F. Schwarz, J. von Delft, and E. Arrigoni, Nonequilibrium kondo effect in a magnetic field: auxiliary master equation approach, New Journal of Physics **20**, 013030 (2018).
[63] The choice of an environment defined by unitary evolution allows us to avoid errors associated with time-discretization of a pre-defined spectral density $\Gamma(\omega)$.
[64] N. Ng, G. Park, A. J. Millis, G. K.-L. Chan, and D. R. Reichman, Real time evolution of anderson impurity models via tensor network influence functionals (2022).
[65] M. M. Wilde, *Quantum information theory* (Cambridge University Press, 2013).
[66] In the strict sense, $\{A_\sigma(m)\}_{m=1}^{M}$ are not superoperators as their bond dimension (and thus the equivalent of the environment operator space) is not guaranteed to be a square integer, and CPTP property is not enforced. Furthermore, this property would require to fix the gauge freedom of the MPS.

Supplemental Material: An efficient method for quantum impurity problems out of equilibrium

Julian Thoenniss,[1] Michael Sonner,[1] Alessio Lerose,[1] and Dmitry A. Abanin[1]

[1] *Department of Theoretical Physics, University of Geneva, Quai Ernest-Ansermet 30, 1205 Geneva, Switzerland*

(Dated: 22nd November 2022)

Appendix A: Derivation of Eq. (4)

We start by recalling the standard derivation of the path integral in Eq. (2). Defining the evolution operator $U = \exp(i\,\delta t\, H)$ for a time step $\delta t = T/M$ ($M \gg 1$) and the Hamiltonian H from Eq. (1), the expectation value of an impurity observable can be expressed as

$$\begin{aligned}&\langle \hat{O}(t_{m^*})\rangle \\ &= \mathrm{Tr}_{\mathrm{imp}}\Big[\mathrm{Tr}_{\mathrm{bath}}\Big(U^{M-m^*}\,\hat{O}\,U^{m^*}\,(\rho_{\mathrm{imp}}\otimes\rho_{\mathrm{bath}})(U^\dagger)^M\Big)\Big].\end{aligned} \tag{A1}$$

Here, $t_{m^*} = m^*\cdot\delta t$ denotes a point on the discrete-time lattice and $m^*\in\{0,1,\dots,M\}$. This expression is cast into path integral form by inserting Grassmann resolutions of identity $\mathbb{1}_\tau = \otimes_\sigma \mathbb{1}_{\sigma,\tau}$, where

$$\begin{aligned}\mathbb{1}_{\sigma,\tau} = \int d(\bar\eta_{\sigma,\tau},\eta_{\sigma,\tau})d(\bar{\boldsymbol{\xi}}_{\sigma,\tau},\boldsymbol{\xi}_{\sigma,\tau})\\ e^{-\bar\eta_{\sigma,\tau}\eta_{\sigma,\tau}-\bar{\boldsymbol{\xi}}_{\sigma,\tau}\boldsymbol{\xi}_{\sigma,\tau}}|\eta_{\sigma,\tau},\boldsymbol{\xi}_{\sigma,\tau}\rangle\langle\bar\eta_{\sigma,\tau},\bar{\boldsymbol{\xi}}_{\sigma,\tau}|,\end{aligned} \tag{A2}$$

between every multiplication of operators. Here, $\bar\eta_{\sigma,\tau},\eta_{\sigma,\tau}$ are impurity variables with index $\tau = 0^\pm,\dots,M^\pm$ on the (discretized) Keldysh contour, while $\bar{\boldsymbol{\xi}}_{\sigma,\tau} = (\bar\xi_{j=1,\sigma,\tau},\dots,\bar\xi_{j=L,\sigma,\tau})^T$, $\boldsymbol{\xi}_{\sigma,\tau} = (\xi_{j=1,\sigma,\tau},\dots,\xi_{j=L,\sigma,\tau})^T$ are the degrees of freedom of the environment (made of L fermionic modes). In total, we thus insert $2(M+1)$ identity resolutions per fermionic mode. In the limit $\delta t\to 0$, Eq. (2) is retrieved following standard textbook passages.

To define a clean prescription for our temporal wave functions overlap, however, it is more convenient to further split the evolution operator U into a local impurity and environment+tunneling evolution operators, i.e. $U\approx U_{\mathrm{imp}}\cdot U_{\mathrm{hyb}}$ (with the same error $\mathcal{O}(\delta t^2)$ as before). Here, we defined $U_{\mathrm{hyb}} = \exp\left(i\,\delta t\, H_{\mathrm{hyb}}\right)$ with

$$\begin{aligned}H_{\mathrm{hyb}} &= H - H_{\mathrm{imp}} = \\ &= \sum_{\substack{k\\ \sigma=\uparrow,\downarrow\\ \alpha=L,R}}\Big[\left(t_k d^\dagger_\sigma c_{k,\alpha,\sigma} + h.c.\right) + \epsilon_k c^\dagger_{k,\alpha,\sigma}c_{k,\alpha,\sigma}\Big],\end{aligned} \tag{A3}$$

and, for later convenience, we choose

$$U_{\mathrm{imp}} = \begin{cases} e^{i\,\delta t H_{\mathrm{imp}}} & \text{for evolution up to time } t_{m^*}\\ \mathbb{1}_{\mathrm{imp}} & \text{for evolution in range } [t_{m^*},T].\end{cases} \tag{A4}$$

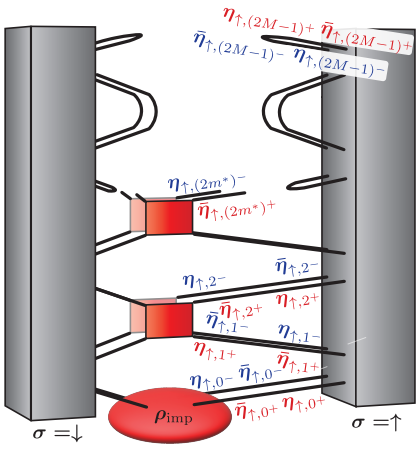

Figure S1. After inserting Grassmann resolutions of identity into Eq. (A1), each leg of the IF and impurity tensor gets associated with a Grassmann variable [red (blue) color refers to the forward (backward) Keldysh branch]. Here, we show the density matrix of the impurity after two time steps. It is obtained from an IM containing $M=4$ time steps. The impurity gates at time steps later than m^* are replaced by the identity operator.

[While this choice is convenient for the conceptual derivation within the Grassmann formalism, we found that a slightly modified prescription, where we replace $\mathbb{1}_{\mathrm{imp}}$ in Eq. (A4) by the perfectly depolarizing channel, is numerically more efficient, see App. B.] In total, with this modified Trotter decomposition, we insert $4M$ Grassmann identity resolutions per spatial site and $\tau = 0^\pm,\dots,(2M-1)^\pm$. In Fig. S1, we illustrate how the resulting $8M$ Grassmann variables are associated with the legs of the IF and impurity tensors, respectively.

In order to arrive at the overlap form of Eq. (4), we manipulate the path integral in a way that results in the following structure: All variables associated with the kernel of the spin-up (down) IF should be conjugate (non-conjugate) and opposite for the impurity kernel. This is achieved by making appropriate variable substitutions in the system-variables of the identity resolution, Eq. (A2). We define these modified identity resolutions as

$\mathbb{1}'_{\sigma,\tau}$ with substitution $\bar\eta_{\sigma,\tau}\to\eta_{\sigma,\tau}$, $\eta_{\sigma,\tau}\to-\bar\eta_{\sigma,\tau}$,

$\mathbb{1}''_{\sigma,\tau}$ with substitution $\bar\eta_{\sigma,\tau}\to-\eta_{\sigma,\tau}$, $\eta_{\sigma,\tau}\to\bar\eta_{\sigma,\tau}$.

With this, Grassmann identities are inserted between the hybridization- and impurity evolution operators on the

forward branch in the following way:

$$U_{\rm imp}\cdot\mathbb{1}_{(2m+1)^+}\cdot U_{\rm hyb}\cdot\mathbb{1}_{(2m)^+}, \tag{A5}$$

with

$$\mathbb{1}_{(2m+1)^+} = \mathbb{1}_{\uparrow,(2m+1)^+}\otimes\mathbb{1}'_{\downarrow,(2m+1)^+}, \tag{A6}$$
$$\mathbb{1}_{(2m)^+} = \mathbb{1}''_{\uparrow,(2m)^+}\otimes\mathbb{1}_{\downarrow,(2m)^+}. \tag{A7}$$

On the backward branch, we insert identities as follows:

$$\mathbb{1}_{(2m)^-}\cdot U^\dagger_{\rm hyb}\cdot\mathbb{1}_{(2m+1)^-}U^\dagger_{\rm imp}, \tag{A8}$$

with

$$\mathbb{1}_{(2m)^-} = \mathbb{1}_{\uparrow,(2m)^-}\otimes\mathbb{1}'_{\downarrow,(2m)^-}, \tag{A9}$$
$$\mathbb{1}_{(2m+1)^-} = \mathbb{1}''_{\uparrow,(2m+1)^-}\otimes\mathbb{1}_{\downarrow,(2m+1)^-}. \tag{A10}$$

With these insertions, one arrives at Eq. (4). Note that these variable substitutions alter the signs of some components of the impurity kernel, while they amount to a simple renaming of variables for the IF.

The resulting discrete-time IF has Gaussian form,

$$\mathcal{I}[\boldsymbol{\eta}_\sigma] = \exp\Big(\sum_{m,m'}\boldsymbol{\eta}^T_{\sigma,m}\mathbf{B}_{mm'}\boldsymbol{\eta}_{\sigma,m'}\Big), \tag{A11}$$

with

$$\boldsymbol{\eta}_{\sigma,m} = (\eta_{\sigma,(2m)^+},\eta_{\sigma,(2m)^-},\eta_{\sigma,(2m+1)^+},\eta_{\sigma,(2m+1)^-})^T.$$

The matrix $\mathbf{B}$ that appears here is the exact Gaussian influence action of the trotterized (Floquet) environment [52]. To understand its relation to the continuous-time result, it is convenient to express it in terms of a discrete-time hybridization matrix $\boldsymbol{\Delta}$,

$$\mathcal{I}[\boldsymbol{\eta}_\sigma] = \exp\left[\sum_{m\geq m'}\boldsymbol{\eta}^T_{\sigma,m}\boldsymbol{\Delta}_{mm'}\boldsymbol{\eta}_{\sigma,m}\right]e^{\eta_{\sigma,0^+}\eta_{\sigma,0^-}}$$
$$\times\, e^{\sum_{m=0}^{M-1}\left(\eta_{\sigma,(2m+1)^+}\eta_{\sigma,(2m)^+}+\eta_{\sigma,(2m)^-}\eta_{\sigma,(2m+1)^-}\right)}, \tag{A12}$$

where the terms in the second and third exponential in Eq. (A12) stem from the overlap of Grassmann coherent states.

For a general discrete-time (Floquet) unitary evolution of the environment, the matrix $\boldsymbol{\Delta}$ has a complicated structure, which we evaluated exactly e.g. for setups with chain-environments [52]. However, the structure greatly simplifies in the Trotter limit $\delta t\to 0$, where $\boldsymbol{\Delta}$ can be written in the form

$$\boldsymbol{\Delta}_{mm'} = (\delta t)^2\Big[\sum_\alpha\int\frac{d\omega}{2\pi}\,\Gamma(\omega)\,\mathbf{G}^\alpha_{mm'}(\omega)\;+\mathcal{O}(\delta t)\Big]. \tag{A13}$$

Here, $\mathbf{G}^\alpha_{mm'}(\omega)$ is a matrix of non-interacting Green's functions of the environment. For fermion-number-conserving Hamiltonians as considered in this work, this yields (omitting ω-dependence for simplicity)

$$\mathbf{G}^\alpha_{m>m'} = \begin{pmatrix} 0 & g^{\alpha,>\,*}_{mm'} & g^{\alpha,<\,*}_{mm'} & 0\\ -g^{\alpha,>}_{mm'} & 0 & 0 & -g^{\alpha,<}_{mm'}\\ -g^{\alpha,>}_{mm'} & 0 & 0 & -g^{\alpha,<}_{mm'}\\ 0 & g^{\alpha,>\,*}_{mm'} & g^{\alpha,<\,*}_{mm'} & 0\end{pmatrix}, \tag{A14}$$

$$\mathbf{G}^\alpha_{m=m'} = \frac{1}{2}\begin{pmatrix} 0 & g^{\alpha,>*}_{mm} & g^{\alpha,>}_{mm} & 0\\ -g^{\alpha,>}_{mm} & 0 & 0 & -g^{\alpha,>*}_{mm}\\ -g^{\alpha,>}_{mm} & 0 & 0 & -g^{\alpha,<}_{mm}\\ 0 & g^{\alpha,>*}_{mm} & g^{\alpha,<*}_{mm} & 0\end{pmatrix}, \tag{A15}$$

with

$$g^{\alpha,<}_{mm'}(\omega) \equiv -n^\alpha_{\rm F}(\omega)\,e^{-i\omega(m-m')\delta t} \tag{A16}$$
$$g^{\alpha,>}_{mm'}(\omega) \equiv \big(1-n^\alpha_{\rm F}(\omega)\big)\,e^{-i\omega(m-m')\delta t}. \tag{A17}$$

These equations make the connection between $\boldsymbol{\Delta}_{mm'}$ and the standard textbook hybridization function $\Delta(\tau,\tau')$ [Eq. (2) of the main text] manifest. Equation (A13) allows to use our formalism to compute impurity dynamics with an environment defined by an arbitrary spectral density $\Gamma(\omega)$.

We emphasize that Eq. (A11) here represents the exact discrete-time IF of a trotterized system, computed from its unitary Floquet dynamics. Thus, in contrast to a brute-force discretization of the textbook expression in Eq. (2) of the main text, Eq. (A11) produces a physically meaningful evolution of the impurity [completely positive and trace preserving (CPTP)] – close by $\mathcal{O}(\delta t)$ to the exact continuous-time Hamiltonian dynamics. Conversely, plugging a spectral density $\Gamma(\omega)$ in Eq. (A13) and neglecting the $\mathcal{O}(\delta t)$ corrections generally (slightly) breaks CPTP.

The impurity tensors $\hat{D}_m$ appearing in the overlap form are obtained directly from the Grassmann kernels corresponding to the impurity evolution: We convert each time-local impurity kernel at time step m to an operator $\hat{D}_m$ that acts between a "↑" two-fermion space (originally corresponding to the tensor product of input and output Hilbert spaces of the ↑ impurity fermion) and a "↓" two-fermion space (originally corresponding to the tensor product of input and output Hilbert spaces of the ↓ impurity fermion), see e.g. superimposed red squares in Fig. S1. Their tensor product, $\hat{D}_{\hat{O},t} = \hat{D}_1\otimes\ldots\otimes\hat{D}_M$ (see main text), defines the product operator which we contract with the IF-MPS as shown in Fig. S1 and described in App. B.

Appendix B: Details on MPS computations

Obtaining the MPS representation of the IF. To obtain a MPS representation of the IF wave function $|I\rangle$, introduced in Eq. (5) of the main text, we apply a generalization of the Fishman-White (FW) algorithm that we adapted to BCS-like wave functions [52,57]. Its input is the two-point correlation matrix Λ whose subblocks are

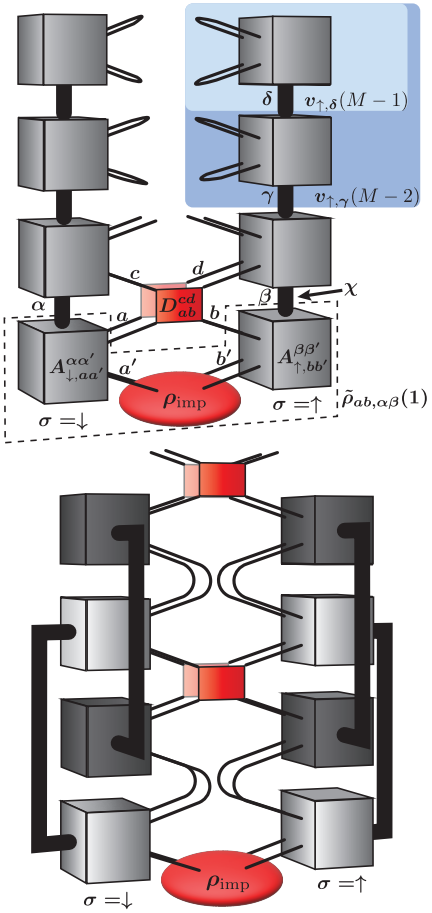

Figure S2. Top: Illustration of the IF-MPS contraction procedure for a single environment and two spin species. Pairs of impurity-legs on the forward and backward branch are combined and labelled by Latin letters, while virtual MPS indices are labelled by Greek letters. Each tensor A of the IF-MPS can be viewed as a linear operator connecting two physical and two virtual spaces. The augmented density matrix $\tilde{\rho}_{ab,\alpha\beta}(1)$ for the first half time step is highlighted by dashed lines. The vectors $v_{\uparrow,\gamma}(M-1)$ and $v_{\uparrow,\beta}(M-2)$, necessary to extract the impurity density matrix from the augmented density matrices, are shaded blue. The whole tensor network corresponds to the vectorized impurity density matrix $\rho_{ef}(3)$ (after the action of IF→impurity→ IF). Bottom: To compute non-equilibrium observables like the current—here for a two-terminal setup—we time evolve $\rho_{\rm imp}(m)$ by contracting it successively with the IF-MPS of the right (light gray) and left (dark gray) environment before applying the impurity gate. In this example, we show the density matrix of the impurity after two full time steps.

given by

$$\Lambda_{\tau\tau'} = \begin{pmatrix} \frac{\langle I|c_\tau c^\dagger_{\tau'}|I\rangle}{\langle I|I\rangle} & \frac{\langle I|c_\tau c_{\tau'}|I\rangle}{\langle I|I\rangle} \\ \frac{\langle I|c^\dagger_\tau c^\dagger_{\tau'}|I\rangle}{\langle I|I\rangle} & \frac{\langle I|c^\dagger_\tau c_{\tau'}|I\rangle}{\langle I|I\rangle} \end{pmatrix}, \tag{B1}$$

where τ, τ' are points on the discretized Keldysh contour. The FW algorithm encodes Λ as a quantum circuit consisting of unitary gates. The accuracy of the circuit representation of $|I\rangle$ is set by an external parameter ϵ that is chosen beforehand. For $\epsilon \to 0$, the circuit representation becomes exact. Applying the circuit to the vacuum (product) state of $4M$ spins yields the MPS representation of $|I\rangle$.

The "local depth" D of the circuit scales logarithmically in evolution time [42,49,52], with a prefactor that increases as ϵ is decreased. For numerical stability, it is advantageous to fix a very small ϵ and continuously reduce the bond dimension χ of the MPS during the circuit contraction. For this, we use conventional singular value decomposition (SVD) where we fix the maximal bond dimension $\chi_{\rm max}$.

In practice, we group all four tensor legs at equal time index m into a single, larger physical Hilbert space of dimension $d = 2^4$; the bond dimension χ refers to these enlarged tensors as depicted in Fig. S2 (top). This procedure yields a MPS that is proportional to the IF wave function, up to errors through finite ϵ and SVD truncation errors. To get the overall normalization $\langle I|I\rangle$, we are in principle free to insert arbitrary impurity evolution operators $U_{\rm imp}$, imposing that the Keldysh partition function equals 1. For environments defined by a continuous spectral density $\Gamma(\omega)$, however, different choices of $U_{\rm imp}$ lead to slightly different normalizations, as time discretization slightly violates the CPTP property of the impurity evolution, as remarked in App. A. For the sake of efficiency, we choose to apply perfectly depolarizing channels on the impurity, which has the effect of connecting the forward and backward legs at a given variable index τ [65] (see upper half of top panel in Fig. S2). This allows us to minimize the cost of normalizing each IF separately.

Once the properly normalized IF-MPS have been obtained, we proceed as follows: The individual tensors of the IF-MPS $\{A_\sigma(m)\}_{m=1}^M$ (gray bricks in Fig. S2) can formally be viewed as "superoperators" acting on the impurity with its physical legs and on the (compressed) environment with its virtual legs [66]. To obtain the full time evolution of the density matrix, we apply these "superoperators" alternately with the local superoperator associated with the impurity Hamiltonian (red bricks in Fig. S2).

Contracting with a single environment. First, let us consider the evolution of an impurity coupled to a single environment which is encoded by two IF-MPS (one for each spin species). This setup is depicted in Fig. S2 (top) and corresponds to the calculations in Fig. 2 and Fig. 4 of the main text.

In the following notation, we use Latin letters to denote combined indices of the forward and backward branch of the Keldysh contour. These indices correspond to physical legs of the IF-MPS. Furthermore, we use Greek letters to label the virtual legs of the MPS. These represent a fictitious state of the compressed environment associated with the MPS virtual bond space as depicted in Fig. S2 (top).

Our starting point is the vectorized initial density mat-

rix ρ_{ab} of the impurity, where the indices a, b correspond to the spin up- and down- fermion respectively. We then add two additional indices, one for each IF, to obtain an augmented density matrix $\tilde{\rho}(0)_{ab,\alpha\beta}$. Each time step consists of i) the combined evolution of the impurity with the environment and ii) the evolution of the impurity only. The former is formally expressed as:

$$\tilde{\rho}_{ab,\alpha\beta}(2m+1) = A^{\alpha\alpha'}_{\downarrow,aa'}(m) A^{\beta\beta'}_{\uparrow,bb'}(m) \tilde{\rho}_{a'b',\alpha'\beta'}(2m), \tag{B2}$$

where $A^{\alpha\alpha'}_{\sigma,aa'}(m)$ is the IF-MPS tensor at time step m. For step ii), we apply the local impurity evolution represented by the superoperator $D^{cd}_{ab}(m)$ (cf. Eq. (4) in main text):

$$\tilde{\rho}_{ab,\alpha\beta}\big(2m+2\big) = D^{ab}_{a'b'}(m) \tilde{\rho}_{a'b',\alpha\beta}(2m+1). \tag{B3}$$

To obtain the density matrix of the impurity from the augmented density matrices at arbitrary intermediate times $\tilde{\rho}(m)$, we recursively compute a set of vectors $v_{\sigma,\alpha}(m)$ for each of the two IF (corresponding to $\sigma = \uparrow$ and $\sigma = \downarrow$, respectively):

$$v_{\sigma,\alpha'}(m-1) = A^{\alpha\alpha'}_{\sigma,aa'}(m) v_{\sigma,\alpha}(m) \frac{1}{2} \mathbb{1}_a \mathbb{1}_{a'}, \tag{B4}$$

with $v_{\sigma,\alpha}(M) = 1$ and $\mathbb{1}_a$ being vectorized identities, see upper panel of Fig. S2. These vectors allow to "trace out the environment" at intermediate times: The density matrix of the impurity $\rho(m)$ can then be obtained from the augmented density matrices as

$$\rho_{ab}(2m) = v_{\downarrow,\alpha}(m) v_{\uparrow,\beta}(m) \tilde{\rho}_{ab,\alpha\beta}(2m), \tag{B5}$$

$$\rho_{ab}(2m-1) = v_{\downarrow,\alpha}(m) v_{\uparrow,\beta}(m) \tilde{\rho}_{ab,\alpha\beta}(2m-1). \tag{B6}$$

Physically, this is equivalent to completing the Keldysh contour to the final time T by evolving the impurity with the perfectly depolarizing channel for each timestep later then m. Numerically, this is slightly more convenient than using identities as in Eq. (A4), as the matrices to be multiplied in Eq. (B4) are smaller.

Computation of the current. To compute the current as in Fig. 3 of the main text, it is necessary to compute the IF of the left and right environment separately, such that we can access the impurity density matrix before and after the individual interaction with the left and with the right environments, as depicted in the bottom panel of Fig. S2. This leads to a modified prescription for time evolution including four independent IF: The augmented density matrix has now four environment indices corresponding to the virtual bond of each of the four IF. For each timestep, we perform the operation in Eq. (B2) twice, once for the left and once for the right environment IF. To extract the impurity density matrix from the augmented density matrix at each substep, all of the additional indices have to be contracted with the corresponding vector $v_{L/R,\uparrow/\downarrow,\alpha}$. This vector is obtained individually for each IF according to Eq. (B4). The required computer memory of the contraction algorithm scales thus as $O(16\chi^4)$, where χ is the maximal bond dimension of each IF. While this requirement of memory resources imposes a bound on manageable bond dimensions in practice, we demonstrate in Fig. 3 that even bond dimensions as low as $\chi = 32$ yield converged results that are competitive with state-of-the-art methods for non-equilibrium dynamics.

7 Conclusion

In this thesis, I introduced a novel ansatz to study the dynamics of local observables in quantum many-body systems. In this approach, the quantum many-body system is treated as a quantum environment and the influence it exerts on its local subsystem is captured in the influence matrix (IM). Analogous to how the knowledge of the density matrix of a quantum state is sufficient to predict the probability distribution of results of all possible quantum measurements, the knowledge of the IM of a quantum environment is sufficient to predict dynamics for arbitrary quantum systems coupled to this environment. The IM is a tensor in the temporal domain, with legs corresponding to different points in time. By treating the IM as a "wave function", we introduced the notion of temporal entanglement (TE). Low TE indicates the existence of an efficient matrix product state (MPS) representation of the IM. Such a parametrization in turn allows the numerical computation of local observables even in very large quantum systems. In this thesis I demonstrated, that for several important classes of systems, such as in many-body localized systems, integrable systems or in circuits close to dual unitarity TE remains low. Together with algorithms to obtain the MPS representation for 1D models and free fermion models, this yields an efficient algorithm for local quantum many-body dynamics.

Dynamical properties like ergodicity, integrability or localization of a quantum system are reflected in the structure of the IM. While TE is low for both integrable [5, 10, 119] and many-body localized systems[2], the entanglement of the "unfolded" IM was shown to be high in the integrable case[6, 97] and low in the localized case [2]. Curiously, for generic thermalizing models, TE appears to scale as volume law [114, 117]. This is surprising, since the defining feature of ergodic systems is that they don't have memory of the initial state. Trying to resolve this apparent contradiction seems to be a relevant part of the wider thermalization puzzle. Furthermore, understanding which temporal correlations contribute to high TE, but potentially are not necessary to compute physical observables, could allow us to expand the scope of the IF approach even further. The entanglement structure of the IM can be used to identify and classify dynamical phases.

The influence matrix approach is also of interest from the point of computational complexity. If an environment can be represented by a IM with polynomial bond dimension, this proves *easiness* the associated impurity problem of constant size arbitrary quantum system coupled to a constant number of such environments. While it is clear from the definitions that *hardness* of such a quantum impurity problem implies super-polynomial scaling of the bond dimension of at least one of the IM involved, it is unclear if and to which extent the converse is true.

The fact that TE is low for large baths of free fermions make this method an ideal candidate for studying out-of-equilibrium phenomena in correlated materials. Studying

the single impurity Anderson model, it was shown in Chap. 6 and Refs. [119, 127, 128] that IM techniques can compete with or even outperform other state-of-the-art methods for non-equilibrium dynamics. Preliminary results for multiple independent reservoirs and impurity orbitals to appear in Ref. [192] show that this performance extends to more complicated setups. This allows usage of these approaches in the context of non-equilibrium dynamic mean field theory and other quantum embedding approaches. Furthermore non-equilibrium effects in mesoscopic systems like quantum dots and quantum point contacts can likely be studied using these techniques.

Bibliography

[1] Alessio Lerose, Michael Sonner, and Dmitry A. Abanin. "Influence Matrix Approach to Many-Body Floquet Dynamics". In: *Physical Review X* 11.2 (2021), p. 021040.

[2] Michael Sonner, Alessio Lerose, and Dmitry A. Abanin. "Characterizing Many-Body Localization via Exact Disorder-Averaged Quantum Noise". In: *Physical Review B* 105.2 (2022), p. L020203.

[3] Julian Thoenniss, Michael Sonner, Alessio Lerose, and Dmitry A. Abanin. "Efficient Method for Quantum Impurity Problems out of Equilibrium". In: *Physical Review B* 107.20 (May 2023), p. L201115. DOI: 10.1103/PhysRevB.107.L201115. (Visited on 08/11/2023).

[4] X. Mi et al. "Noise-Resilient Edge Modes on a Chain of Superconducting Qubits". In: *Science* 378.6621 (Nov. 2022), pp. 785–790. DOI: 10.1126/science.abq5769. (Visited on 08/31/2023).

[5] Alessio Lerose, Michael Sonner, and Dmitry A. Abanin. "Scaling of Temporal Entanglement in Proximity to Integrability". In: *Physical Review B* 104.3 (2021), p. 035137.

[6] Alessio Lerose, Michael Sonner, and Dmitry A. Abanin. "Overcoming the Entanglement Barrier in Quantum Many-Body Dynamics via Space-Time Duality". In: *Physical Review B* 107.6 (Feb. 2023), p. L060305. DOI: 10.1103/PhysRevB.107.L060305. (Visited on 02/01/2024).

[7] Michael Sonner, Maksym Serbyn, Zlatko Papić, and Dmitry A. Abanin. "Thouless Energy across the Many-Body Localization Transition in Floquet Systems". In: *Physical Review B* 104.8 (2021), p. L081112.

[8] Michael Sonner, Alessio Lerose, and Dmitry A. Abanin. "Influence Functional of Many-Body Systems: Temporal Entanglement and Matrix-Product State Representation". In: *Annals of Physics* 435 (2021), p. 168677.

[9] Benedikt Kloss, Julian Thoenniss, Michael Sonner, Alessio Lerose, Matthew T. Fishman, E. M. Stoudenmire, Olivier Parcollet, Antoine Georges, and Dmitry A. Abanin. "Equilibrium Quantum Impurity Problems via Matrix Product State Encoding of the Retarded Action". In: *Physical Review B* 108.20 (Nov. 2023), p. 205110. DOI: 10.1103/PhysRevB.108.205110. (Visited on 04/28/2024).

[10] Giacomo Giudice, Giuliano Giudici, Michael Sonner, Julian Thoenniss, Alessio Lerose, Dmitry A. Abanin, and Lorenzo Piroli. "Temporal Entanglement, Quasiparticles, and the Role of Interactions". In: *Physical Review Letters* 128.22 (2022), p. 220401.

[11] Immanuel Bloch, Jean Dalibard, and Wilhelm Zwerger. "Many-Body Physics with Ultracold Gases". In: *Reviews of Modern Physics* 80.3 (July 2008), pp. 885–964. DOI: 10.1103/RevModPhys.80.885. (Visited on 12/12/2023).

[12] Tim Langen, Remi Geiger, and Jörg Schmiedmayer. "Ultracold Atoms Out of Equilibrium". In: *Annual Review of Condensed Matter Physics* 6.1 (2015), pp. 201–217. DOI: 10.1146/annurev-conmatphys-031214-014548. (Visited on 12/12/2023).

[13] D. Bluvstein et al. "Controlling Quantum Many-Body Dynamics in Driven Rydberg Atom Arrays". In: *Science* 371.6536 (Mar. 2021), pp. 1355–1359. DOI: 10.1126/science.abg2530. (Visited on 04/29/2024).

[14] Ehud Altman et al. "Quantum Simulators: Architectures and Opportunities". In: *PRX Quantum* 2.1 (Feb. 2021), p. 017003. DOI: 10.1103/PRXQuantum.2.017003. (Visited on 01/31/2024).

[15] J. Eisert, M. Friesdorf, and C. Gogolin. "Quantum Many-Body Systems out of Equilibrium". In: *Nature Physics* 11.2 (Feb. 2015), pp. 124–130. ISSN: 1745-2481. DOI: 10.1038/nphys3215. (Visited on 04/29/2024).

[16] Ramón Aguado and David C. Langreth. "Out-of-Equilibrium Kondo Effect in Double Quantum Dots". In: *Physical Review Letters* 85.9 (Aug. 2000), pp. 1946–1949. DOI: 10.1103/PhysRevLett.85.1946. (Visited on 04/29/2024).

[17] S. De Franceschi, R. Hanson, W. G. van der Wiel, J. M. Elzerman, J. J. Wijpkema, T. Fujisawa, S. Tarucha, and L. P. Kouwenhoven. "Out-of-Equilibrium Kondo Effect in a Mesoscopic Device". In: *Physical Review Letters* 89.15 (Sept. 2002), p. 156801. DOI: 10.1103/PhysRevLett.89.156801. (Visited on 04/29/2024).

[18] Sebastian Krinner, Tilman Esslinger, and Jean-Philippe Brantut. "Two-Terminal Transport Measurements with Cold Atoms". In: *Journal of Physics: Condensed Matter* 29.34 (July 2017), p. 343003. ISSN: 0953-8984. DOI: 10.1088/1361-648X/aa74a1. (Visited on 01/31/2024).

[19] Vedika Khemani, Achilleas Lazarides, Roderich Moessner, and S. L. Sondhi. "Phase Structure of Driven Quantum Systems". In: *Physical Review Letters* 116.25 (June 2016), p. 250401. DOI: 10.1103/PhysRevLett.116.250401. (Visited on 12/12/2023).

[20] Xiao Mi et al. "Time-Crystalline Eigenstate Order on a Quantum Processor". In: *Nature* 601.7894 (Jan. 2022), pp. 531–536. ISSN: 1476-4687. DOI: 10.1038/s41586-021-04257-w. (Visited on 02/07/2024).

[21] Soonwon Choi et al. "Observation of Discrete Time-Crystalline Order in a Disordered Dipolar Many-Body System". In: *Nature* 543.7644 (Mar. 2017), pp. 221–225. ISSN: 1476-4687. DOI: 10.1038/nature21426. (Visited on 12/12/2023).

[22] J. Zhang et al. "Observation of a Discrete Time Crystal". In: *Nature* 543.7644 (Mar. 2017), pp. 217–220. ISSN: 1476-4687. DOI: 10.1038/nature21413. (Visited on 12/12/2023).

[23] Frederik Nathan, Dmitry Abanin, Erez Berg, Netanel H. Lindner, and Mark S. Rudner. "Anomalous Floquet Insulators". In: *Physical Review B* 99.19 (May 2019), p. 195133. DOI: 10.1103/PhysRevB.99.195133. (Visited on 12/12/2023).

[24] A. Abragam. *The Principles of Nuclear Magnetism*. Clarendon Press, 1961. ISBN: 978-0-19-852014-6.

[25] M. H. Devoret, A. Wallraff, and J. M. Martinis. *Superconducting Qubits: A Short Review*. Nov. 2004. DOI: 10.48550/arXiv.cond-mat/0411174. arXiv: cond-mat/0411174. (Visited on 04/29/2024).

[26] John Preskill. "Lecture Notes for Physics 229: Quantum Information and Computation". In: *California Institute of Technology* 16.1 (1998), pp. 1–8.

[27] Erhard Schmidt. "Zur Theorie der linearen und nichtlinearen Integralgleichungen. III. Teil". In: *Mathematische Annalen* 65.3 (Sept. 1908), pp. 370–399. ISSN: 1432-1807. DOI: 10.1007/BF01456418. (Visited on 04/15/2024).

[28] E. Schrödinger. "Probability Relations between Separated Systems". In: *Mathematical Proceedings of the Cambridge Philosophical Society* 32.3 (Oct. 1936), pp. 446–452. ISSN: 1469-8064, 0305-0041. DOI: 10.1017/S0305004100019137. (Visited on 05/02/2024).

[29] Lane P. Hughston, Richard Jozsa, and William K. Wootters. "A Complete Classification of Quantum Ensembles Having a given Density Matrix". In: *Physics Letters A* 183.1 (Nov. 1993), pp. 14–18. ISSN: 0375-9601. DOI: 10.1016/0375-9601(93)90880-9. (Visited on 05/02/2024).

[30] Nicolas Gisin. "Stochastic Quantum Dynamics and Relativity". In: *Helvetica Physica Acta* 62.4 (1989), pp. 363–371.

[31] C. E. Shannon. "A Mathematical Theory of Communication". In: *The Bell System Technical Journal* 27.3 (July 1948), pp. 379–423. ISSN: 0005-8580. DOI: 10.1002/j.1538-7305.1948.tb01338.x. (Visited on 04/19/2024).

[32] John Von Neumann. *Mathematical Foundations of Quantum Mechanics: New Edition*. Vol. 53. Princeton university press, 2018.

[33] R. Clausius. "Ueber Die Bewegende Kraft Der Wärme Und Die Gesetze, Welche Sich Daraus Für Die Wärmelehre Selbst Ableiten Lassen". In: *Annalen der Physik* 155.3 (1850), pp. 368–397. ISSN: 1521-3889. DOI: 10.1002/andp.18501550306. (Visited on 05/02/2024).

[34] J. Eisert, M. Cramer, and M. B. Plenio. "Colloquium: Area Laws for the Entanglement Entropy". In: *Reviews of Modern Physics* 82.1 (Feb. 2010), pp. 277–306. DOI: 10.1103/RevModPhys.82.277. (Visited on 03/17/2024).

[35] G. Vidal, J. I. Latorre, E. Rico, and A. Kitaev. "Entanglement in Quantum Critical Phenomena". In: *Physical Review Letters* 90.22 (June 2003), p. 227902. DOI: 10.1103/PhysRevLett.90.227902. (Visited on 05/02/2024).

[36] Israel Klich, Gil Refael, and Alessandro Silva. "Measuring Entanglement Entropies in Many-Body Systems". In: *Physical Review A* 74.3 (Sept. 2006), p. 032306. DOI: 10.1103/PhysRevA.74.032306. (Visited on 04/19/2024).

[37] Dmitry A. Abanin and Eugene Demler. "Measuring Entanglement Entropy of a Generic Many-Body System with a Quantum Switch". In: *Physical Review Letters* 109.2 (July 2012), p. 020504. DOI: 10.1103/PhysRevLett.109.020504. (Visited on 04/19/2024).

[38] Rajibul Islam, Ruichao Ma, Philipp M. Preiss, M. Eric Tai, Alexander Lukin, Matthew Rispoli, and Markus Greiner. "Measuring Entanglement Entropy in a Quantum Many-Body System". In: *Nature* 528.7580 (Dec. 2015), pp. 77–83. ISSN: 1476-4687. DOI: 10.1038/nature15750. (Visited on 04/19/2024).

[39] Per-Olov Löwdin. "On Operators, Superoperators, Hamiltonians, and Liouvillians". In: *International Journal of Quantum Chemistry* 22.S16 (1982), pp. 485–560. ISSN: 1097-461X. DOI: 10.1002/qua.560220847. (Visited on 05/02/2024).

[40] Göran Lindblad. "Completely Positive Maps and Entropy Inequalities". In: *Communications in Mathematical Physics* 40.2 (June 1975), pp. 147–151. ISSN: 1432-0916. DOI: 10.1007/BF01609396. (Visited on 05/02/2024).

[41] Man-Duen Choi. "Completely Positive Linear Maps on Complex Matrices". In: *Linear Algebra and its Applications* 10.3 (June 1975), pp. 285–290. ISSN: 0024-3795. DOI: 10.1016/0024-3795(75)90075-0. (Visited on 04/02/2024).

[42] W Forrest Stinespring. "Positive Functions on C^*-Algebras". In: *Proceedings of the American Mathematical Society* 6.2 (1955), pp. 211–216.

[43] Felix A. Pollock, César Rodríguez-Rosario, Thomas Frauenheim, Mauro Paternostro, and Kavan Modi. "Non-Markovian Quantum Processes: Complete Framework and Efficient Characterization". In: *Physical Review A* 97.1 (Jan. 2018), p. 012127. DOI: 10.1103/PhysRevA.97.012127. (Visited on 07/14/2023).

[44] Gregory A. L. White, Felix A. Pollock, Lloyd C. L. Hollenberg, Charles D. Hill, and Kavan Modi. *From Many-Body to Many-Time Physics*. May 2022. DOI: 10.48550/arXiv.2107.13934. arXiv: 2107.13934 [quant-ph]. (Visited on 04/02/2024).

[45] Mathias R. Jørgensen and Felix A. Pollock. "Exploiting the Causal Tensor Network Structure of Quantum Processes to Efficiently Simulate Non-Markovian Path Integrals". In: *Physical Review Letters* 123.24 (Dec. 2019), p. 240602. DOI: 10.1103/PhysRevLett.123.240602. (Visited on 04/02/2024).

[46] G. Lindblad. "On the Generators of Quantum Dynamical Semigroups". In: *Communications in Mathematical Physics* 48.2 (June 1976), pp. 119–130. ISSN: 1432-0916. DOI: 10.1007/BF01608499. (Visited on 12/28/2023).

[47] Luca D'Alessio, Yariv Kafri, Anatoli Polkovnikov, and Marcos Rigol. "From Quantum Chaos and Eigenstate Thermalization to Statistical Mechanics and Thermodynamics". In: *Advances in Physics* 65.3 (May 2016), pp. 239–362. ISSN: 0001-8732. DOI: 10.1080/00018732.2016.1198134. (Visited on 12/12/2023).

[48] Joshua M. Deutsch. "Eigenstate Thermalization Hypothesis". In: *Reports on Progress in Physics* 81.8 (July 2018), p. 082001. ISSN: 0034-4885. DOI: 10.1088/1361-6633/aac9f1. (Visited on 04/26/2024).

[49] J. H. Christenson, J. W. Cronin, V. L. Fitch, and R. Turlay. "Evidence for the $2\ensuremath{\pi}$ Decay of the K_{2}^{0} Meson". In: *Physical Review Letters* 13.4 (July 1964), pp. 138–140. DOI: 10.1103/PhysRevLett.13.138. (Visited on 03/19/2024).

[50] Nándor Simányi. "Proof of the Ergodic Hypothesis for Typical Hard Ball Systems". In: *Annales Henri Poincaré* 5.2 (Apr. 2004), pp. 203–233. ISSN: 1424-0661. DOI: 10.1007/s00023-004-0166-8. (Visited on 04/24/2024).

[51] Ya G. Sinai. "Dynamical systems with elastic reflections". In: *Russian Mathematical Surveys* 25.2 (Apr. 1970), pp. 137–189. ISSN: 0036-0279. DOI: 10.1070/RM1970v025n02ABEH003794. (Visited on 04/24/2024).

[52] LA Bunimovich. "Decay of Correlations in Dynamical Systems with Chaotic Behavior". In: *Zhurnal Éksperimentalnoi i Teoreticheskoi Fiziki* 89 (1985), pp. 1452–1471.

[53] J. -P. Eckmann and D. Ruelle. "Ergodic Theory of Chaos and Strange Attractors". In: *Reviews of Modern Physics* 57.3 (July 1985), pp. 617–656. DOI: 10.1103/RevModPhys.57.617. (Visited on 04/17/2024).

[54] J. M. Deutsch. "Quantum Statistical Mechanics in a Closed System". In: *Physical Review A* 43.4 (Feb. 1991), pp. 2046–2049. DOI: 10.1103/PhysRevA.43.2046. (Visited on 04/27/2024).

[55] Sanjay Hortikar and Mark Srednicki. "Random Matrix Elements and Eigenfunctions in Chaotic Systems". In: *Physical Review E* 57.6 (June 1998), pp. 7313–7316. DOI: 10.1103/PhysRevE.57.7313. (Visited on 06/08/2024).

[56] Mark Srednicki. "Chaos and Quantum Thermalization". In: *Physical Review E* 50.2 (Aug. 1994), pp. 888–901. DOI: 10.1103/PhysRevE.50.888. (Visited on 04/23/2024).

[57] Maksym Serbyn and Joel E. Moore. "Spectral Statistics across the Many-Body Localization Transition". In: *Physical Review B* 93.4 (Jan. 2016), p. 041424. DOI: 10.1103/PhysRevB.93.041424. (Visited on 04/27/2024).

[58] Rodney J Baxter. "One-Dimensional Anisotropic Heisenberg Chain". In: *Annals of Physics* 70.2 (Apr. 1972), pp. 323–337. ISSN: 0003-4916. DOI: 10.1016/0003-4916(72)90270-9. (Visited on 04/27/2024).

[59] Vincenzo Alba. "Eigenstate Thermalization Hypothesis and Integrability in Quantum Spin Chains". In: *Physical Review B* 91.15 (Apr. 2015), p. 155123. DOI: 10.1103/PhysRevB.91.155123. (Visited on 04/27/2024).

[60] Markus P. Müller, Emily Adlam, Lluís Masanes, and Nathan Wiebe. "Thermalization and Canonical Typicality in Translation-Invariant Quantum Lattice Systems". In: *Communications in Mathematical Physics* 340.2 (Dec. 2015), pp. 499–561. ISSN: 1432-0916. DOI: 10.1007/s00220-015-2473-y. (Visited on 04/27/2024).

[61] D. M. Basko, I. L. Aleiner, and B. L. Altshuler. "Metal–Insulator Transition in a Weakly Interacting Many-Electron System with Localized Single-Particle States". In: *Annals of Physics* 321.5 (May 2006), pp. 1126–1205. ISSN: 0003-4916. DOI: 10.1016/j.aop.2005.11.014. (Visited on 03/17/2024).

[62] I. V. Gornyi, A. D. Mirlin, and D. G. Polyakov. "Interacting Electrons in Disordered Wires: Anderson Localization and Low-T Transport". In: *Physical Review Letters* 95.20 (Nov. 2005), p. 206603. DOI: 10.1103/PhysRevLett.95.206603. (Visited on 03/17/2024).

[63] John Z. Imbrie. "On Many-Body Localization for Quantum Spin Chains". In: *Journal of Statistical Physics* 163.5 (June 2016), pp. 998–1048. ISSN: 1572-9613. DOI: 10.1007/s10955-016-1508-x. (Visited on 03/17/2024).

[64] P. W. Anderson. "Absence of Diffusion in Certain Random Lattices". In: *Physical Review* 109.5 (Mar. 1958), pp. 1492–1505. DOI: 10.1103/PhysRev.109.1492. (Visited on 04/24/2024).

[65] Maksym Serbyn, Z. Papić, and Dmitry A. Abanin. "Local Conservation Laws and the Structure of the Many-Body Localized States". In: *Physical Review Letters* 111.12 (Sept. 2013), p. 127201. DOI: 10.1103/PhysRevLett.111.127201. (Visited on 03/17/2024).

[66] V. Ros, M. Müller, and A. Scardicchio. "Integrals of Motion in the Many-Body Localized Phase". In: *Nuclear Physics B* 891 (Feb. 2015), pp. 420–465. ISSN: 0550-3213. DOI: 10.1016/j.nuclphysb.2014.12.014. (Visited on 03/17/2024).

[67] Anushya Chandran, Isaac H. Kim, Guifre Vidal, and Dmitry A. Abanin. "Constructing Local Integrals of Motion in the Many-Body Localized Phase". In: *Physical Review B* 91.8 (Feb. 2015), p. 085425. DOI: 10.1103/PhysRevB.91.085425. (Visited on 03/17/2024).

[68] David A. Huse, Rahul Nandkishore, and Vadim Oganesyan. "Phenomenology of Fully Many-Body-Localized Systems". In: *Physical Review B* 90.17 (Nov. 2014), p. 174202. DOI: 10.1103/PhysRevB.90.174202. (Visited on 03/17/2024).

[69] Pasquale Calabrese and John Cardy. "Evolution of Entanglement Entropy in One-Dimensional Systems". In: *Journal of Statistical Mechanics: Theory and Experiment* 2005.04 (Apr. 2005), P04010. ISSN: 1742-5468. DOI: 10.1088/1742-5468/2005/04/P04010. (Visited on 12/27/2023).

[70] Hyungwon Kim and David A. Huse. "Ballistic Spreading of Entanglement in a Diffusive Nonintegrable System". In: *Physical Review Letters* 111.12 (Sept. 2013), p. 127205. DOI: 10.1103/PhysRevLett.111.127205. (Visited on 12/27/2023).

[71] Adam Nahum, Jonathan Ruhman, Sagar Vijay, and Jeongwan Haah. "Quantum Entanglement Growth under Random Unitary Dynamics". In: *Physical Review X* 7.3 (July 2017), p. 031016. DOI: 10.1103/PhysRevX.7.031016. (Visited on 12/26/2023).

[72] Rahul Nandkishore and David A. Huse. "Many-Body Localization and Thermalization in Quantum Statistical Mechanics". In: *Annual Review of Condensed Matter Physics* 6.1 (2015), pp. 15–38. DOI: 10.1146/annurev-conmatphys-031214-014726. (Visited on 12/12/2023).

[73] Dmitry A. Abanin, Ehud Altman, Immanuel Bloch, and Maksym Serbyn. "Colloquium: Many-body Localization, Thermalization, and Entanglement". In: *Reviews of Modern Physics* 91.2 (May 2019), p. 021001. DOI: 10.1103/RevModPhys.91.021001. (Visited on 12/12/2023).

[74] Ehud Altman and Ronen Vosk. "Universal Dynamics and Renormalization in Many-Body-Localized Systems". In: *Annual Review of Condensed Matter Physics* 6.1 (2015), pp. 383–409. DOI: 10.1146/annurev-conmatphys-031214-014701. (Visited on 12/12/2023).

[75] Fabien Alet and Nicolas Laflorencie. "Many-Body Localization: An Introduction and Selected Topics". In: *Comptes Rendus Physique*. Quantum Simulation / Simulation Quantique 19.6 (Sept. 2018), pp. 498–525. ISSN: 1631-0705. DOI: 10.1016/j.crhy.2018.03.003. (Visited on 12/12/2023).

[76] D. Perez-Garcia, F. Verstraete, M. M. Wolf, and J. I. Cirac. *Matrix Product State Representations*. May 2007. DOI: 10.48550/arXiv.quant-ph/0608197. arXiv: quant-ph/0608197. (Visited on 04/15/2024).

[77] F. Verstraete, V. Murg, and J.I. Cirac. "Matrix Product States, Projected Entangled Pair States, and Variational Renormalization Group Methods for Quantum Spin Systems". In: *Advances in Physics* 57.2 (Mar. 2008), pp. 143–224. ISSN: 0001-8732. DOI: 10.1080/14789940801912366. (Visited on 04/15/2024).

[78] Ulrich Schollwöck. "The Density-Matrix Renormalization Group in the Age of Matrix Product States". In: *Annals of Physics*. January 2011 Special Issue 326.1 (Jan. 2011), pp. 96–192. ISSN: 0003-4916. DOI: 10.1016/j.aop.2010.09.012. (Visited on 12/27/2023).

[79] Román Orús. "A Practical Introduction to Tensor Networks: Matrix Product States and Projected Entangled Pair States". In: *Annals of Physics* 349 (Oct. 2014), pp. 117–158. ISSN: 0003-4916. DOI: 10.1016/j.aop.2014.06.013. (Visited on 01/30/2024).

[80] Ian Affleck, Tom Kennedy, Elliott H. Lieb, and Hal Tasaki. "Rigorous Results on Valence-Bond Ground States in Antiferromagnets". In: *Physical Review Letters* 59.7 (Aug. 1987), pp. 799–802. DOI: 10.1103/PhysRevLett.59.799. (Visited on 04/15/2024).

[81] A. Klümper, A. Schadschneider, and J. Zittartz. "Groundstate Properties of a Generalized VBS-model". In: *Zeitschrift für Physik B Condensed Matter* 87.3 (Oct. 1992), pp. 281–287. ISSN: 1431-584X. DOI: 10.1007/BF01309281. (Visited on 04/15/2024).

[82] A. K. Kolezhuk, H.-J. Mikeska, and Shoji Yamamoto. "Matrix-Product-States Approach to Heisenberg Ferrimagnetic Spin Chains". In: *Physical Review B* 55.6 (Feb. 1997), R3336–R3339. DOI: 10.1103/PhysRevB.55.R3336. (Visited on 04/15/2024).

[83] I. V. Oseledets. "Tensor-Train Decomposition". In: *SIAM Journal on Scientific Computing* 33.5 (Jan. 2011), pp. 2295–2317. ISSN: 1064-8275. DOI: 10.1137/090752286. (Visited on 04/15/2024).

[84] Jakob Unfried, Johannes Hauschild, and Frank Pollmann. "Fast Time Evolution of Matrix Product States Using the QR Decomposition". In: *Physical Review B* 107.15 (Apr. 2023), p. 155133. DOI: 10.1103/PhysRevB.107.155133. (Visited on 04/15/2024).

[85] Guifré Vidal. "Efficient Classical Simulation of Slightly Entangled Quantum Computations". In: *Physical Review Letters* 91.14 (Oct. 2003), p. 147902. DOI: 10.1103/PhysRevLett.91.147902. (Visited on 12/12/2023).

[86] Guifré Vidal. "Efficient Simulation of One-Dimensional Quantum Many-Body Systems". In: *Physical Review Letters* 93.4 (July 2004), p. 040502. DOI: 10.1103/PhysRevLett.93.040502. (Visited on 12/27/2023).

[87] Jutho Haegeman, J. Ignacio Cirac, Tobias J. Osborne, Iztok Pižorn, Henri Verschelde, and Frank Verstraete. "Time-Dependent Variational Principle for Quantum Lattices". In: *Physical Review Letters* 107.7 (Aug. 2011), p. 070601. DOI: 10.1103/PhysRevLett.107.070601. (Visited on 04/01/2024).

[88] Sebastian Paeckel, Thomas Köhler, Andreas Swoboda, Salvatore R. Manmana, Ulrich Schollwöck, and Claudius Hubig. "Time-Evolution Methods for Matrix-Product States". In: *Annals of Physics* 411 (Dec. 2019), p. 167998. ISSN: 0003-4916. DOI: 10.1016/j.aop.2019.167998. (Visited on 12/12/2023).

[89] Laurens Vanderstraeten, Jutho Haegeman, and Frank Verstraete. "Tangent-Space Methods for Uniform Matrix Product States". In: *SciPost Physics Lecture Notes* (Jan. 2019), p. 007. ISSN: 2590-1990. DOI: 10.21468/SciPostPhysLectNotes.7. (Visited on 12/12/2023).

[90] J. Ignacio Cirac, David Pérez-García, Norbert Schuch, and Frank Verstraete. "Matrix Product States and Projected Entangled Pair States: Concepts, Symmetries, Theorems". In: *Reviews of Modern Physics* 93.4 (Dec. 2021), p. 045003. DOI: 10.1103/RevModPhys.93.045003. (Visited on 02/14/2024).

[91] Eyal Leviatan, Frank Pollmann, Jens H. Bardarson, David A. Huse, and Ehud Altman. *Quantum Thermalization Dynamics with Matrix-Product States*. Oct. 2017. DOI: 10.48550/arXiv.1702.08894. arXiv: 1702.08894 [cond-mat, physics:quant-ph]. (Visited on 12/27/2023).

[92] Christopher David White, Michael Zaletel, Roger S. K. Mong, and Gil Refael. "Quantum Dynamics of Thermalizing Systems". In: *Physical Review B* 97.3 (Jan. 2018), p. 035127. DOI: 10.1103/PhysRevB.97.035127. (Visited on 12/27/2023).

[93] Bingtian Ye, Francisco Machado, Christopher David White, Roger S. K. Mong, and Norman Y. Yao. "Emergent Hydrodynamics in Nonequilibrium Quantum Systems". In: *Physical Review Letters* 125.3 (July 2020), p. 030601. DOI: 10.1103/PhysRevLett.125.030601. (Visited on 12/27/2023).

[94] J. Surace, M. Piani, and L. Tagliacozzo. "Simulating the Out-of-Equilibrium Dynamics of Local Observables by Trading Entanglement for Mixture". In: *Physical Review B* 99.23 (June 2019), p. 235115. DOI: 10.1103/PhysRevB.99.235115. (Visited on 12/27/2023).

[95] Tibor Rakovszky, C. W. von Keyserlingk, and Frank Pollmann. "Dissipation-Assisted Operator Evolution Method for Capturing Hydrodynamic Transport". In: *Physical Review B* 105.7 (Feb. 2022), p. 075131. DOI: 10.1103/PhysRevB.105.075131. (Visited on 11/01/2022).

[96] Jerome Lloyd, Tibor Rakovszky, Frank Pollmann, and Curt von Keyserlingk. *The Ballistic to Diffusive Crossover in a Weakly-Interacting Fermi Gas*. Oct. 2023. DOI: 10.48550/arXiv.2310.16043. arXiv: 2310.16043 [cond-mat, physics:quant-ph]. (Visited on 12/27/2023).

[97] M. C. Bañuls, M. B. Hastings, F. Verstraete, and J. I. Cirac. "Matrix Product States for Dynamical Simulation of Infinite Chains". In: *Physical Review Letters* 102.24 (June 2009), p. 240603. DOI: 10.1103/PhysRevLett.102.240603. (Visited on 07/14/2023).

[98] Alexander Müller-Hermes, J. Ignacio Cirac, and Mari Carmen Bañuls. "Tensor Network Techniques for the Computation of Dynamical Observables in One-Dimensional Quantum Spin Systems". In: *New Journal of Physics* 14.7 (July 2012), p. 075003. ISSN: 1367-2630. DOI: 10.1088/1367-2630/14/7/075003. (Visited on 12/27/2023).

[99] M. B. Hastings and R. Mahajan. "Connecting Entanglement in Time and Space: Improving the Folding Algorithm". In: *Physical Review A* 91.3 (Mar. 2015), p. 032306. DOI: 10.1103/PhysRevA.91.032306. (Visited on 12/28/2023).

[100] Miguel Frías-Pérez and Mari Carmen Bañuls. "Light Cone Tensor Network and Time Evolution". In: *Physical Review B* 106.11 (Sept. 2022), p. 115117. DOI: 10.1103/PhysRevB.106.115117. (Visited on 07/14/2023).

[101] Steven R. White and Adrian E. Feiguin. "Real-Time Evolution Using the Density Matrix Renormalization Group". In: *Physical Review Letters* 93.7 (Aug. 2004), p. 076401. DOI: 10.1103/PhysRevLett.93.076401. (Visited on 01/30/2024).

[102] C. Karrasch, J. H. Bardarson, and J. E. Moore. "Reducing the Numerical Effort of Finite-Temperature Density Matrix Renormalization Group Calculations". In: *New Journal of Physics* 15.8 (Aug. 2013), p. 083031. ISSN: 1367-2630. DOI: 10.1088/1367-2630/15/8/083031. (Visited on 12/27/2023).

[103] Johannes Hauschild, Eyal Leviatan, Jens H. Bardarson, Ehud Altman, Michael P. Zaletel, and Frank Pollmann. "Finding Purifications with Minimal Entanglement". In: *Physical Review B* 98.23 (Dec. 2018), p. 235163. DOI: 10.1103/PhysRevB.98.235163. (Visited on 12/27/2023).

[104] R. P. Feynman and F. L. Vernon. "The Theory of a General Quantum System Interacting with a Linear Dissipative System". In: *Annals of Physics* 281.1 (Apr. 2000), pp. 547–607. ISSN: 0003-4916. DOI: 10.1006/aphy.2000.6017. (Visited on 07/14/2023).

[105] Heinz-Peter Breuer and Francesco Petruccione. *The Theory of Open Quantum Systems*. Oxford University Press, 2002. ISBN: 978-0-19-852063-4.

[106] A. Jamiołkowski. "Linear Transformations Which Preserve Trace and Positive Semidefiniteness of Operators". In: *Reports on Mathematical Physics* 3.4 (Dec. 1972), pp. 275–278. ISSN: 0034-4877. DOI: 10.1016/0034-4877(72)90011-0. (Visited on 04/02/2024).

[107] A. Strathearn, P. Kirton, D. Kilda, J. Keeling, and B. W. Lovett. "Efficient Non-Markovian Quantum Dynamics Using Time-Evolving Matrix Product Operators". In: *Nature Communications* 9.1 (Aug. 2018), p. 3322. ISSN: 2041-1723. DOI: 10.1038/s41467-018-05617-3. (Visited on 12/13/2023).

[108] Erika Ye and Garnet Kin-Lic Chan. "Constructing Tensor Network Influence Functionals for General Quantum Dynamics". In: *The Journal of Chemical Physics* 155.4 (July 2021), p. 044104. ISSN: 0021-9606. DOI: 10.1063/5.0047260. (Visited on 12/26/2023).

[109] Moritz Cygorek, Michael Cosacchi, Alexei Vagov, Vollrath Martin Axt, Brendon W. Lovett, Jonathan Keeling, and Erik M. Gauger. "Simulation of Open Quantum Systems by Automated Compression of Arbitrary Environments". In: *Nature Physics* 18.6 (June 2022), pp. 662–668. ISSN: 1745-2481. DOI: 10.1038/s41567-022-01544-9. (Visited on 12/13/2023).

[110] Gerald E. Fux, Dainius Kilda, Brendon W. Lovett, and Jonathan Keeling. "Tensor Network Simulation of Chains of Non-Markovian Open Quantum Systems". In: *Physical Review Research* 5.3 (Aug. 2023), p. 033078. DOI: 10.1103/PhysRevResearch.5.033078. (Visited on 04/02/2024).

[111] M. Akila, D. Waltner, B. Gutkin, and T. Guhr. "Particle-Time Duality in the Kicked Ising Spin Chain". In: *Journal of Physics A: Mathematical and Theoretical* 49.37 (Aug. 2016), p. 375101. ISSN: 1751-8121. DOI: 10.1088/1751-8113/49/37/375101. (Visited on 12/12/2023).

[112] Bruno Bertini, Pavel Kos, and Tomaž Prosen. "Exact Correlation Functions for Dual-Unitary Lattice Models in $1+1$ Dimensions". In: *Physical Review Letters* 123.21 (Nov. 2019), p. 210601. DOI: 10.1103/PhysRevLett.123.210601. (Visited on 12/27/2023).

[113] Katja Klobas, Bruno Bertini, and Lorenzo Piroli. "Exact Thermalization Dynamics in the "Rule 54" Quantum Cellular Automaton". In: *Physical Review Letters* 126.16 (Apr. 2021), p. 160602. DOI: 10.1103/PhysRevLett.126.160602. (Visited on 12/27/2023).

[114] Lorenzo Piroli, Bruno Bertini, J. Ignacio Cirac, and Tomaž Prosen. "Exact Dynamics in Dual-Unitary Quantum Circuits". In: *Physical Review B* 101.9 (Mar. 2020), p. 094304. DOI: 10.1103/PhysRevB.101.094304. (Visited on 12/27/2023).

[115] Filippo Caruso, Vittorio Giovannetti, Cosmo Lupo, and Stefano Mancini. "Quantum Channels and Memory Effects". In: *Reviews of Modern Physics* 86.4 (Dec. 2014), pp. 1203–1259. DOI: 10.1103/RevModPhys.86.1203. (Visited on 04/02/2024).

[116] Gilad Gour and Mark M. Wilde. "Entropy of a Quantum Channel". In: *Physical Review Research* 3.2 (May 2021), p. 023096. DOI: 10.1103/PhysRevResearch.3.023096. (Visited on 04/02/2024).

[117] Alessandro Foligno, Tianci Zhou, and Bruno Bertini. "Temporal Entanglement in Chaotic Quantum Circuits". In: *Physical Review X* 13.4 (Oct. 2023), p. 041008. ISSN: 2160-3308. DOI: 10.1103/PhysRevX.13.041008. arXiv: 2302.08502 [cond-mat, physics:hep-th, physics:math-ph, physics:quant-ph]. (Visited on 02/01/2024).

[118] Tomaž Prosen and Iztok Pižorn. "Operator Space Entanglement Entropy in a Transverse Ising Chain". In: *Physical Review A* 76.3 (Sept. 2007), p. 032316. DOI: 10.1103/PhysRevA.76.032316. (Visited on 04/02/2024).

[119] Julian Thoenniss, Alessio Lerose, and Dmitry A. Abanin. "Nonequilibrium Quantum Impurity Problems via Matrix-Product States in the Temporal Domain". In: *Physical Review B* 107.19 (May 2023), p. 195101. DOI: 10.1103/PhysRevB.107.195101. (Visited on 08/11/2023).

[120] *OpenBLAS : An Optimized BLAS Library*. https://www.openblas.net/. (Visited on 03/22/2024).

[121] Kazushige Goto and Robert A. van de Geijn. "Anatomy of High-Performance Matrix Multiplication". In: *ACM Transactions on Mathematical Software* 34.3 (May 2008), 12:1–12:25. ISSN: 0098-3500. DOI: 10.1145/1356052.1356053. (Visited on 03/22/2024).

[122] A. J. Leggett, S. Chakravarty, A. T. Dorsey, Matthew P. A. Fisher, Anupam Garg, and W. Zwerger. "Dynamics of the Dissipative Two-State System". In: *Reviews of Modern Physics* 59.1 (Jan. 1987), pp. 1–85. DOI: 10.1103/RevModPhys.59.1. (Visited on 12/26/2023).

[123] Eric Lutz. "Fractional Transport Equations for L\'evy Stable Processes". In: *Physical Review Letters* 86.11 (Mar. 2001), pp. 2208–2211. DOI: 10.1103/PhysRevLett.86.2208. (Visited on 06/08/2024).

[124] Jinshuang Jin, Matisse Wei-Yuan Tu, Wei-Min Zhang, and YiJing Yan. "Non-Equilibrium Quantum Theory for Nanodevices Based on the Feynman–Vernon Influence Functional". In: *New Journal of Physics* 12.8 (Aug. 2010), p. 083013. ISSN: 1367-2630. DOI: 10.1088/1367-2630/12/8/083013. (Visited on 04/03/2024).

[125] Elliott H. Lieb and Derek W. Robinson. "The Finite Group Velocity of Quantum Spin Systems". In: *Communications in Mathematical Physics* 28.3 (Sept. 1972), pp. 251–257. ISSN: 1432-0916. DOI: 10.1007/BF01645779. (Visited on 12/27/2023).

[126] Matthew B. Hastings and Tohru Koma. "Spectral Gap and Exponential Decay of Correlations". In: *Communications in Mathematical Physics* 265.3 (Aug. 2006), pp. 781–804. ISSN: 1432-0916. DOI: 10.1007/s00220-006-0030-4. (Visited on 02/05/2024).

[127] Nathan Ng, Gunhee Park, Andrew J. Millis, Garnet Kin-Lic Chan, and David R. Reichman. "Real-Time Evolution of Anderson Impurity Models via Tensor Network Influence Functionals". In: *Physical Review B* 107.12 (Mar. 2023), p. 125103. DOI: 10.1103/PhysRevB.107.125103. (Visited on 02/01/2024).

[128] Ruofan Chen, Xiansong Xu, and Chu Guo. "Grassmann Time-Evolving Matrix Product Operators for Quantum Impurity Models". In: *Physical Review B* 109.4 (Jan. 2024), p. 045140. DOI: 10.1103/PhysRevB.109.045140. (Visited on 02/01/2024).

[129] J. Dubail. "Entanglement Scaling of Operators: A Conformal Field Theory Approach, with a Glimpse of Simulability of Long-Time Dynamics in 1 + 1d". In: *Journal of Physics A: Mathematical and Theoretical* 50.23 (May 2017), p. 234001. ISSN: 1751-8121. DOI: 10.1088/1751-8121/aa6f38. (Visited on 03/06/2024).

[130] Huajia Wang and Tianci Zhou. "Barrier from Chaos: Operator Entanglement Dynamics of the Reduced Density Matrix". In: *Journal of High Energy Physics* 2019.12 (Dec. 2019), p. 20. ISSN: 1029-8479. DOI: 10.1007/JHEP12(2019)020. (Visited on 03/06/2024).

[131] Isaac Reid and Bruno Bertini. "Entanglement Barriers in Dual-Unitary Circuits". In: *Physical Review B* 104.1 (July 2021), p. 014301. DOI: 10.1103/PhysRevB.104.014301. (Visited on 03/07/2024).

[132] Sofia Gonzalez-Garcia, Shengqi Sang, Timothy H. Hsieh, Sergio Boixo, Guifre Vidal, Andrew C. Potter, and Romain Vasseur. *Random Insights into the Complexity of Two-Dimensional Tensor Network Calculations*. July 2023. DOI: 10.48550/arXiv.2307.11053. arXiv: 2307.11053 [cond-mat, physics:quant-ph]. (Visited on 01/29/2024).

[133] Bruno Bertini, Pavel Kos, and Tomaž Prosen. "Exact Spectral Form Factor in a Minimal Model of Many-Body Quantum Chaos". In: *Physical Review Letters* 121.26 (Dec. 2018), p. 264101. DOI: 10.1103/PhysRevLett.121.264101. (Visited on 03/17/2024).

[134] Boris Gutkin, Petr Braun, Maram Akila, Daniel Waltner, and Thomas Guhr. "Exact Local Correlations in Kicked Chains". In: *Physical Review B* 102.17 (Nov. 2020), p. 174307. DOI: 10.1103/PhysRevB.102.174307. (Visited on 12/28/2023).

[135] Thomas Gorin, Tomaž Prosen, Thomas H. Seligman, and Marko Žnidarič. "Dynamics of Loschmidt Echoes and Fidelity Decay". In: *Physics Reports* 435.2 (Nov. 2006), pp. 33–156. ISSN: 0370-1573. DOI: 10.1016/j.physrep.2006.09.003. (Visited on 12/28/2023).

[136] Pablo R. Zangara and Horacio M. Pastawski. "Loschmidt Echo in Many-Spin Systems: A Quest for Intrinsic Decoherence and Emergent Irreversibility". In: *Physica Scripta* 92.3 (Feb. 2017), p. 033001. ISSN: 1402-4896. DOI: 10.1088/1402-4896/aa5bee. (Visited on 12/28/2023).

[137] R. Moessner and S. L. Sondhi. "Equilibration and Order in Quantum Floquet Matter". In: *Nature Physics* 13.5 (May 2017), pp. 424–428. ISSN: 1745-2481. DOI: 10.1038/nphys4106. (Visited on 03/17/2024).

[138] M. C. Bañuls, N. Y. Yao, S. Choi, M. D. Lukin, and J. I. Cirac. "Dynamics of Quantum Information in Many-Body Localized Systems". In: *Physical Review B* 96.17 (Nov. 2017), p. 174201. DOI: 10.1103/PhysRevB.96.174201. (Visited on 03/17/2024).

[139] Wojciech De Roeck and François Huveneers. "Stability and Instability towards Delocalization in Many-Body Localization Systems". In: *Physical Review B* 95.15 (Apr. 2017), p. 155129. DOI: 10.1103/PhysRevB.95.155129. (Visited on 03/17/2024).

[140] Kartiek Agarwal, Ehud Altman, Eugene Demler, Sarang Gopalakrishnan, David A. Huse, and Michael Knap. "Rare-Region Effects and Dynamics near the Many-Body Localization Transition". In: *Annalen der Physik* 529.7 (2017), p. 1600326. ISSN: 1521-3889. DOI: 10.1002/andp.201600326. (Visited on 03/17/2024).

[141] Sarang Gopalakrishnan, Kartiek Agarwal, Eugene A. Demler, David A. Huse, and Michael Knap. "Griffiths Effects and Slow Dynamics in Nearly Many-Body Localized Systems". In: *Physical Review B* 93.13 (Apr. 2016), p. 134206. DOI: 10.1103/PhysRevB.93.134206. (Visited on 03/17/2024).

[142] Kartiek Agarwal, Sarang Gopalakrishnan, Michael Knap, Markus Müller, and Eugene Demler. "Anomalous Diffusion and Griffiths Effects Near the Many-Body Localization Transition". In: *Physical Review Letters* 114.16 (Apr. 2015), p. 160401. DOI: 10.1103/PhysRevLett.114.160401. (Visited on 03/17/2024).

[143] D. A. Abanin, J. H. Bardarson, G. De Tomasi, S. Gopalakrishnan, V. Khemani, S. A. Parameswaran, F. Pollmann, A. C. Potter, M. Serbyn, and R. Vasseur. "Distinguishing Localization from Chaos: Challenges in Finite-Size Systems". In: *Annals of Physics* 427 (Apr. 2021), p. 168415. ISSN: 0003-4916. DOI: 10.1016/j.aop.2021.168415. (Visited on 03/17/2024).

[144] Alex Kamenev and Anton Andreev. "Electron-Electron Interactions in Disordered Metals: Keldysh Formalism". In: *Physical Review B* 60.4 (July 1999), pp. 2218–2238. DOI: 10.1103/PhysRevB.60.2218. (Visited on 03/17/2024).

[145] Alex Kamenev and Alex Levchenko. "Keldysh Technique and Non-Linear σ-Model: Basic Principles and Applications". In: *Advances in Physics* 58.3 (May 2009), pp. 197–319. ISSN: 0001-8732. DOI: 10.1080/00018730902850504. (Visited on 02/01/2024).

[146] B. Paredes, F. Verstraete, and J. I. Cirac. "Exploiting Quantum Parallelism to Simulate Quantum Random Many-Body Systems". In: *Physical Review Letters* 95.14 (Sept. 2005), p. 140501. DOI: 10.1103/PhysRevLett.95.140501. (Visited on 03/17/2024).

[147] Liangsheng Zhang, Vedika Khemani, and David A. Huse. "A Floquet Model for the Many-Body Localization Transition". In: *Physical Review B* 94.22 (Dec. 2016), p. 224202. DOI: 10.1103/PhysRevB.94.224202. (Visited on 03/17/2024).

[148] Talía L. M. Lezama, Soumya Bera, and Jens H. Bardarson. "Apparent Slow Dynamics in the Ergodic Phase of a Driven Many-Body Localized System without Extensive Conserved Quantities". In: *Physical Review B* 99.16 (Apr. 2019), p. 161106. DOI: 10.1103/PhysRevB.99.161106. (Visited on 03/18/2024).

[149] V. Ros and M. Müller. "Remanent Magnetization: Signature of Many-Body Localization in Quantum Antiferromagnets". In: *Physical Review Letters* 118.23 (June 2017), p. 237202. DOI: 10.1103/PhysRevLett.118.237202. (Visited on 03/17/2024).

[150] S. J. Garratt and J. T. Chalker. "Many-Body Delocalization as Symmetry Breaking". In: *Physical Review Letters* 127.2 (July 2021), p. 026802. DOI: 10.1103/PhysRevLett.127.026802. (Visited on 12/13/2023).

[151] P. Schlottmann and P.D. Sacramento. "Multichannel Kondo Problem and Some Applications". In: *Advances in Physics* 42.6 (Dec. 1993), pp. 641–682. ISSN: 0001-8732. DOI: 10.1080/00018739300101534. (Visited on 04/11/2024).

[152] Yaakov Kleeorin and Yigal Meir. "Quantum Phase Transition in a Realistic Double-Quantum-Dot System". In: *Scientific Reports* 8.1 (July 2018), p. 10539. ISSN: 2045-2322. DOI: 10.1038/s41598-018-28822-y. (Visited on 04/11/2024).

[153] Guangjie Li, Yuval Oreg, and Jukka I. Väyrynen. "Multichannel Topological Kondo Effect". In: *Physical Review Letters* 130.6 (Feb. 2023), p. 066302. DOI: 10.1103/PhysRevLett.130.066302. (Visited on 04/11/2024).

[154] Zhanyu Ma, Cheolhee Han, Yigal Meir, and Eran Sela. "Identifying an Environment-Induced Localization Transition from Entropy and Conductance". In: *Physical Review Letters* 131.12 (Sept. 2023), p. 126502. DOI: 10.1103/PhysRevLett.131.126502. (Visited on 04/11/2024).

[155] Yigal Meir, Ned S. Wingreen, and Patrick A. Lee. "Low-Temperature Transport through a Quantum Dot: The Anderson Model out of Equilibrium". In: *Physical Review Letters* 70.17 (Apr. 1993), pp. 2601–2604. DOI: 10.1103/PhysRevLett.70.2601. (Visited on 04/09/2024).

[156] Michael Pustilnik and Leonid Glazman. "Kondo Effect in Quantum Dots". In: *Journal of Physics: Condensed Matter* 16.16 (Apr. 2004), R513. ISSN: 0953-8984. DOI: 10.1088/0953-8984/16/16/R01. (Visited on 04/09/2024).

[157] Johannes Bauer, Christophe Salomon, and Eugene Demler. "Realizing a Kondo-Correlated State with Ultracold Atoms". In: *Physical Review Letters* 111.21 (Nov. 2013), p. 215304. DOI: 10.1103/PhysRevLett.111.215304. (Visited on 04/09/2024).

[158] Márton Kanász-Nagy, Yuto Ashida, Tao Shi, Cătălin Paşcu Moca, Tatsuhiko N. Ikeda, Simon Fölling, J. Ignacio Cirac, Gergely Zaránd, and Eugene A. Demler. "Exploring the Anisotropic Kondo Model in and out of Equilibrium with Alkaline-Earth Atoms". In: *Physical Review B* 97.15 (Apr. 2018), p. 155156. DOI: 10.1103/PhysRevB.97.155156. (Visited on 03/03/2023).

[159] L. Riegger, N. Darkwah Oppong, M. Höfer, D. R. Fernandes, I. Bloch, and S. Fölling. "Localized Magnetic Moments with Tunable Spin Exchange in a Gas of Ultracold Fermions". In: *Physical Review Letters* 120.14 (Apr. 2018), p. 143601. DOI: 10.1103/PhysRevLett.120.143601. (Visited on 04/09/2024).

[160] Antoine Georges, Gabriel Kotliar, Werner Krauth, and Marcelo J. Rozenberg. "Dynamical Mean-Field Theory of Strongly Correlated Fermion Systems and the Limit of Infinite Dimensions". In: *Reviews of Modern Physics* 68.1 (Jan. 1996), pp. 13–125. DOI: 10.1103/RevModPhys.68.13. (Visited on 12/29/2022).

[161] Hideo Aoki, Naoto Tsuji, Martin Eckstein, Marcus Kollar, Takashi Oka, and Philipp Werner. "Nonequilibrium Dynamical Mean-Field Theory and Its Applications". In: *Reviews of Modern Physics* 86.2 (June 2014), pp. 779–837. DOI: 10.1103/RevModPhys.86.779. (Visited on 12/29/2022).

[162] A. N. Rubtsov, V. V. Savkin, and A. I. Lichtenstein. "Continuous-Time Quantum Monte Carlo Method for Fermions". In: *Physical Review B* 72.3 (July 2005), p. 035122. DOI: 10.1103/PhysRevB.72.035122. (Visited on 04/11/2024).

[163] E. Gull, P. Werner, O. Parcollet, and M. Troyer. "Continuous-Time Auxiliary-Field Monte Carlo for Quantum Impurity Models". In: *Europhysics Letters* 82.5 (May 2008), p. 57003. ISSN: 0295-5075. DOI: 10.1209/0295-5075/82/57003. (Visited on 04/11/2024).

[164] Philipp Werner and Andrew J. Millis. "Hybridization Expansion Impurity Solver: General Formulation and Application to Kondo Lattice and Two-Orbital Models". In: *Physical Review B* 74.15 (Oct. 2006), p. 155107. DOI: 10.1103/PhysRevB.74.155107. (Visited on 04/11/2024).

[165] Kenneth G. Wilson. "The Renormalization Group: Critical Phenomena and the Kondo Problem". In: *Reviews of Modern Physics* 47.4 (Oct. 1975), pp. 773–840. DOI: 10.1103/RevModPhys.47.773. (Visited on 04/09/2024).

[166] Ralf Bulla, Theo A. Costi, and Thomas Pruschke. "Numerical Renormalization Group Method for Quantum Impurity Systems". In: *Reviews of Modern Physics* 80.2 (Apr. 2008), pp. 395–450. DOI: 10.1103/RevModPhys.80.395. (Visited on 04/11/2024).

[167] Olivier Parcollet, Michel Ferrero, Thomas Ayral, Hartmut Hafermann, Igor Krivenko, Laura Messio, and Priyanka Seth. "TRIQS: A Toolbox for Research on Interacting Quantum Systems". In: *Computer Physics Communications* 196 (Nov. 2015), pp. 398–415. ISSN: 0010-4655. DOI: 10.1016/j.cpc.2015.04.023. (Visited on 04/11/2024).

[168] Rok Zitko. *NRG Ljubljana*. Zenodo. May 2021. DOI: 10.5281/zenodo.4841076. (Visited on 04/11/2024).

[169] Priyanka Seth, Igor Krivenko, Michel Ferrero, and Olivier Parcollet. "TRIQS/CTHYB: A Continuous-Time Quantum Monte Carlo Hybridisation Expansion Solver for Quantum Impurity Problems". In: *Computer Physics Communications* 200 (Mar. 2016), pp. 274–284. ISSN: 0010-4655. DOI: 10.1016/j.cpc.2015.10.023. (Visited on 04/11/2024).

[170] Lothar Mühlbacher and Eran Rabani. "Real-Time Path Integral Approach to Nonequilibrium Many-Body Quantum Systems". In: *Physical Review Letters* 100.17 (May 2008), p. 176403. DOI: 10.1103/PhysRevLett.100.176403. (Visited on 04/09/2024).

[171] Philipp Werner, Takashi Oka, and Andrew J. Millis. "Diagrammatic Monte Carlo Simulation of Nonequilibrium Systems". In: *Physical Review B* 79.3 (Jan. 2009), p. 035320. DOI: 10.1103/PhysRevB.79.035320. (Visited on 04/09/2024).

[172] Marco Schiró and Michele Fabrizio. "Real-Time Diagrammatic Monte Carlo for Nonequilibrium Quantum Transport". In: *Physical Review B* 79.15 (Apr. 2009), p. 153302. DOI: 10.1103/PhysRevB.79.153302. (Visited on 04/09/2024).

[173] Emanuel Gull, David R. Reichman, and Andrew J. Millis. "Numerically Exact Long-Time Behavior of Nonequilibrium Quantum Impurity Models". In: *Physical Review B* 84.8 (Aug. 2011), p. 085134. DOI: 10.1103/PhysRevB.84.085134. (Visited on 04/09/2024).

[174] Guy Cohen and Eran Rabani. "Memory Effects in Nonequilibrium Quantum Impurity Models". In: *Physical Review B* 84.7 (Aug. 2011), p. 075150. DOI: 10.1103/PhysRevB.84.075150. (Visited on 04/09/2024).

[175] Guy Cohen, Emanuel Gull, David R. Reichman, Andrew J. Millis, and Eran Rabani. "Numerically Exact Long-Time Magnetization Dynamics at the Nonequilibrium Kondo Crossover of the Anderson Impurity Model". In: *Physical Review B* 87.19 (May 2013), p. 195108. DOI: 10.1103/PhysRevB.87.195108. (Visited on 04/09/2024).

[176] Guy Cohen, Emanuel Gull, David R. Reichman, and Andrew J. Millis. "Taming the Dynamical Sign Problem in Real-Time Evolution of Quantum Many-Body Problems". In: *Physical Review Letters* 115.26 (Dec. 2015), p. 266802. DOI: 10.1103/PhysRevLett.115.266802. (Visited on 10/07/2022).

[177] Martin Nuss, Martin Ganahl, Enrico Arrigoni, Wolfgang von der Linden, and Hans Gerd Evertz. "Nonequilibrium Spatiotemporal Formation of the Kondo Screening Cloud on a Lattice". In: *Physical Review B* 91.8 (Feb. 2015), p. 085127. DOI: 10.1103/PhysRevB.91.085127. (Visited on 10/07/2022).

[178] F. Alexander Wolf, Ian P. McCulloch, and Ulrich Schollwöck. "Solving Nonequilibrium Dynamical Mean-Field Theory Using Matrix Product States". In: *Physical Review B* 90.23 (Dec. 2014), p. 235131. DOI: 10.1103/PhysRevB.90.235131. (Visited on 04/09/2024).

[179] F. Schwarz, I. Weymann, J. von Delft, and A. Weichselbaum. "Nonequilibrium Steady-State Transport in Quantum Impurity Models: A Thermofield and Quantum Quench Approach Using Matrix Product States". In: *Physical Review Letters* 121.13 (Sept. 2018), p. 137702. DOI: 10.1103/PhysRevLett.121.137702. (Visited on 04/09/2024).

[180] Gabriela Wójtowicz, Justin E. Elenewski, Marek M. Rams, and Michael Zwolak. "Open-System Tensor Networks and Kramers' Crossover for Quantum Transport". In: *Physical Review A* 101.5 (May 2020), p. 050301. DOI: 10.1103/PhysRevA.101.050301. (Visited on 04/09/2024).

[181] Lucas Kohn and Giuseppe E. Santoro. "Quench Dynamics of the Anderson Impurity Model at Finite Temperature Using Matrix Product States: Entanglement and Bath Dynamics". In: *Journal of Statistical Mechanics: Theory and Experiment* 2022.6 (June 2022), p. 063102. ISSN: 1742-5468. DOI: 10.1088/1742-5468/ac729b. (Visited on 04/26/2023).

[182] Javier Prior, Alex W. Chin, Susana F. Huelga, and Martin B. Plenio. "Efficient Simulation of Strong System-Environment Interactions". In: *Physical Review Letters* 105.5 (July 2010), p. 050404. DOI: 10.1103/PhysRevLett.105.050404. (Visited on 04/09/2024).

[183] Alexander Nüßeler, Ish Dhand, Susana F. Huelga, and Martin B. Plenio. "Efficient Simulation of Open Quantum Systems Coupled to a Fermionic Bath". In: *Physical Review B* 101.15 (Apr. 2020), p. 155134. DOI: 10.1103/PhysRevB.101.155134. (Visited on 04/09/2024).

[184] Frithjof B. Anders and Avraham Schiller. "Real-Time Dynamics in Quantum-Impurity Systems: A Time-Dependent Numerical Renormalization-Group Approach". In: *Physical Review Letters* 95.19 (Oct. 2005), p. 196801. DOI: 10.1103/PhysRevLett.95.196801. (Visited on 02/14/2024).

[185] H. T. M. Nghiem and T. A. Costi. "Time Evolution of the Kondo Resonance in Response to a Quench". In: *Physical Review Letters* 119.15 (Oct. 2017), p. 156601. DOI: 10.1103/PhysRevLett.119.156601. (Visited on 04/09/2024).

[186] Alex W. Chin, Ángel Rivas, Susana F. Huelga, and Martin B. Plenio. "Exact Mapping between System-Reservoir Quantum Models and Semi-Infinite Discrete Chains Using Orthogonal Polynomials". In: *Journal of Mathematical Physics* 51.9 (Sept. 2010), p. 092109. ISSN: 0022-2488. DOI: 10.1063/1.3490188. (Visited on 04/11/2024).

[187] J. Bardeen, L. N. Cooper, and J. R. Schrieffer. "Microscopic Theory of Superconductivity". In: *Physical Review* 106.1 (Apr. 1957), pp. 162–164. DOI: 10.1103/PhysRev.106.162. (Visited on 04/11/2024).

[188] Matthew T. Fishman and Steven R. White. "Compression of Correlation Matrices and an Efficient Method for Forming Matrix Product States of Fermionic Gaussian States". In: *Physical Review B* 92.7 (Aug. 2015), p. 075132. DOI: 10.1103/PhysRevB.92.075132. (Visited on 09/25/2023).

[189] P. W. Anderson. "Localized Magnetic States in Metals". In: *Physical Review* 124.1 (Oct. 1961), pp. 41–53. DOI: 10.1103/PhysRev.124.41. (Visited on 04/09/2024).

[190] Jun Kondo. "Resistance Minimum in Dilute Magnetic Alloys". In: *Progress of Theoretical Physics* 32.1 (July 1964), pp. 37–49. ISSN: 0033-068X. DOI: 10.1143/PTP.32.37. (Visited on 04/11/2024).

[191] Corentin Bertrand, Serge Florens, Olivier Parcollet, and Xavier Waintal. "Reconstructing Nonequilibrium Regimes of Quantum Many-Body Systems from the Analytical Structure of Perturbative Expansions". In: *Physical Review X* 9.4 (Oct. 2019), p. 041008. DOI: 10.1103/PhysRevX.9.041008. (Visited on 10/28/2022).

[192] Michael Sonner, Julian Thoenniss, Alessio Lerose, and Dmitry A. Abanin. "Efficient Real-Time Simulation of Multi-Orbital Impurity Models (in Preparation)". In: ().